VU VRIJE UNIVERSITEIT AMSTERDAM

VU Research Portal

Feedforward and feedback processing in monkey visual cortex

van Kerkoerle, T.J.

2015

document version
Publisher's PDF, also known as Version of record

Link to publication in VU Research Portal

citation for published version (APA)
van Kerkoerle, T. J. (2015). *Feedforward and feedback processing in monkey visual cortex*. [PhD-Thesis - Research and graduation internal, Vrije Universiteit Amsterdam].

General rights
Copyright and moral rights for the publications made accessible in the public portal are retained by the authors and/or other copyright owners and it is a condition of accessing publications that users recognise and abide by the legal requirements associated with these rights.

- Users may download and print one copy of any publication from the public portal for the purpose of private study or research.
- You may not further distribute the material or use it for any profit-making activity or commercial gain
- You may freely distribute the URL identifying the publication in the public portal ?

Take down policy
If you believe that this document breaches copyright please contact us providing details, and we will remove access to the work immediately and investigate your claim.

E-mail address:
vuresearchportal.ub@vu.nl

Download date: 05. May. 2023

Feedforward and Feedback Processing in Monkey Visual Cortex

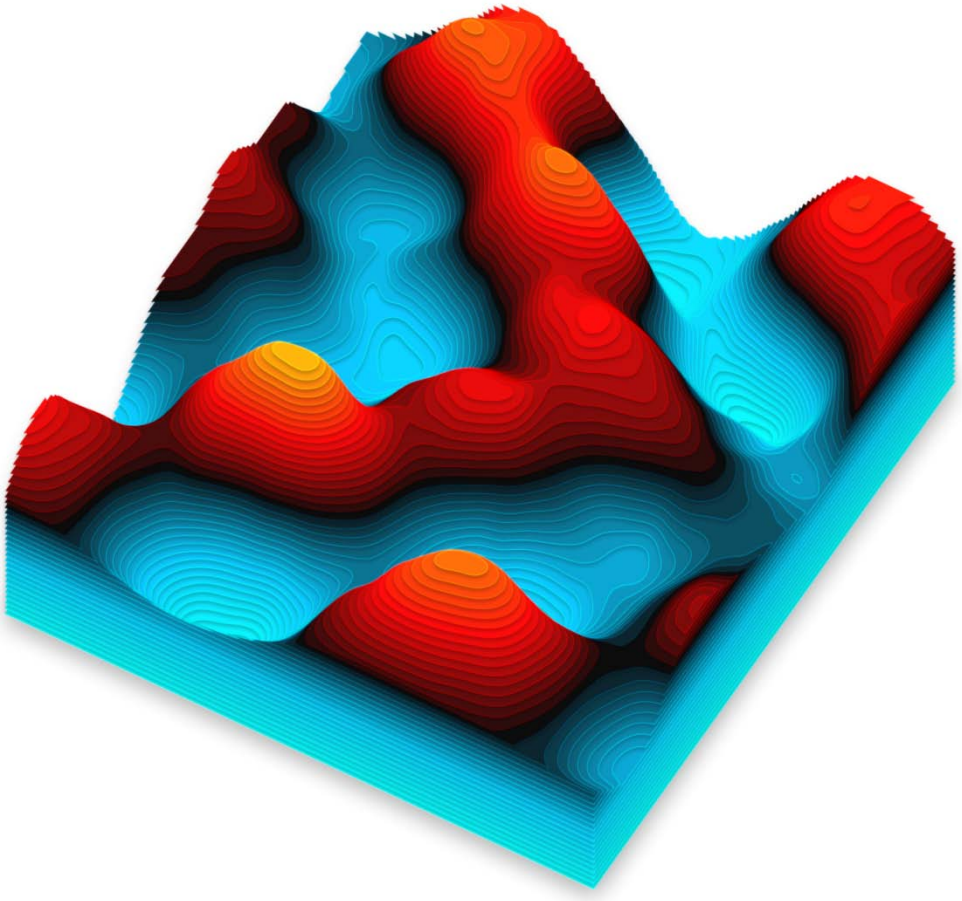

Timo van Kerkoerle

2015

VRIJE UNIVERSITEIT

Feedforward and Feedback Processing in Monkey Visual Cortex

ACADEMISCH PROEFSCHRIFT

ter verkrijging van de graad Doctor aan
de Vrije Universiteit Amsterdam,
op gezag van de rector magnificus
prof.dr. F.A. van der Duyn Schouten,
in het openbaar te verdedigen
ten overstaan van de promotiecommissie
van de Faculteit der Aard- en Levenswetenschappen
op donderdag 3 december 2015 om 13.45 uur
in de aula van de universiteit,
De Boelelaan 1105

door

Timo Johannes van Kerkoerle

geboren te Maastricht

promotor: prof.dr. P.R. Roelfsema

copromotor: dr. M.W. Self

Overige commissieleden: prof.dr. R. Desimone

prof.dr. P. Fries

prof.dr. O. Jensen

prof.dr. H.D. Mansvelder

prof.dr. E.J.W. van Someren

Opgedragen aan

Floor van den Hout (1977-2013)

Je zult altijd bij ons zijn

Cover design: Michiel Schuurman

Lay-out: Timo van Kerkoerle

Printed by: Proefschriftmaken.nl || Uitgeverij BOXPress

Content

Chapter 1 | Introduction

Visual perception

Every morning we wake up and open our eyes we see the world, we see colors, shapes and objects. The outside world appears to us, immediate, in detail and seemingly without any effort. We trust this experience, we don't question that this is the actual world we live in. Why should we, as it is continuously being confirmed by our interaction with it, holding a glass of water, our feet touching the ground.

However, when we close one eye we can clearly see the tip of our own nose (**Figure 1**). The fact that we normally overlook this is a surprise to most, as we often forget that we need our eyes to see.

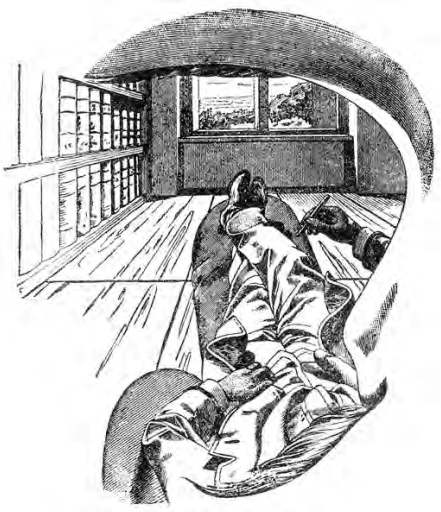

Figure 1 | Inner perspective. A drawing by Ernst Mach showing the boundaries of our visual field.[47]

Our view of the world not only has limits, it even has holes in it, the so called 'blind spots' (**Figure 2**), created by the fiber bundles that exit through the back of our eyeballs. And the colors we see are not veridical either. The visual world outside is comprised of electromagnetic waves with different wavelengths. We just interpret light with a certain wavelengths as having a certain color, colorizing the images we see as in a coloring book.

Figure 2 | Blind Spot. An illustration by which you can experience the blind spots in your eye. Close your left eye and focus on the black cross in the middle. Start with your eyes at around 10cm distance and slowly move backwards. At around 20cm distance you can see that the red dot disappears. Moreover, the blue lines seem to continue at the location of the red dot. This is partly due to mechanisms in the cortex.

These examples illustrate that we don't have a direct perception of the outside world, but that our visual experience is a construct of our brain. We are living in a simulation that is so convincingly real that it can be hard to believe it is generated by this bulk of tissue in our heads. How does our brain create the images that we see? What are the neural mechanisms that are underlying our visual perception?

The retina & the LGN

A crucial step towards visual perception takes place in the first layer of cells in the retina where photoreceptors transform electromagnetic waves into electrical charges across the cell membrane. Light is now being represented by the activity in brain tissue. A photoreceptor only responds to a small patch of the visual field, this is called it's receptive field (RF)[1], similar to a pixel of a digital camera (**Figure 3**).

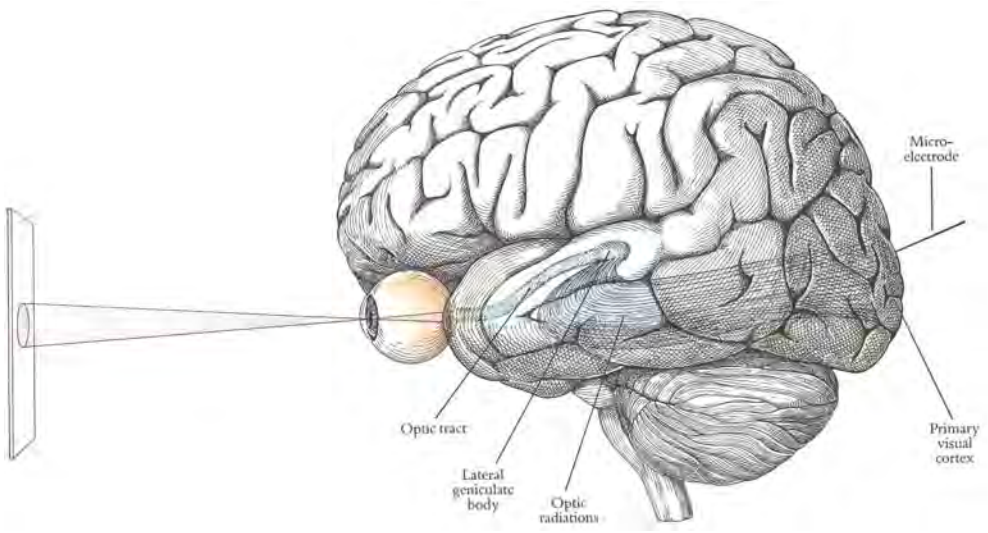

Figure 3 | The visual stream. An illustration showing how visual information propagates from the eyes to the lateral geniculate nucleus (LGN), and onwards to the primary visual cortex (V1) at the back of the brain.[48] From V1, activity travels towards the front of the brain (see also Figure 5).

The electrical activity of the photoreceptor is passed on to the next layer of neurons, the bipolar cells. Another group of neurons called horizontal cells also receive input from the photoreceptors as well and locally inhibit bipolar cells. A bipolar cell that is activated by light thereby only becomes active if it receives more light than its neighbors, and it gets suppressed if it receives less light than it's neighbors. The receptive field of bipolar cells thereby have a so called 'center-surround organization' (**Figure 4A**)[2]. This elegant trick makes bipolar cells relatively independent of how bright or dark the image is that you're looking at.

The next station from the retina is the lateral geniculate nucleus (LGN), a knob of neurons within the thalamus, a structure in the middle of the brain. The receptive fields of neurons in the LGN are similar to the ones in the retina[3]. From the LGN, the activity is sent directly to the first visual area in the cortex, the primary visual cortex (V1) (**Figure 3**).

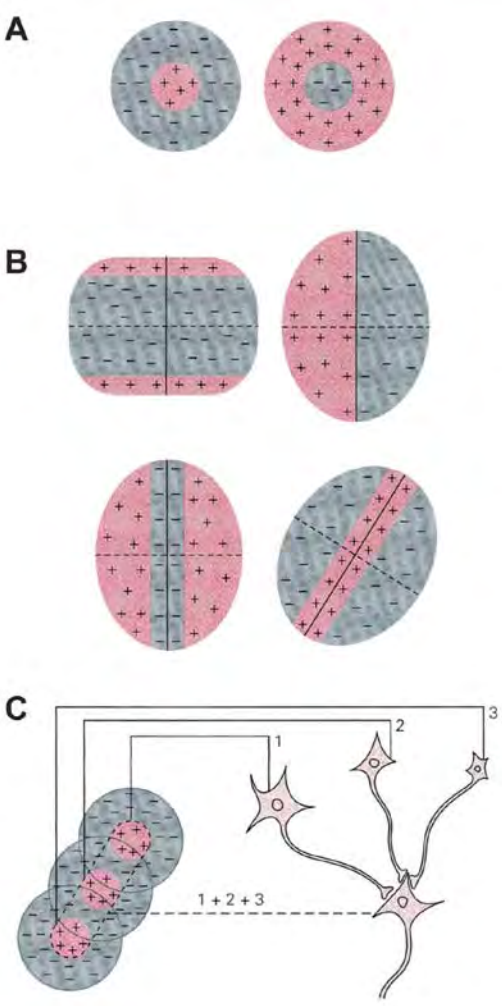

Figure 4 | Receptive fields. An illustration of receptive fields in the retina and the LGN (**A**) and in V1 (**B**). Receptive fields can either have a positive center and a negative surround, or vice versa. Receptive fields in the retina and the LGN are concentric while in V1 they are elongated. Panel **C** illustrates a simple circuit by which an elongated receptive field can be made up from three concentric receptive fields which are aligned.[49]

The cortex

The first layer in V1 where activity arrives at is layer 4C (some activity is also being send to layer 6 and to layer 4A)[4]. For primates, the neurons in layer 4C behave similar to neurons in the LGN[5]. Layer 4 subsequently targets superficial layers 2 & 3[4]. Here, cells behave differently, they do no longer respond to dots of light, but to bars, or edges (**Figure 4B**)[5]. And they only respond if the bar has a specific orientation. You could imagine that the combined input from a couple of layer 4C neurons to a layer 2-3 neuron create this property (**Figure 4C**).

From layers 2 and 3 in V1, activity flows onwards to layer 4 of the next cortical area, which is V2. In V2 the properties of the neurons change again, seemingly combining the input they receive from V1. With every step that activity travels down the visual hierarchy, the properties of the neurons become more and more complex (**Figure 5**). The information processing in this direction is called 'feed-forward'.

All the way down the visual stream, in the inferotemporal cortex (IT), cells only respond to very specific objects, to faces or houses for example. Moreover, cells have been found that only respond to pictures of specific persons, Jennifer Aniston for example[6]. And they not only respond to an image of her face, but also to an image of her standing among other people, and even when reading just her name. Similar cells have been found for Bill Clinton and the Simpsons. These so- called 'grandmother cells' only respond when you see or just think about a certain person.

The path towards IT is called the ventral stream, representing what we see. Another path in the cortex represents where we see it and where it is moving towards, the dorsal stream[7]. These paths both give input to an area in the front of the brain, the prefrontal cortex (PFC). This brain structure is thought to be involved in planning, setting goals and deciding on what to do to reach those goals[8].

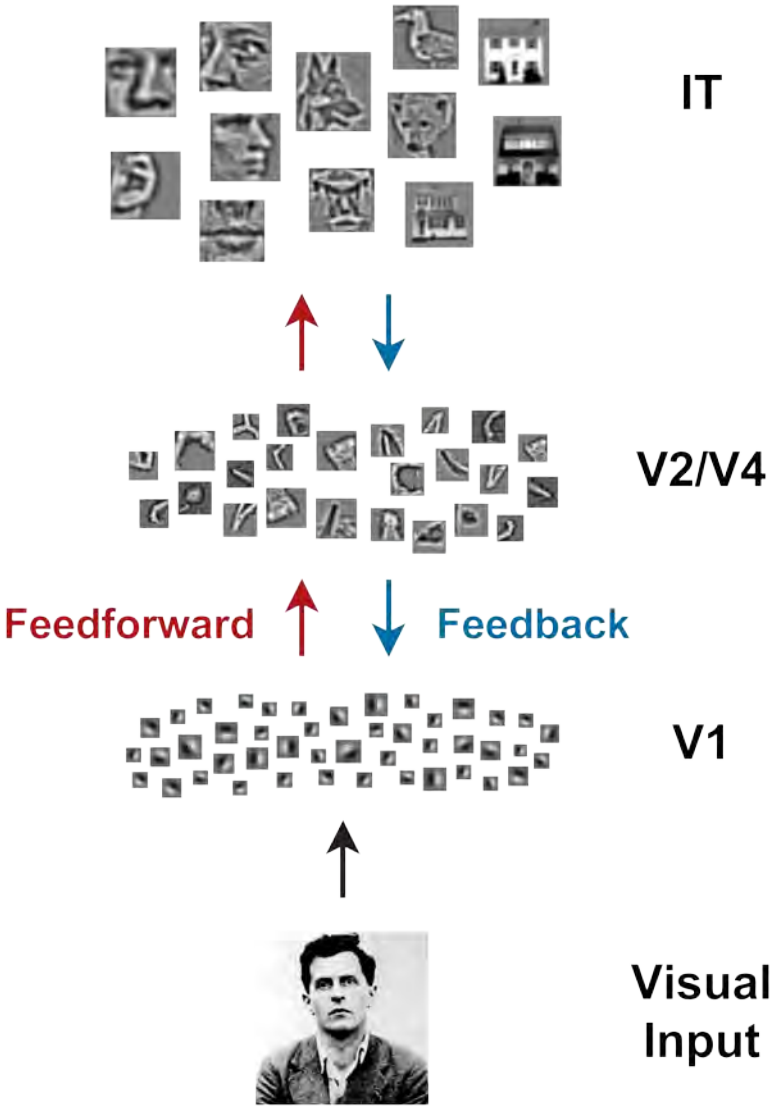

Figure 5 | Visual Hierarchy. Illustration of the feedforward (in red) and feedback (in blue) flow of information between visual areas in the cortex. The tiled images represent receptive fields of neurons in the different cortical areas. Note that while the number of neurons decreases towards higher visual areas, their receptive fields become larger and more complex. (Adapted from ref. 50).[50]

Feedback processing, selective attention and working memory

The feedforward processing stream that we just described can fully explain the activity of grandmother cells in IT cortex[9-12]. However, there is a 'feedback' processing stream sending information in the opposite direction (from the PFC to IT, IT to V4 etc.), which is as least as dense as the feedforward stream[13]. The function and mechanisms of this feedback pathway are much less understood.

One cognitive function that is thought to involve feedback connections is 'selective attention', the filtering of information dependent on what is relevant for us at a given moment in time[14-16]. This is crucial in everyday life, for example when focusing on a headline from the front page of a newspaper. The effects of attention on visual perception can be quite dramatic, see **Figure 6**. By sheer thought we can perceive this drawing as either a duck or a rabbit. Your visual experiences switches, while the drawing stays exactly the same.

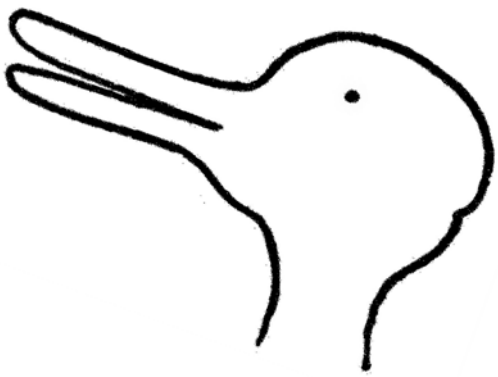

Figure 6 | Duck rabbit illusion. A drawing by Ludwig Wittgenstein in which you can see this drawing either as a duck or as a rabbit. You can even try to switch between one and the other while fixating your eyes on the dot in the middle. Once you have seen the duck and the rabbit it becomes impossible to see neither, to simply observe the drawing as a set of lines. This illustrates that we always interpret what we see.[51]

A related cognitive function is working memory, keeping relevant information in mind when a stimulus is no longer present. To understand this sentence for example, you have to

keep track of the individual words to be able to combine them at the end into a message with coherent meaning. You only have to store the words for a short period of time and can forget them once you have distilled the gist of the sentence.

Both selective attention and working memory are thought to involve feedback from the PFC to early visual areas. The PFC maintains the information about the task at hand and sends feedback to early visual areas to enhance the visual representation of task-relevant versus task-irrelevant stimuli. This suggests that early visual areas are not only involved in the processing of information when a stimulus is present, but also when retaining information about that stimulus when it has disappeared.

How crucial working memory and selective attention are becomes apparent when they are impaired, as is the case in mental illnesses as varied as autism, schizophrenia, ADHD, depression and old age[17-24]. Therefore, investigating the neural mechanisms of cortical feedback is not only important to understanding visual perception, but it is also highly relevant for the understanding of many mental illnesses.

Laminar recordings

Neurons in the visual cortex receive both feedforward and feedback input and it has therefore been difficult to separate the two streams of processing. Luckily, the feedforward and feedback inputs to cortical areas arrives in separate layers, in particular in area V1. As mentioned before, the feedforward connections to V1 arrive mainly in layer 4C. In contrast, the feedback connections target layer 1-3 and layer 5. This allows us to distinguish feedforward from feedback influences by measuring inputs to neurons in different layers of V1.

Techniques that are used in humans rely on signals that can be picked up on top of the scalp, which generally cannot distinguish between cortical layers. Simultaneously recording throughout the depth of cortex is possible with an invasive laminar probe (**Figure 7**). Monkeys can be trained to perform similar tasks that are used to test cognitive impairments in patients with mental illnesses[25], which provides a unique way to study the underlying cortical mechanisms and the role of feedback in visual attention and working memory.

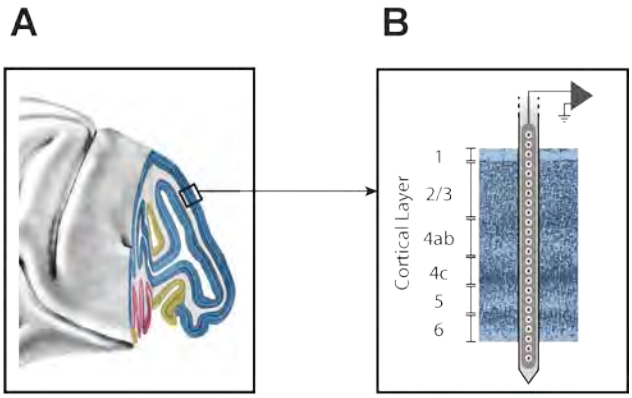

Figure 7 | Monkey brain and laminar recordings. (**A**) Lateral view of a macaque brain with a part cut out exposing the calcarine sulcus. Blue indicates V1, yellow indicates V2 and red indicates V3. (**B**) Illustration of a laminar recording using a high density laminar probe.

Chapter 2

A cognitive task that is thought to involve feedback to V1 and is well studied in humans and monkeys is the figure-ground task (**Figure 8A**,**B**)[26-31]. A display of texture elements of a certain orientation is presented with one square containing elements of the opposite orientation, giving the perception of a figure popping out against a background. A monkey can be trained to make an eye movement to the center of a figure, indicating that he perceived it.

Neurons in V1 have a small receptive field (red and blue circles in **Figure 8A**,**B**), confined within the figure. Note that the stimulus elements inside these circles are identical, receptive fields in V1 are too small to distinguish whether they are lying on a figure or on a background. That explains why the initial transient responses in these neurons are identical for the figure and ground conditions (**Figure 8C**). Still, neurons in V1 with their receptive fields lying on the figure enhance their activity relative to when they are lying on the background, with a delay of about 100ms (**Figure 8C**). This difference in activity is called 'figure-ground modulation'. Neurons in higher visual areas have larger receptive fields that would be able to see whether they are lying on a figure or on a background. This suggests that neurons in V1 receive feedback input from higher visual areas; this input enhances the

activity of neurons with receptive fields lying on the figure and suppresses the activity of neurons with receptive fields lying on the background. The delay is thought to arise from the fact that activity first has to propagate to higher visual areas before it can be send back to V1[15].

To directly investigate whether the figure-ground task involves feedback to V1, we recorded activity in the different layers of monkey V1 with a laminar probe. Our hypothesis is that the initial response to the figure and ground stimulus evokes a laminar pattern in V1 that indicates feedforward input to layer 4 and 6. In contrast, the modulation between the figure and ground condition is expected to indicate feedback input to layer 1-3 and layer 5.

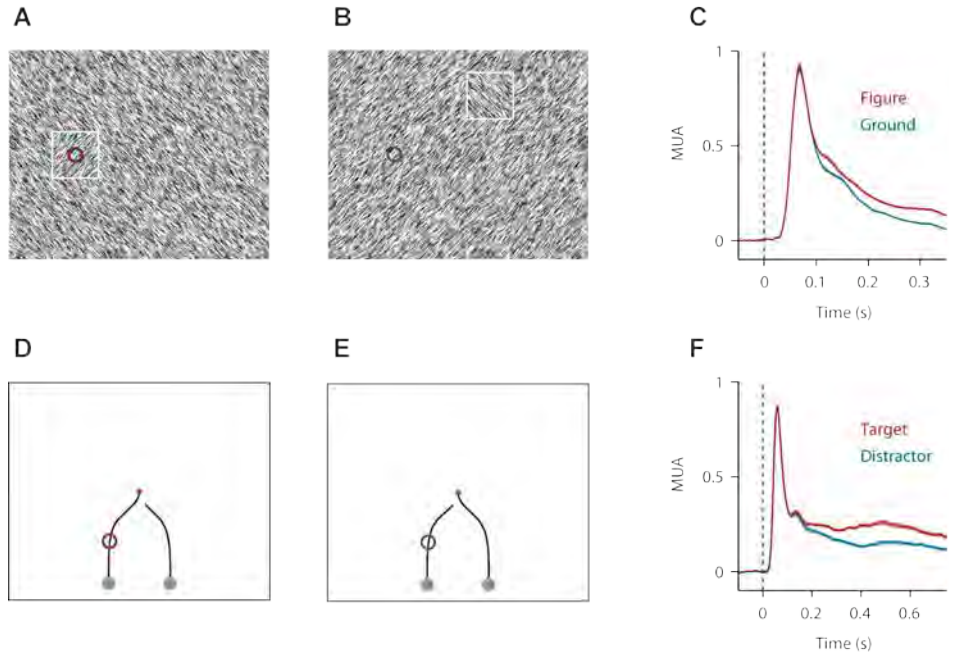

Figure 8 | Figure-ground and curve-tracing task. (**A**,**B**) Texture-segregation stimuli with a figure of one orientation placed on a background with the orthogonal orientation. The monkey was trained to make an eyemovement to the center of the figure. The neurons' receptive field (circle) fell either on the figure (A) or on the background (B). The white square was not visible to the monkey. (**C**) Average MUA response in V1 evoked by the figure (red trace) and the background (blue trace). The dashed line indicates the stimulus onset. (**D**,**E**) The monkey had to mentally trace the target curve that was connected to the fixation point. Either the target curve (D) (red circle) or the distractor curves was placed in the RF (**E**) (blue circle). (**F**) Average MUA response in V1 evoked by the target (red trace) and the distractor curve (blue trace).

Chapter 3

Horizontal connections within V1 have been shown to provide contextual input to the receptive fields of neurons in V1[32]. Figure-ground modulation could thereby rely on input from neurons within V1 instead of feedback from higher visual areas[33, 34]. Yet the modulation has been shown to depend on whether it is the goal of the monkey to report the figure, indicating the involvement of feedback from higher cortical areas like the PFC[31].

A task that is not thought to rely on horizontal connections, and more clearly involves the selection of one object among distractors is the curve-tracing task (**Figure 8D**,**E**)[35]. Monkeys are trained to mentally trace a curve and make an eye movement to the end of the curve that is connected to the fixation dot[35]. Again, the receptive fields of neurons in V1 are too small to see whether they are lying on a task-relevant (**Figure 8D**) or a task-irrelevant part of the stimulus (**Figure 8E**). Still, neurons on the target curve become enhanced over the distractor curve after a certain delay, again indicating feedback (**Figure 8F**).

The curve-tracing task allowed us to measure the laminar profile of both selective attention and spatial working memory in V1, by presenting the curves either for the full duration of the trial or only for a short time period. It is still an open question whether a working memory trace is present in terms of spiking activity in V1. Furthermore, we can now investigate the role of feedback in both selective attention and working memory by analyzing the laminar pattern of activity in V1.

Chapter 4

The brain also generates rhythmic activity. Visual input generates a high frequency rhythm in the visual cortex called 'gamma' (**Figure 9**)[36]. This rhythm corresponds to spiking activity and is enhanced when the stimulus is attended[37].

Another rhythm of a lower frequency called 'alpha' is generated in the visual cortex when you close your eyes (**Figure 10**)[38]. It has been suggested that the alpha rhythm therefore reflects the state of the cortex when it is at rest[38-40]. In line with this, the alpha rhythm is found to be suppressed at attended locations[41, 42].

It has been suggested that the gamma rhythm selectively propagates in the feedforward direction through the visual hierarchy, while the alpha rhythms propagates in the feedback direction. Rhythmic activity could thereby provide markers to distinguish feedforward from feedback processing. As the alpha and gamma rhythm can also be picked up outside the scalp this could be highly useful to investigate these processing streams in humans.

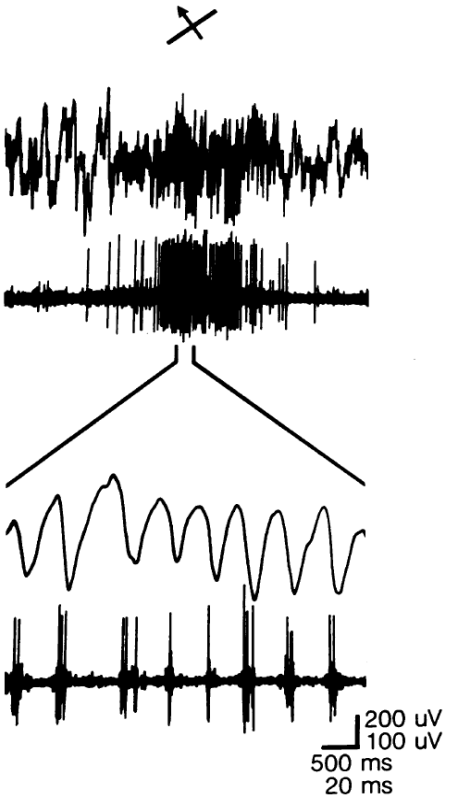

Figure 9 | Gamma oscillations in V1 with visual stimulation. Recording in cat V1 with the local field potential (LFP) on the top and single unit recordings below it. The upper two traces show a slower times scale, the inset below it shows a faster time scale. At the onset of a moving bar, the low frequency oscillations in the LFP can be seen to be replaced by high frequency activity, simultaneous the spiking activity is increased. In the inset it can be seen that this high frequency activity also consists of oscillations where spiking activity it locked to a specific phase of the LFP.[52]

We analyzed the alpha and gamma rhythm during the figure-ground and the curve-tracing task, using both laminar recordings in V1, and combined recordings in V1 and V4. Moreover, using pharmacological manipulations and electrical microstimulation we causally investigated the hypothesis that the alpha and gamma rhythms travel in opposite direction through the visual cortex.

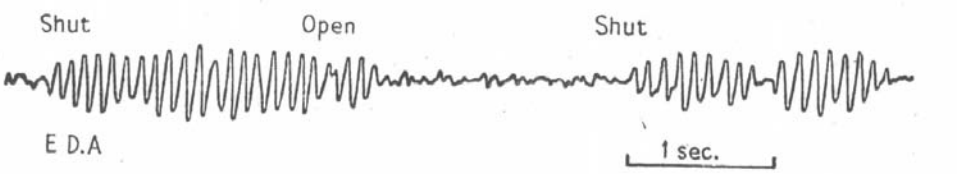

Figure 10 | Alpha oscillation with eyes closing. EEG recording showing large amplitude alpha oscillations when eyes are closed, which disappear when eyes are open.[53]

Chapter 5

Finally, we investigated how the PFC maintains task relevant information during working memory. Neurons in the PFC which are selective for a task relevant stimulus show persistent activity when the stimulus has disappeared[43]. The neural mechanisms behind this persistent activity are not well understood.

Neurons contain two major classes of channels by which they receives excitatory input, AMPA and NMDA channels. While AMPA channels open and close rapidly, NMDA channels have slower dynamics. Furthermore, NMDA channels can only open once the cell has been depolarized[44]. Modeling work therefore suggested that NMDA channels could be essential in working memory, maintaining sustained activity after an initial feedforward activation[45]. Moreover, a deficit in NMDA channels has been suggested to underlie schizophrenia, which is in line with working memory impairments in schizophrenia patients[46].

Using pharmacological manipulations we studied the roles of AMPA and NMDA channels located in PFC neurons for working memory.

Conclusion

Taken together, we investigated the cortical mechanisms of selective attention and working memory in monkey visual cortex. We investigated the mechanisms of the source of cortical feedback in the PFC, and the signatures of feedback in the laminar profile and in rhythmic activity in early visual areas. This line of research has the potential to unravel the function and mechanisms of cortical feedback, which could have applications with huge benefits to society.

References

1. Hartline,H.K. The response of single optic nerve fibers of the vertebrate eye to illumination of the retina. *Am. J. Physiol.* **121**, 400-415 (1938).
2. Kuffler,S.W. Discharge patterns and functional organization of mammalian retina. *J. Neurophysiol.* **16**, 37-68 (1953).
3. Hubel,D.H. Single unit activity in lateral geniculate body and optic tract of unrestrained cats. *J. Physiol* **150**, 91-104 (1960).
4. Lund,J.S. Anatomical organization of macaque monkey striate visual cortex. *Annu. Rev. Neurosci.* **11**, 253-288 (1988).
5. Hubel,D.H. & Wiesel,T.N. Receptive fields and functional architecture of monkey striate cortex. *J. Physiol* **195**, 215-243 (1968).
6. Quiroga,R.Q., Reddy,L., Kreiman,G., Koch,C., & Fried,I. Invariant visual representation by single neurons in the human brain. *Nature* **435**, 1102-1107 (2005).
7. Goodale,M.A. & Milner,A.D. Separate visual pathways for perception and action. *Trends Neurosci.* **15**, 20-25 (1992).
8. Miller,E.K. & Cohen,J.D. An integrative theory of prefrontal cortex function. *Annu. Rev. Neurosci.* **24**, 167-202 (2001).
9. Riesenhuber,M. & Poggio,T. Neural mechanisms of object recognition. *Curr. Opin. Neurobiol.* **12**, 162-168 (2002).
10. Rust,N.C., Mante,V., Simoncelli,E.P., & Movshon,J.A. How MT cells analyze the motion of visual patterns. *Nat. Neurosci.* **9**, 1421-1431 (2006).
11. Serre,T., Oliva,A., & Poggio,T. A feedforward architecture accounts for rapid categorization. *Proc. Natl. Acad. Sci. U. S. A* **104**, 6424-6429 (2007).
12. DiCarlo,J.J., Zoccolan,D., & Rust,N.C. How does the brain solve visual object recognition? *Neuron* **73**, 415-434 (2012).

13. Markov,N.T. *et al.* Weight consistency specifies regularities of macaque cortical networks. *Cereb. Cortex* **21**, 1254-1272 (2011).

14. Hochstein,S. & Ahissar,M. Views from the top: hierarchies and reverse hierarchies in the visual system. *Neuron* **36**, 791-804 (2002).

15. Lamme,V.A.F. & Roelfsema,P.R. The distinct modes of vision offered by feedforward and recurrent processing. *Trends Neurosci.* **23**, 571-579 (2000).

16. Gilbert,C.D. & Li,W. Top-down influences on visual processing. *Nat. Rev. Neurosci.* **14**, 350-363 (2013).

17. Burack,J.A. Selective attention deficits in persons with autism: preliminary evidence of an inefficient attentional lens. *J. Abnorm. Psychol.* **103**, 535-543 (1994).

18. Barkley,R.A. Behavioral inhibition, sustained attention, and executive functions: constructing a unifying theory of ADHD. *Psychol. Bull.* **121**, 65-94 (1997).

19. Tavares,J., Drevets,W.C., & Sahakian,B.J. Cognition in mania and depression. *Psychological Medicine* **6**, 959-967 (2003).

20. Gazzaley,A., Cooney,J.W., Rissman,J., & D'Esposito,M. Top-down suppression deficit underlies working memory impairment in normal aging. *Nature Neurosci.* **8**, 1298-1300 (2005).

21. Booth,J.R. *et al.* Larger deficits in brain networks for response inhibition than for visual selective attention in attention deficit hyperactivity disorder (ADHD). *J. Child Psychol. Psychiatry* **46**, 94-111 (2005).

22. Desseilles,M. *et al.* Abnormal neural filtering of irrelevant visual information in depression. *J. Neurosci.* **29**, 1395-1403 (2009).

23. Hahn,B. *et al.* Failure of schizophrenia patients to overcome salient distractors during working memory encoding. *Biol. Psychiatry* **68**, 603-609 (2010).

24. Lakatos,P., Schroeder,C.E., Leitman,D.I., & Javitt,D.C. Predictive suppression of cortical excitability and its deficit in schizophrenia. *J. Neurosci.* **33**, 11692-11702 (2013).

25. Goldman-Rakic,P.S. Cellular basis of working memory. *Neuron* **14**, 477-485 (1995).

26. Lamme,V.A.F., van Dijk,B.W., & Spekreijse,H. Texture segregation is processed by primary visual cortex in man and monkey: evidence from VEP experiments. *Vision Res.* **32**, 797-807 (1992).

27. Lamme,V.A.F. The neurophysiology of figure-ground segregation in primary visual cortex. *J. Neurosci.* **15**, 1605-1615 (1995).

28. Lamme,V.A., Zipser,K., & Spekreijse,H. Figure-ground activity in primary visual cortex is suppressed by anesthesia. *Proc. Natl. Acad. Sci. U. S. A* **95**, 3263-3268 (1998).

29. Lamme,V.A.F., Supèr,H., & Spekreijse,H. Feedforward, horizontal, and feedback processing in the visual cortex. *Curr. Opin. Neurobiol.* **8**, 529-535 (1998).

30. Hupe,J.M. *et al.* Cortical feedback improves discrimination between figure and background by V1, V2 and V3 neurons. *Nature* **394**, 784-787 (1998).

31. Poort,J. *et al.* The role of attention in figure-ground segregation in areas V1 and V4 of the visual cortex. *Neuron* **75**, 143-156 (2012).

32. Das,A. & Gilbert,C.D. Topography of contrextual modulations mediated by short-range interactions in primary visual cortex. *Nature* **399**, 655-661 (1999).

33. Li,Z. Contextual influences in V1 as a basis for pop out and asymmetry in visual search. *Proc. Natl. Acad. Sci. USA* **96**, 10539-10535 (1999).

34. Stettler,D.D., Das,A., Bennett,J., & Gilbert,C.D. Lateral connectivity and contextual interactions in macaque primary visual cortex. *Neuron* **36**, 739-750 (2002).

35. Roelfsema,P.R., Lamme,V.A.F., & Spekreijse,H. Object-based attention in the primary visual cortex of the macaque monkey. *Nature* **395**, 376-381 (1998).

36. Gray,C.M., König,P., Engel,A.K., & Singer,W. Oscillatory responses in cat visual cortex exibit inter-columnar synchronization which reflects global stimulus properties. *Nature* **338**, 334-337 (1989).

37. Fries,P., Reynolds,J.H., Rorie,A.E., & Desimone,R. Modulation of oscillatory neuronal synchronization by selective visual attention. *Science* **291**, 1560-1563 (2001).

38. Berger,H. Über das elektroenkephalogramm des menschen. *Arch. Psychiatr. Nervenkr* **87**, 527-570 (1929).

39. Adrian,E. Brain Rhythms. *Nature* **153**, 360-362 (1944).

40. Yu,J. & Ferster,D. Membrane potential synchrony in primary visual cortex during sensory stimulation. *Neuron* **68**, 1187-1201 (2010).

41. Fries,P., Womelsdorf,T., Oostenveld,R., & Desimone,R. The effects of visual stimulation and selective visual attention on rhythmic neuronal synchronization in macaque area V4. *J. Neurosci.* **28**, 4823-4835 (2008).

42. Buffalo,E.A., Fries,P., Landman,R., Buschman,T.J., & Desimone,R. Laminar differences in gamma and alpha coherence in the ventral stream. *Proc. Natl. Acad. Sci. USA* **108**, 11262-11267 (2011).

43. Funahashi,S., Bruce,C.J., & Goldman-Rakic,P.S. Mnemonic coding of visual space in the monkey's dorsolateral prefrontal cortex. *J. Neurophysiol.* **61**, 331-349 (1989).

44. Hestrin,S., Nicoll,R.A., Perkel,D.J., & Sah,P. Analysis of excitatory synaptic action in pyramidal cells using whole-cell recording from rat hippocampal slices. *J. Physiol* **422**, 203-225 (1990).

45. Lisman,J.E., Fellous,J.M., & Wang,X.J. A role for NMDA-receptor channels in working memory. *Nat. Neurosci.* **1**, 273-275 (1998).

46. Lewis,D.A., Hashimoto,T., & Volk,D.W. Cortical inhibitory neurons and schizophrenia. *Nat. Rev. Neurosci.* **6**, 312-324 (2005).

47. Mach,E. *Die Analyse der Empfindungen* (Verlag von Gustav Fischer, Jena, 1885).

48. Hubel,D.H. *Eye, brain, and vision* (Freeman, New York, 1988).

49. Kandel,E.R., Schwartz,J.H., Jessell,T.M., & Eds. *Principles of Neural Science, 4/e* (McGraw-Hill,2000).

50. Thorpe,S.J. *Spikes and recognition* (slide from the presentation during the Visual Neuroscience European Summer School, 2012).

51. Wittgenstein,l. *Tractatus Logico-Philosophicus* (Kegan Paul, Trench, Trubener & Co., Ltd., London, 1922).

52. Gray,C.M. & Singer,W. Stimulus-specific neuronal oscillations in orientation columns of cat visual cortex. *Proc. Natl. Acad. Sci. USA* **86**, 1698-1702 (1989).

53. Adrian,E.D. & Matthews,B.H. The Berger rhythm: potential changes from the occipital lobes in man. *Brain* **57**, 355-385 (1934).

Chapter 2 | Distinct roles of the cortical layers of area V1 in figure-ground segregation

Matthew W. Self, Timo van Kerkoerle, Hans Supèr &

Pieter R. Roelfsema

ABSTRACT

What roles do the different cortical layers play in visual processing? We recorded simultaneously from all layers of the primary visual cortex while monkeys performed a figure-ground segregation task. This task can be divided into different sub-processes which are thought to engage feedforward, horizontal and feedback processes at different time-points. These different connection types have different patterns of laminar terminations in V1 and can therefore be distinguished with laminar recordings. We found that the visual response started 40ms after stimulus presentation in layers 4 and 6, which are targets of feedforward connections from the LGN and distribute activity to the other layers. Boundary detection started shortly after the visual response. In this phase, boundaries of the figure induced synaptic currents and stronger neuronal responses in upper layer 4 and the superficial layers ~70ms after stimulus onset, consistent with the hypothesis that they are detected by horizontal connections. In the next phase, ~30ms later, synaptic inputs arrived in layers 1, 2 and 5 that receive feedback from higher visual areas which caused the filling-in of the representation of the entire figure with enhanced neuronal activity. The present results reveal unique contributions of the different cortical layers to the formation a visual percept. This new blueprint of laminar processing may generalize to other tasks and to other areas of the cerebral cortex, where the layers are likely to have similar roles as those in area V1.

INTRODUCTION

Neocortex is often divided into six layers on the basis of histological data. Every layer receives a characteristic pattern of inputs and gives rise to a distinct set of projections to other layers and brain structures. While the anatomy of the different layers is fairly well defined[1-4] the roles of the different layers in cortical processing are still poorly understood and their elucidation remains a central challenge for systems neuroscience[5]. In the present study we examined the role of the layers in the primary visual cortex (V1) of monkeys. V1 receives feedforward connections from the LGN that terminate primarily in layers 4 and 6[6,7], there are horizontal connections between the V1 columns which are present in all layers but predominantly terminate in upper layer 4 and the superficial layers[8,9] and there are feedback connections from higher visual areas, which terminate primarily in layers 1, and 5 and tend to avoid layer 4[9-12]. What is the role of these different inputs? Do they give rise to distinct types of firing behavior in the different layers?

To determine the role of the layers we used a texture-segmentation task (**Figure 1A**) because electrophysiological[13], psychophysical[14,15] and computational[16-18] studies have suggested that cortical processing in this task consists of a number of processing phases for which feedforward, horizontal and feedback connections play different roles. Firstly, the orientation of the line elements is extracted by the spatial arrangement of feedforward connections from the LGN to V1[19]. Then the edges between figure and background are detected at locations where the orientation changes abruptly (**Figure 1B**). This is thought to be achieved through horizontal inhibition between neurons with nearby RFs tuned to the same orientation[16,17,20,21], suppressing neuronal responses to homogeneous image regions.

Finally, all image elements of the figure must be grouped together in perception (**Figure 1C**). Electrophysiological studies have shown that neuronal responses evoked by the figure are enhanced relative to the background, an effect known as figure-ground modulation (FGM)[22]. FGM in the figure center is thought to arise from feedback projections from higher visual areas back to V1 as it is modulated by attention[18] and absent when a monkey fails to detect the figure[23] or is anesthetized[24].

The aim of our study was to identify the laminar circuits engaged by the different processing phases in the texture-segregation task of **Figure 1A**. We simultaneously

recorded multi-unit neural activity (MUA) from all layers of V1 using a multi-contact depth electrode. The advantage of this electrode is that we were also able to measure the flow of synaptic currents in the different layers underlying changes in firing-rate using current-source density (CSD) analysis[25]. The laminar profile of these currents can be compared to the targets of feedforward, horizontal and feedback connections, allowing us to estimate the contributions of these connection types to figure-ground segregation.

RESULTS

We trained two monkeys to perform a texture-segregation task (**Figure 1D**,**E**) where they saw a square figure of one orientation on a background of the opposite orientation. Both monkeys performed this task with an accuracy of greater than 95%.

Twenty-five percent of trials were catch-trials without a figure and on these trials the monkey was rewarded for maintaining fixation. The performance on catch trials was slightly lower (77% for Monkey S and 89% for Monkey E) due to the longer fixation time.

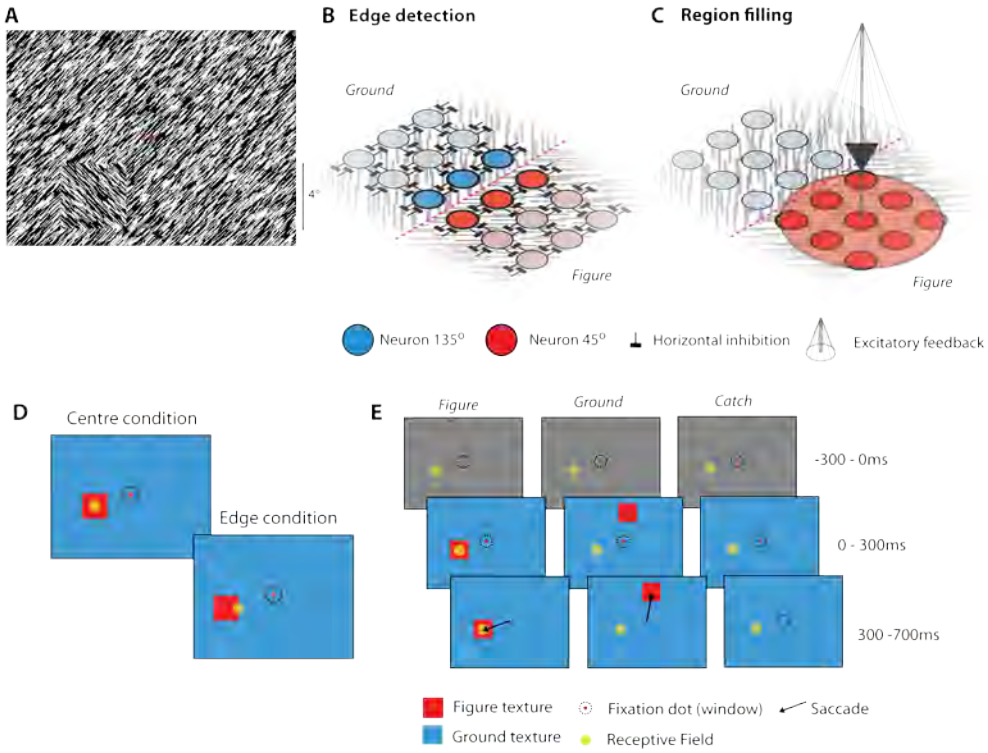

Figure 1. (**A**) Example texture with an orientation defined figure used in the present study. (**B**) A model of neural responses at either side of a texture-boundary (pink dashed line). Neurons tuned to the same orientation inhibit each other (black bars). A neuron at the edge of the figure receives less inhibition than a neuron in the middle of the texture and therefore has a relatively enhanced firing-rate (saturated colors, thicker outlines). (**C**) Models of region-filling suggest that the figure-region becomes perceptually grouped through excitatory feedback from neurons in higher visual areas tuned to the figural orientation (red cone) causing an enhanced firing rate in the entire figure region. (**D**) We varied the eccentricity of the figure in blocks of 200-500 trials so that the RF of the neurons fell on either the figure center or edge. (**E**) Schematic representation of the time-course of the task. Monkeys started a trial by fixating within a small window (1^{o}) centered on a fixation point. After 300ms a figure-ground texture appeared. There were three possible figure locations. One was centered on the neurons' RF (figure condition) and the other two were at an angle of 120^{o} (ground conditions). The orientation of the line elements (45^{o} or 135^{o}) was chosen so that the texture inside the RFs was on average the same across conditions. The fixation dot was extinguished after another 300ms and the monkeys were rewarded for an eye movement to the figure (arrow). On catch trials there was no figure and the monkey was rewarded for maintaining fixation. The yellow circle denotes the RF and the red square illustrates the location of the figure.

Visually driven activity in the different cortical laminae

We recorded multi-unit spiking activity (MUA) simultaneously from the different laminae of area V1 using a multi-contact electrode (**Figure 2A**). We estimated the cortical layer of each electrode site using current source density (CSD) analysis (see **Methods** and **Figure S1A-C**). The CSD profile provides a reliable measure for the boundary between layers 4c and 5. We estimated boundaries between the other layers using data from previous anatomical studies[3,4,26] and these boundaries are therefore more tentative. For each electrode contact we measured the orientation tuning and the multi-unit receptive-field (RF) with a moving bar stimulus (**Figure S1D-E**, **Supplementary Methods**). We then examined the neural responses induced by the appearance of the textures in the catch-trial condition in which there is no figure-ground organization. Visual response latency (calculated using a curve-fitting technique, **Figure 2B**,**C** and **Supplementary Methods**) varied across the cortical layers, being earliest in layer 4c and layer 6. Visually driven activity then spread to layer 5 and considerably (10-15ms) later to the superficial layers. For statistical analysis we grouped the layers into four laminar compartments (deep layers, layer 4c, layer 4a/b and superficial layers, see **Methods**). The differences in latency across the compartments were highly significant (assessed by a mixed linear model which corrects for the correlations within penetrations, see **Supplementary Methods** for details; $F_{3,119.7}=116$, $p<0.001$, n=43 penetrations). Post-hoc tests showed that layer 4c had a significantly shorter latency and that the superficial layers had a significantly longer latency than all other compartments (all $p<0.05$, Bonferroni corrections were applied to all post-hoc tests).

Figure 2D shows the MUA response induced by the appearance of the texture, averaged across all penetrations. **Figure 2E** shows the MUA and CSD responses during the initial peak response phase (30-90ms). The CSD profile gives information about the currents that flow in the cortical layers[25]. Current sinks mark the locations where excitatory input arrives and causes inward currents, whereas current sources arise at locations where the current flows out of cells. The first current in the average CSD was a sink in layer 4c reflecting the thalamic input into this layer (black arrow in **Figure 2E**). This sink coincided with a source in layer 5, which reflects the passive return of current[25]. This initial sink/source pair was followed by a pattern of current sinks and sources in superficial and deep layers that reflects

the anatomy of the cortical micro-circuitry[1]. Thus, the laminar recordings reveal how the visual response activates successive layers of V1.

The initial burst of activity evoked by the onset of the texture stimulus was followed a period of sustained spiking activity (**Figure 2F**). We measured the strength of the sustained activity as the average MUA in a window from 100-300ms after stimulus onset. The strength of this sustained response differed significantly between the cortical compartments (mixed model, $F_{3,119.8}=9.9$, $p<0.001$, n=43 penetrations). Spiking activity in layer 4 was relatively transient whereas the response was more sustained in the superficial layers and particularly in layer 5.

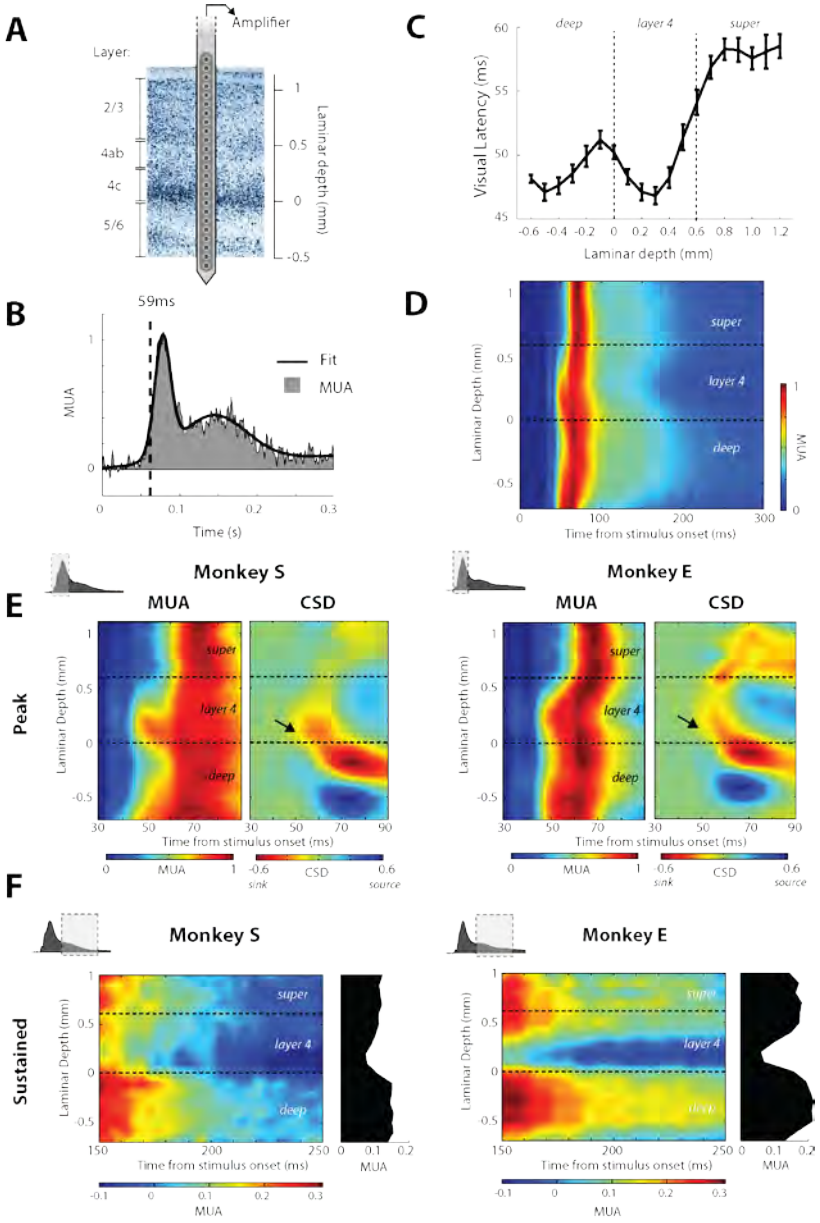

Figure 2. (**A**) Laminar electrode for the simultaneous recording of MUA and CSD at different cortical depths. The electrode ('U-probe', Plexon) contained 24 contact points spaced 100µm apart which allowed us to record simultaneously from every layer of cortex. The diagram shows the approximate thickness of V1 cortex and the division into four layer compartments: 2/3, 4ab, 4c and 5/6. We assigned the depth of 0mm to the reversal in the CSD, which marks the boundary between layer 4c and layer 5. (**B**) Example MUA response in the catch-trial condition (averaged across 235 trials) at

one of the recording sites. A curve was fitted to estimate the visual response latency as the point at which it reached 33% of its maximum (dashed-line). (**C**) The black curve shows visual latencies in the different laminae, averaged across all penetrations, the error-bars show s.e.m. (Figure S5 specifies number of recording sites per cortical depth). (**D**) The average multi-unit activity (MUA) response across penetrations (n = 43) to the oriented texture (catch-trial condition). Dashed lines mark the boundaries between layer compartments. (**E**) The average MUA and current source density (CSD) responses evoked by the onset of the oriented texture across the different laminae in an early time window (30-90ms). These responses were averaged across 29 penetrations for monkey S and 14 for monkey E. For the CSD plots on the right warmer colors indicate current sinks (i.e. current flowing into neurons), cooler colors indicate current sources (current flowing out of neurons). The first MUA response occurred in layers 4c and 6 and it was accompanied by a current sink in layer 4 (indicated by the black arrows). (**F**) MUA during the more sustained phase of the response (150-250ms). The plots to the right of each graph show the average MUA in this time-period for each layer. Note the U-shaped profile indicating that responses in layer 4 are more transient than in the superficial and deep layers.

The laminar profile of region-filling in V1

To examine the differences between neural responses evoked by the center of the figure and the background we placed the figure so that the RF fell on its center or on the background. Figure 3 shows an example penetration from each monkey and illustrates several effects that we consistently observed across penetrations. The laminar profiles of the responses evoked by the figure and background were similar during the initial peak-response, but at later time-points (>100ms) responses were stronger when the figure fell on the RF (**Figure 3A**,**B**). This can best be visualized by subtracting the background response from the figure response to compute FGM (**Figure 3C**). In both example penetrations FGM was strongest in the superficial and deep layers and considerably weaker in layer 4. The laminar pattern of FGM resembled the pattern of sustained activity (compare **Figure 3C** and **Figure 2F**). The strength of FGM differed significantly between laminar compartments of V1 in both example penetrations (two-way ANOVA, interaction between condition and compartment, Monkey S: n=155 trials, $F_{3,612}$=3.3, p=0.02; Monkey E: n=828 trials, $F_{3,3304}$=12.2, p<0.001).

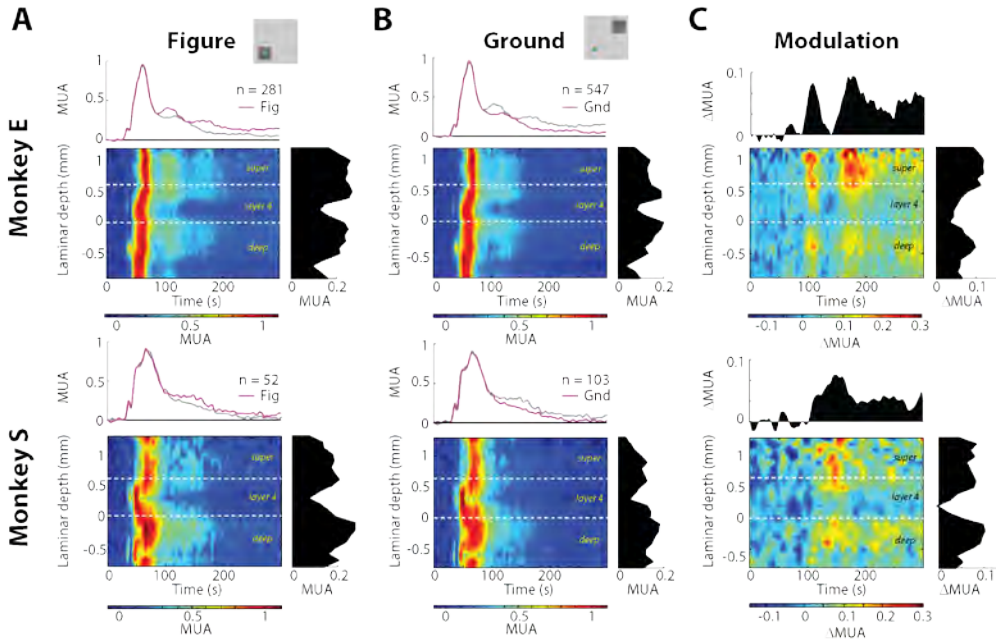

Figure 3. (**A**,**B**) MUA responses across the layers from an example penetration in Monkey E (top graphs) and Monkey S (bottom graphs) evoked by the figure (A) and background (B). The panels above show the MUA-response averaged across all laminae; the relevant condition is highlighted in pink. Panels to the right show the MUA response averaged across time (0-300ms post stimulus onset). Note that the high levels of sustained activity in the superficial layers and in layer 5 are most pronounced in the figure condition. *n,* number of trials. (**C**) FGM, which is the difference between activity evoked by a figure and the background. The upper graphs show how FGM develops in time and the right graph shows the variation across laminae. Note that FGM is weakest in layer 4.

We observed a similar laminar profile of FGM at the population level (**Figure 4A**). We quantified center-FGM as the difference in normalized activity evoked by the figure and background (in a window from 100-300ms). In Monkey E the average FGM was 0.072, i.e. the difference in response evoked by figure and ground was on average 7.2% of the peak response (mixed model, $F_{1,13.1}$=382, p<0.001, n=14 penetrations). FGM was significant (p<0.05, two-sample t-test) at 98% of individual recording sites. In Monkey S the average FGM was 5.8% (mixed model, $F_{1,27.5}$=88.8, p<0.001, n=29 penetrations) and was significant at 68% of sites. We did not observe cases where the background evoked significantly stronger activity than the figure. The absolute FGM strength may appear small, but this is

due to the normalization to the peak response. During the sustained response period (100-300ms) the figure evoked responses were 46% (monkey E) and 28% (monkey S) stronger than the background. FGM was strongest in the superficial and deep layers, which are targets of feedback connections, and weaker in layer 4, the main target of feedforward input from the LGN (**Figure 4A**, data and statistical maps from the individual monkeys are shown in **Figure S2**). For statistical analysis we again grouped the layers into four compartments (**Figure 4C**). FGM differed significantly between these compartments (mixed model, Monkey S: $F_{3,78.0}=5.4$, $p=0.002$; Monkey E: $F_{3,38.2}=35.2$, $p<0.001$). Post-hoc analyses showed that the deep and superficial layers modulated significantly more than the layer 4 sites ($p<0.05$) and were not significantly different from each other ($p>0.5$). Control analyses showed that these results did not depend on the orientation-tuning of the recording sites and were not caused by variations in eye position within the fixation window (**Supplementary Results**). Thus, FGM is strong in the superficial and deep layers, targets of feedback connections.

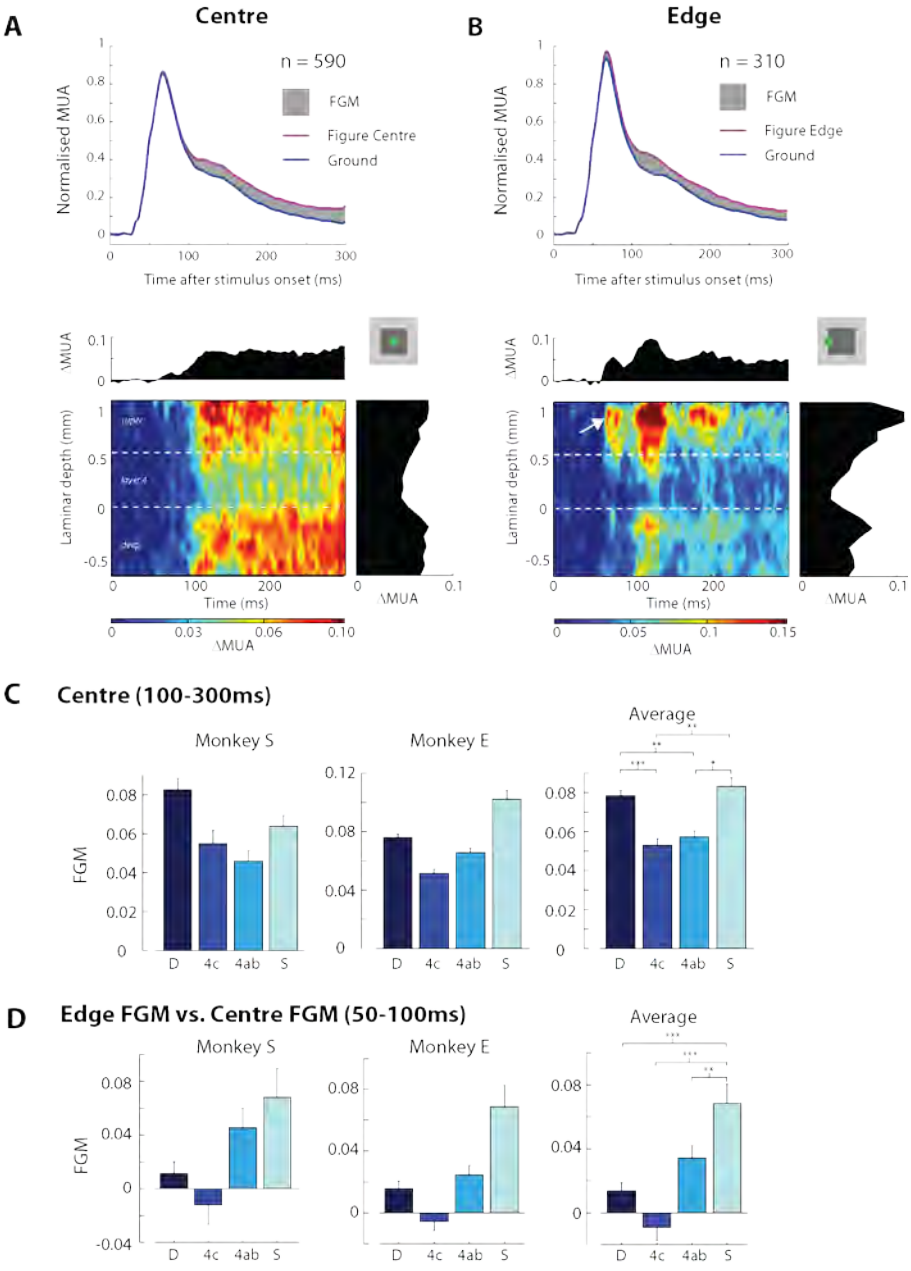

Figure 4. (**A**,**B**) FGM in the center of the figure (A) and at the edge (B) averaged across all penetrations. The upper plots show MUA averaged across layers. The shaded grey region shows the difference in activity evoked by the figure and background (FGM). *n*, number of recording sites. The lower plots show the laminar profile of FGM. The edge causes early FGM in the superficial layers (white arrow in B). (**C**) The average FGM evoked by the figure center in the four layer compartments.

Error-bars, s.e.m. Significant differences from post-hoc tests in the average across both animals are indicated by the asterisks, * = $p < 0.05$, ** = $p < 0.01$, *** = $p < 0.001$, after Bonferroni correction. (**D**) Difference between the level of FGM in the edge and center conditions during the early (50-100ms) time period. Note that the difference is strongest in the superficial layers and, to a lesser extent, layer 4ab. Number of recording sites in panels C and D have been specified in Figure S5.

To examine the synaptic inputs responsible for FGM we computed the difference between the CSD evoked by the figure and the background (**Figure 5A**). FGM was associated with an altered current flow in layer 5 and very superficially in putative layer 1 or upper layer 2 (black arrows in **Figure 5A**). There appears to be an additional current sink in the figure condition, but because **Figure 5A** is the result of a subtraction it is also possible that there was an additional current source in the background condition (**Figure S3A** shows the figure and ground conditions separately). Cluster-based statistics indicated that the differences between the figure and background CSD described above were all statistically significant (**Figure 5C**, **Supplementary Methods**). The latency of the CSD difference in layer 5 and layer 1/2 was approximately 100ms and it began at the same time as the modulation of the MUA response (see below and **Figure S4**). Thus, our results indicate that region-filling is caused by a putative excitatory input into layers 1, 2 and 5, the major targets of cortico-cortical feedback connections[10,11].

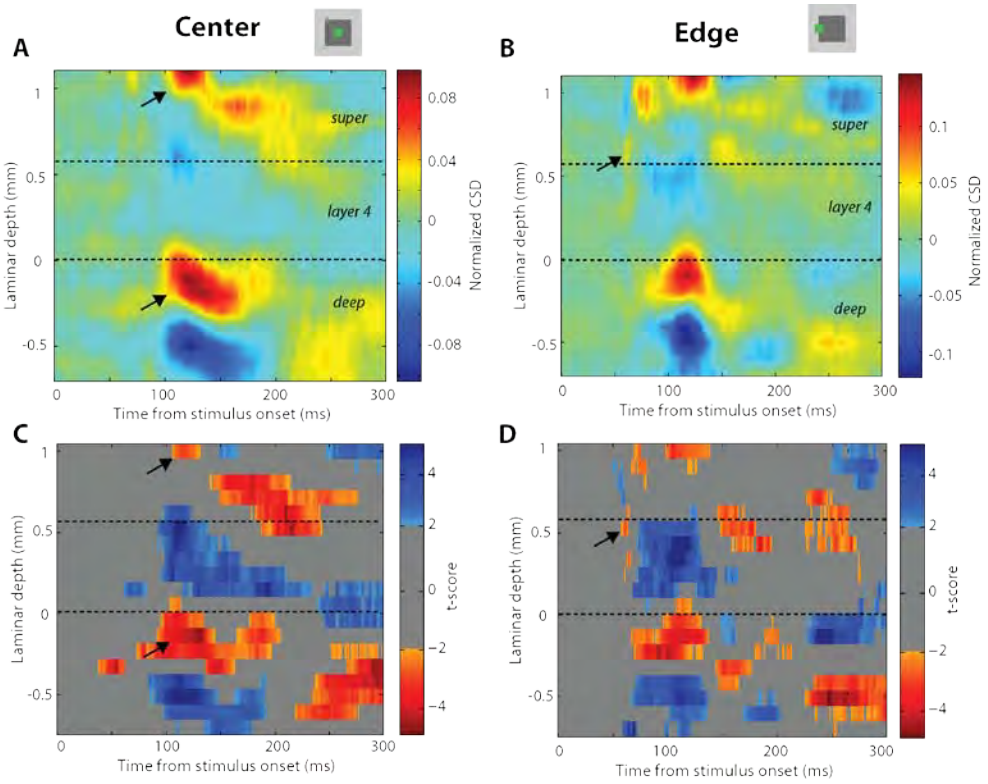

Figure 5 | (**A**) Difference in the normalized CSD evoked by the figure center and background. Warm colors show stronger sinks in the figure condition (and/or stronger sources in the ground condition) and cooler colors stronger sources. The black arrows indicate the first sinks that differentiate between figure and background at a latency of ~100ms in layer 5 and layer 1/2. (**B**) The difference in CSD between the figure edge and the background. The earliest, weak sink occurs in upper layer 4/superficial layers (black-arrow). This sink was consistent across penetrations (see **Figure S3B**,**C**). (**C**,**D**) A statistical map indicating the *t*-score of the difference between the CSD evoked by the figure center (C) or figure edge (D) and the background. Cluster-statistics were used to calculate the significance of sinks and sources. Non-significant clusters are not shown (grey area). **Figure S5** specifies the number of recording sites per cortical depth.

Laminar profile of FGM at boundaries between figure and background

The boundary between figure and background was defined by an orientation-discontinuity, which might be detected locally in V1. To examine the laminar profile of the boundary detection process, we placed the neurons' RF on the edge between figure and background

(**Figure 1D**). We observed significant FGM at the figure edge for both monkeys (mixed model: monkey S: n=16 penetrations, $F_{1,16.3}$=43.6, p<0.001; monkey E: n=12 penetrations, $F_{1,11.2}$=197.3, p<0.001). At first sight, the laminar profile of edge-FGM was similar to that of center-FGM (**Figure 4A**,**B**, **Figure S2**). However, the edge of the figure evoked an additional, early increase in neuronal activity that was strong in the superficial layers (arrow in **Figure 4B**) and somewhat weaker but significant in upper layer 4 (**Figure 4D**, **6C**). We tested almost all recording sites in the edge and the center condition so that we could compare the FGM for matched penetrations. FGM in an early analysis window (50-100ms) was significantly stronger when the RF was on the edge of the figure than when it fell on the center (mixed model, n=27 matched penetrations, $F_{1,26.6}$=6.3, p=0.02). This difference in FGM between the center and the edge varied between the laminar compartments ($F_{3,67.2}$=7.2, p<0.001) being significantly larger in the superficial layers than in the other layers (post-hoc tests, all p<0.05) (**Figure 4D**).

To further characterize edge FGM, we measured its latency using the same curve-fitting procedure used for the visual latency (**Figure 6A**,**B**). Across the population of recording sites the early detection of edges in upper layer 4 and the superficial layers caused the latency of edge-FGM to differ significantly between layers (mixed model, $F_{3,55.6}$=6.4, p=0.001). Edge FGM in the superficial layers begun on average at 71ms after stimulus onset (**Figure 6C**). In contrast, the latency of FGM in the center of the figure was very similar across the layer compartments (mixed model, F<1) beginning at 100ms. Center-FGM was significantly later than edge-FGM in the superficial layers and layer 4ab (paired t-test, both p<0.005). Edge FGM was accompanied by an extra current sink in putative upper layer 4/lower layer 3 (black arrow, **Figure 5B**,**D**) and a source in layer 2. Although these currents appear weak in **Figure 5B**, they were reproducible across penetrations and animals (**Figure S3B**,**C**) and occurred at a latency of 58ms, just prior to the edge-modulation of the MUA response (**Figure S4**), which suggests that they underlie the edge FGM. Thus, edge detection was associated with an early MUA increase in superficial layers and upper layer 4, caused by a characteristic pattern of synaptic input into these layers.

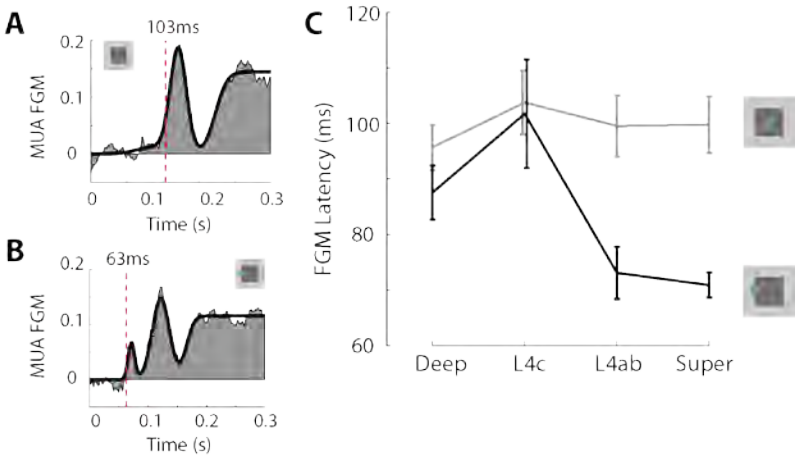

Figure 6 | (**A**) Time-course of FGM at an example recording site in the superficial layers with RF in the center of the figure. The black-line shows the function (the sum of two Gaussians and a cumulative Gaussian) used to estimate the latency of FGM (the same function was used to estimate visual latency). The latency was estimated as the time point at which the function reached 33% of its first maximum. (**B**) Example FGM time course at a superficial layer electrode with the RF on the edge. Note that the first Gaussian captures the early edge modulation. (**C**) The average latency across penetrations of the center-FGM (grey line) and edge-FGM (black line), calculated by fitting a curve to the FGM in each layer compartment for every penetration. Error-bars show s.e.m.

DISCUSSION

Here we have examined the roles of the different cortical layers within a single visual task that requires a number of different computations. The segregation of a figure from the background starts with the registration of features, is followed by the detection of feature discontinuities at the figure boundaries and completes with a region filling process that labels all figural image elements with enhanced activity[13,18]. We observed distinct contributions of the cortical layers to the successive processing phases, corresponding well to the anatomy of feedforward, horizontal and feedback connections (summarized in **Figure 7**).

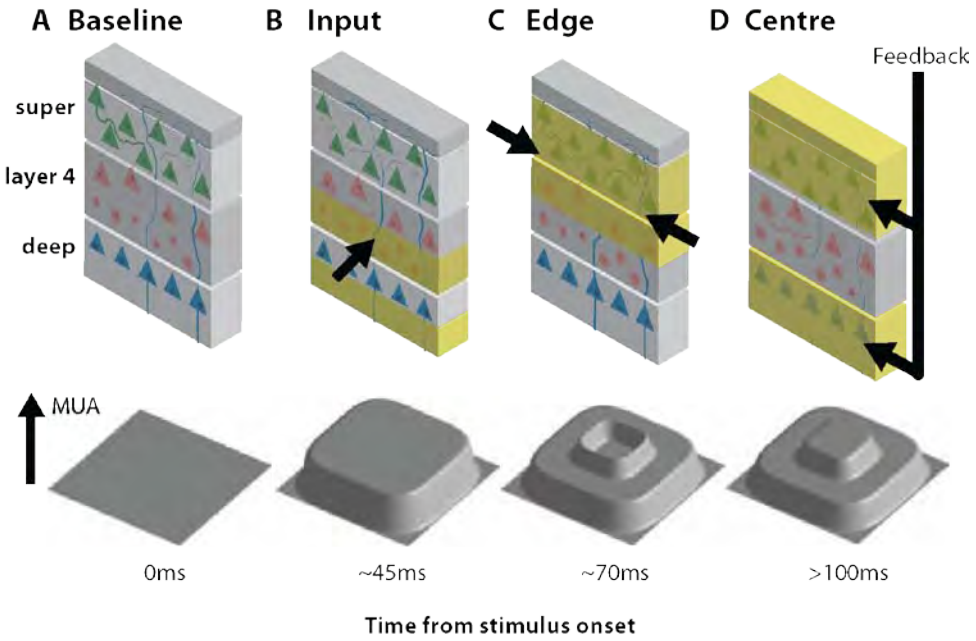

Figure 7 | The processes for figure-ground segregation have different time-courses and also specific laminar profiles within area V1 (**A**-**D**). The registration of features started in layers 4 and 6 (yellow region in B), the layers that receive input from the LGN, causing an early current sink in layer 4c (black arrow in B). Whereas the textures produced a transient response in layers 4 and 6, the response in the other layers was more sustained, especially in layers 2/3 and layer 5. After 65-70ms boundary detection occurred in the superficial layers (yellow regions in C) because image locations where the features changed caused stronger MUA activity than image locations with a homogeneous orientation. This edge-enhancement was accompanied by current sinks in upper layer 4 and the superficial layers, which receive input from horizontally projecting axons within V1 (black arrows in C). After approximately 100ms, FGM also occurred in the center of the figure (yellow region in D). Center-FGM was significantly weaker in layer 4 than in the deep and superficial layers and it coincided with additional current sinks in the upper superficial layers and in layer 5 (black arrows in D), known targets of cortico-cortical feedback connections.

Flow of visual information through the cortical column

The initial input from the LGN into layer 4c causes large sinks in the CSD and this input robustly drives responses in all cortical layers (**Figure 7B**). We observed that the latency of the visual response varies across the cortical laminae, in accordance with previous

studies[27,28]. The shortest latencies occurred in the input layers 4c and 6, with longer latencies in layer 5 and particularly in the superficial layers. This result is surprising as the anatomy of the micro-circuitry of V1 appears to predict shorter latencies in superficial layers than layer 5[2,29]. Long response latencies in the superficial layers has been observed previously[27] and their cause is unknown. One possibility is that neurons in the superficial layers must summate the input from layer 4 for a longer period before they reach spike-threshold. Layer 5 neurons receive a small amount of direct input from layer 4[30] onto their apical dendrites in layers 2/3[31], which is highly effective in driving the neuron to threshold[32] and may allow layer 5 neurons to fire at a shorter latency. We also observed a laminar difference in the balance between transient and sustained activity. Layers 4 and 6 had a strong transient response but their activity decreased after ~100ms. Visually driven activity was more sustained in the superficial layers and layer 5[33] and these layers may therefore play an important role in representing the stimulus at later times. These laminar differences contrast with a recent study in V1 of anesthetized monkeys[34] showing that the level of sustained activity evoked by moving gratings is relatively homogeneous across the layers. This discrepancy may have been caused by our use of stationary texture patterns, which cause stronger adaptation, or by a difference between the awake and anesthetized state.

Detection of feature discontinuities at figure edges

The figures used in this study were delimited by orientation-defined edges. Neurocomputational models have suggested that boundary detection is caused by inhibition between neurons tuned to the same orientation[20,21]. This "iso-orientation inhibition" suppresses activity in image regions with a homogeneous orientation and is weaker at edges, thus accounting for edge-FGM (**Figure 1B**)[35]. It has also been implicated in orientation pop-out detection in V1[36,37].

We observed early enhancements in spiking activity at orientation-defined edges within 10-15ms after the visual response in the superficial layers and upper layer 4 (**Figure 7C**). This finding is in line with a recent study demonstrating that iso-orientation inhibition is most pronounced in these layers[38] and the latency is also in good agreement with previous studies[35,36,39]. Horizontal connections within V1 are a likely source of the required orientation-tuned inhibition. Many pyramidal neurons in V1 have axonal arbors that

project horizontally over large distances[8,40,41] and that are particularly prominent in upper layer 4 and the superficial layers[9] although these connections are also present in the other layers. These horizontal connections preferentially link cortical columns tuned to the same orientation and they could therefore provide the required iso-orientation inhibition[42]. In accordance with a contribution of the horizontal connections, the earliest difference in current flow between the edge and center-FGM was in upper layer 4 and the superficial layers (**Figure 5B**, **Figure S3B**,**C**)[8,40]. An important role for local processing within V1 for boundary detection is also supported by a study demonstrating that blocking V2 did not reduce pop-out effects in V1[43] and by a recent study showing that boundary detection depends little on the animal's attentional state[18]. Our results combined with these previous findings support the idea that texture-defined boundaries are first detected locally in V1 through iso-orientation inhibition.

FGM at the center of the figure

Iso-orientation inhibition for boundary detection would cause suppression of neuronal activity in the center of the figure, where image elements are surrounded by the same orientation. We have previously postulated a complementary region-filling process where neurons in higher areas that register the figural orientation provide feedback to excite V1 neurons coding the same orientation[16,44] (**Figure 1C**). This "iso-orientation excitation" feedback mechanism can explain why FGM in V1 labels all image elements of the figure with enhanced activity at a longer delay and is supported by a number of previous studies. FGM in V1 in the center of the figure is abolished if higher areas are lesioned[45] or if the monkey is anesthetized[24], and it is reduced if the animal directs attention away from the figure[18]. FGM in the figure center is also reduced if the monkey fails to detect the figure[23]. The present results provide further support for this view. Center-FGM was strongest in the superficial and deep layers (**Figure 7D**), which receive feedback from higher areas, and it was weaker in the input layer 4 (**Figure 4A**,**C**). Moreover, the center-FGM coincided with strong current sinks in layers 1,2 and 5 (**Figure 5A**), which are prime targets of feedback connections to area V1[9,10,46]. The areas that provide these feedback signals cannot be determined from our data, but the most likely candidates are V2 and ventral stream areas (e.g. V4) where neurons are selective for orientation and send feedback connections to the

deep and superficial layers of V1[9,10,12,46]. The pattern of feedback targets we observe is less consistent with a contribution from dorsal stream areas such as MT which target layer 4B[47].

The influence of figure-ground organization on spiking activity was more widespread than the CSD sinks. We note, however, that these sinks may also reflect input into the dendrites of cells with somas located in different cortical layers. Furthermore, FGM can be passed around the cortical micro-circuitry through the many interlaminar connections[1,2]. Layer 4c neurons have only few dendrites extending into layers 1, 2 and 5[2], which might cause them to receive little feedback from higher areas and this could explain the weak FGM in this layer. However, it is also conceivable that the weaker FGM in layer 4 is the result of the weaker level of sustained activity. Previous studies suggested that feedback effects are particularly pronounced for neurons that are well driven by a stimulus and weaker for neurons that are not[48,49]. Such a multiplicative interaction between feedback effects and visually driven activity could be conveyed by NMDA-receptor mediated feedback[50]. NMDA-receptors only pass current if the membrane is depolarized, which could explain why FGM is strongest in layers with a high level of sustained activity.

In conclusion, the present results reveal distinct laminar patterns of neuronal activity in V1 for the visual response, the detection of boundaries and the labeling of figural image regions with enhanced neuronal activity. Future studies can now determine whether the laminar patterns observed in the present task comprise a canonical pattern for tasks that require feedforward activation, combined with local intra-areal processing and feedback from higher visual areas.

METHODS

All procedures complied with the NIH Guide for Care and Use of Laboratory Animals, and were approved by the institutional animal care and use committee of the Royal Netherlands Academy of Arts and Sciences. We recorded from 2 adult macaque monkeys (monkeys S and E) using laminar electrodes (Figure 2A). The monkeys were implanted with a headpost and recording chamber as described previously[50]. We targeted the operculum of area V1 (visualized using ultrasonic imaging, Figure S1B), as well as from the calcarine portion of V1 by inserting the electrode deeper into the cortex (Figure S1D).

We recorded the spiking responses of neurons as the envelope of the multi-unit activity (MUA) (**Supplementary Methods**). The local field potential (LFP) was recorded by filtering the raw signal from the electrodes (digitized at 24.4kHz) using a low-pass filter (2nd order Butterworth filter, corner frequency 200Hz), and sampling it at 763Hz. The current-source density was calculated as:

$$CSD(x) = -\sigma \cdot \frac{\varphi(x-h) - 2\varphi(x) + \varphi(x+h)}{h^2}$$

φ is the voltage (in μV), x is the point at which the CSD is calculated, h is the spacing of recording sites for the computation (here 200μm) and σ is tissue conductivity (we used 0.4 $S.m^{-1}$).

The MUA response at each recording site was normalized by subtracting the spontaneous activity, measured from -150ms to 0ms before stimulus onset, and by dividing the response by the peak response (maximum in a 50-90ms window after stimulus onset) in the catch-trial condition. FGM was calculated as the difference between normalized figure and ground MUA responses in a time window from 100-300ms after stimulus onset. We normalized the CSD of each penetration by dividing by the maximum absolute value of the CSD across layers during the peak period (50-90ms) in the catch-trial condition.

To generate average MUAs and CSDs per electrode depth we aligned the depth of the different penetrations using the CSD (**Supplementary Methods**). The realigned, normalized CSD data and normalized MUA signals were then averaged across penetrations.

We assigned recording sites to one of four laminar compartments based on their distance from the layer 4c/layer 5 boundary. The assignments were made with reference to previous anatomical studies[3,4,26] which measured the thickness of the cortical layers in V1. These assignments come with an inherent degree of uncertainty as histological measurements of layer thicknesses vary between studies, aside from the CSD reversal at the boundary between layer 4 and layer 5 that is reliable[25]. The compartment labels we use in this paper should therefore be taken as guides and do not imply a one-to-one correspondence with histological data. Recording sites between 0.7 and 0.1mm below the 4c/5-boundary were assigned to the deep layers, sites between 0 and 0.2mm above the boundary were assigned to layer 4c, sites between 0.3 and 0.5mm were assigned to upper layer 4 (which we refer to as layer 4ab) and sites more than 0.5mm above the boundary were assigned to the superficial layers. Recording sites more than 0.7mm below or more than 1.1mm above the boundary were removed from the analysis because we did not obtain sufficient data from these very deep and very shallow locations (14.9% of all recording sites).

References

1. Douglas,R.J. & Martin,K.A. Neuronal circuits of the neocortex. *Annu. Rev. Neurosci.* **27**, 419-451 (2004).
2. Callaway,E.M. Local circuits in primary visual cortex of the macaque monkey. *Annu. Rev. Neurosci.* **21**, 47-74 (1998).
3. Lund,J.S. Anatomical organization of macaque monkey striate visual cortex. *Annu. Rev. Neurosci.* **11**, 253-288 (1988).
4. Henry,G.H., Harvey,A.R., & Lund,J.S. The afferent connections and laminar distribution of cells in the cat striate cortex. *J. Comp Neurol.* **187**, 725-744 (1979).
5. Larkum,M. A cellular mechanism for cortical associations: an organizing principle for the cerebral cortex. *Trends Neurosci.* **36**, 141-151 (2013).
6. Blasdel,G.G. & Lund,J.S. Termination of afferent axons in macaque striate cortex. *J. Neurosci.* **3**, 1389-1413 (1983).
7. Hubel,D.H. & Wiesel,T.N. Laminar and columnar distribution of geniculo-cortical fibers in the macaque monkey. *J. Comp Neurol.* **146**, 421-450 (1972).
8. Gilbert,C.D. & Wiesel,T.N. Clustered intrinsic connections in cat visual cortex. *J. Neurosci.* **3**, 1116-1133 (1983).

9. Rockland,K.S. & Pandya,D.N. Laminar origins and terminations of cortical connections of the occipital lobe in the rhesus monkey. *Brain Res.* **179**, 3-20 (1979).

10. Rockland,K.S. & Virga,A. Terminal arbors of individual "feedback" axons projecting from area V2 to V1 in the macaque monkey: a study using immunohistochemistry of anterogradely transported Phaseolus vulgaris-leucoagglutinin. *J. Comp Neurol.* **285**, 54-72 (1989).

11. Anderson,J.C. & Martin,K.A. The synaptic connections between cortical areas V1 and V2 in macaque monkey. *J. Neurosci.* **29**, 11283-11293 (2009).

12. Felleman,D.J. & Van Essen,D.C. Distributed hierarchical processing in the primate cerebral cortex. *Cereb. Cortex* **1**, 1-47 (1991).

13. Lamme,V.A. & Roelfsema,P.R. The distinct modes of vision offered by feedforward and recurrent processing. *Trends Neurosci.* **23**, 571-579 (2000).

14. Mumford,D., Kosslyn,S.M., Hillger,L.A., & Herrnstein,R.J. Discriminating figure from ground: the role of edge detection and region growing. *Proc. Natl. Acad. Sci. U. S. A* **84**, 7354-7358 (1987).

15. Wolfson,S.S. & Landy,M.S. Examining edge- and region-based texture analysis mechanisms. *Vision Res.* **38**, 439-446 (1998).

16. Roelfsema,P.R., Lamme,V.A., Spekreijse,H., & Bosch,H. Figure-ground segregation in a recurrent network architecture. *J. Cogn Neurosci.* **14**, 525-537 (2002).

17. Grossberg,S. & Mingolla,E. Neural dynamics of form perception: boundary completion, illusory figures, and neon color spreading. *Psychol. Rev.* **92**, 173-211 (1985).

18. Poort,J. *et al.* The role of attention in figure-ground segregation in areas v1 and v4 of the visual cortex. *Neuron* **75**, 143-156 (2012).

19. Ferster,D. & Miller,K.D. Neural mechanisms of orientation selectivity in the visual cortex. *Annu. Rev. Neurosci.* **23**, 441-471 (2000).

20. Bhatt,R., Carpenter,G.A., & Grossberg,S. Texture segregation by visual cortex: perceptual grouping, attention, and learning. *Vision Res.* **47**, 3173-3211 (2007).

21. Li,Z. Visual segmentation by contextual influences via intra-cortical interactions in the primary visual cortex. *Network.* **10**, 187-212 (1999).

22. Lamme,V.A. The neurophysiology of figure-ground segregation in primary visual cortex. *J. Neurosci.* **15**, 1605-1615 (1995).

23. Supèr,H., Spekreijse,H., & Lamme,V.A. Two distinct modes of sensory processing observed in monkey primary visual cortex (V1). *Nature Neuroscience* **4**, 304-310 (2001).

24. Lamme,V.A., Zipser,K., & Spekreijse,H. Figure-ground activity in primary visual cortex is suppressed by anesthesia. *Proc. Natl. Acad. Sci. U. S. A* **95**, 3263-3268 (1998).

25. Mitzdorf,U. Current source-density method and application in cat cerebral cortex: investigation of evoked potentials and EEG phenomena. *Physiol Rev.* **65**, 37-100 (1985).

26. Lund,J.S. Organization of neurons in the visual cortex, area 17, of the monkey (Macaca mulatta). *J. Comp Neurol.* **147**, 455-496 (1973).

27. Maunsell,J.H. & Gibson,J.R. Visual response latencies in striate cortex of the macaque monkey. *J. Neurophysiol.* **68**, 1332-1344 (1992).

28. Nowak,L.G., Munk,M.H., Girard,P., & Bullier,J. Visual latencies in areas V1 and V2 of the macaque monkey. *Vis. Neurosci.* **12**, 371-384 (1995).

29. Gilbert,C.D. Microcircuitry of the visual cortex. *Annu. Rev. Neurosci.* **6**, 217-247 (1983).

30. Katz,L.C., Gilbert,C.D., & Wiesel,T.N. Local circuits and ocular dominance columns in monkey striate cortex. *J. Neurosci.* **9**, 1389-1399 (1989).

31. Binzegger,T., Douglas,R.J., & Martin,K.A. A quantitative map of the circuit of cat primary visual cortex. *J. Neurosci.* **24**, 8441-8453 (2004).

32. Larkum,M.E., Senn,W., & Luscher,H.R. Top-down dendritic input increases the gain of layer 5 pyramidal neurons. *Cereb. Cortex* **14**, 1059-1070 (2004).

33. Maier,A., Aura,C.J., & Leopold,D.A. Infragranular sources of sustained local field potential responses in macaque primary visual cortex. *J. Neurosci.* **31**, 1971-1980 (2011).

34. Xing,D., Yeh,C.I., Burns,S., & Shapley,R.M. Laminar analysis of visually evoked activity in the primary visual cortex. *Proc. Natl. Acad. Sci. U. S. A* **109**, 13871-13876 (2012).

35. Nothdurft,H.C., Gallant,J.L., & Van Essen,D.C. Response profiles to texture border patterns in area V1. *Vis. Neurosci.* **17**, 421-436 (2000).

36. Knierim,J.J. & Van Essen,D.C. Neuronal responses to static texture patterns in area V1 of the alert macaque monkey. *J. Neurophysiol.* **67**, 961-980 (1992).

37. Nothdurft,H.C., Gallant,J.L., & Van Essen,D.C. Response modulation by texture surround in primate area V1: correlates of "popout" under anesthesia. *Vis. Neurosci.* **16**, 15-34 (1999).

38. Henry,C.A., Joshi,S., Xing,D., Shapley,R.M., & Hawken,M.J. Functional characterization of the extraclassical receptive field in macaque v1: contrast, orientation, and temporal dynamics. *J. Neurosci.* **33**, 6230-6242 (2013).

39. Lamme,V.A., Rodriguez-Rodriguez,V., & Spekreijse,H. Separate processing dynamics for texture elements, boundaries and surfaces in primary visual cortex of the macaque monkey. *Cereb. Cortex* **9**, 406-413 (1999).

40. Hirsch,J.A. & Gilbert,C.D. Synaptic physiology of horizontal connections in the cat's visual cortex. *J. Neurosci.* **11**, 1800-1809 (1991).

41. Gilbert,C.D. & Wiesel,T.N. Morphology and intracortical projections of functionally characterised neurones in the cat visual cortex. *Nature* **280**, 120-125 (1979).

42. Malach,R., Amir,Y., Harel,M., & Grinvald,A. Relationship between intrinsic connections and functional architecture revealed by optical imaging and in vivo targeted biocytin injections in primate striate cortex. *Proc. Natl. Acad. Sci. U. S. A* **90**, 10469-10473 (1993).

43. Hupe,J.M., James,A.C., Girard,P., & Bullier,J. Response modulations by static texture surround in area V1 of the macaque monkey do not depend on feedback connections from V2. *J. Neurophysiol.* **85**, 146-163 (2001).

44. Craft,E., Schutze,H., Niebur,E., & von der Heydt,R. A neural model of figure-ground organization. *J. Neurophysiol.* **97**, 4310-4326 (2007).

45. Lamme,V.A., Supèr,H., & Spekreijse,H. Feedforward, horizontal, and feedback processing in the visual cortex. *Curr. Opin. Neurobiol.* **8**, 529-535 (1998).

46. Rockland,K.S., Saleem,K.S., & Tanaka,K. Divergent feedback connections from areas V4 and TEO in the macaque. *Vis. Neurosci.* **11**, 579-600 (1994).

47. Rockland,K.S. & Knutson,T. Feedback connections from area MT of the squirrel monkey to areas V1 and V2. *J. Comp Neurol.* **425**, 345-368 (2000).

48. Moore,T. & Armstrong,K.M. Selective gating of visual signals by microstimulation of frontal cortex. *Nature* **421**, 370-373 (2003).

49. Ekstrom,L.B., Roelfsema,P.R., Arsenault,J.T., Bonmassar,G., & Vanduffel,W. Bottom-up dependent gating of frontal signals in early visual cortex. *Science* **321**, 414-417 (2008).

50. Self,M.W., Kooijmans,R.N., Super,H., Lamme,V.A., & Roelfsema,P.R. Different glutamate receptors convey feedforward and recurrent processing in macaque V1. *Proc. Natl. Acad. Sci. U. S. A* **109**, 11031-11036 (2012).

SUPPLEMENTARY INFORMATION

Supplementary Results

Influence of orientation tuning on FGM

We examined whether FGM depended on the neurons' orientation tuning. We first calculated an orientation index based upon the response of the multi-units to the texture stimuli (OTI):

$$OTI = \frac{CTH_{45} - CTH_{135}}{CTH_{45} + CTH_{135}}$$

Where CTH_{45} was the average MUA response during the catch trial condition (0-300ms) with a 45° texture and CTH_{135} was the response to the 135° texture. We considered a multi-unit recording site to be tuned to orientation if this index was greater than 0.1 (prefers 45°) or less than -0.1 (prefers 135°). We then examined how these recording sites responded to figure and ground textures which either matched the preferred orientation of the cell or not. We carried out a 2x2 repeated measures ANOVA with factors context (figure or ground) and orientation of the texture in the RF (preferred or non-preferred). As expected, we found significant main-effects of context and orientation (Orientation: $F_{1,1045} = 1463$, $p<10^{-6}$. Context: $F_{1,1045}=2640$, $p<10^{-6}$), however these two factors did not interact ($F_{1,1045} = 2.12$, $p = 0.15$). We also examined if FGM depended on the strength of the orientation-tuning by correlating the OTI with FGM-strength, but we found no significant correlation ($r^2 = 0.0005$, $p > 0.5$). Thus, the strength of FGM does not depend strongly on the orientation tuning of the recording sites.

Eye movement analysis

During this experiment the animals fixated on a fixation dot of 0.3° in diameter inside a circular window of 1° diameter. We performed an analysis to control for possible differences in fixational eye-position within this window between the figure and ground conditions. We performed a stratification analysis as described previously[1]. For each penetration we binned the mean horizontal and vertical eye positions from each trial (bin size 0.25° x 0.25°). We equated the number of trials in each bin across conditions (figure and ground) by randomly removing surplus trials in one of the conditions, thus ensuring that the eye-position distribution was similar across the different conditions. We then reanalyzed the data using the remaining trials. After stratification we still found significant differences in FGM in the centre condition across layer compartments ($F_{3,81.3}$ = 6.5, p = 0.001). FGM was weakest in layer 4c (FGM in superficial layers and deep layers was significantly stronger than in layer 4c, post-hoc test, both $p < 0.01$, Bonferroni corrected). After stratification, we also replicated the laminar profile of FGM if the RF fell on the edge, with significant differences between the layer compartments (window from 50-100ms, $F_{3,66.4}$= 4.5, p = 0.006) . Thus, the laminar differences between the centre and edge FGM were not caused by variations in eye-position.

Supplementary Methods

Stimuli and task

After 300ms of fixation, we presented a figure-ground stimulus that was comprised of an oriented texture with a square figure (4°x4°) of the orthogonal orientation (**Figure 1A**). The textures consisted of randomly placed black line elements (45° or 135°) on a white background. We made four different textures for each recording session (two of each orientation) and these were presented in a counter-balanced order to ensure that precisely the same line-elements were present in the RF for each condition. After another 300ms, the fixation dot was extinguished and the monkeys were rewarded for making an eye movement to the figure. There were three possible figure locations. One was centered on the neurons' RF (figure condition) and the other two were at an angle of 120° (ground conditions, **Figure 1E**). Twenty-five percent of trials were catch-trials without a figure and

on these trials the monkey was rewarded for maintaining fixation. Within a block of trials (between 200-500 correct trials) the figure was always presented at the same eccentricity. In different blocks we varied the eccentricity of the figure to create the 'Center' and 'Edge' conditions (**Figure 1D**).

Aligning penetrations based on CSD analysis

To align different penetrations in depth we used current source density (CSD) analysis. A full-screen, full-contrast checkerboard was presented (duration 250ms, check size 0.3°) while the monkey fixated. The sudden appearance of the checkerboard produced a characteristic and highly repeatable laminar CSD pattern (Fig. S1A,C) with a clear reversal from current sources in the deep layers to a current sink in layer 4c. We identified this reversal point online for each penetration and placed the electrode so that the reversal was as close as possible to the 8th contact from the tip to ensure coverage of all cortical laminae. We also used this reversal point to align all our recordings in depth at the data analysis stage. Taking one penetration as a reference, we used an automated procedure to shift the other penetrations to minimize the sum-of-squares errors between the CSD of the reference and target penetration between 50 and 100ms after stimulus onset (as this time period gives the most reliable CSD profiles).

Receptive-field measurement

We measured the extent of the multi-unit receptive-field (RF) by determining the onset and offset of the response at each recording site evoked by a moving bar. The RF dimensions were measured precisely by sweeping the bar in the four cardinal directions while the monkey maintained fixation. We measured the average response to a minimum of eight repeats of each direction, and fitted a Gaussian curve to the responses (adjusting mean and standard deviation). The onset and offset of the response were taken as two standard deviations on either side of the mean. The RF border was taken to be the average between the onset position of one direction averaged with the offset position from the opposite direction, a procedure which automatically compensates for the delay between the stimulus and the onset of the neural response[2]. The RF size varied with laminar compartment

(**Figure S1E**) (Mixed model, $F_{3,118.7}$= 46.2, $p < 0.001$). The smallest RFs were found in layer 4c in accordance with some[3,4] but not all[5,6] previous studies, whereas the RFs in the deepest layers were particularly large, as has been reported previously[5].

Orientation tuning indices (OTIs) were calculated as the ratio between the average response to the preferred orientation of the moving light bar and the response to the least-preferred orientation. The strength of orientation tuning of the multi-unit activity also varied significantly across the cortical layers (**Figure S1E**) (Mixed model, $F_{3,120.1} = 8.9$, $p < 0.001$) being weakest in layer 4c, as has been reported previously for single units[4,6-9].

Multi-unit envelope

To study spiking activity we used a multi-unit recording technique that was introduced by Legatt et al.[10], and was used in several studies from other labs[11,12]. The method measures the spiking of neurons in the vicinity of the electrodes as the amplitude of the envelope of the multi-unit signal (MUA)[2]. The signal from the electrode is first filtered between 500Hz and 5kHz to extract high-frequency (spiking) activity, rectified (negative values become positive) and low-pass filtered at 200Hz to produce MUA. MUA provides an instantaneous measure of the number and amplitude of spikes in the vicinity of the electrode and its measurement does not require the setting of an (arbitrary) spike-detection threshold. We have previously compared responses obtained using MUA with both thresholded multi-unit data and single-unit data and found the responses to be very similar[2,13]. Furthermore, we observed that the MUA signal contains contributions from spiking neurons within ~150µm of the contact point[13], which corresponds to the distance over which the same V1 cell can be recorded with single-unit recording[14,15]. The limited distance over which cells are recorded with MUA is supported by the well-localized receptive fields with a size corresponding to the composite receptive field of a few V1 single units (**Figure S1D**).

MUA Statistics

Statistics assessing the level of FGM for the example penetrations were generated using the average activity on each trial from a laminar compartment as the dependent variable. These

values were entered into a two-way independent ANOVA with the factors being condition (figure, ground) and compartment (deep, layer 4c, layer 4ab, superficial).

We carried out our population statistics at the level of laminar compartments. Specifically, data from individual recording sites within a laminar compartment of the same penetration were first averaged and these averages entered into the statistical tests. We corrected for the fact that data from electrode sites from the same penetration are correlated (i.e. not independent) with a hierarchical mixed linear regression model (referred to as a 'mixed model' in the text) with one fixed effect (laminar compartment, 4 levels) and one random effect (penetration). The model contained an intercept term for the random effect and was fit using restricted maximum likelihood in SPSS (IBM, vs. 20). This approach produces identical results to a standard repeated-measures ANOVA if there is no missing data. However, in some penetrations there were insufficient numbers of electrode sites passing our exclusion criteria (or in the case of latency analyses, insufficient sites generating a measurable latency) to generate a compartment average. In these cases the mixed model approach is more powerful. The same mixed model approach was used for testing figure-ground modulation, visual latency, latency of modulation and the level of sustained activity. For *post-hoc* testing a 95% confidence interval was constructed around the estimated marginal means and the Bonferroni correction for multiple comparisons was applied.

Latency Analysis

Our method to calculate the latency of the visual response was based on a previously described method[16]. The latency of both the visual response and FGM were calculated by fitting a function to the data. We fitted the visual response, *y*, at each time-point, *t*, with the sum of two Gaussians and a cumulative Gaussian using non-linear least-squares fitting (MATLAB, Mathworks Inc.):

$$y(t) = \frac{G_1 e^{-0.5\left(\frac{t-\mu_1}{\sigma_1}\right)^2}}{\sqrt{2\pi}\sigma_1} + \frac{G_2 e^{-0.5\left(\frac{t-\mu_2}{\sigma_2}\right)^2}}{\sqrt{2\pi}\sigma_2} + 0.5G_3\left[1 + erf\left(\frac{t-\mu_3}{\sqrt{2{\sigma_3}^2}}\right)\right]$$

Free parameters of the fit are the amplitudes ($G_{1\text{-}3}$), means ($\mu_{1\text{-}3}$) and standard deviations ($\sigma_{1\text{-}3}$) of the Gaussians, and *erf* stands for the error function.

To calculate the latency of FGM we fitted the same function to the difference between the responses evoked by the figure and the background, separately for every layer compartment. The method resulted in good fits of both the visual response (median adjusted r^2 = 0.94) and FGM (median adjusted r^2 = 0.73). We (arbitrarily) defined the latency as the time point at which the fitted curve reached 33% of the maximum of the earliest Gaussian.

An important advantage of this technique is that the latency does not strongly depend on the signal-to-noise ratio of the response or the number of trials (in contrast, latency measurements based on the first of a number of significant time bins tend to yield shorter latencies when more data has been acquired). Moreover, we could use the same curve to fit the visually driven response, the centre FGM and the edge FGM so that these latencies could be directly compared.

Number of penetrations and exclusion criteria

We recorded from a total of 43 penetrations in which we acquired data from the center position (29 from monkey S and 14 from monkey E) yielding a total of 590 recording sites (370 in monkey S and 220 in monkey E) after applying our exclusion criteria (See below). We also recorded data from the edge of the figure in 16 penetrations in monkey S (154 recording sites) and 12 penetrations in monkey E (156 sites). For all of the penetrations in which we recorded data from the edge condition we also recorded data from the center condition, with the exception of one penetration in which we only recorded edge data yielding 27 matched penetrations for the center and edge data. We included eight penetrations from Monkey S with a laminar probe containing a fluid-line for the injections of drugs. The effects of the drug injections were reported elsewhere[13], whereas the data included here came from the pre-injection period. The number of included of recording sites per layer per condition per monkey is reported in **Figure S5**.

We removed recording sites with a signal-to-noise ratio (SNR) of less than 1. SNR was calculated as the difference between the evoked visual response (in a window from 0-300ms) and the spontaneous activity during the pre-stimulus period (-150-0ms) normalized to the standard deviation across trials of activity in the pre-stimulus period. We also

removed recordings sites for which the RF was not well defined or if the RF was larger than 2.5°. For the analysis of FGM in the center of the figure we did not evaluate activity at recording sites where the RF edge came within 0.2° of the figure edge. For the analysis of edge FGM, we only included recording sites with an RF which included the figure edge. The exclusion criteria together (too high/low cortical depth, low signal-to-noise ratio, RF too large, not well defined or at wrong location) resulted in the exclusion of 41.3% of all potential MUA-recording sites, but the CSD at these sites could generally be used.

CSD cluster statistics

The statistical analysis of the significance of differences in the CSD between figure and background was based on a non-parametric cluster analysis[17]. First, we calculated *t*-scores for the difference in the CSD evoked by the figure and the background across penetrations for each time-sample/depth pair, thus producing a 2-dimensional array of *t*-scores (time-samples x depth). The *t*-map was thresholded, setting non-significant *t*-values ($p < 0.05$) to zero (**Figure 5C**,**D**). We clustered adjacent *t*-scores with the same sign and calculated a cluster statistic; the sum of the absolute *t*-scores per cluster. To determine the significance of these clusters, we carried out a bootstrapping analysis. We randomly shuffled the data (mixing trials from the figure and ground condition) to produce 1000 CSD difference maps (see below for details) and subjected them to the same procedures as the real data. We took the maximum of the sum of the *t*-values in each cluster as the bootstrap statistic and generated a shuffled distribution of this statistic. We then compared the calculated *t*-values from each cluster of the actual data to the shuffled distribution. Clusters were considered significant if their absolute *t*-value fell above the 95th percentile of the shuffled distribution. We also applied a size-threshold, excluding clusters that were smaller than 10 time-sample/depth pairs. The advantage of this statistic is that it uses both the magnitude of the *t*-scores within a cluster and also the size of the cluster so that is sensitive to strong sinks and sources and also to weak, but spatially extended, sinks and sources.

The bootstrapping procedure was as follows:

1) For each electrode site of a penetration, the LFP from the figure and ground trials were collected and placed into one large distribution, with one entry per trial.

2) Two reshuffled conditions ($Figure_r$ and $Ground_r$) were created for every penetration by sampling (with replacement) from this pooled distribution of trials. The same number of trials per condition were drawn as were present in the original data set. The average LFP for each condition was then calculated from the reshuffled trials and stored for each electrode site in the penetration.

3) The LFP maps were converted into CSD-profiles using the equation described in the Experimental Procedures. The resulting CSD maps were converted into a CSD difference map by subtracting the CSD map of the simulated ground condition from that of the simulated figure condition.

4) Steps 1-3 were repeated for each penetration and the CSD difference maps of different penetrations were aligned in depth.

5) One-sample t-tests were performed for each time/depth sample (229 time-samples [0-300ms] x 19 depths). The resulting t-maps were thresholded and non-significant ($p < 0.05$) samples were set to zero.

6) The thresholded t-maps were clustered. Negative and positive t-scores were separately clustered and a cluster-statistic, the sum of the absolute t-values in the cluster, was calculated for each cluster. The maximum of the summed cluster values was then taken as the bootstrap statistic.

7) Steps 1-6 were repeated 1000 times to produce a distribution of cluster statistics.

8) The cluster statistics from the original data were compared to the cluster-distribution.

Supplementary Figures

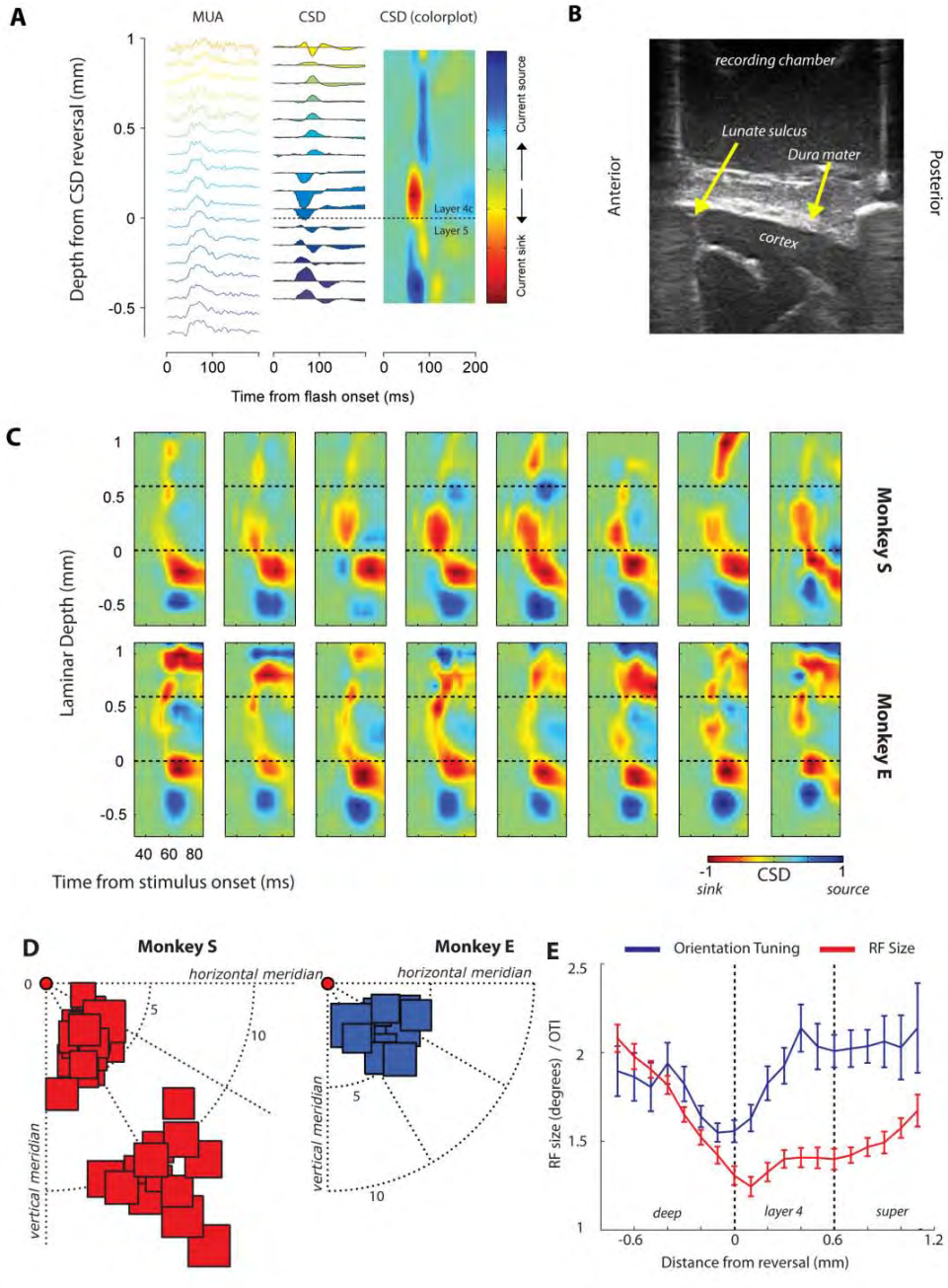

Figure S1 | (**A**) An example penetration showing the MUA (left graph) and CSD (middle and right graph) triggered by the sudden appearance of a full-screen, full-contrast checkerboard stimulus. Simultaneous responses from 17 contacts are shown stacked (the other contacts were excluded due to low signal to noise ratio). In the leftmost columns blue colors indicate deeper channels and green/yellow colors indicate shallow channels. In the rightmost column the red colors show current sinks and the blue colors current sources. The CSD shows a reversal from a current source in the deep layers to a current sink in layer 4c, the boundary is marked by the dashed line. (**B**) An ultrasound image taken through the recording chamber showing the operculum of V1. The lunate sulcus is visible at the anterior side of the image and all penetrations were targeted posterior to the lunate. The cortical surface is relatively flat here allowing penetrations orthogonal to the cortical layers. This is important for achieving accurate current source density profiles. (**C**) Example current-source density profiles from 8 penetrations in monkey S (top row) and monkey E (bottom row). These profiles show the CSD pattern produced by the onset of the full-screen texture (catch-trial condition). (**D**) Location of RFs from monkey S (red, left graph) from opercular (central RFs) and calcarine V1 recordings (eccentric RFs) and monkey E (blue, right graph) from recordings in the operculum. (**E**) The average RF size (square-root of the RF area, red line) and orientation tuning index (OTI) as a function of cortical depth. Lower OTIs indicate weaker orientation tuning.

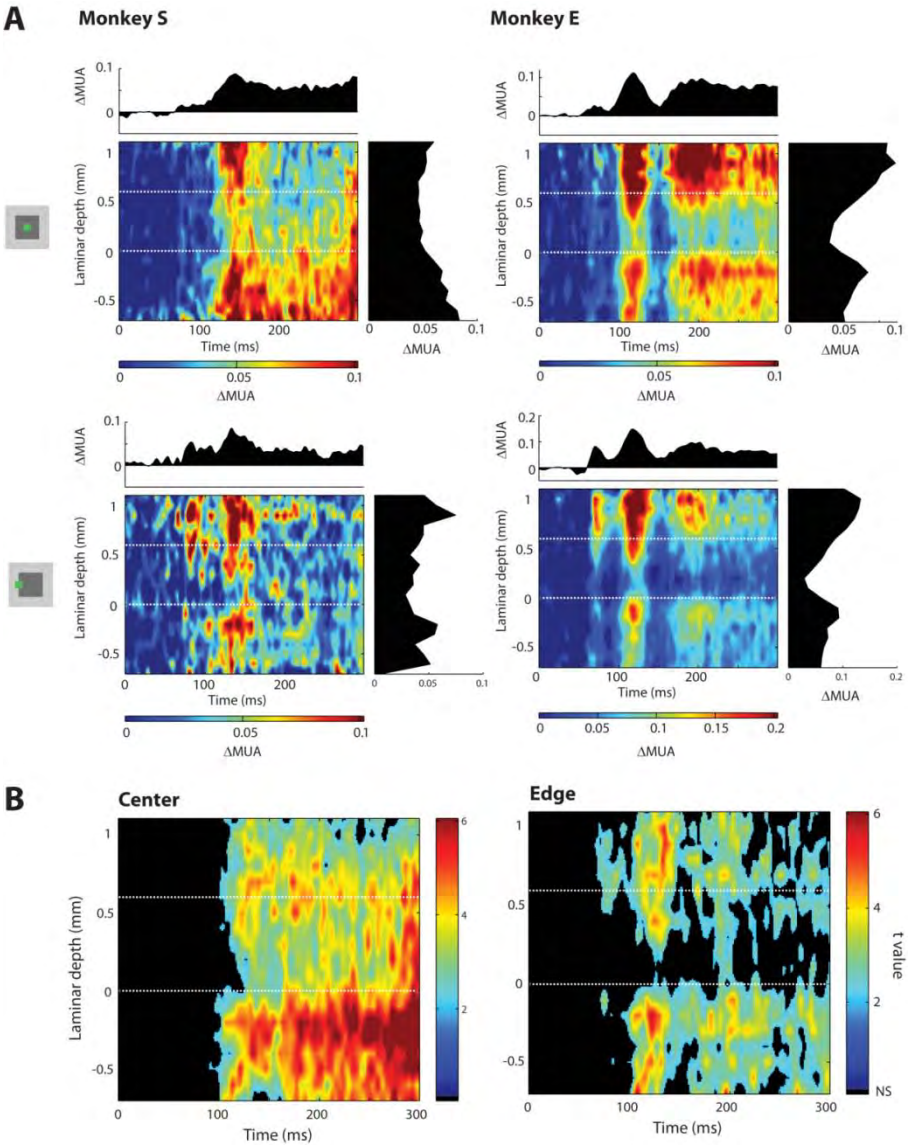

Figure S2 | (**A**) MUA data from the individual animals in the same format as Figure 4A,B. Both the temporal and laminar patterns of FGM were similar. One difference was a lower level of FGM in the superficial layers of Monkey S in a later phase (>200ms), although it was similar to the FGM in Monkey E in an earlier phase (100-200ms). (**B**) Statistical maps showing t-values from sample-by-sample t-tests between the figure and ground conditions from the centre (left) and edge (right) positions. Non-significant tests ($p < 0.05$, NS) are colored black.

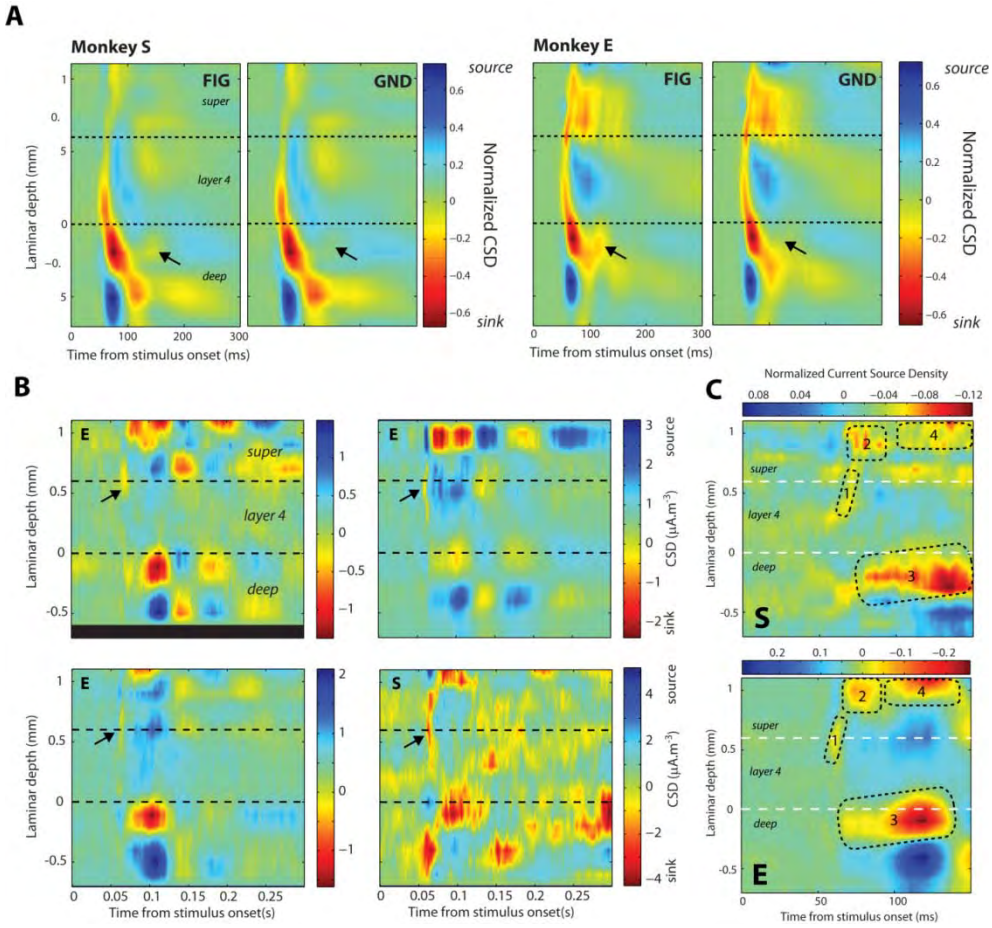

Figure S3 | (**A**) The average normalized CSD patterns from monkey S (left graphs) and monkey E (right graphs) in the figure center and ground conditions individually. The location of the modulatory current sink in layer 5 is indicated by the arrow. This modulatory current arrives at a time-point where there is no obvious net current flow in the ground condition. (**B**) Example penetrations showing the CSD difference between the response evoked by the figure edge and the background. Conventions are as in Figure 5B. These examples demonstrate the consistency of the extra sink in upper layer 4/superficial layers (black arrow) caused by the presence of the edge in the RF. E/S indicates the monkey. (**C**) Average data from the individual monkeys showing the CSD difference between the response evoked by the figure edge and the background. Four additional sinks in the edge condition (labeled 1-4) are identified. Note the similar timing and laminar position in both monkeys.

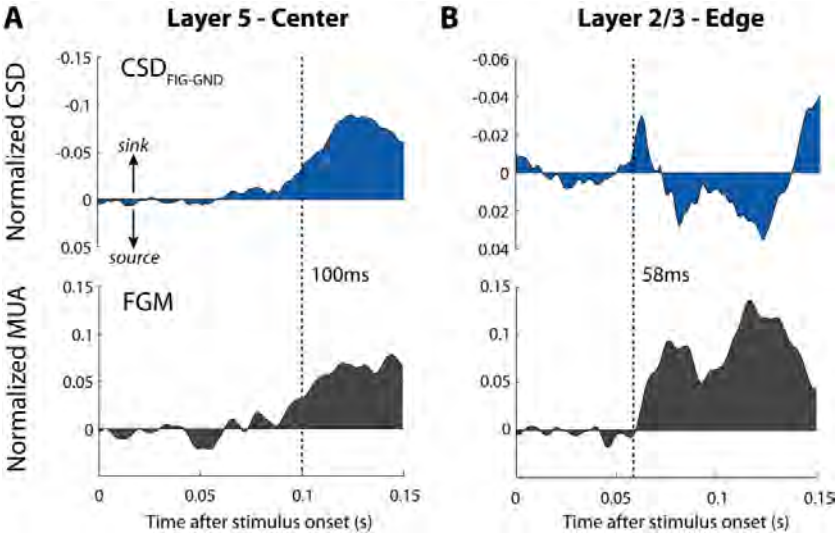

Figure S4 | (**A**) The top graph shows the difference in the CSD between the figure and ground conditions in layer 5 in the center condition (the average of the two electrode sites immediately below layer 4c were used, i.e. -0.1 and -0.2mm). The dashed line shows the latency of the CSD modulation (100ms) which was estimated by taking the point at which the trace reached 33% of the maximum response (it is not necessary to fit the CSD trace with a curve to estimate latency as it is already a low-passed signal). We also calculated the latency of the CSD modulation in layer 1, which was very similar to that of layer 5 (102.3ms). The lower graph shows the level of FGM from the same laminar depth with the CSD latency overlaid. (**B**) The same format as in (A) but now showing the early edge-related modulation in the superficial layers (depths 0.6 and 0.7mm were averaged). The latency of the CSD sink (58ms) was estimated in the same way as in (A).

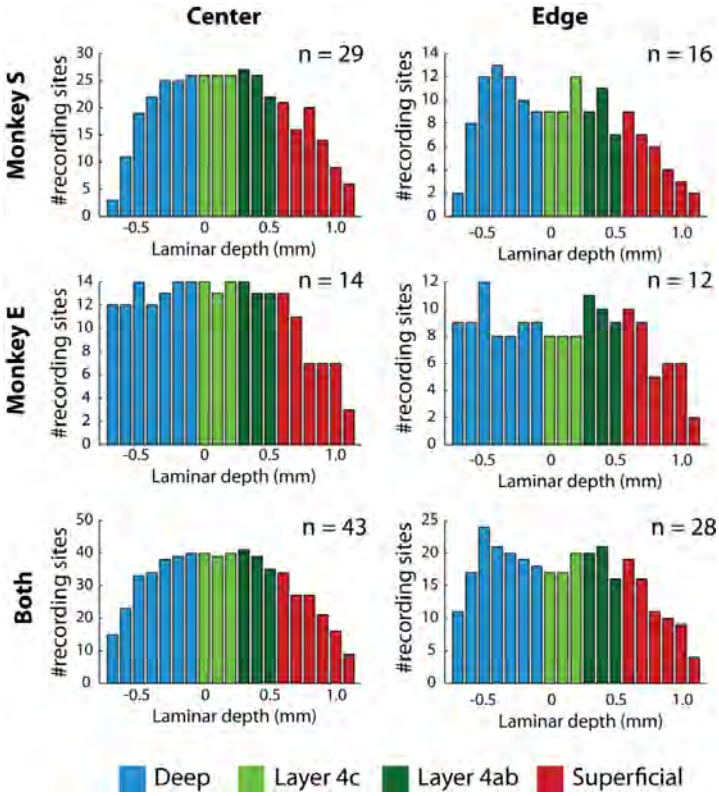

Figure S5 | The number of recording sites included in the analysis per layer. The color of the bars indicates the laminar compartment that the electrode site was assigned to. The *n* values indicate the number of penetrations in each data set.

Supplementary References

1. Roelfsema P.R., Lamme,V.A., & Spekreijse,H. Object-based attention in the primary visual cortex of the macaque monkey. *Nature* **395**, 376-381 (1998).

2. Supèr,H. & Roelfsema,P.R. Chronic multiunit recordings in behaving animals: advantages and limitations. *Prog. Brain Res.* **147**, 263-282 (2005).

3. Schiller,P.H., Finlay,B.L., & Volman,S.F. Quantitative studies of single-cell properties in monkey striate cortex. II. Orientation specificity and ocular dominance. *J. Neurophysiol.* **39**, 1320-1333 (1976).

4. Hubel,D.H. & Wiesel,T.N. Ferrier lecture. Functional architecture of macaque monkey visual cortex. *Proc. R. Soc. Lond B Biol. Sci.* **198**, 1-59 (1977).

5. Sceniak,M.P., Hawken,M.J., & Shapley,R. Visual spatial characterization of macaque V1 neurons. *J. Neurophysiol.* **85**, 1873-1887 (2001).

6. Snodderly,D.M. & Gur,M. Organization of striate cortex of alert, trained monkeys (Macaca fascicularis): ongoing activity, stimulus selectivity, and widths of receptive field activating regions. *J. Neurophysiol.* **74**, 2100-2125 (1995).

7. Ringach,D.L., Shapley,R.M., & Hawken,M.J. Orientation selectivity in macaque V1: diversity and laminar dependence. *J. Neurosci.* **22**, 5639-5651 (2002).

8. Gur,M., Kagan,I., & Snodderly,D.M. Orientation and direction selectivity of neurons in V1 of alert monkeys: functional relationships and laminar distributions. *Cereb. Cortex* **15**, 1207-1221 (2005).

9. Blasdel,G.G. & Fitzpatrick,D. Physiological organization of layer 4 in macaque striate cortex. *J. Neurosci.* **4**, 880-895 (1984).

10. Legatt,A.D., Arezzo,J., & Vaughan,H.G., Jr. Averaged multiple unit activity as an estimate of phasic changes in local neuronal activity: effects of volume-conducted potentials. *J. Neurosci. Methods* **2**, 203-217 (1980).

11. Logothetis,N.K., Pauls,J., Augath,M., Trinath,T., & Oeltermann,A. Neurophysiological investigation of the basis of the fMRI signal. *Nature* **412**, 150-157 (2001).

12. Xing,D., Yeh,C.I., & Shapley,R.M. Spatial spread of the local field potential and its laminar variation in visual cortex. *J. Neurosci.* **29**, 11540-11549 (2009).

13. Self,M.W., Kooijmans,R.N., Super,H., Lamme,V.A., & Roelfsema,P.R. Different glutamate receptors convey feedforward and recurrent processing in macaque V1. *Proc. Natl. Acad. Sci. U. S. A* **109**, 11031-11036 (2012).

14. Henze,D.A. *et al.* Intracellular features predicted by extracellular recordings in the hippocampus in vivo. *J. Neurophysiol.* **84**, 390-400 (2000).

15. Gray,C.M., Maldonado,P.E., Wilson,M., & McNaughton,B. Tetrodes markedly improve the reliability and yield of multiple single-unit isolation from multi-unit recordings in cat striate cortex. *J. Neurosci. Methods* **63**, 43-54 (1995).

16. Roelfsema,P.R., Tolboom,M., & Khayat,P.S. Different processing phases for features, figures, and selective attention in the primary visual cortex. *Neuron* **56**, 785-792 (2007).

17. Maris,E. & Oostenveld,R. Nonparametric statistical testing of EEG- and MEG-data. *J. Neurosci. Methods* **164**, 177-190 (2007).

Chapter 3 | The influence of attention and working memory on neuronal activity in the different layers of primary visual cortex

Timo van Kerkoerle, Matthew W. Self and Pieter R. Roelfsema

ABSTRACT

Selective attention and working memory are essential in daily life. Attention serves to select relevant stimuli while working memory retains the information when the stimulus has disappeared. Selective attention causes a top-down modulation of neurons in sensory areas, but the influence of working memory is less well understood. We here compared the influence of top-down selection signals on neuronal activity in the different layers of primary visual cortex (V1) in the presence and absence of a visual stimulus. Current-source density analysis revealed a profile of top-down inputs in the superficial layers and layer 5, irrespective of the presence of the stimulus. The top-down signal caused an increase in the neuronal firing rates that was most pronounced in the superficial and deep layers and weaker in input layer 4. This increase was strongest in the presence of the stimulus but we also found a highly reliable memory trace when the stimulus had disappeared. A visual mask erased the V1 memory activity, but it then reappeared at a later point in time. These results provide new insights in the role of V1 in working memory, and in the laminar circuits involved in top-down modulation of activity in early visual cortex.

INTRODUCTION

A brief visual stimulus can leave a lasting trace in the visual system. Visual memories consist of successive phases that differ in stability. The first phase is iconic memory, a high capacity store that lasts about 100ms and resembles a snapshot of what was just seen[1,2]. Iconic memory traces are fragile and are overwritten when new information is presented. During the decay of iconic memory, a subset of visual items can be transferred into visual working memory[3], which is a more robust memory store that can last several seconds but has a small capacity[4].

At the neuronal level, iconic memory is thought to correspond to the decaying activity that follows the response elicited by the stimulus in low-level areas of the visual cortex. Neuronal activity underlying the more stable working memories is found in higher areas of the visual, parietal and frontal cortex where neurons exhibit persistent firing even if the stimulus has disappeared[5-7]. The role of low-level areas in the maintenance of visual information as persistent activity is less well understood[8]. On the one hand, a recent study[9] demonstrated that persistent firing elicited by briefly presented motion stimulus is virtually absent from area MT, a lower level motion sensitive area, but that it is strong in the next higher area MST and in the frontal cortex. This finding suggests that persistent firing is a unique property of higher cortical areas. On the other hand, studies in human observers demonstrated that memory traces of low-level stimulus attributes may persist for seconds[10], and fMRI studies revealed that is it possible to decode the orientation of a stimulus in working memory from activity in primary visual cortex (V1)[11,12]. It not known, however, whether the fMRI signals elicited by working memories reflect subthreshold synaptic events or whether neurons also increase their spiking activity[13-15]. There has been one electrophysiological study in monkeys that demonstrated that working memory influences firing rates in V1[16], but this study used a stimulus with texture elements that drove the neurons even during the delay period. It is therefore unknown if V1 neurons exhibit persistent activity when there is no stimulus in the receptive field (RF).

To resolve this issue we here used a curve-tracing task, which requires an analysis of the location and orientation of multiple contour elements, which are represented at a high resolution in the lower visual areas. An example curve-tracing stimulus has been illustrated in **Figure 1C-F** where the task is to determine the green circle that is connected to the

fixation point by a target curve. Previous studies used version of this task where the stimulus remained in view and demonstrated that the feedforward response is followed by a phase where horizontal connections and feedback connections , modulate V1 activity[17-20]. In this later phase, enhanced neuronal activity spreads along the V1 representation of the target curve, starting at the fixation point until the entire curve has been labeled with an enhanced response[17,21]. This propagation of enhanced activity corresponds to the spread of object-based attention at a psychological level of description[22,23]. Human observers can continue tracing for a few hundred milliseconds if the stimulus is presented only briefly[24]. This capacity to trace a mental image of a curve that disappeared implies that the observers had access to the curves' precise shapes. We therefore hypothesized that early visual areas might also contribute to curve tracing after the stimulus has disappeared.

We trained monkeys in a curve-tracing task where the stimulus was presented only briefly to address a number of questions. First, we wanted to test if monkeys can trace curves that are only briefly presented. If so, do V1 neurons exhibit persistent activity and does it depend on the relevance of previously presented contour elements? Second, we aimed to compare the putative V1 memory signal to the attentional response modulation when the curves remain visible. Third, we wanted to measure the influence of a strong visual mask on the activity in area V1 because masking interferes with iconic memory whereas working memories can be preserved[25]. Fourth and finally, we used a laminar electrode so that we could determine the contribution of the different V1 layers to curve tracing in the presence and absence of the stimulus.

RESULTS

We recorded multi-unit activity (MUA) and local field potentials (LFPs) in the different layers of monkey V1 using a high-density depth probe with a spacing of 100um between electrodes (**Figure 1A,B**). We used a version of a curve tracing task (**Figure 1C,D**)[17] that allowed a direct comparison between selective attention for stimuli that remained on the screen and working memory for stimuli that were only presented briefly. The monkeys directed their gaze to a red dot and we then presented four curves with green circles at their ends. One of the curves was a target curve that connected the fixation dot to one of the

green circles. The monkeys were rewarded for making a saccade to this target circle after a delay of 750ms. In every recording session we showed a total of eight stimuli that were randomly interleaved and varied at three locations (**Figure 1C-F** shows the variations at locations 1 and 2, **Figure S1** shows all stimuli). We adapted the stimulus so that the neurons' receptive field fell on one of the possible segments at location 2, and the initial segment at location 1 determined whether the this segment belonged to the target curve (**Figure 1C**) or a distractor curve (**Figure 1D**), while receptive field stimulation was constant. For the two other stimuli the target (**Figure 1E**) or distractor curve was adjacent to the receptive field (**Figure 1F**) so that we could determine the spatial specificity of attentional modulation and persistent activity. We held the orientation of the contour element in the neurons' RF constant to obtain a sufficient number of trials per condition and did not determine orientation tuning.

In the standard curve-tracing task (performed in blocks of ~100 trials), the monkeys' accuracy was high (94% for monkey E and 97% for monkey R). The appearance of a contour segment in the receptive field elicited a feedforward MUA response in the different V1 layers, starting in layers 4C and 6 and then spreading into the superficial and deep layers (**Figure 1G,H**). We also computed the current source density (CSD) profile to determine the putative location of synaptic inputs. The small contour element in the receptive field elicited a relatively weak initial current sink in layer 4C (arrow in **Figure 1I**), which was followed by current sinks and sources in the superficial and deep layers[26,27]. This laminar pattern is consistent with the projection from the LGN to layers 4C and 6[28] which, in turn, target the superficial and deep layers[29], although the later CSD profile presumably also includes contributions from horizontal and feedback connections[27].

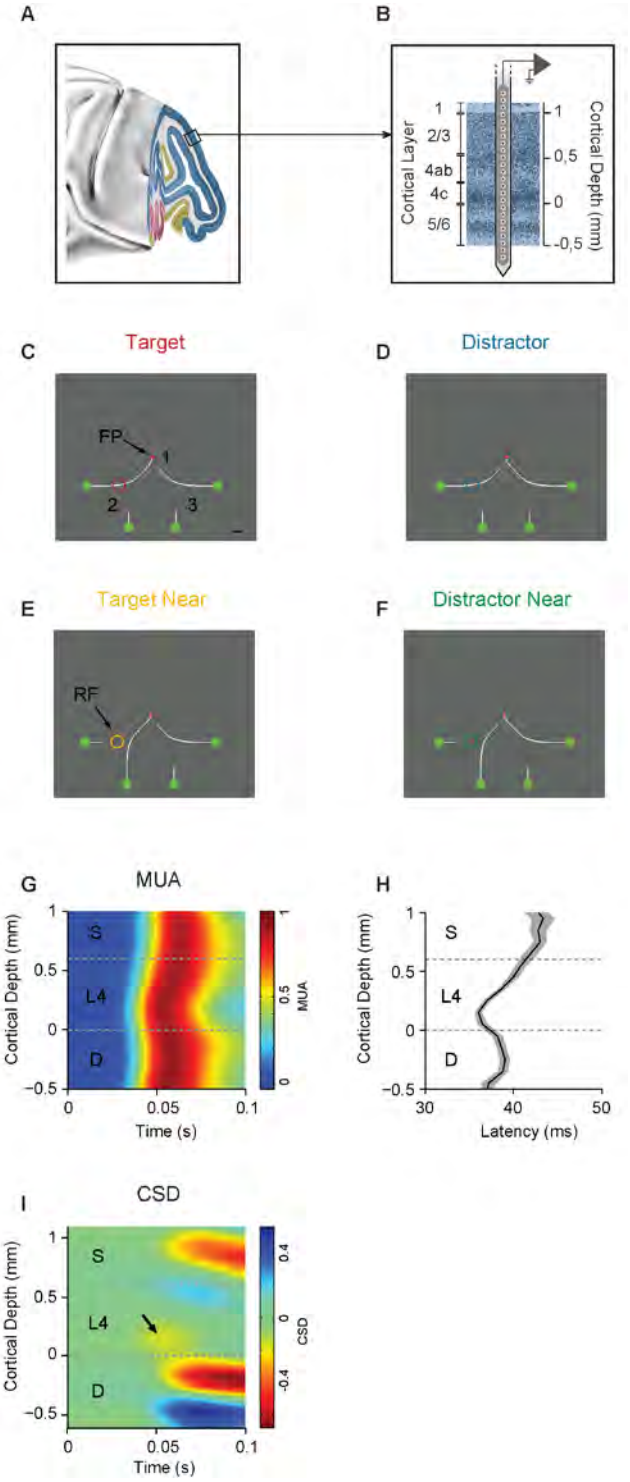
A
B
Cortical Layer
1
2/3
4ab
4c
5/6
Cortical Depth (mm)
1
0,5
0
-0,5
C
Target
FP
1
2
3
D
Distractor
E
Target Near
RF
F
Distractor Near
G
MUA
Cortical Depth (mm)
S
L4
D
Time (s)
MUA
H
Latency (ms)
I
CSD

Figure 1 | Laminar recordings and visual stimuli. (**A**) Lateral view of the macaque brain. V1 is the blue region. (**B**) Laminar recording with the multi-site linear electrode (Plexon Inc. U-probe). (**C-F**) The monkey had to mentally trace the target curve that was connected to the fixation point (FP). We placed the target curve (C, red circle) or a distractor curves in the RF (D, blue). In other conditions the target (E, yellow) or distractor curve (F, green) was next to the RF. Bar in panel C, 1 degree. (**G**) The average MUA response evoked by the onset of the target curve across the layers. Note the slight differences in the timing of the onset of the MUA response between layers. (**H**) Visual latencies in the different layers, averaged across all penetrations, shaded areas indicate s.e.m. (*n*=38 penetrations). The earliest neuronal activity occurred in layers 4C and 6. (**H**) Average CSD evoked by the appearance of the target curve. Warm colors indicate current sinks, cooler colors current sources. The appearance of the curve causes an early sink in layer 4C (arrow).

The initial MUA response did not distinguish between the target and distractor curve (**Figure 2B**), but after a delay the representation of the target curve was enhanced over the representation of the distractor (200-750ms after stimulus onset, t-test: monkey E: n=25 penetrations, $p<0.001$; monkey R: n=13 penetrations, $p<0.001$), in line with previous studies[17,19,30]. The reliability of the attentional modulation in V1 was high as it occurred in every penetration (**Figure 2C**). A target or distractor curve that fell next to the receptive elicited only a weak, transient and delayed response (**Figure 2B**)[31] that did not discriminate between target and distractor (t-test: $p>0.1$ for both monkeys). Thus, attention only influenced neurons that were well activated by a contour element in their receptive field.

In alternating blocks of trials (of ~100 trials) we examined if the monkeys were able to trace curves that were presented for 150ms, followed by a delay of 600ms with only the fixation point left on the screen. At the end of the trial, the stimulus reappeared, except the middle line elements which had to be remembered (locations 2 and 3, **Figure 2D**). The monkeys' performance was comparable to that in the regular curve-tracing task (90% for monkey E and 97% for monkey R; t-test: $p>0.1$ for both monkeys), suggesting that they could trace the image of a curve that had been presented only briefly, just like human observers[24]. In this version of the task, the MUA exhibited an off-response and the activity then gradually decreased to baseline (**Figure 2E**), a decrease in activity that presumably corresponds to the decay of iconic memory.

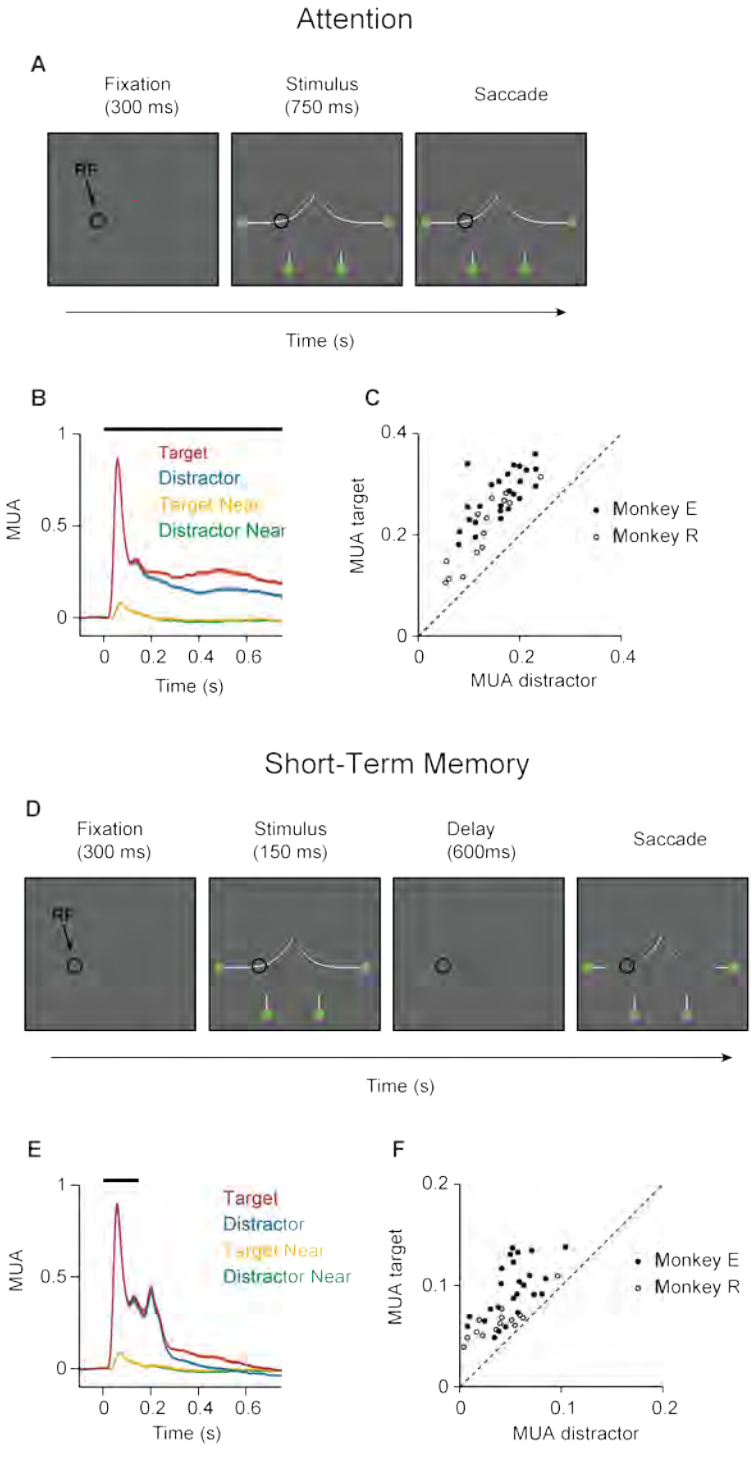
Attention
A
Fixation
(300 ms)
Stimulus
(750 ms)
Saccade
RF
Time (s)
B
C
MUA
Target
Distractor
Target Near
Distractor Near
Time (s)
MUA target
MUA distractor
Monkey E
Monkey R
Short-Term Memory
D
Fixation
(300 ms)
Stimulus
(150 ms)
Delay
(600ms)
Saccade
RF
Time (s)
E
F
MUA
Target
Distractor
Target Near
Distractor Near
Time (s)
MUA target
MUA distractor
Monkey E
Monkey R

Figure 2 | Selective attention and short-term memory; task and MUA response. (**A**,**D**) After a 300 ms fixation period, four curves appeared on the screen. One of them was the target curve that was connected to the fixation point. The monkeys had to make a saccade to a green circle at the end of this curve. In the regular task (A), the stimulus remained on the screen whereas the stimulus disappeared after 150ms in the short duration task (D). After an additional delay (600ms), part of the stimulus reappeared, but the segment at locations 2 and 3 did not, so that the animal had to remember the configuration of the target curve. Black circle, typical receptive field location. (**B**,**E**) Neuronal activity averaged across all V1 recording sites in the standard task (B) and the short stimulus duration task (E). The RF fell on the target (red trace), distractor curve (blue), or next to the target (yellow) or distractor curve (green). Shaded areas show s.e.m. (*n*=38 penetrations; when they are difficult to see the s.e.m. is small). (**C**,**F**) Data of the individual penetrations in monkeys E (black data points) and R (white) in the standard task (C) and the task with short stimulus duration (F). Abscissa, MUA elicited by the distractor curve (200-750ms after stimulus onset). Ordinate, MUA elicited by the target curve.

Strikingly, the response elicited by the contour element that had been part of the target curve remained stronger than the distractor response for the full duration of the trial (**Figure 2E**) (t-test: monkey E: n=25 penetrations, $p<0.001$; monkey R: n=13 penetrations, $p<0.001$). Although this modulation of persistent activity was weaker than the attentional modulation in the presence of the stimulus (two sample t-test: monkey E: n=25 penetrations, $p<0.001$; monkey R: n=13 penetrations, $p<0.01$), it was present in all penetrations in both monkeys (**Figure 2F**). No modulation of V1 activity occurred when the target or distractor curve was adjacent to the receptive field (t-test: $p>0.05$ for both monkeys), indicating that the modulation of persistent activity depended on the brief stimulation of the neurons' receptive field. We also considered the possibility that the modulation of persistent activity was related to the trajectory of the impending eye movement, but we ruled this possible explanation out in a control experiment, in which we varied the shape of the target curve while keeping the eye movement target the same (**Figure S2**). Thus, persistent activity was strongest for task-relevant parts of the representation in memory and not due to eye movement preparation.

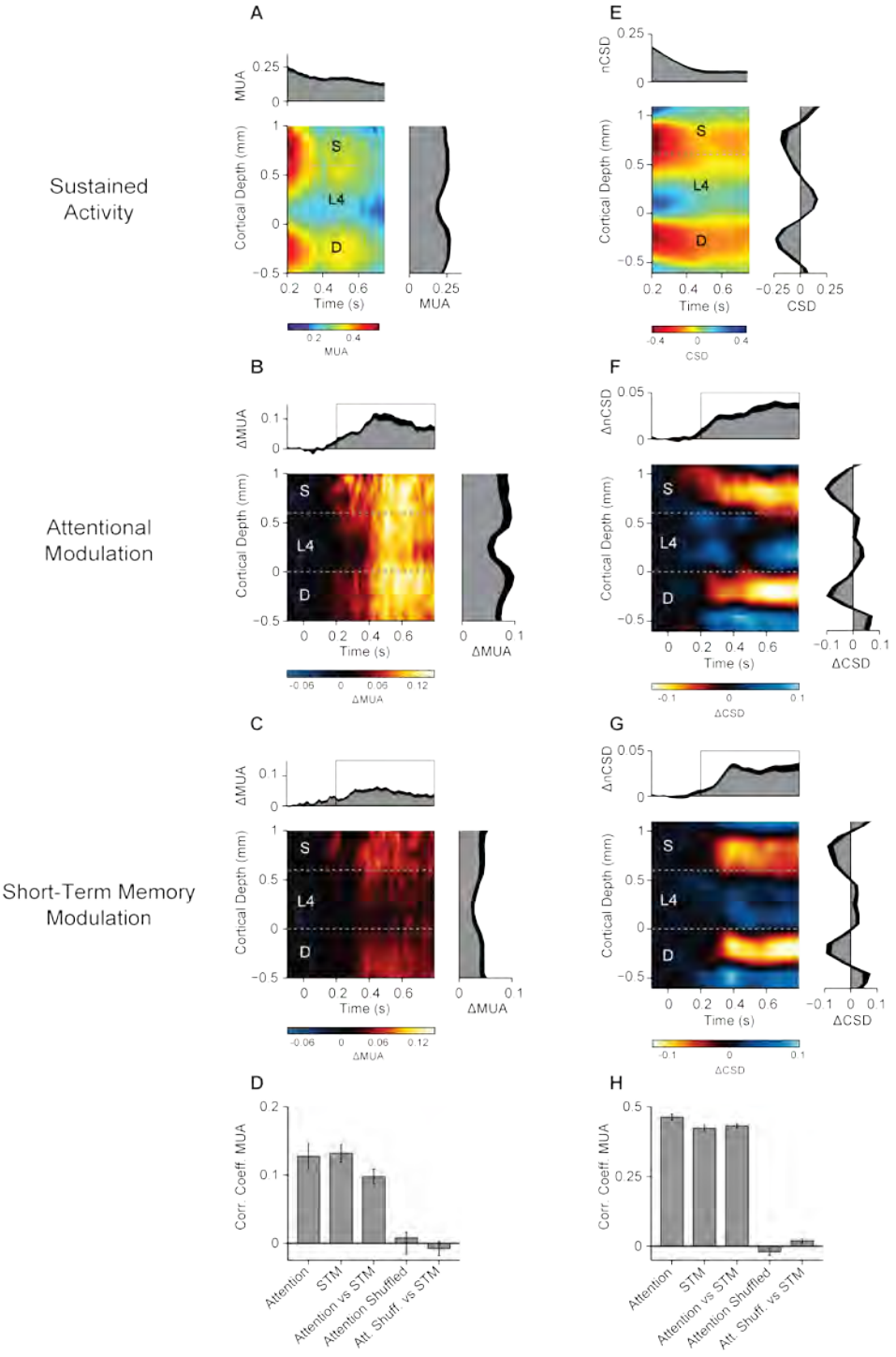
Sustained Activity
Attentional Modulation
Short-Term Memory Modulation
A
B
C
D
E
F
G
H
MUA
ΔMUA
nCSD
ΔnCSD
CSD
ΔCSD
Cortical Depth (mm)
S
L4
D
Time (s)
Corr. Coeff. MUA
Attention
STM
Attention vs STM
Attention Shuffled
Att. Shuff. vs STM

Figure 3 | The laminar profile of selective attention and short-term memory. (**A**) Laminar pattern of spiking activity in the epoch after the peak response. (**B,C**) The attentional modulation (B) and short-term memory effect (**C**) on spiking activity across the depth of the cortex. The figures show the difference in activity elicited by the (memory of) the target and the distractor curve (red minus blue traces in Figure 2B,F). For the MUA, graphs above and at the side show the averages across layers and across the modulation period (200-750ms after stimulus onset, indicated by the black square in graphs at the top). Graphs at the side show the average across the modulation period. Graphs at the top show the amplitude of this laminar profile over time (inner product of the laminar profile at a particular time point and the average normalized laminar profile in the modulation period). Black lines indicate s.e.m. (**D**) Consistency of the laminar MUA profile as assessed with an analysis of correlations between penetrations in the modulation period in the attention and short-term memory conditions and between these conditions. Also shown are the controls when the data are shuffled. Error bars indicate s.e.m. (**E**) Average CSD during the episode when the peak response has subsided. The average laminar CSD profile is plotted on the right. The upper panel shows the inner product of this profile with the CSD at the different time points (nCSD). (**F**,**G**) Average difference in CSD between target and distractor curve. Plots on the side and top are as defined in panel E. (**H**) Analysis of the consistency of the laminar CSD profile across penetrations by computing pair-wise correlations.

We next examined the activity profile in the presence and absence of the stimulus across the depth of the cortex. **Figure 3A** shows the sustained spiking activity (200-750ms after stimulus onset) elicited by a contour element of the distractor curve (blue in **Figure 2B**) in the different layers. For statistical analysis we normalized activity at every electrode to the peak response and we assigned electrodes to three compartments, superficial layers, layer 4 and the deep layers. The sustained activity level differed significantly between layers (one-way repeated measure ANOVA, monkey E: $F(2,48)=9.4$, $p<0.05$; monkey R: $F(2,24)=6.63$, $p<0.005$). It was stronger in the superficial and deep layers than in layer 4 (t-test: $p<0.01$ for both comparisons and both monkeys). There were also differences between layers in the strength of the attentional modulation (**Figure 3B**; one-way repeated measures ANOVA, monkey E: $F(2,48)=9.4$, $p=0.001$; monkey R: $F(2,24)=6.63$, $p=0.005$), which was strongest in the superficial and deep layers and weaker in layer 4 (t-test: $p<0.05$ for both comparisons and both monkeys), in accordance with the anatomy of feedback connections to V1 which tend to avoid layer 4[32,33]. The laminar profile of attentional modulation was consistent across penetrations (**Figure 3B**) (test of correlation across penetrations; t-test: $p<0.001$ for both monkeys; unlike a shuffle control; t-test: $p>0.5$ for both monkeys).

When the stimulus disappeared, the difference between activity elicited by the target and distractor was weaker than when it did not, but the laminar profile was similar (**Figure 3C**), with a significant difference between the layers (ANOVA, monkey E: $F(2,48)=12.7$, $p<0.001$; monkey R: $F(2,24)=4.733$, $p=0.025$). The extra activity elicited by the target curve was more pronounced in the superficial and deep layers than in layer 4 (t-test: $p<0.05$ for both comparisons and both monkeys). This laminar profile of MUA modulation was similar between tasks (analysis of correlations; t-test: $p<0.001$ for both monkeys) (**Figure 3D**), suggesting a common feedback source for selective attention and spatial working memory.

To investigate the synaptic sources underlying the MUA, we calculated the current source density (CSD). If the distractor curve remained visible it evoked two sinks in the CSD, one in the deep layers and the other one straddling the superficial layers and upper layer 4 (**Figure 3E**). When we subtracted the distractor response from the target response to isolate the attentional modulation, we observed two sinks that were more confined. One was in the superficial layers and the other one in layer 5 (**Figure 3F**), i.e. in the layers that receive feedback connections from higher visual areas[32,33]. This CSD pattern was highly consistent across recording sessions (t-test: $p<0.001$ for both monkeys) (**Figure 3H**). The CSD associated with the modulation of persistent activity if the stimulus was not visible exhibited a surprisingly similar laminar profile (200-750ms after stimulus onset; t-test: $p<0.001$ for both monkeys), with sinks in layer 1-3 and 5 (**Figure 3G**). It did not differ significantly from the profile of attentional modulation with the stimulus in view (two-way ANOVA, monkey E: $F(17,204)=1.2$, $p=0.3$; monkey R: $F(17,408)=1.7$, $p=0.15$). Thus, both tasks gave rise to similar laminar patterns of spiking activity and synaptic input, in accordance with the anatomy of feedback connections to V1.

The amplitude of the CSD modulation was also similar in the presence and absence of the stimulus (t-test: $p>0.15$ for both monkeys), although the MUA modulation was stronger if the curves were visible (causing an interaction between signal type [MUA vs. CSD] and task in a two-way ANOVA, monkey E: $F(1,48)=53.2$, $p<0.001$; monkey R: $F(1,24)=45.7$, $p<0.001$), which indicates that the presence of a curve in the receptive field amplified the influence on the firing rate. These results, taken together, demonstrate that tracing a briefly presented curve causes a modulation of persistent activity in V1.

The influence of masking on persistent activity in V1

Is the modulation of persistent activity a spatial working memory trace or does it represent an influence of attention on iconic memory? Iconic memories are sensitive to masking, while information becomes resistant against masks once it has been transferred into working memory[1,2,4]. In our next experiment we therefore tested the influence of masks on persistent firing in V1. We showed two full contrast checkerboard stimuli at locations 2 and 3, 400ms after the onset of the stimulus (225ms after the offset). One of these masks covered the neurons' receptive field (**Figure 4A**). The performance for this task was slightly, but not significantly lower than in the memory task without a mask (84% for monkey E and 95% for monkey R; t-test, $p>0.3$ for both monkeys). The mask elicited a strong MUA response that abolished the curve-tracing modulation (window from 450-550ms after stimulus onset, t-test: $p>0.25$ for both monkeys). Notably, the modulation returned ~200ms after mask offset (**Figure 4B**; t-test: monkey E: n=12 penetrations, $p<0.01$; monkey R: n=8 penetrations, $p<0.01$), an effect that occurred for nearly all penetrations in both monkeys (**Figure 4C**). The magnitude of the modulation in this epoch was similar to that when no mask had been shown (650-750ms after stimulus onset, t-test: $p>0.2$ for both monkeys) and the profile across the layers was similar (**Figure 4D**,**F** test of correlations, t-test: $p<0.01$ for both monkeys). The mask also disrupted the characteristic CSD profile with sinks in the superficial layers and layer 5 (**Figure 4E**), associated with the selection of the target curve in memory, but the CSD pattern reappeared at about the same time as the MUA modulation (**Figure 4D**; 650-750ms after stimulus onset, t-test: $p<0.05$ for both monkeys). During this phase, the CSD profile was similar to that in the task without a mask (two-way repeated measure ANOVA, monkey E: $F(17,595)=1.2$, $p=0.3$; monkey R: $F(17,323)=2.1$, $p=0.1$). Thus during the mask, V1 spiking activity apparently does not store the memory of the stimulus but the response modulation is restored later, presumably due to feedback from higher areas. The reappearance of the V1 modulation suggests that these putative higher areas enable a stable form of memory, and it excludes the possibility that the modulation of the V1 response depends on iconic memory.

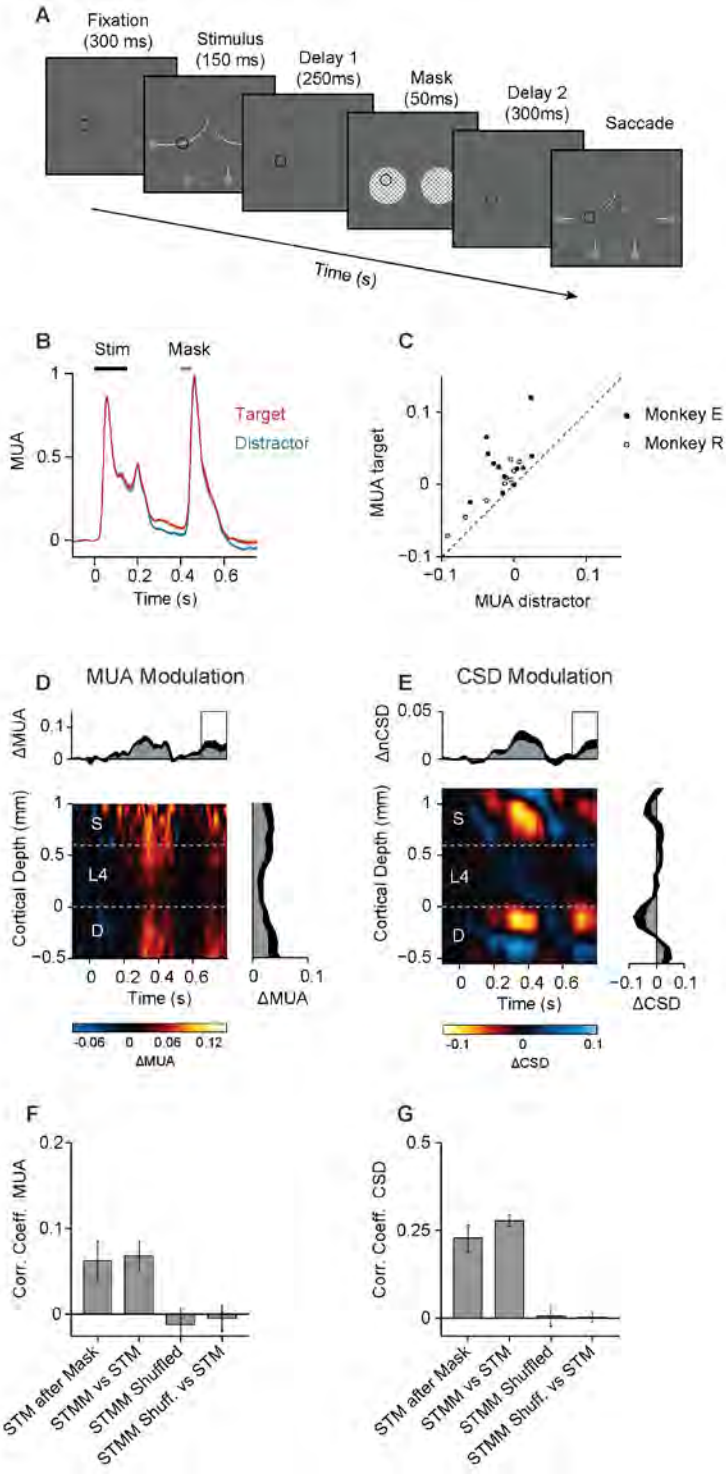
A
Fixation (300 ms)
Stimulus (150 ms)
Delay 1 (250ms)
Mask (50ms)
Delay 2 (300ms)
Saccade
Time (s)
B
Stim
Mask
Target
Distractor
MUA
Time (s)
C
Monkey E
Monkey R
MUA target
MUA distractor
D
MUA Modulation
ΔMUA
Cortical Depth (mm)
S
L4
D
Time (s)
E
CSD Modulation
ΔnCSD
ΔCSD
F
Corr. Coeff. MUA
STM after Mask
STMM vs STM
STMM Shuffled
STMM Shuff. vs STM
G
Corr. Coeff. CSD

Figure 4 | The influence of a mask. (**A**) The stimulus was shown for 150ms and 250ms later a mask appeared (50ms) followed by another delay of 300ms. (**B**) Neuronal activity averaged across all V1 recording sites in two monkeys evoked by the target (red trace) and the distractor curve (blue). Shaded areas show s.e.m. (*n*=20 penetrations, if it is difficult to see, the s.e.m. is small). (**C**) MUA evoked by the target (ordinate) and distractor curve (abscissa) during the modulation period (650-750ms after stimulus onset). Filled circles for monkey E, open circles for monkey R. (**D**) Difference in MUA elicited by the target and distractor curve across cortical depth. Upper panel, average across layers. Right panel, average in window from 650-750ms after stimulus onset (black square in upper panel). (**E**) CSD difference between target and distractor curve. Upper panel, time course (inner product with the average laminar profile from 650-750ms). Right panel, average from 650-750ms. Black lines, s.e.m. (**F**,**G**) Correlation coefficients of the MUA (F) and CSD (G) across penetrations from 650-750ms. STMM, consistency across penetration of short-term memory modulation after the mask. STMM vs. STM, correlation coefficient between STM modulation after the mask and when there was no mask. Error bars, s.e.m.

A limitation in keeping multiple curves in memory

We next investigated whether the monkey could maintain two the configuration of two curves in memory by only presenting the cue at location 1 after the locations 2 and 3 had been masked (**Figure 5A**). After 150ms the crucial segments disappeared while the 'skeleton' of the stimulus remained in view, to aid the monkeys in a task that was relatively difficult for them. The accuracy was lower than in the task of **Figure 2D** (74% for monkey E and 81% for monkey R; t-test, $p<0.05$ for both monkeys) and close to 75%, which is predicted if the monkeys are able to hold the configuration of only one of the two masked locations in memory (100% for the memorized configuration and 50% for the other one). As expected, the MUA response elicited by the target and distractor curves overlapped during the first delay (**Figure 5B**), but approximately 200ms after the appearance of the contour element at location 1, the representation of the target curve increased (900-1150ms after stimulus onset, t-test: monkey E: n=14 penetrations, $p<0.001$; monkey R: n=9 penetrations, $p<0.001$). This modulation of spiking activity occurred in nearly all penetrations in both monkeys (**Figure 5C**). The modulation in the both the MUA and the CSD exhibited their characteristic laminar pattern (**Figure 5D**,**E**), which was also significant (900-1150ms after stimulus onset, t-test: $p<0.001$ for both monkeys). Thus the cue near the fixation point initiated a feedback signal from higher areas back to V1, which enhanced the representation of the relevant curve in memory.

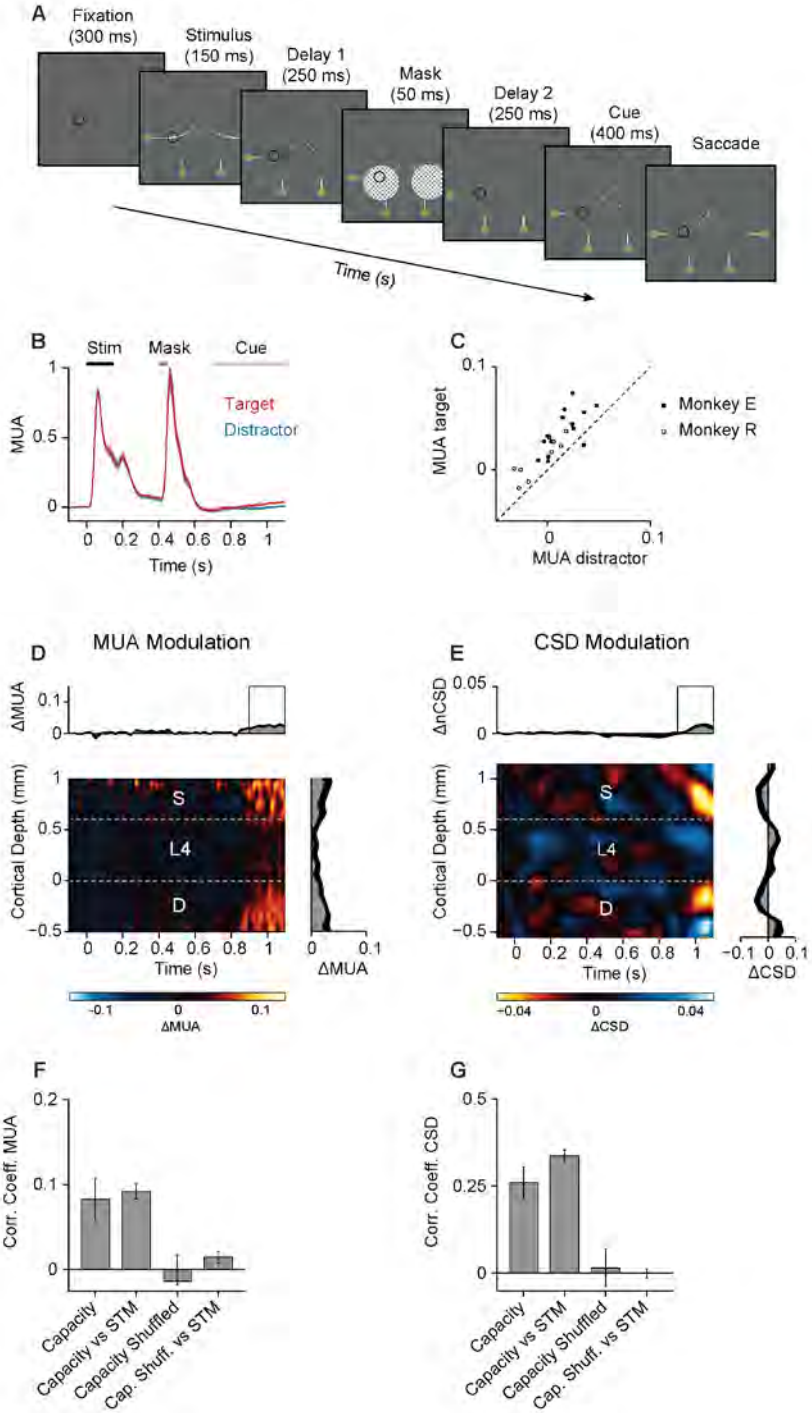
A
Fixation (300 ms)
Stimulus (150 ms)
Delay 1 (250 ms)
Mask (50 ms)
Delay 2 (250 ms)
Cue (400 ms)
Saccade
Time (s)
B
Stim
Mask
Cue
Target
Distractor
MUA
Time (s)
C
MUA target
MUA distractor
Monkey E
Monkey R
D
MUA Modulation
ΔMUA
Cortical Depth (mm)
S
L4
D
Time (s)
E
CSD Modulation
ΔnCSD
ΔCSD
F
Corr. Coeff. MUA
Capacity
Capacity vs STM
Capacity Shuffled
Cap. Shuff. vs STM
G
Corr. Coeff. CSD

Figure 5 | The influence of a delayed central cue. (**A**) The contours in or near the receptive field disappeared after 150ms and a mask (50ms) appeared after 250ms, followed by a second delay of 250ms. The connection to the fixation point was shown after the second delay cueing one of the curves as target. (**B**) Average MUA response evoked by the target (red trace) and the distractor curve (blue). Shaded areas show s.e.m. (*n*=23 penetrations). (**C**) MUA elicited by target (ordinate) and distractor (abscissa) from 850-1100ms after stimulus onset. (**D,E**) Difference in MUA (D) and CSD (E) elicited by target and distractor curve. (**F**,**G**) The left bar represents the average correlation coefficients of the laminar pattern of the MUA (F) and CSD (G) between penetrations, from 850-1100ms. The second bar (capacity vs. STM) compares the laminar profile to that in the task without a mask. Error bars show s.e.m.

The monkeys' accuracy suggested that they memorized, on average, only one of the two masked configurations. We therefore hypothesized that V1 activity during the first delay might predict which configuration was remembered and compared the neuronal activity in correct and erroneous trials. V1 activity elicited by the probed side of the stimulus was stronger in correct trials than that in erroneous trials (t-test, $p<0.05$ for both monkeys). In contrast, if the distractor was in the receptive field, activity was slightly weaker on correct trials, but this effect was not significant (t-test, $p=0.2$ for monkey and $p=0.06$ for monkey R). Thus, V1 activity during the first delay predicted the accuracy of the memory on that side of the stimulus.

DISCUSSION

Human observers can trace curves that are presented only briefly, as if they can inspect a mental image of a previously presented stimulus at a high spatial resolution for a few hundred milliseconds[24]. Here we compared the mechanisms of this mental tracing process to the mechanisms for curve tracing with the stimulus in view, directly comparing of spatial attention and working memory in the different layers of V1. Like humans, monkeys are able to trace curves that are only briefly shown to them. Remarkably, the relevance of contour elements modulated the spiking activity of V1 neurons, during a phase in which they were no longer in view. This modulation of spiking activity was most pronounced in the superficial and deep cortical layers and an analysis of the CSD revealed strong current sinks

in the superficial layers and layer 5, in accordance with an important contribution of feedback connections from higher visual areas to the modulation of V1 activity.

Iconic memory and working memory

Theories about visual memory for briefly presented stimuli distinguish between an early iconic memory store with a rapid decay and a later working memory store that lasts longer[1,2]. A distinguishing feature of iconic memory, which differentiates it from working memory, is its sensitivity to masking. Masks erase iconic memories but they usually do not interfere with items that have been transferred into working memory. The transfer from iconic memory to working memory has to be selective because the capacity of working memory is much smaller than that of iconic memory[1,2,34]. Our results suggest that the delayed V1 response modulation after a briefly presented stimulus is a neuronal correlate of working memory, for at least two reasons. First, the mask briefly erased the influence of memory on V1 spiking activity, but the response modulation reappeared thereafter. In other words, the memory resisted the mask. Second, V1 activity predicted the probability that the memory for the curve in the receptive field would survive the mask, and this memory store had a limited capacity of approximately one contour configuration. These results, taken together, imply that the late modulation of V1 activity provides a neuronal correlate of working memory. At the same time, it is conceivable that the early visually driven but quickly decaying V1 response provides a neuronal correlate of iconic memory, a conjecture that could be addressed in future work.

Working memory representations in early visual cortical areas

Many previous studies in monkeys performing working memory tasks focused on higher cortical areas where the persistent firing for items in working memory can be strong[5-7]. It has remained less clear if working memory also relies on persistent activity in early visual cortical areas[8]. On the one hand, fMRI studies in humans revealed signatures of the items in working memory in higher but also in lower visual areas[35-37]. Indeed, it is possible to decode the stimulus in memory in early visual areas by analyzing the pattern of the fMRI signal across multiple voxels[11,12], even when the visually driven fMRI response has decayed back to

baseline[38,39]. One the other hand, it was unknown whether these fMRI signals reflect an influence of memory on spiking activity or on subthreshold synaptic activity[13-15]. In accordance with such a subthreshold influence, a recent study on the influence of working memory on neuronal firing rates reported that persistent firing was virtually absent from motion sensitive area MT, but pronounced in the higher visual area MST and prefrontal cortex[9]. Nevertheless, the present results reveal that tracing a curve in memory modulates V1 spiking activity, during a phase where the overall V1 firing rate is close to spontaneous activity levels. It is of interest that masks briefly eliminated this memory trace. The response modulation restored when the mask had disappeared. This finding is consistent with the hypothesis that the target curve was also stored in higher cortical areas where masks may have less impact, which then fed back to restore the pattern of response modulation in V1. We note, however, that the masking results do not rule out local storage of information within V1 by processes other than spiking activity, such as rapid synaptic potentiation[40].

We do not know why we observed such a robust influence of memory on V1 activity where previous studies failed to find such an effect. One possibility is that tracing a curve in memory necessitates the access to a high-resolution representation of the location and orientation of contour elements, which is made available by V1. Compared to other tasks, the attentional selection of contour elements during the tracing of visible curves also causes a relatively strong modulation of V1 activity compared to some other tasks that demand attention shifts[17,41]. Another difference is that we investigated the spatial working memory for a relevant curve, whereas previous studies focused on memory features other than space, like motion direction. A sustained spatial attention signal that is directed to the locations that were previously occupied by a relevant curve might therefore also account for our results, although one previous study reported that attention does not influence ongoing V1 activity if there is no stimulus in the RF[41]. It is generally difficult, if not impossible, to dissociate working memory for spatial locations from sustained attention to these locations and a sustained attention signal implies a memory for the locations where attention should be directed. It is therefore of interest that the working memory trace specifically encoded the course of the target curve (**Figure 2F**, **S2**), as if it was contingent on the preceding visual response[42].

Neuronal activity underlying working memory and attention

The present study is the first to directly compare the influence of selective attention and working memory on neuronal activity in the different layers of cortex. Attention and working memory both increased spiking activity with pronounced effects on spiking in the superficial and deep layers and an almost identical CSD profile. Our findings therefore support theories that suggest that the mechanisms for controlling attention strongly overlap with those for working memory [37,43,44]. Attention and working memory caused current sinks in the superficial layers and layer 5 of similar magnitude, yet the modulation of MUA was highest with a stimulus in the neurons' RF. This finding suggests that the feedforward drive provided by a RF stimulus enhances the impact of feedback input on the firing rates. This amplification of the feedback influence by the visual stimulus should not distract from the new finding that working memory also had a robust influence on V1 firing rates if there was no stimulus in the RF. Thus, our results support studies that demonstrated short-term memory for location[16] and figure-ground organization[45] in early visual cortex while driving cells with a texture or an edge. Yet, they also go beyond by demonstrating short-term memory signals in the absence of a visual stimulus.

Role of the different V1 layers

Although models of the visual system have often emphasized the importance of feedforward connections[46-49], early visual areas receive at least as much feedback as feedforward input[50]. Area V1 is an extreme case in this respect, because only ~1% of the external input connections come from the LGN and ~95% from higher visual areas[50]. Feedforward and feedback connections target different V1 layers[28,32,33], which allowed us to distinguish between these two processing streams. The visually driven spiking response started in input layer 4[51,52] and then quickly spread to the superficial and deep layers. In accordance with previous work, the initial visual response coincided with a sink in layer 4, the target of feedforward connections from the LGN[26,27]. The laminar pattern of the feedback influences was drastically different because the increase in spiking activity caused by attention and working memory was most pronounced in the superficial and deep layers. The modulation of the firing rate was accompanied with strong current sinks in the superficial layer and layer 5, which are the main targets of cortical feedback connections[32,33]. The laminar pattern

caused by selective attention and working memory resembles the pattern of activity across the V1 layers when monkeys segregate a texture into figure and background[27], although figure-ground segmentation also occurs when attention is directed elsewhere[30]. These results, taken together, suggest that these sinks in the superficial layers and layer 5 represent a reliable signature of feedback influences onto lower cortical areas, which are driven by figure-ground organization, selective attention as well as working memory.

METHODS

Stimuli

We trained two macaque monkeys (E and R) to perform the curve tracing tasks. A trial began with the fixation point (a red circle of 0.3° diameter) presented on a grey background. The monkey initiated the trial when the eye position was within a one degree window centred on the fixation point. We presented the curve-tracing stimulus after 300ms of fixation and extinguished the fixation point after another 750ms in most of tasks (**Figure 2A**,**D** and **Figure 4A**), but after 1100ms in task with the delayed presentation of the cue near fixation (**Figure 5A**). The monkey was required to make a saccadic eye-movement into a target-window (3 degrees diameter) centered on the green disc at the end of the target curve. Correct responses were rewarded with apple juice. We aborted trials in which the animal broke fixation before the fixation point was extinguished. All stimulus conditions were presented in a pseudorandom order.

The stimuli were generated using in-house software and were presented on a CRT monitor with a resolution of 1024x768 pixels and refresh rate of 85Hz, which was viewed from a distance of 75cm. The stimulus consisted of two main branches that could split into two curves each, with an initial segment (location 1 in **Figure 2A**) that determined which of the two main branches was relevant and two additional segments (locations 2 and 3) determining the relevance of contour elements within the branch, so that there were a total of 8 stimuli (**Figure S1**). We placed one of the contour elements at location 2 in the center of the receptive field. The configuration at location 3 was not relevant for our analyses and we therefore averaged across these two configurations so that there were a total of four conditions left.

Surgical procedures

The animals underwent two surgeries under general anesthesia that was induced with ketamine (15mg/kg injected intramuscularly) and maintained after intubation by ventilation with a mixture of 70% N_2O and 30% O_2, supplemented with 0.8% isoflurane, fentanyl (0.005mg/kg intravenously) and midazolam (0.5mg/kg/h intravenously). We implanted a head holder in the first operation. We trained the monkeys until they could reliably perform the task, and we then implanted a recording chamber (Crist Instruments) over the operculum of V1 and performed a craniotomy inside the chamber for the laminar recordings. All procedures complied with the NIH Guide for Care and Use of Laboratory Animals (National Institutes of Health, Bethesda, Maryland), and were approved by the institutional animal care and use committee of the Royal Netherlands Academy of Arts and Sciences.

Data acquisition and preprocessing

We collected neuronal data with TDT (Tucker Davis Technology) recording equipment using a high-impedance headstage (RA16AC) and a preamplifier (either RA16SD or PZ2) with a hardware high-pass filter of 2.2Hz, a low-pass filter of 7.5 kHz (-3dB point) and sampled with a rate of 24.4kHz. As in previous studies[14,53,54], the digitized signals were band-pass filtered (500Hz-5kHz), full-wave rectified and low-pass filtered (200Hz) to produce an envelope of the multi-unit activity (MUA). This MUA signal provides an average of spiking activity of a number of neurons in the vicinity of the tip of the electrode and the population response obtained with this method is therefore expected to be identical to the population response obtained by pooling across single units[55-57]. We applied a low-pass filter (<200Hz) to record the local field potential (LFP), and sampled it at 763Hz. We corrected the LFP for the amplitude changes and phase shifts that were induced by the filters in the preamplifier, as has been described in Supplementary Information.

We corrected for the change in amplitude and phase shifts induced by the hardware filters (Nelson et al. 2008). To determine the filter characteristics we generated 15 windows of 60 seconds white noise in Matlab (The MathWorks, Inc), used the sound card of the PC for

output and attenuated the signal with a voltage divider. We fed the signal to the headstage and preamplifier, and for comparison also to a DC amplifier (TDT RA8GA). As expected, the power spectrum of the signal recorded with the DC amplifier was flat, while the lower frequencies were attenuated in the signal recorded through the head-stage and preamplifier. We calculated the phase spectrum between the two signals as well as the amplitude spectrum of the regular preamplifier and fitted sigmoidal functions to these spectra. We used the fitted functions to correct LFP signals in the frequency domain.

We used multi-contact 'U' probes (Plexon) for the laminar recordings with 24 contact points spaced 100µm apart (**Figure 1B**). Either the metal shaft of the probe or a silver/silver chloride wire in the recording chamber served as reference. We used a blunt guide tube to exert slight pressure on the dura and we then quickly inserted the tip of the probe using a micro-manipulator (Narishige, Japan). The moment when the first contact point passed the dura was ascertained by careful visual inspection of the LFP and listening to the MUA. Once the probe passed through the dura, the guide tube and the probe were moved upward until the dura showed no sign of dimpling. This procedure was done quickly to minimize the time of applying pressure to the cortex. The probe was then lowered into the cortex at very low speeds (~2-5µm/s). We obtained high quality spiking activity with this method and observed no shifts in the depth of the probe the during recording sessions.

We calculated the one-dimensional current source density (CSD) from the LFP following Mitzdorf [58] as:

$$CSD(x) = -\sigma \cdot \frac{\phi(x-h) - 2\phi(x) + \phi(x+h)}{h^2}$$

Where ϕ is the voltage, x is the point at which the CSD is calculated, h is the spacing of electrodes for the computation (here we used a spacing of 200µm) and σ is the conductivity of cortical tissue (we used a value of $0.4 S.m^{-1}$)[59]. The CSD is negative if currents flow towards the electrode (sink) and positive if currents flow away from the contact points (source)[58,60].

To determine the depth of the electrode we measured the CSD evoked by a full-screen 100% contrast checkerboard (presented for 250ms while the monkey fixated, check size 0.3°)[26,27,58].

We estimated the location of the border between layer 5 and layer 4C as the polarity reversal from current sinks in layer 4C to current sources in the deep layers around 40ms after stimulus onset[26,61]. We placed the electrode so that the CSD reversal was as close as possible to the 8th contact from the tip to ensure coverage of all cortical layers. Final alignment was done on the basis of evoked potential by the curve stimuli (**Figure 1I**). We estimated the position of the other layers on the basis of published histological data[62,63]. We mapped the receptive fields (RFs) of the neurons at every recording site of the electrode (see below for the RF mapping methods). When the RFs of the recording sites in different layers did not overlap, indicating that the probe was not perpendicular to the cortical surface, the probe was retracted and inserted at a different location. We calculated the signal-to-noise-ratios (SNR) of every MUA recording site as the height of the peak of the stimulus-evoked response divided by the standard deviation of activity in the prestimulus period. Only recording sites with an SNR>3 were included in the analysis.

Eye movements were recorded with a video eye-tracker (Thomas recordings) with a sampling rate of 350Hz. Trials containing microsaccades were discarded, microsaccades were defined as a minimum of 5 consecutive samples in which the speed of the eye movement was higher than 5 times the standard deviation.

We corrected for the change in amplitude and phase shifts induced by the hardware filters (Nelson et al. 2008). To determine the filter characteristics we generated 15 windows of 60 seconds white noise in Matlab (The MathWorks, Inc), used the sound card of the PC for output and attenuated the signal with a voltage divider. We fed the signal to the headstage and preamplifier, and for comparison also to a DC amplifier (TDT RA8GA). As expected, the power spectrum of the signal recorded with the DC amplifier was flat, while the lower frequencies were attenuated in the signal recorded through the head-stage and preamplifier. We calculated the phase spectrum between the two signals as well as the amplitude spectrum of the regular preamplifier and fitted sigmoidal functions to these spectra. We used the fitted functions to correct LFP signals in the frequency domain.

Data analysis and statistics

The MUA response at each recording site was normalized by subtracting the spontaneous activity, measured from -150ms to 0ms before stimulus onset, and by dividing the response by the peak response (calculated as the maximum response in a window 50-90ms after stimulus onset) of the recording site in the distractor condition. We normalized the CSD of each penetration by dividing by the maximum absolute value of the CSD across layers during the fixation period in the target curve condition.

To generate the average MUA and CSD per electrode depth we first aligned the depth of the different penetrations using the CSD for realigning the probes. The realigned, normalized CSD data and normalized MUA signals were then averaged across penetrations. We assigned recording sites to one of three laminar compartments based on their distance from the layer 4c/layer 5 boundary. The assignments were made with reference to previous anatomical studies[62,63], which measured the thickness of the cortical layers in V1. Recording sites between 0.55 and 0.05mm below the 4c/5-boundary were assigned to the deep layers, sites between 0.05 and 0.55mm above the boundary were assigned to layer 4 and sites between 0.65mm and 1.15mm above the boundary were assigned to the superficial layers.

Our method to calculate the latency of the visual response was similar to previously described methods[19,64]. We fitted the sum of a Gausian and a cumulative Gausian to the data and determined the latency as the time point at which the fitted curve reached 33% of its maximum.

We quantified the amplitude of the normalized CSD pattern over time (nCSD). To this aim, we first computed the laminar template, which we defined as the average laminar profile in the modulation period which we normalized the laminar template to the channel with the strongest sink. The nCSD is the inner product of the laminar template and the momentary CSD.

To calculate the correlation coefficient an average over pair-wise correlations was taken. For the comparisons within tasks, all possible comparisons were taken, i.e. the number of paired correlations equaled 0.5*N*(N-1), where N is the number of penetrations. For the comparisons between tasks, only the comparisons from the same penetration were taken, i.e

the number of paired correlations equaled N. For shuffled controls, the channels from one element of the comparison were randomly shuffled.

Receptive-field measurements

We measured the V1 receptive field dimensions by determining the onset and offset of the response to a slowly moving light bar for each of eight movement directions (**Figure S3**)[65]. The MUA RF size was 1.4 deg on average (with an s.d. of 0.25 deg) and the eccentricity was between 2.1 and 7.8 deg (median = 5.3 deg). No difference between average eye position or the standard deviation of the eye position was observed between conditions (**Figure S4**).

Statistics

We used ANOVAs to estimate the significance of MUA and CSD patterns across the layers with laminar compartment as factor for MUA (deep, layer 4 and superficial) and the channels of the laminar electrode for CSD because this method corrects for correlated data of channels of individual penetrations. For the MUA, data from individual recording sites within a laminar compartment of the same penetration were first averaged and these averages entered into the statistical tests. If necessary, we applied the Greenhouse-Geisser correction for deviations from sphericity. For post-hoc testing we used t-tests and we used two sampled t-tests to compare results from different tasks. Welch's t-tests were used if there were differences in variance between the two datasets.

References

1. Sperling,G. The information available in brief visual presentations. *Psychological Monographs: General and Applied* **74**, 1-29 (1960).

2. Phillips,W.A. Short-term visual memory. *Phil. Trans. R. Soc. Lond. B* **302**, 295-309 (1983).

3. Luck,S.J. & Vogel,E.K. The capacity of visual working memory for features and conjunctions. *Nature* **390**, 279-281 (1997).

4. Sligte,I.G., Scholte,H.S., & Lamme,V.A. Are there multiple visual short-term memory stores? *PLoS. ONE.* **3**, e1699 (2008).

5. Fuster,J.M. & Alexander,G.E. Neuron activity related to short-term memory. *Science* **173**, 652-654 (1971).

6. Funahashi,S., Bruce,C.J., & Goldman-Rakic,P.S. Mnemonic coding of visual space in the monkey's dorsolateral prefrontal cortex. *J. Neurophysiol.* **61**, 331-349 (1989).

7. Miller,E.K., Erickson,C.A., & Desimone,R. Neural mechanisms of visual working memory in prefrontal cortex of the macaque. *J. Neurosci.* **16**, 5154-5167 (1996).

8. Pasternak,T. & Greenlee,M.W. Working memory in primate sensory systems. *Nature Reviews Neuroscience* **6**, 97-107 (2005).

9. Mendoza-Halliday,D., Torres,S., & Martinez-Trujillo,J.C. Sharp emergence of feature-selective sustained activity along the dorsal visual pathway. *Nat. Neurosci.* **17**, 1255-1262 (2014).

10. Tanaka,Y. & Sagi,D. A perceptual memory for low-contrast visual signals. *Proc. Natl. Acad. Sci. U. S. A* **95**, 12729-12733 (1998).

11. Harrison,S.A. & Tong,F. Decoding reveals the contents of visual working memory in early visual areas. *Nature* **485**, 632-635 (2009).

12. Serences,J.T., Ester,E.F., Vogel,E.K., & Awh,E. Stimulus-specific delay activity in human primary visual cortex. *Psychol. Sci.* **20**, 207-214 (2009).

13. Viswanathan,A. & Freeman,R.D. Neurometabolic coupling in cerebral cortex reflects synaptic more than spiking activity. *Nat. Neurosci.* **10**, 1308-1312 (2007).

14. Logothetis,N.K., Pauls,J., Augath,M., & Oeltermann,A. Neurophysiological investigation of the basis of the fMRI signal. *Nature* **412**, 150-157 (2001).

15. Maier,A. *et al.* Divergence of fMRI and neural signals in V1 during perceptual suppression in the awake monkey. *Nat. Neurosci.* **11**, 1193-1200 (2008).

16. Supèr,H., Spekreijse,H., & Lamme,V.A.F. A neural correlate of working memory in the monkey primary visual cortex. *Science* **293**, 120-124 (2001).

17. Roelfsema,P.R., Lamme,V.A.F., & Spekreijse,H. Object-based attention in the primary visual cortex of the macaque monkey. *Nature* **395**, 376-381 (1998).

18. Roelfsema,P.R. Cortical algorithms for perceptual grouping. *Annu. Rev. Neurosci.* **29**, 203-227 (2006).

19. Roelfsema,P.R., Tolboom,M., & Khayat,P.S. Different processing phases for features, figures, and selective attention in the primary visual cortex. *Neuron* **56**, 785-792 (2007).

20. Gilbert,C.D. & Li,W. Top-down influences on visual processing. *Nat. Rev. Neurosci.* **14**, 350-363 (2013).

21. Pooresmaeili,A. & Roelfsema,P.R. A Growth-Cone Model for the Spread of Object-Based Attention during Contour Grouping. *Curr. Biol.* **24**, 2869-2877 (2014).

22. Houtkamp,R., Spekreijse,H., & Roelfsema,P.R. A gradual spread of attention during mental curve tracing. *Percept. Psychophys.* **65**, 1136-1144 (2003).

23. McCormick,P.A. & Jolicoeur,P. Capturing visual attention and the curve tracing operation. *J. Exp. Psychol. : Hum. Percept. Perform.* **18**, 72-89 (1992).

24. Jolicoeur,P., Ullman,S., & MacKay,M. Visual curve tracing properties. *J. Exp. Psychol. : Hum. Percept. Perform.* **17**, 997-1022 (1991).

25. Sligte,I.G., Scholte,H.S., & Lamme,V.A. V4 activity predicts the strength of visual short-term memory representations. *J. Neurosci.* **29**, 7432-7438 (2009).

26. Schroeder,C.E., Tenke,C.E., Givre,S.J., Arezzo,J.C., & Vaughan,H.G., Jr. Striate cortical contribution to the surface-recorded pattern-reversal VEP in the alert monkey. *Vision Res.* **31**, 1143-1157 (1991).

27. Self,M.W., van,K.T., Super,H., & Roelfsema,P.R. Distinct roles of the cortical layers of area V1 in figure-ground segregation. *Curr. Biol.* **23**, 2121-2129 (2013).

28. Lund,J.S. Anatomical organization of macaque monkey striate visual cortex. *Annu. Rev. Neurosci.* **11**, 253-288 (1988).

29. Binzegger,T., Douglas,R.J., & Martin,K.A. A quantitative map of the circuit of cat primary visual cortex. *J. Neurosci.* **24**, 8441-8453 (2004).

30. Poort,J. *et al.* The role of attention in figure-ground segregation in areas V1 and V4 of the visual cortex. *Neuron* **75**, 143-156 (2012).

31. Li,W., Thier,P., & Wehrhahn,C. Contextual influence on orientation discrimination of humans and responses of neurons in V1 of alert monkeys. *J. Neurophysiol.* **83**, 941-954 (2000).

32. Rockland,K.S. & Virga,A. Terminal arbors of individual "feedback" axons projecting from area V2 to V1 in the macaque monkey: a study using immunohistochemistry of anterogradely transported Phaseolus vulgaris-leucoagglutinin. *J. Comp. Neurol.* **285**, 54-72 (1989).

33. Anderson,J.C. & Martin,K.A. The synaptic connections between cortical areas V1 and V2 in macaque monkey. *J. Neurosci.* **29**, 11283-11293 (2009).

34. Alvarez,G.A. & Cavanagh,P. The capacity of visual short-term memory is set both by visual information load and number of objects. *Psychol. Sci.* **15**, 106-111 (2004).

35. Cabeza,R. & Nyberg,L. Imaging cognition II: An empirical review of 275 PET and fMRI studies. *J. Cogn Neurosci.* **12**, 1-47 (2000).

36. Cabeza,R. & Nyberg,L. Imaging Cognition: An Empirical Review of PET Studies with Normal Subjects. *J. Cogn Neurosci.* **9**, 1-26 (1997).

37. Olivers,C.N. Interactions between visual working memory and visual attention. *Front Biosci.* **13**, 1182-1191 (2008).

38. Riggall,A.C. & Postle,B.R. The relationship between working memory storage and elevated activity as measured with functional magnetic resonance imaging. *J. Neurosci.* **32**, 12990-12998 (2012).

39. Albers,A.M., Kok,P., Toni,I., Dijkerman,H.C., & de Lange,F.P. Shared representations for working memory and mental imagery in early visual cortex. *Curr. Biol.* **23**, 1427-1431 (2013).

40. Mongillo,G., Barak,O., & Tsodyks,M. Synaptic theory of working memory. *Science* **319**, 1543-1546 (2008).

41. Luck,S.J., Chelazzi,L., Hillyard,S.A., & Desimone,R. Neural mechanisms of spatial selective attention in areas V1, V2, and V4 of macaque visual cortex. *J. Neurophysiol.* **77**, 24-42 (1997).

42. Ekstrom,L.B., Roelfsema,P.R., Arsenault,J.T., Bonmassar,G., & Vanduffel,W. Bottom-up dependent gating of frontal signals in early visual cortex. *Science* **321**, 414-417 (2008).

43. Gazzaley,A. & Nobre,A.C. Top-down modulation: bridging selective attention and working memory. *Trends Cogn. Sci.* **16**, 129-135 (2012).

44. Awh,E. & Jonides,J. Overlapping mechanisms of attention and spatial working memory. *Trends Cogn. Sci.* **5**, 119-126 (2001).

45. O'Herron,P. & von der Heydt,R. Short-term memory for figure-ground organization in the visual cortex. *Nature Neurosci.* **61**, 801-809 (2009).

46. Riesenhuber,M. & Poggio,T. Neural mechanisms of object recognition. *Curr. Opin. Neurobiol.* **12**, 162-168 (2002).

47. Rust,N.C., Mante,V., Simoncelli,E.P., & Movshon,J.A. How MT cells analyze the motion of visual patterns. *Nat. Neurosci.* **9**, 1421-1431 (2006).

48. Serre,T., Oliva,A., & Poggio,T. A feedforward architecture accounts for rapid categorization. *Proc. Natl. Acad. Sci. U. S. A* **104**, 6424-6429 (2007).

49. DiCarlo,J.J., Zoccolan,D., & Rust,N.C. How does the brain solve visual object recognition? *Neuron* **73**, 415-434 (2012).

50. Markov,N.T. *et al.* Weight consistency specifies regularities of macaque cortical networks. *Cereb. Cortex* **21**, 1254-1272 (2011).

51. Maunsell,J.H.R. & Gibson,J.R. Visual response latencies in striate cortex of the macaque monkey. *J. Neurophysiol.* **68**, 1332-1344 (1992).

52. Nowak,L.G., Munk,M.H.J., Girard,P., & Bullier,J. Visual latencies in areas V1 and V2 of the macaque monkey. *Vis. Neurosci.* **12**, 371-384 (1995).

53. Supèr,H. & Roelfsema,P.R. Chronic multi-unit recordings in behaving animals: advantages and limitations. *Prog. Brain Res.* **147**, 263-282 (2005).

54. Xing,D., Yeh,C.-I., & Shapley,R.M. Spatial spread of the local field potential and its laminar variation in visual cortex. *J. Neurosci.* **29**, 11540-11549 (2009).

55. Logothetis,N.K. The neural basis of the blood-oxygen-level-dependent functional magnetic resonance imaging signal. *Philos. Trans. R. Soc. Lond B Biol. Sci.* **357**, 1003-1037 (2002).

56. Super,H. & Roelfsema,P.R. Chronic multiunit recordings in behaving animals: advantages and limitations. *Prog. Brain Res.* **147**, 263-282 (2005).

57. Cohen,M.R. & Maunsell,J.H. Attention improves performance primarily by reducing interneuronal correlations. *Nat. Neurosci.* **12**, 1594-1600 (2009).

58. Mitzdorf,U. Current source-density method and application in cat cerebral cortex: investigation of evoked potentials and EEG phenomena. *Physiol. Rev.* **65**, 37-100 (1985).

59. Logothetis,N.K., Kayser,C., & Oeltermann,A. In vivo measurement of cortical impedance spectrum in monkeys: implications for signal propagation. *Neuron* **55**, 809-823 (2007).

60. Buzsaki,G., Anastassiou,C.A., & Koch,C. The origin of extracellular fields and currents--EEG, ECoG, LFP and spikes. *Nat. Rev. Neurosci.* **13**, 407-420 (2012).

61. Mitzdorf,U. & Singer,W. Excitatory synaptic ensemble properties in the visual cortex of the macaque monkey: a current source density analysis of electrically evoked potentials. *J. Comp Neurol.* **187**, 71-83 (1979).

62. Lund,J.S. Organization of neurons in the visual cortex, area 17, of the monkey (macaca mulatta). *J. Comp. Neurol.* **147**, 455-495 (1973).

63. O'Kusky,J. & Colonnier,M. A laminar analysis of the number of neurons, glia, and synapses in the adult cortex (area 17) of adult macaque monkeys. *J. Comp Neurol.* **210**, 278-290 (1982).

64. Self,M.W., van,K.T., Super,H., & Roelfsema,P.R. Distinct roles of the cortical layers of area V1 in figure-ground segregation. *Curr. Biol.* **23**, 2121-2129 (2013).

65. Kato,H., Bishop,P.O., & Orban,G.A. Hypercomplex and simple/complex cell classifications in cat striate cortex. *J. Neurophysiol.* **41**, 1072-1095 (1978).

SUPPLEMENTARY INFORMATION

Supplementary Figures

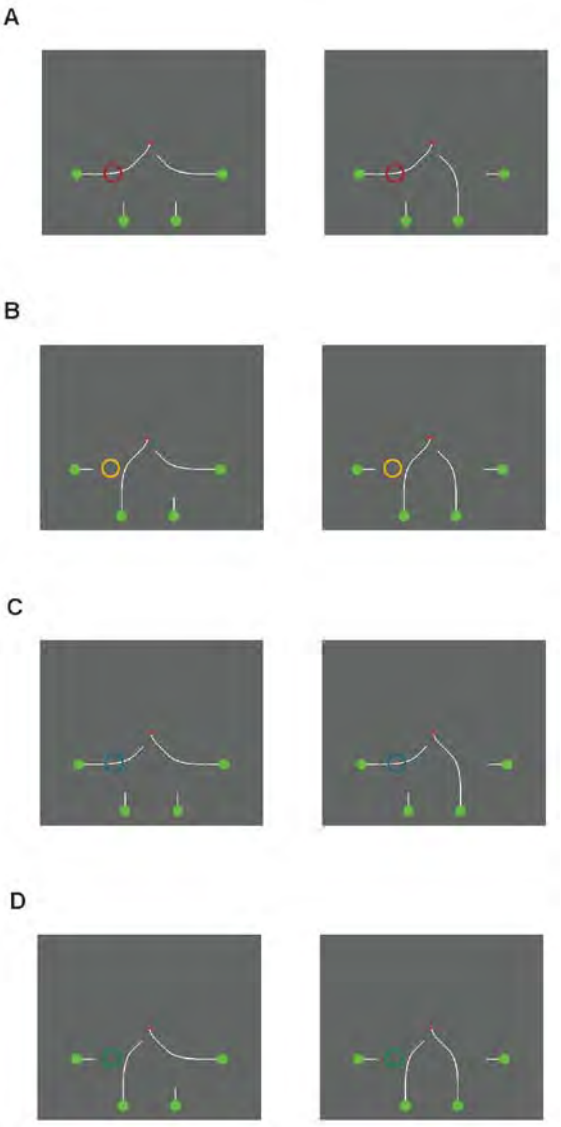

Figure S1 | The stimulus conditions. There were two stimuli for each of the conditions. The target (**A**) or distractor curve (**B**) fell in the receptive field or the target (**C**) or distractor curve (**D**) fell next to the receptive field. Circles indicate the position of the receptive fields.

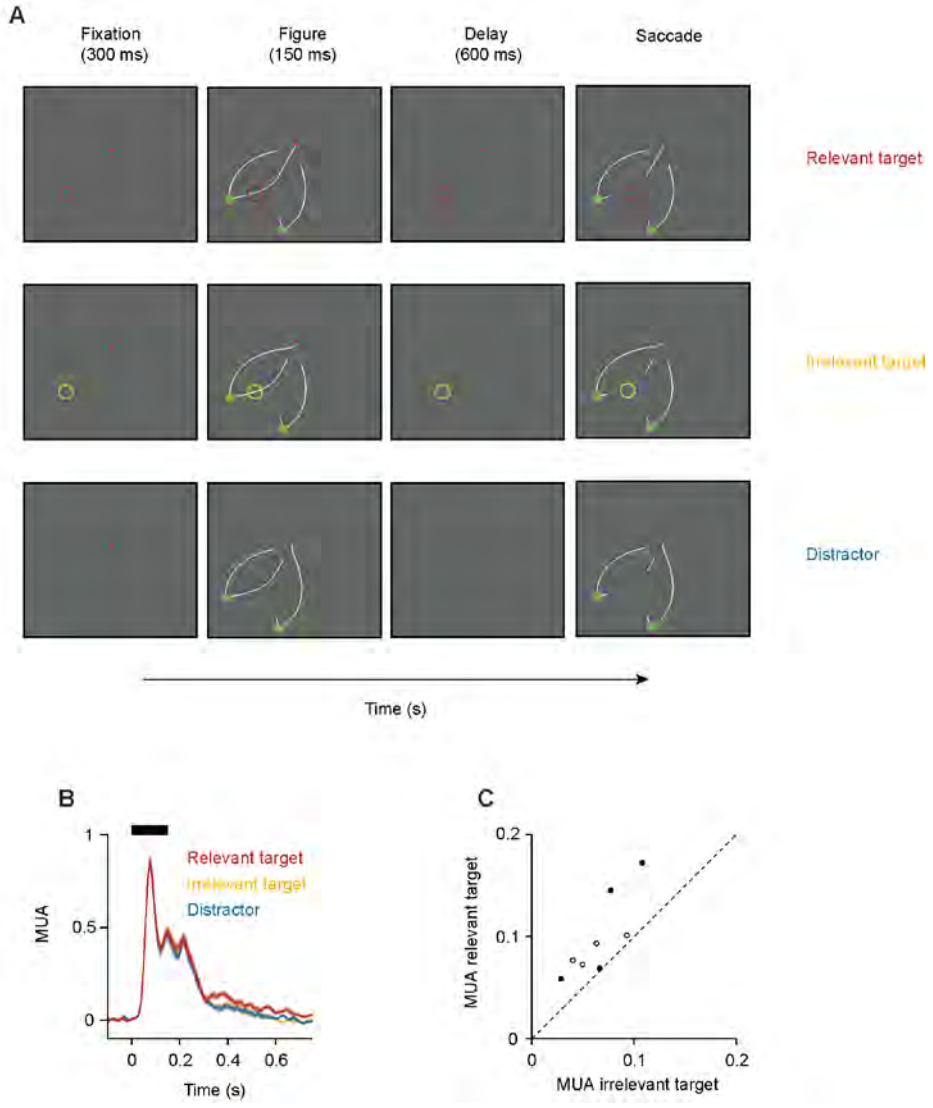

Figure S2 | Dissociating short-term memory from the saccade plan. (**A**) The monkeys were trained to fixate on the red dot and to make an eye movement to the target at the end of the curve that was connected to the fixation dot, after a memory delay. The receptive field could be on the target curve (red condition, upper row), on an adjacent distractor curve (yellow condition, middle row) or on a far distractor curve (blue condition, lower row). Note that the eye movements in the target and adjacent distractor conditions were identical, but that the receptive field only fell on (the memory of) the relevant curve in the target condition. (**B**) The average MUA response elicited by the memory

of the target curve is elevated relative to that elicited by the adjacent and far distractor. Thus, the V1 working memory trace depends on the course of the curve and not on the impending eye movement. Shaded areas show s.e.m. (*n*=8 penetrations). (**C**) MUA elicited by the target condition and the adjacent distractor in a window from 200-750ms after stimulus onset (filled circles for monkey E, open circles for monkey R). All data points lie above the diagonal, indicating that the MUA for the memory of the target curve was stronger than that for the adjacent distractor in all penetrations(t-test, $p<0.001$ for both monkeys).

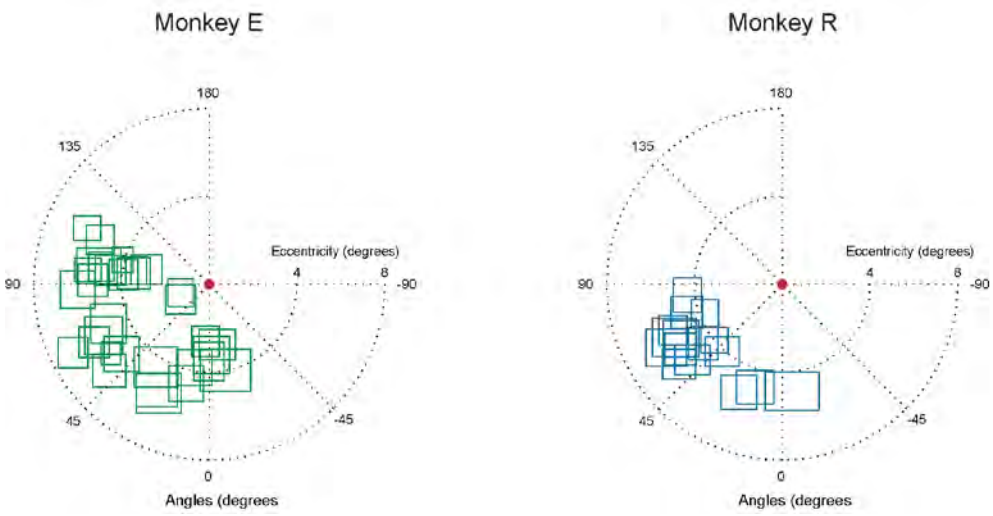

Figure S3 | Position and size of the multiunit RFs. The rectangles indicate the average position and size of the RFs in each penetration. Monkey E, green squares. Monkey R, blue squares.

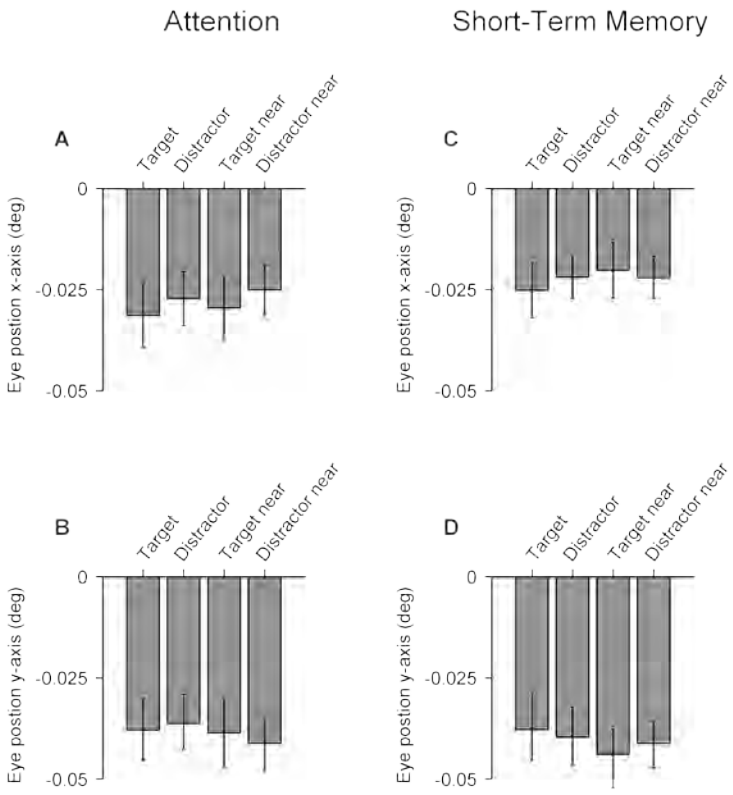

Figure S4 | Eye position. (**A**, **C**) X and (**B**, **D**) Y eye position for (A, B) the attentional and (C, D) the short-term memory task.

Chapter 4 | Alpha and gamma oscillations characterize feedback and feedforward processing in monkey visual cortex

Timo van Kerkoerle, Matthew W. Self, Bruno Dagnino, Marie-Alice Gariel-Mathis, Jasper Poort, Chris van der Togt, and Pieter R. Roelfsema

ABSTRACT

Cognitive functions rely on the coordinated activity of neurons in many brain regions but the interactions between cortical areas are not yet well understood. Here we investigated whether low-frequency (alpha) and high-frequency (gamma) oscillations characterize different directions of information flow in monkey visual cortex. We recorded from all layers of the primary visual cortex (V1) and found that gamma waves are initiated in input layer 4 and propagate to the deep and superficial layers of cortex, whereas alpha waves propagate in the opposite direction. Simultaneous recordings from V1 and downstream area V4 confirmed that gamma and alpha waves propagate in the feedforward and feedback direction, respectively. Microstimulation in V1 elicited gamma oscillations in V4, whereas microstimulation in V4 elicited alpha oscillations in V1, thus providing causal evidence for the opposite propagation of these rhythms. Furthermore, blocking NMDA receptors, thought to be involved in feedback processing, suppressed alpha while boosting gamma. These results provide new insights into the relation between brain rhythms and cognition.

INTRODUCTION

Areas of the visual cortex are arranged hierarchically with low-level areas representing simple features and higher areas representing the more complex aspects of the visual world[1,2]. Neurons in many visual areas are co-active during the perception of a visual stimulus and it is difficult to disentangle the influences of lower areas onto higher areas from the effects that go in the opposite direction [3]. Studies of visual cognition could benefit enormously from markers of cortical activity that distinguish between feedforward and feedback effects. One such putative marker is cortical oscillatory activity, because oscillations of different frequencies have been proposed to propagate either in feedforward or in the feedback direction[4,5], but experimental evidence for this view is sparse[6].

Low frequency rhythms, like the alpha rhythm which is particularly pronounced in the visual cortex, have been proposed to characterize spontaneous activity[7,8] as the alpha rhythm increases when the subject closes the eyes[9]. More recent observations have also implicated alpha oscillations in the active suppression of irrelevant, unattended information[10,11]. In contrast, the high-frequency gamma rhythm increases if visual stimuli are presented, and in particular if they are task-relevant[12,13]. One influential hypothesis has been that gamma oscillations play a role in feature binding[14], but later studies casted doubt on this proposal[15,16]. A more recent hypothesis holds that gamma oscillations facilitate the communication between cortical areas[17], but both evidence in favor of this proposal[18] and against it[19-22] has been presented. Although the causal role of oscillatory rhythms in cognition is therefore not undisputed, it would also be of great value if oscillations could be used as markers for feedforward and feedback effects[23].

We therefore aimed to resolve, for the first time, the laminar pattern of low and high frequency oscillations in V1 with a high spatial resolution during a texture segregation task that requires interactions between visually driven activity and top-down influences from higher areas. For comparison, we also examined oscillatory coupling between V1 and extrastriate area V4 in the same task. Moreover, we here used two new, causal approaches to test directionality. First, we applied microstimulation in one area while recording the oscillations in the other area. Second, we locally infused blockers of AMPA and NMDA-receptors thought to be differentially involved in feedforward and feedback processing[24,25].

All our results converged onto a straightforward conclusion: gamma oscillations in visual cortex travel in the feedforward direction whereas alpha oscillations index feedback effects.

RESULTS

We first investigated the power and the timing of oscillatory activity in the different layers of area V1. Anatomical studies demonstrated that the feedforward input from the lateral geniculate nucleus arrives predominantly in layer 4C with a weaker input into layer 6[26], whereas feedback connections from higher visual areas target layers 1, 2 and 5, avoiding layer 4[27,28]. If alpha and gamma activity travel in opposite directions through the cortex this might therefore be visible in the laminar profile of these rhythms in V1.

To measure oscillatory activity in V1, we recorded multi-unit neuronal activity (MUA) and local field potentials (LFP) using laminar electrodes that span the cortical depth with contact points spaced 100μm apart (**Figure 1A**,**B**). An important advantage of these laminar electrodes is that they permit the computation of the current-source density (CSD), which estimates currents flowing into and out of neurons in different layers[29,30]. We determined the cortical depth of the laminar electrode in each recording session with the CSD response triggered by the appearance of a checkerboard stimulus[31]. The stimulus evoked a characteristic CSD profile with a current sink in layer 4C and a current source in the deep layers (**Figure S1**). These sinks and sources coincided with the onset of the visual response in the MUA.

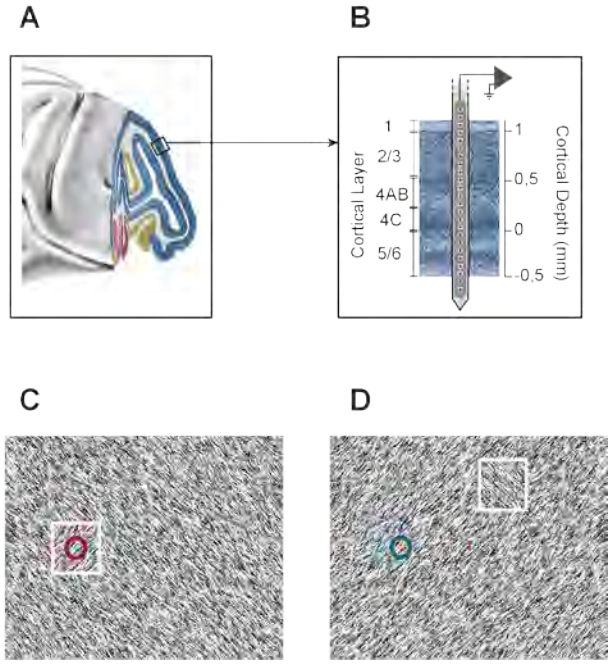

Figure 1 | Laminar recordings. (**A**) Lateral view of the macaque brain. Blue region corresponds to area V1. (**B**) Laminar recording with the multi-site linear electrode (Plexon Inc. U-probe). (**C**,**D**) Texture segregation stimulus with a figure of one orientation placed on a background with the orthogonal orientation. The neurons' receptive field (circle) fell on the figure (white square, not visible to the monkey) (C) or on the background (D).

Oscillatory activity in V1 in a texture-segregation task

We trained monkeys to carry out a figure-ground segregation task in which they detected an orientation defined figure (**Figure 1C**,**D**)[32]. The monkeys started a trial by directing their gaze to a fixation point, and after a delay of 300ms a full screen texture appeared with texture elements with one orientation and a square figure (4 deg size) of the opposite orientation (**Figure 1C**). After an additional 300ms of fixation, the monkey made an eye movement towards the figure to obtain a juice reward. On each trial, the figure appeared at one of three locations at the same eccentricity. In one of these conditions, the neurons' receptive fields (RFs) fell on the figure centre, in the other two conditions the RFs fell on the background (**Figure 1D**). We balanced the orientation of the line elements across trials so that the texture elements inside the RFs were on average identical across conditions and we ensured that the RFs of none of the recording sites overlapped with the figure edge. As

previously reported[32], MUA in V1 (24 penetrations with a total of n=493 recording sites, 13 penetrations in monkey S and 11 penetrations in monkey E) was stronger if the neurons' RF fell on the figure than when it fell on the background (**Figure 2A**), a modulatory effect that most likely depends on feedback from higher areas[33-35].

Examination of the LFP also revealed a prominent signature of figure-ground organization. The background texture evoked a strong low frequency oscillation, which could be seen in single trials (arrows in **Figure 2B**), but the low frequency oscillations elicited by the figure were weaker. To further characterize these oscillations, we computed the power spectrum in a window from 150-350ms from stimulus onset. This analysis revealed a prominent peak in the lower frequencies (5-15Hz), which was larger if the RF fell on the background than if it fell on the figure (**Figure 2*C***; **Figure S2A**,**D**) and also stronger than in the pre-stimulus period (**Figure 2C**; **S2C**) (t–test, n=493, P<0.001 for both comparisons). We next analyzed of the LFP-MUA coherence, focusing on the internally generated oscillations by first subtracting the evoked potential (**Figure S3**), and found that the MUA was also more strongly locked to the low-frequency rhythm if the RF fell on the background (**Figure 2D**, **Figure S2F**). The spectral resolution for the low frequencies was limited by the short duration of the computational window (200ms), but we obtained a comparable results when we analyzed trials with longer reaction times so that we could use a longer time window of 300ms (**Figure S4**). We also analyzed catch trials with a homogeneous background where the monkeys were required to maintain gaze on the fixation point for 700ms (**Figure S5A**-**C**). The MUA in these catch trials was similar to when the figure was placed outside the neurons' RF (**Figure S5H**). The LFP power spectrum and the LFP-MUA coherence in the catch trials were similar to that in the background condition (time-window of 550ms; spectral resolution of ~1.8Hz) with a peak at ~10Hz, indicative of an alpha oscillation (**Figure S5F**,**G**). The alpha peak also remained in a later time-window (400-700ms after stimulus onset) (**Figure S5I**), confirming that the alpha oscillation did not depend on the initial stimulus-evoked activity. The increase of the alpha rhythm when the RF fell on the background compared to when it fell on the figure and compared to the pre-stimulus period is in line with previous reports that alpha indexes the suppression of irrelevant information[10,11]. Moreover, we found that trials with more LFP alpha power (5-15Hz) had a weaker MUA response (**Figure 2E**; cor. coef.= -0.05, t-test, n=493, P<0.05)[36] in further support of this idea.

In contrast to the low-frequency rhythm, the gamma rhythm was stronger in the figure representation than in the background. This increase in gamma was visible in the LFP power spectrum (**Figure 2C**, **Figure S2A**,**E**) and also in the coherence between the MUA and the LFP (**Figure 2D**, **Figure S2G**) (*t*–test, n=493, P<0.001 for both comparisons). When we sorted trials according to gamma power (40-90Hz), trials with a higher gamma were associated with a stronger MUA response (**Figure 2E**; cor. coef.=0.3, *t*-test, P<0.001)[37]. We also investigated the intermediate beta band (15-30Hz), but beta power and coherence was only weakly modulated by the task (**Figure 2C**,**D** and **Figure S2A**). The weak beta oscillations differentiate V1 from the primary somatosensory cortex where beta power is much more prominent[38].

To analyze the profile of LFP power across the layers, we divided them into four compartments: layers 1/2, layer 3, layer 4 and layers 5/6. The alpha power was strongest in layers 5/6 (*t*-test, n=24 penetrations, all Ps<0.001) with a secondary peak in layer 1/2 (layers 1/2 higher than layers 3 and 4*;* *t*-test, P<0.001) (**Figure 2F**,**G**) as has been observed previously[13,39]. In contrast, gamma power was stronger in layer 3 than in the other layers (**Figure 2F**,**G***;* *t*-test, all Ps<0.001)[39,40]. The laminar pattern of LFP power was similar, irrespective of whether the RF fell on figure or ground (**Figure 2*G***). Thus, the cortical mechanisms that generate the alpha and gamma rhythm appear to be similar for figure and background, but task-relevance modulates the amplitude of these rhythms.

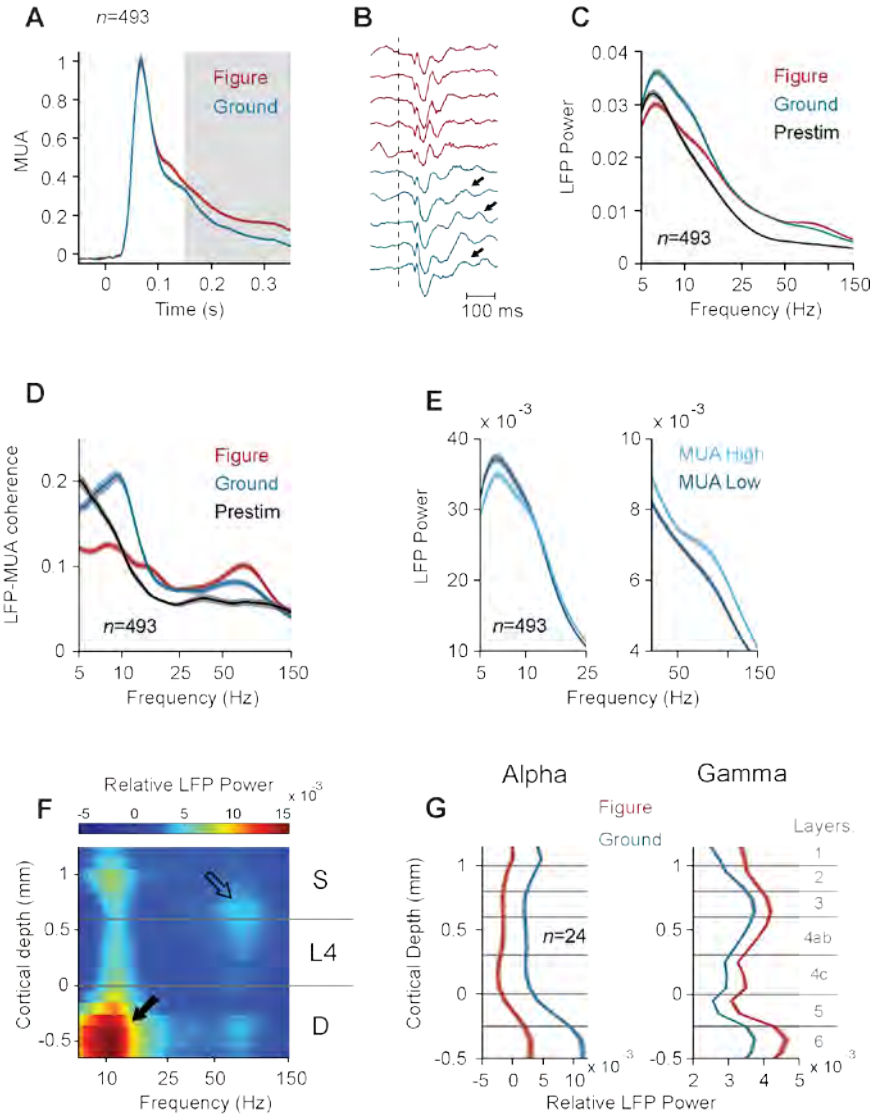

Figure 2 | Neuronal activity in the texture-segregation task. (**A**) Average MUA response in V1 evoked by the figure (red trace) and the background (blue trace) (*n*=493 recording sites). Grey area highlights the modulation period (150-350ms after stimulus onset). (**B**) Example LFP responses in successive trials at an example electrode, elicited by image elements of the figure (red) and background (blue). Dotted line indicates the stimulus onset, arrows indicate slow frequency oscillations. (**C**) Average LFP power spectrum (arbitrary units) evoked by the figure (red trace) and background (blue trace) during the modulation period and the pre-stimulus period (200-0ms before stimulus onset) (black trace). (**D**) Average LFP-MUA coherence in the figure (red trace) and

background condition (blue trace) during the modulation period, and the pre-stimulus period (black trace). The dashed lines indicate the LFP-MUA coherence for shuffled trials. (**E**) LFP power spectra calculated for the 50% trials with lowest (dark blue lines) and highest MUA response (light blue lines) in the conditions with the RF on the background. (**F**) Laminar profile of the increase in LFP power evoked by the background (power is shown in pseudocolor, arbitrary units, log scale). Black arrow, alpha activity in the deep layers. Open arrow, gamma activity in upper layer 4 and the superficial layers. (**G**) Laminar profile of LFP power in the alpha (5-15Hz) and gamma band (40-90 Hz) in the conditions with the RF on the figure (red traces) and background (blue traces). Shaded areas show s.e.m. in all plots (*n*=493 recording sites), when they are difficult to see the s.e.m. is small.

Propagation of alpha and gamma oscillations through the layers of V1

The use of a laminar electrode with a fine spacing between contact points provided us with a unique opportunity to investigate the propagation of rhythmic activity from one layer to the next. We investigated the LFP in all layers, aligning activity to the LFP troughs in layer 4C (**Figure S6**). To detect the time of alpha troughs we filtered the LFP between 8 and 12Hz and registered the times of the minima. These narrow filter settings were only used to detect trough times; all further analyses were performed with the broad-band LFP signal (**Figure S6D**). We used the alpha troughs time-points to compute the average trough-aligned LFP, in the same way that one would align the LFP to the stimulus presentations to compute the evoked potential. We applied this analysis to the broad-band LFP in the background condition where alpha was most pronounced and averaged across all penetrations (n=24). In the LFP, the alpha oscillations were relatively coherent across cortical depth (**Figure 3*A***), but this signal also contains contributions from volume conduction. The CSD provides a local measure for the sinks and sources underlying the LFP in the different layers. The CSD profile had the shape of a chevron with a succession of sinks starting in feedback recipient layers 1, 2 and 5 that propagated towards layer 4 during the alpha cycle (**Figure 3B**). The MUA was also coupled to the LFP troughs (**Figure 3C**), as predicted by the significant coherence between these signals in the alpha range (**Figure 2D**). Interestingly, we also observed phase differences between MUA in different cortical layers. The earliest MUA coincided with the current sinks in layers 1, 2 and 5 (**Figure 3C**). MUA in layer 4 lagged MUA in the deep and superficial layers by 12 and 10ms, respectively (t-test, n=24 penetrations, both comparisons P<0.005). When we repeated this analysis for other frequency bands, we found that MUA in superficial and deep layers preceded MUA in layer

4 for all frequencies between 5 and 15Hz (**Figure S7**). The same laminar profile was found before stimulus onset, indicating that it was general feature of alpha oscillations, which did not depend on the presence of a visual stimulus (**Figure S8**).

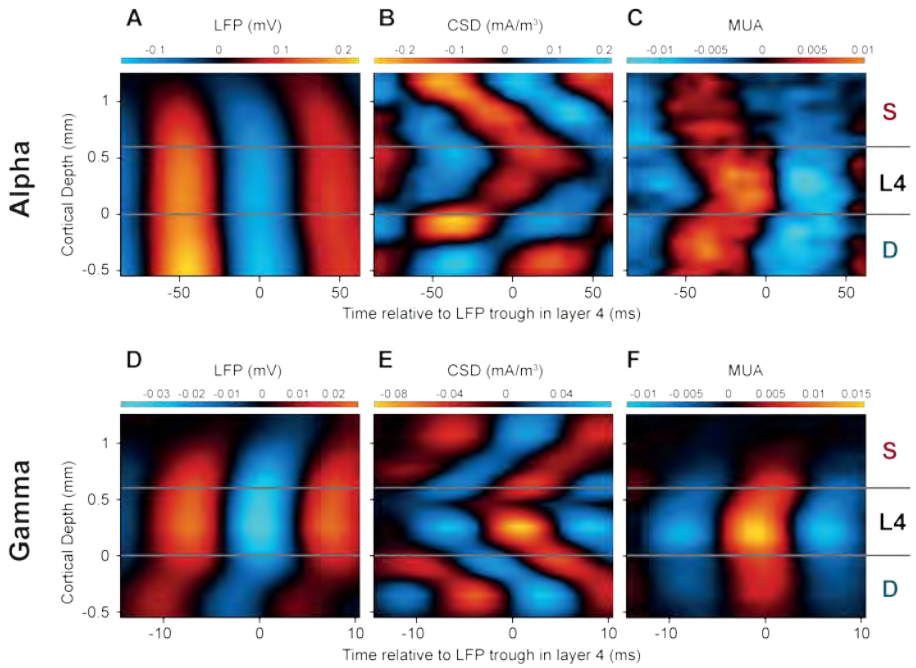

Figure 3 | Laminar profile of cortical oscillations. To determine the average laminar profile of the LFP, CSD and MUA relative to the alpha and gamma oscillations, we aligned the data to the troughs of the LFP in layer 4. (**A**) Laminar profile of the LFP (mV) relative to the alpha troughs in a window from 150-300ms after stimulus onset, averaged across 24 penetrations. The LFP was relatively homogeneous across the layers. Negative potentials are shown in blue, positive potentials in red. (**B**) Average laminar profile of the CSD (mA/m^3) relative to LFP troughs in layer 4 for the alpha rhythm. Current sinks are shown in red, sources in blue. (**C**) MUA aligned to the LFP troughs in layer 4. Red colors show MUA that is higher than the average and blue colors MUA lower than the average. The MUA was normalized to the visually driven activity 150-300ms after stimulus onset. The scale therefore denotes the fraction of the visually driven MUA response that synchronized to the LFP troughs in layer 4 in the 8-12Hz frequency range. (**D-F**) Same analysis as in A-D, but now the data were aligned to the troughs of the gamma rhythm (55-65Hz) in layer 4.

The phase lags in the MUA were less pronounced than in the CSD (**Figure 3B**,**C**), smaller phase differences that might be explained by the neurons' extended dendritic trees.

Neurons sample synaptic input from multiple layers so that the timing of somatic spikes across layers might become more similar than the timing of synaptic inputs in different layers. For example, some layer 4 cells receive input trough their dendrites in layer 2/3 so that they can start to fire action potentials before the alpha related synaptic input arrives in layer 4. To directly investigate the phase relationship between spikes and synaptic input we analyzed the coherence between the MUA and the layer specific CSD for the alpha frequencies (**Figure 4A**). In this analysis we averaged MUA across layers, but we obtained qualitatively comparable results if we separately analyzed MUA from the superficial layers, layer 4 or deep layers (**Figure S9**). We found four coherence peaks; in layers 1/2, 4, 5 and 6. The phase analysis for the alpha rhythm revealed that MUA was in phase with sinks in layers 1/2 and 5 (mean phase advance of CSD sink relative to MUA in L1/2, 23±6° (s.e.m.); L5, -2±8°; n=24) but with sources in layers 4 and 6 (mean phase in L4, -174±7°; L6, 171±5°). These results suggest that the spikes locking to the alpha rhythm are driven by sinks in layers 1/2 and 5, which are the main targets of feedback connections.

We next analyzed the propagation of activity during gamma oscillations. We detected troughs by filtering the LFP between 55 and 65 Hz and then used these time-points to analyze the broad-band LFP, CSD and the MUA (**Figure S6**). Strikingly, gamma oscillations exhibited the opposite sequence of sinks across the layers (**Figure 3D**-**F**). The gamma cycle started with a sink in layer 4, the recipient of feedforward input, and the sinks then propagated to the superficial and deep layers. Spiking activity in layer 4 coincided with the layer 4 current sink, and was delayed by 1ms in the deep layers (t-test, n=24, P<0.05) and by 2ms in the superficial layers (P<0.005)[41], a phase delay that occurred for all frequencies between 20 and 100Hz (**Figure S7**). The analysis of gamma-coherence between MUA and CSD revealed two peaks. The first coherence peak reflected the coincidence of the MUA with a current sink in layer 4 (mean phase advance of CSD sink relative to MUA: 17±4° (s.e.m); n=24) and the second coherence peak occurred in layer 6 where a current sink lagged the MUA by 116±5° (**Figure 4B**). These results suggest that the gamma cycle starts with excitatory input into layer 4, the main target of feedforward connections from the LGN.

The propagation of alpha and gamma oscillations through the layers was highly consistent between monkeys (**Figure S10**). Interestingly, it was also relatively invariant across

conditions with the RF on the background (**Figure 3**), the figure (**Figure S11A-F**) and catch trials (**Figure S11G-L**). We observed a comparable invariance in the phase relation between CSD and MUA, which did not depend strongly on the presence of a figure in the RF (compare **Figure 4** to **Figure S12**). Thus, figure-ground segregation influences the amplitude of the oscillations, but the cortical mechanisms that generate these rhythms appear to be invariant.

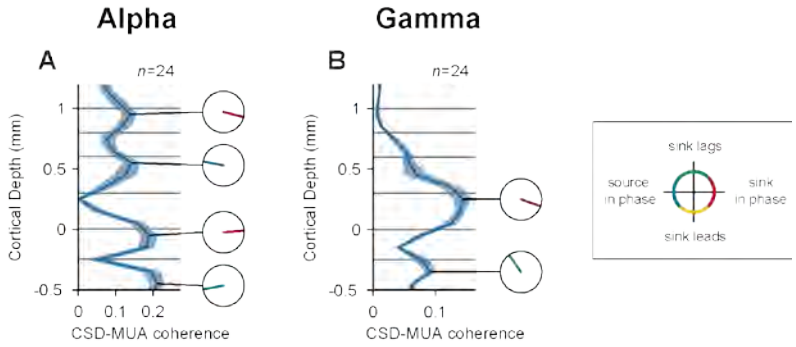

Figure 4 | Laminar profile of CSD-MUA coherence and phase. (**A**) Laminar profile of coherence between the layer-specific CSD and the MUA averaged across all layers, for the alpha band (RF on the background). There were four peaks in the coherence and the small circles show the phase of the CSD relative to the MUA. Red colors indicate that MUA was in phase with a sink in layers 1/2 and 5. Blue colors indicate that the MUA was in phase with a source. (**B**) Laminar profile of the CSD-MUA coherence in the gamma frequency range. Note that the MUA was in phase with a sink in layer 4.

We replicated these results with a phase coherency analysis that does not depend on the detection of troughs. We analyzed the phase of the CSD and MUA in the different layers relative to the LFP in layer 4. For the gamma oscillations, the phase of the CSD and MUA in layer 4 was earlier than that in the other layers (**Figure S13**; *t*-test, n=24, P<0.001 for both MUA and CSD), in accordance with the feedforward laminar profile. Alpha oscillatory activity showed the opposite profile with a phase advance of the deep and superficial layers relative to layer 4 (**Figure S13**; P<0.001 for both MUA and CSD). Thus, the opposite propagation of alpha and gamma oscillations through the cortical layers is a robust finding that does not depend on details of the analysis method.

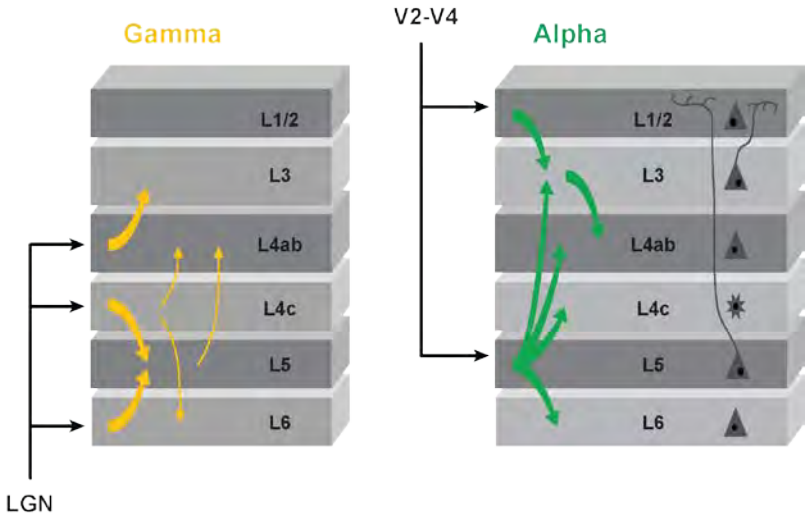

Figure 5 | Schematic representation of Granger causality between layers for the gamma (left) and alpha band (right). Thick arrows indicate Granger causality stronger than 0.015, thin arrows for the gamma band indicate Granger causality between 0.005 and 0.015 (not shown for the alpha band to prevent crowding).

We complemented the analysis of phase differences by measuring Granger causality between the CSDs in the different layers. If oscillations are propagated between layers, then activity in one layer should forecast activity in the next better than the other way around, implying a significant directionality in the Granger causal interactions[38]. As a first step in this analysis, we calculated the average coherence of CSDs between sites on the laminar probe with a distance of 200μm, and found peaks at 10 and 80Hz (**Figure S14**), in accordance with the LFP-MUA coherence (**Figure 2*D***). The Granger causality analysis also revealed a peak around 10Hz, in accordance with a previous study[42], and a broader peak in the gamma range (**Figure S15**). **Figure 5** summarizes the Granger-causal interactions between layers with a significant directionality in the alpha and gamma range. It can be seen that Granger causality in the alpha range was directed from the superficial and deep layers towards layer 4, in accordance with the analysis of phase differences (**Figure 3*B***). The Granger causality showed a strong directionality from layer 5 to layer 6, 4C, 4AB and 3 (permutation test, $P<0.001$), from layer 1/2 to layer 3 (permutation test, $P<0.001$), and from layer 3 to layer 4AB (permutation test, $P<0.001$), indicating that the alpha rhythm originates

from the feedback recipient layers in V1. The Granger causality in the gamma range (30-90Hz) showed a strong directionality from layer 4AB to layer 3, from layers 4C to layer 5 and 6 and from layer 6 to layer 5 (permutation test, all *Ps*<0.001) (**Figure 5**, **Figure S15**), in line with the trough-triggering analysis (**Figure 3**), implying that the gamma rhythm originates from the V1 layers that receive feedforward input from the LGN.

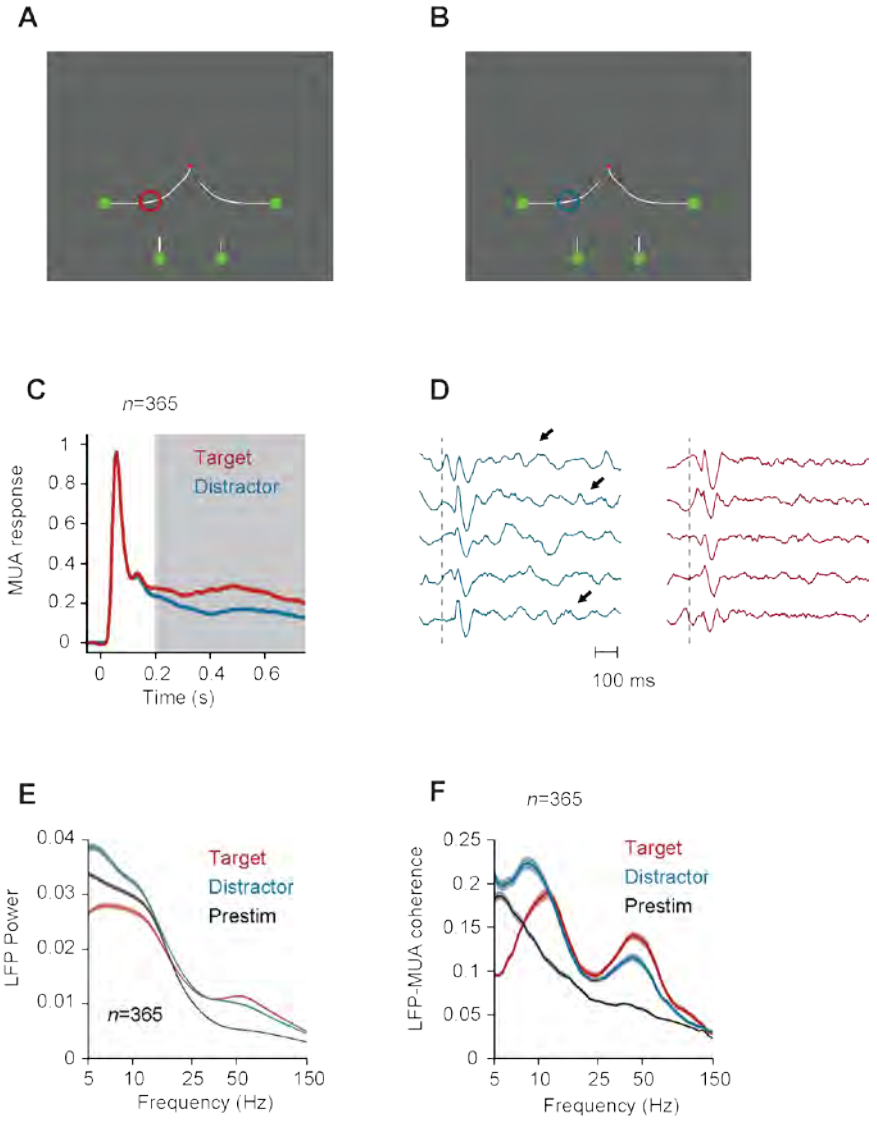

Figure 6 | Curve-tracing task where the monkey had to mentally trace the target curve that was connected to the fixation point. (**A**,**B**) We place either the target curve (A) (red circle) or one of the distractor curves in the RF (B) (blue circle). (**C**) Neuronal activity averaged across all V1 recording sites in two monkeys evoked by the target (red trace) and the distractor curve (blue trace). Grey area highlights the time window for spectral analysis (200-750ms after stimulus onset). (**D**) Example LFP responses in successive single trials elicited by the target (red) and distractor curve (blue). Dotted line indicates the stimulus onset, arrows point to low frequency oscillations. (**E**) LFP power spectrum elicited by the target and distractor curve and during pre-stimulus period (200-0ms before stimulus onset) (black trace). (**F**) LFP-MUA coherence evoked by the target and distractor curve during the epoch of response modulation (200-750ms after stimulus onset) and during the pre-stimulus period (black trace). Shaded areas show s.e.m. in all plots (*n*=365 recording sites), when they are difficult to see the s.e.m. is small.

Curve-tracing task

Texture defined figures are intrinsically salient and induce stimulus driven attention shifts[43]. We therefore investigated if these results generalize to another task where the attention shifts depend on familiarity with the task. Two monkeys mentally traced a target curve, which was connected to a red fixation point, while ignoring three distractor curves (**Figure 6A**,**B**). We showed previously that subjects solve this task by directing attention to the target curve and by ignoring the distractors[44,45]. The monkeys viewed the stimulus for 750ms and we ensured that the contour element in the neurons' RF was the same across conditions so that we could directly investigate the influence of attention shifts on neuronal activity in V1 (8 penetrations in monkey R and 8 penetrations in monkey E with a total of *n*=365 recording sites). As in previous work[e.g. 46] the attended curve evoked a stronger MUA response than the distractor curves (**Figure 6C**) ($p<0.001$, sign-test). Also in this task, the ignored curve elicited a low frequency oscillation that was visible in individual trials (**Figure 6*D***), and we could now examine LFP power and LFP-MUA coherence in a longer time window (from 200-750ms after stimulus onset) (**Figure 6E**,**F**). Our results replicated those in the texture-segregation (compare to **Figure 2**). The distractor curve evoked a significant increase in low frequency power ($p<0.001$, sign-test), whereas the target curve elicited stronger power in the gamma frequency range ($p<0.001$, sign-test). The LFP-MUA coherence revealed that MUA was locked to these rhythms (**Figure 6*F***) and demonstrated that the center frequency of the low frequency oscillation was 10Hz. Moreover, the

propagation of neuronal activity through the cortical layers was comparable to that in the texture-segregation task (**Figure S16**), implying that these results generalized across tasks.

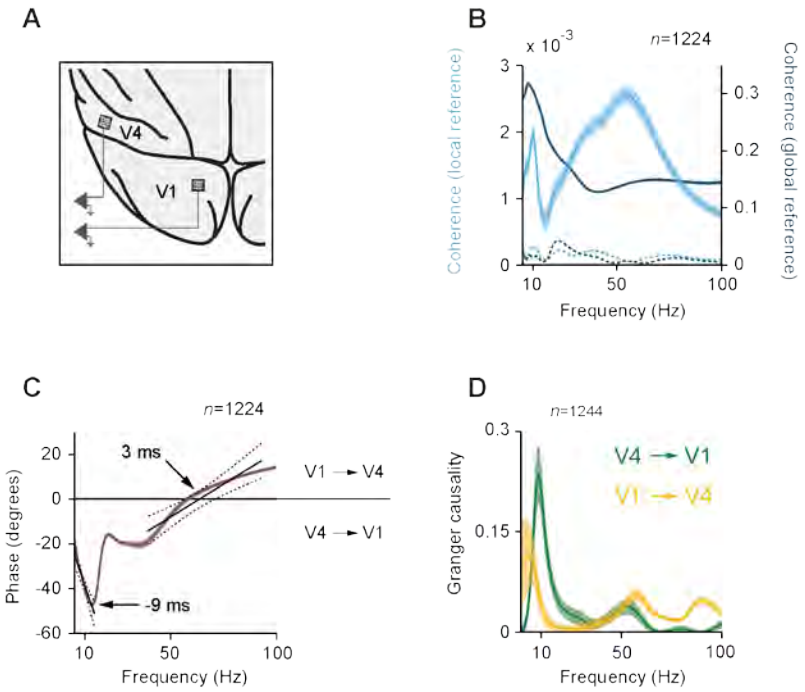

Figure 7 | Array recordings in areas V1 and V4. (**A**) Schematic representation of implanted electrode arrays in V1 and V4 with overlapping RF's. (**B**) Coherence between the LFP in V1 and V4 in a window from 150-350 ms after stimulus onset when the neurons' receptive fields fell on the background. Shaded areas show s.e.m. (*n*=1224 pairs). The cyan curve shows the coherence between the locally referenced LFP in the two areas (Y-axis scale shown left). Blue curve, coherence between LFP signals referenced to a low-impedance epidural electrode (Y-axis scale on the right). Dotted lines indicate the V1-V4 coherence for shuffled trials. (**C**) Phase relationship between LFP in V1 and V4. Black lines show least square linear fits to the phase of alpha and gamma as function of frequency. Dashed lines indicate 95% confidence intervals (*P*<0.001). (**D**) Average Granger causality of the LFP from V1 to V4 (yellow line) and from V4 to V1 recording sites (green line). Shaded areas show s.e.m. (n=1224 pairs).

Coupling between V1 and V4

We found that gamma waves start in input layer 4 whereas alpha waves start in feedback recipient layers 1, 2 and 5. Is this opposite progression of oscillations through the cortical

layers associated with corresponding time-lags between lower and higher visual areas? Previous studies in cats and using EEG recordings in humans suggested a phase lead of lower areas over higher areas for gamma oscillations and a phase lag for alpha oscillations[6,47,48]. To investigate the synchrony between areas of the monkey visual cortex in the texture-segregation task, we simultaneously recorded the LFP in V1 and downstream area V4 with chronically implanted microelectrode arrays with an electrode length of 1 or 1.5mm in two other monkeys (n=34 recording sites in V1, n=36 recording sites in V4, 7 recording sessions) (**Figure 7A**). The V1 and V4 RFs overlapped (**Figure S17**). We first examined the coherence between the LFPs in the two areas in the background condition and observed that it was significant for both the alpha and the gamma range compared to a shuffle control (t-test, n=1224 pairs, P<0.001) (**Figure 7B**). For the coherence and power analysis we referenced the LFP to another electrode within the same array (inter-electrode distance of 0.4 mm). The inter-areal coherence was much lower than in a recent study using epidural EEG recording above V1 and V4 [49] (inter-electrode distance of 2-3mm), as predicted by previous work [50]. Indeed, the coherence between the V1 and V4 LFP referenced to a low impedance epidural electrode was two orders of magnitude higher (blue in **Figure 6B**), but coherence computed in this way may also contain the contribution of sources that are picked up by the common reference. The LFP-MUA coherence between V1 and V4 also showed a low and a high frequency peak (**Figure S18**). We next examined the phase relation (epidural reference) and observed a phase-lead of area V4 for the lower frequencies (**Figure 7C**), which increased with frequencies between 5 and 12Hz. This finding is consistent with a relatively fixed time delay between V4 and V1 that translates into larger phase lags at higher frequencies. The slope of the phase relation provides an estimate of this delay for the alpha band, which was approximately 9ms (limitations of this method have been pointed out by[51]). The slope inverted above 15Hz, and the V1 phase lag changed into a phase lead in the gamma band. Although less linear, the slope of this phase relation in the gamma range suggested that V1 led V4 by approximately 3ms. We used Granger causality (global reference) to further investigate the directionality of the coupling between V1 and V4 (**Figure 7D**). We observed a narrow peak around 10Hz directed in the feedback direction, from V4 to V1 (permutation test, P<0.01). In contrast, Granger causality in the gamma range was stronger in the feedforward direction, from V1 to V4 (permutation test P<0.01), in accordance with the analysis of phase delays (**Figure 7C**).

Thus, the inter-areal coupling during figure-ground segregation supports the hypothesis that gamma and alpha rhythms index feedforward and feedback processing, respectively.

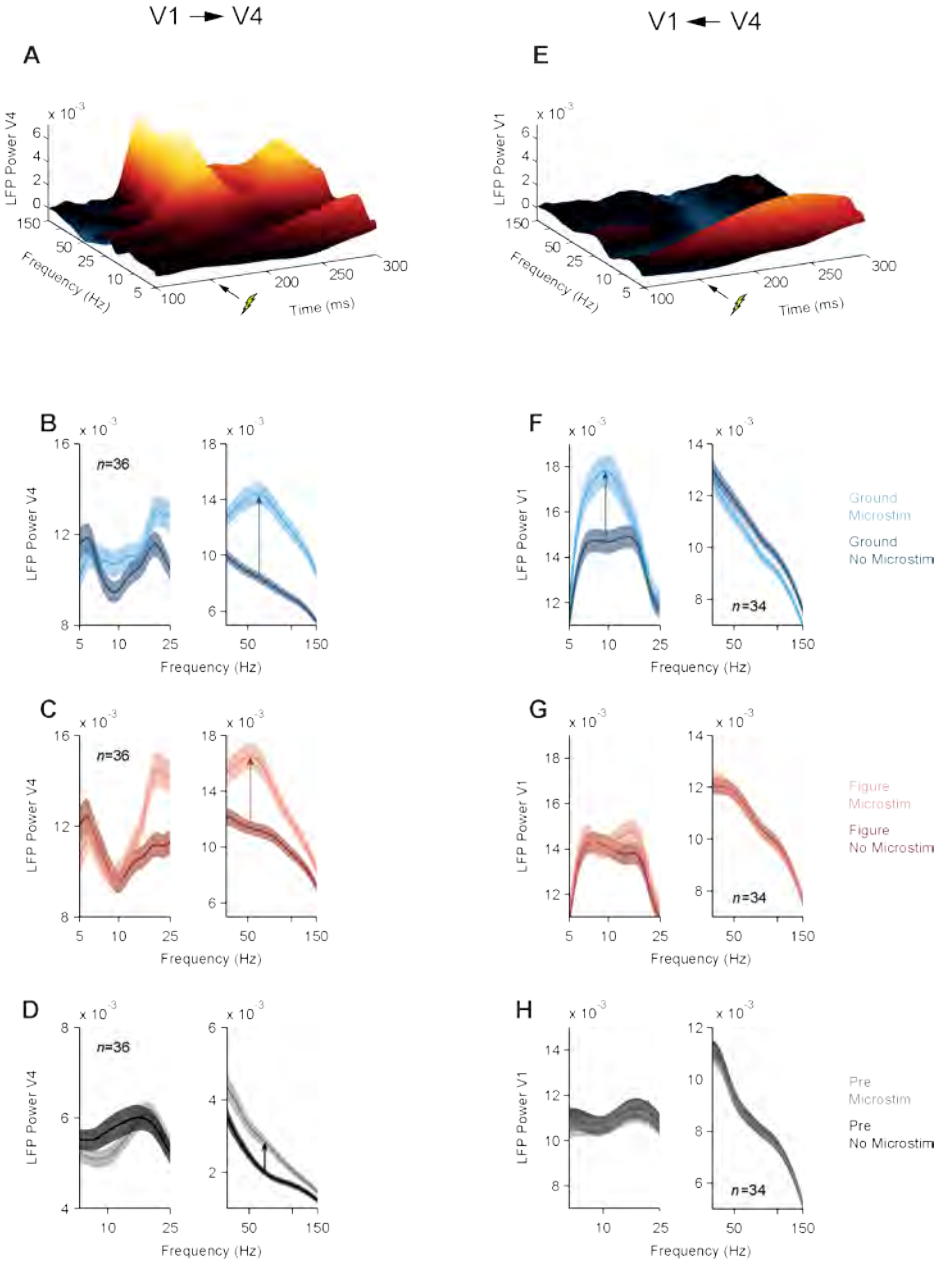

Figure 8 | Effects of microstimulation in areas V1 and V4. (**A**) Effect of microstimulation of V1 on the LFP power spectrum in V4. Stimulation (5 pulses, 200Hz) was applied in the conditions with the RF on the background from 150-170ms after stimulus onset in the texture segregation task. The power in each time bin represents the center of a time window (Morlet wavelet) with a length equal to one cycle of the corresponding frequency. (**B**,**C**) Power spectrum in V4 with (lighter curve) and without V1 microstimulation (darker curve) if the RF fell on the background (B) or figure (C). The analysis window was from 0-200ms (50-100ms) after microstimulation for alpha (gamma). Shaded areas show s.e.m. (*n*=36 recording sites). (**D**) Influence of V1 microstimulation from 150-130ms before stimulus onset on V4 power. (**E**) Effect of V4 microstimulation on the power spectrum in V1 in the background condition (*n*=34 recording sites). (**F**-**H**) Power spectrum in V1 with (lighter curves) and without V4 microstimulation (darker curves) if the RFs fell on the background (F), figure (G) or in the pre-stimulus epoch (H).

Microstimulation in V1 and V4

We next tested this hypothesis with a causal approach by combining electrical microstimulation in one area with the recording of LFP in the other area, in two monkeys (6 and 8 recording sessions with stimulation in V1 and V4, respectively). We again used the chronically implanted microarrays with overlapping RFs, but we now stimulated one area and recorded neuronal activity in the other one. We applied microstimulation in V1 for 20ms (5 pulses at 200Hz; amplitude 50-100μA), starting 150ms after the onset of the texture segregation stimulus. Microstimulation had a negligible effect on the monkeys' accuracy (above 98%), which was expected because the task was not designed to provide sensitive measures of the monkeys' performance. It induced gamma oscillations in V4 (*t*-test, *n*=36 V4 recording sites, $P<0.001$, 200-250ms after stimulus onset, both in the figure and background condition) but had little effect on V4 alpha power ($P>0.3$, 150-350ms after stimulus onset) (**Figure 8A**-**C**). The effect of V1 microstimulation did not strongly depend on whether the neurons' RF fell on the background (**Figure 8B**) or figure (**Figure 8C**). Moreover, a similar effect occurred if microstimulation occurred in the fixation epoch, 150ms before the texture was presented (*t*-test, *n*=36, $P<0.001$ for gamma, $P>0.25$ for alpha) (**Figure 8D**). Thus, the effect of V1 microstimulation on V4 power did not depend strongly on the visual stimulus, which is in accordance with a driving effect of the feedforward connections.

We also carried out the opposite experiment, microstimulating in V4 while recording in V1. If the neurons' RF fell on the background, V4 microstimulation with the same timing (amplitude 30-60μA) caused an increase in the V1 alpha rhythm (*t*-test, n=34 V1 recording sites, P<0.001, 150-350ms after stimulus onset), while it suppressed the gamma rhythm (P<0.05, 200-250ms after stimulus onset) (**Figure 8E,F**). The effect of V4 microstimulation on V1 was stimulus dependent. If the figure fell in the neurons' RFs, it blocked the increase in alpha elicited by V4 microstimulation as well as the decrease in gamma (**Figure 8G**). Interestingly, V4 microstimulation also had little effect on V1 power in the fixation epoch, when the monkeys were looking at a blank screen (*t*-test, n=34, P>0.5 for alpha and gamma, 150-0ms before stimulus onset) (**Figure 8H**). Thus, V1 neurons are particularly susceptible for the V4 feedback effects when their RFs fall on the background. Furthermore, these microstimulation results, taken together, provide causal evidence that gamma oscillations travel in the feedforward direction, whereas alpha waves travel in the feedback direction.

Pharmacological intervention in V1

We used pharmacology as an additional causal method to probe the directionality of alpha and gamma oscillations. Theoretical studies proposed that the feedforward drive of a cortical neuron depends on AMPA-receptors whereas feedback effects depend more on NMDA-receptors[24]. A recent neurophysiological study using the texture-segregation task demonstrated that AMPA-blockers indeed reduce the visually driven response whereas NMDA-blockers decrease the difference in activity evoked by the figure and background[25], which depends on feedback connections[33,35]. If alpha oscillations signify feedback processing, then alpha power might decrease if NMDA-receptors are blocked. We used laminar probes with a fluid line for local pressure injection of small quantities (<80nL) of pharmacological substances in V1 while the monkeys carried out the texture segregation task (**Figure S19A**). We first measured the effective diffusion distance of our injections with CNQX (an AMPA-receptor blocker), which reliably reduces neural responses. CNQX injections reduced neural activity over a distance of approximately 1.5mm (**Figure S19B**).

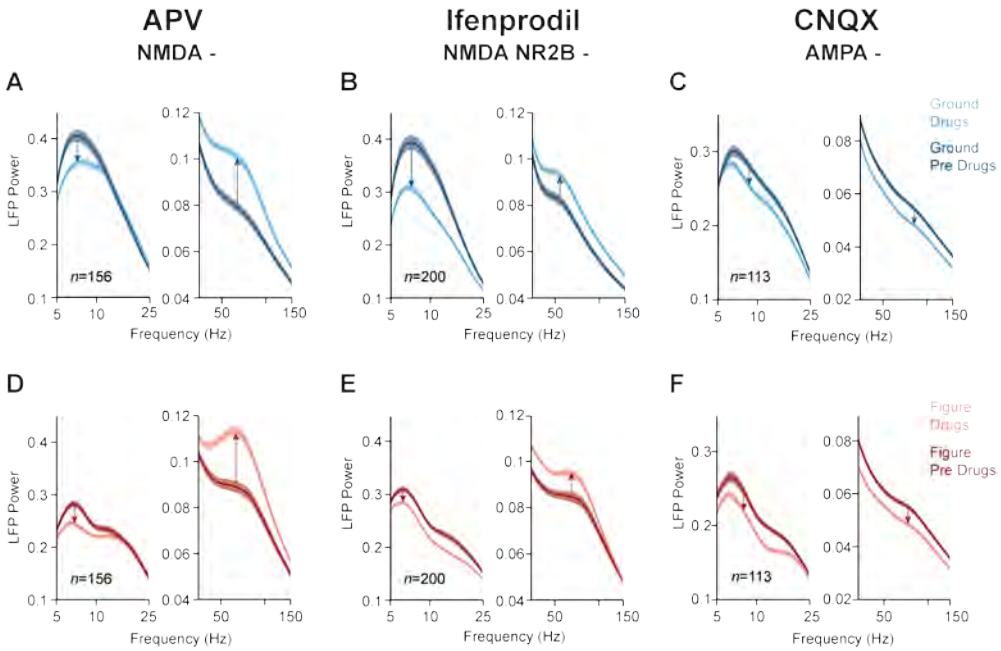

Figure 9 | Effects of glutamate-receptor antagonists in V1. (**A**) Effect of the NMDA-receptor blocker APV on the LFP power spectrum (*n*=156 sites), in a window from 150-350 ms after stimulus onset with the RF on the background. Blue trace, pre-drug epoch. Cyan trace, after drug application. (**B**) Effect of ifenprodil, another blocker of the NMDA-receptor (*n*=200). (**C**) Effect of the AMPA-receptor blocker CNQX (*n*=113). (**D**-**F**) Same as A-C but for the condition with the RF on the figure. Shaded areas show s.e.m.

To block NMDA-receptors we applied the broad spectrum NMDA-antagonists APV (8 penetrations in two monkeys) and ifenprodil, which blocks NMDA-receptors with the NR2B subunit (11 penetrations in two monkeys). The small drug injections generally did not interfere with the monkeys' accuracy, which was higher than 97%, but they did have a profound influence on the power spectrum of the LFP. Both NDMA-receptor blockers suppressed the alpha frequencies of the LFP, while enhancing the gamma frequencies (**Figure 9**). These effects occurred if the neurons' RF fell on the background (**Figure 9A**,**B**; *t*-test, APV *n*=156 sites, ifenprodil *n*=200, both drugs $P<0.001$ for alpha; $P<0.05$ for APV and $P<0.001$ for ifenprodil for gamma) and also if it fell on the figure (**Figure 9D**,**E**; both drugs $P<0.001$ for alpha; $P<0.05$ for APV and $P<0.001$ for ifenprodil for gamma). The two NMDA-blockers have opposing effects on visually driven activity[25], which implies that their

influence on alpha and gamma oscillations are not caused by changes in neuronal excitability. In the control experiments where we blocked the AMPA-receptors with CNQX (n=113 sites in 7 penetrations in two monkeys) we observed a reduction in the LFP power across all frequencies (**Figure 9C,F**; t-test, n=113, P<0.001 for alpha and gamma in either stimulus condition), as is expected for a drug that causes a general decrease of cortical activity. Thus, NMDA-receptor activity is important for the alpha rhythm, which fits with the relatively long time constant of these receptors[52] and is in accordance with their role in feedback processing[24,25].

DISCUSSION

Our results provide four convergent lines of evidence that the gamma rhythm is a signature of feedforward processing whereas the alpha rhythm indexes feedback effects. First, our results demonstrate for the first time that gamma waves start in layer 4, the input layer of cortex, and are then propagated to the superficial and deep layers. Alpha waves are initiated in layers 1, 2 and 5, the targets of corticocortical feedback connections in V1[27] and propagate in the opposite direction, towards layer 4. Second, simultaneous recordings in V1 and V4 showed that the gamma rhythm propagates from V1 to V4 whereas the alpha rhythm propagates in the opposite direction. Third, electrical microstimulation provided the first causal evidence that feedforward processing induces gamma oscillations in a higher visual area and that feedback causes alpha activity in a lower area. Fourth, we found that local application of blockers of the NMDA-receptor, which is important for feedback effects[25], suppressed alpha oscillations while enhancing gamma oscillations. These results, taken together, provide strong evidence for the opposite directionality of alpha and gamma oscillations.

Figure-ground organization mainly influenced the amplitude of the oscillations but their laminar patterns remained the same, and we obtained similar results with shifts of attention in the curve-tracing task. Thus, task-relevance influences the amplitude of the rhythms, but the cortical mechanisms that generate them appear to be task and stimulus invariant.

Mechanisms underlying the alpha rhythm

Our analysis of the coherence between MUA and the CSD during alpha oscillations revealed that spikes coincide with sinks in feedback recipient layers 1/2 and 5[27,28] and with sources in layers 4 and 6[26] (**Figure 4**). This is of considerable interest because layer 5 cells, thought to be involved in the generation of alpha[53,54], are particularly sensitive to coincident input to their basal and apical dendritic trees[55,56] and their apical dendrites have a resonance in the 5-10Hz frequency range[5,57]. Alpha coherence between spikes and the CSD was also measured by Bollimunta et al.[42] but the present study is the first to resolve the laminar pattern with a high resolution because of a denser spacing of contact points on the electrodes.

The sinks that started in layers 1/2 and 5 propagated towards input layer 4 during the alpha cycle. We obtained a similar result for MUA, which also started in the superficial and deep layers and was delayed in layer 4 during the alpha cycle. The propagation of activity towards layer 4 could rely on the input it receives from layers 5/6[58-61] and 2/3[60]. The results therefore support the hypothesis that alpha is a signature of feedback effects.

Mechanisms underlying the gamma rhythm

Our data revealed that spiking activity during the gamma cycle coincided with a sink in layer 4C, which was followed by a succession of sinks propagating towards the superficial and deep layers. Moreover, layer 4 MUA locking to the gamma rhythm preceded MUA in superficial and deep layers, in line with a previous study in squirrel monkey[41]. These results suggest that the gamma oscillation in V1 is elicited by thalamic input, which is in accordance with the finding that trials with a stronger MUA response also elicited more gamma. In combination with in vitro studies demonstrating that gamma oscillations are of cortical origin[5], our results suggest that the thalamic input enables a cortical loop that generates these high frequency rhythms.

Our laminar recordings thereby provided new mechanistic insight into generation of cortical rhythms. The opposite directionalities of gamma and alpha oscillations represent a strong constraint for cortical circuit models that aim to explain the generation of these rhythms.

Directionality between V1 and V4

The simultaneous V1-V4 recordings demonstrated that the opposite directionalities of the alpha and gamma rhythms co-exist for a single combination of visual cortical areas within a single task. The relationship between the frequency and phase-delay in the two areas suggested that V1 leads V4 by 3ms for the gamma rhythm but lags V4 by 9ms for alpha. This difference between time-lags may seem surprising because feedforward and feedback connections have similar conduction times[62], but our pharmacological results suggest that it may be explained by a difference in synaptic integration. The time constant of NMDA channels, which play a role in the feedback effects, is longer than that of AMPA channels that are important for the feedforward propagation of activity to higher visual areas[25].

Our analysis of phase shifts and Granger causality between V1 and V4 confirmed the propagation of alpha waves in the feedback direction, in accordance with some[48,63] but not all[64] previous EEG-recordings in humans. At first sight, this result appears to contradict a recent finding that Granger causality between V1 and V2 in the alpha range is strongest in the feedforward direction[18]. We suspect that methodological differences (the previous study only selected electrode combinations with high gamma coherence) and perhaps differences between tasks are responsible for this discrepancy.

The feedforward signature of gamma is in line with recent studies showing stronger Granger causality for gamma from V1 to V2 and from V1 to V4 than in the opposite direction[18,49,65]. It is also reminiscent of a study in cats, showing that gamma oscillations propagate from the LGN to V1 with an average delay of approximately 2ms[47].

A modeling study by Vierling-Claassen et al.[66] suggested that pyramidal cells interact with fast-spiking interneurons to generate gamma oscillations whereas they interact with low threshold spiking interneurons to generate the alpha rhythm. In this context, our findings raise the possibility that feedforward connections preferentially influence the putative loop that involves fast-spiking cells, whereas feedback connections target low-threshold spiking interneurons, a hypothesis that could be explored in future work, e.g. by recording from genetically identified single neurons during alpha and gamma oscillations in mice.

Causal tests of directionality

Our electrical microstimulation experiments provided the first causal evidence that feedforward processing induces gamma oscillations in a higher visual area and that feedback causes alpha activity in a lower area. We used electrode arrays for microstimulation, positioned 1 or 1.5mm below the cortical surface. They were presumably in layers 4 or 5, but the effects of microstimulation on neuronal activity are relatively homogeneous across cortical depth[67,68]. Microstimulation activates axons in the vicinity of the electrode tip[68,69] and can cause orthodromic and antidromic stimulation effects in another area. Antidromic effects occur if axon terminals of projection neurons are stimulated and action potentials travel back to their cell-bodies in another area. Orthodromic effects occur either by the direct or by trans-synaptic activation of projection neurons with cell bodies in the area that is stimulated. At the current levels used by us, most neurons are stimulated trans-synaptically[68]. Accordingly, previous studies demonstrated that orthodromic stimulation effects are many times stronger than antidromic effects even between areas with strong direct projections[62,70,71]. The direct connectivity between V1 and V4 is relatively sparse[72] and the antidromic contribution to our findings was therefore presumably even smaller than in these previous studies.

V4 microstimulation only caused an increase in V1 alpha if the neurons' RF fell on the background (**Figure 8**). This finding is important for two reasons. First, antidromic stimulation effects should be invariant across visual stimulation conditions. The stimulus dependence of V4 microstimulation effects therefore confirms the predominance of orthodromic, trans-synaptic stimulation effects. Second, the finding that V4 stimulation only induced alpha in V1 if the neurons' RFs fell on the background suggests that alpha oscillations are signature of suppressive feedback effects. This suggestion is supported by our finding that trials with strong alpha were associated with a weak MUA response as well as preliminary results that V4 microstimulation reduces firing rates of V1-neurons in the texture segregation task [73]. The influence of V4 stimulation on the V1 alpha rhythm could be generated by the cortico-cortical feedback connections, but our results do not exclude the possibility that these effects are mediated in part through the thalamus[74]. Specifically, connections from the pulvinar also target the superficial layers of V1 and may provide a source of top-down influences[75-77]. We used V1 microstimulation to probe the feedforward

effects and found that it elicited gamma power in area V4 without a strong influence on the V4 alpha rhythm. Interestingly, this increase in gamma was relatively independent of the visual stimulus in the neurons' RF, in accordance with a driving influence of the feedforward connections, and indeed, our preliminary results revealed that V1 microstimulation increases V4 spiking activity[73].

Our second causal experiment influenced the activity of glutamate receptors with a pharmacological approach. Theoretical work[24] implicated NMDA-receptor activity in cortico-cortical feedback effects. A recent study[25] confirmed this prediction by demonstrating that figure-ground modulation in V1, which depends on feedback[35], indeed requires NMDA-receptor activity, whereas visually driven activity in V1 primarily depends on AMPA-receptors. Thus, NMDA-blockers reduce feedback influences, and our finding that they reduce alpha oscillations is in line with the hypothesis that alpha oscillations signify feedback effects. This finding is also in accordance with previous results in cortical slices where NMDA blockers suppress the lower frequencies[53]. At the same time, we found that NMDA-receptor blockers enhanced gamma oscillations, in accordance with previous results obtained with the systemic application of NMDA antagonists in rodents[78] and with local application in the visual cortex of monkeys[79].

The influence of perceptual organization on the alpha and gamma rhythm

The finding that the gamma and alpha rhythms signal feedforward and feedback processing is neutral with respect to their putative role in information processing. Many studies have reported that selective attention enhances the gamma rhythm[12,13,49,80]. The increased gamma may be instrumental in the propagation of sensory information towards higher areas[17], but it could also be a side-effect of a more efficient feedforward information flow for attended stimuli. Earlier studies reported that the presentation of a visual stimulus suppresses the alpha rhythm[80-83]. Our laminar recordings only revealed alpha suppression at the representation of the figure and only in the middle and superficial layers (**Figure 2G**), in line with a recent study[13,84]. The selective enhancement of the alpha rhythm in the background of the texture stimulus and its association with weaker neuronal activity suggests that it reflects the active suppression of irrelevant information[10,11,85]. Such a suppressive feedback effect is in accordance with a role of corticocortical feedback in

surround suppression[86-88] and inhibitory effects of selective attention in early visual areas[89,90]. A previous model of the interactions between cortical areas for texture segregation proposed that the orientation of the image elements that are part of the figure is registered in higher visual areas, which feedback to suppress V1 responses to background elements with the orthogonal orientation and disinhibit activity evoked by figural image elements with the same orientation[91]. The putative disinhibitory top-down feedback influence on the figure representation is in line with the low alpha power with the figure in the neuron's RF. Our results do not exclude that feedback, in addition to its putative disinhibitory effect, also has direct excitatory effects to enhance the neuronal representation of relevant image elements[92,93]. Such an excitatory feedback signal might be weaker, or not show up in a spectral analysis if it targets different synapses that do not cause synchronized activity. Our experiments with the curve-tracing task and a comparison with previous work[12,13,49,80] indicate that the effects of task-relevance of alpha and gamma power generalize across tasks.

Irrespective of the precise functional significance of these brain rhythms, our results demonstrate that alpha and gamma oscillations characterize feedback and feedforward processing in visual cortex. This new insight can now be exploited to gain a deeper understanding of the role of feedforward and feedback influences in visual cognition.

METHODS

Six adult macaque monkeys (S, E, R, B, J and C) were trained to do a texture segregation task. A texture stimulus was presented 300ms after the monkey directed gaze to a fixation period. The stimulus was a whole screen texture with one orientation with a figural region of 4x4 degrees with the orthogonal orientation (Figure 1D,E). After another fixation epoch of 300ms the monkey received a reward for making a saccade to the texture defined figure. The figure could appear at 3 possible locations, with the location of the figure rotated by 120 degrees. The texture stimuli were constructed so that on average precisely the same contour elements were present inside the RF across the different conditions (details in SI Appendix).

In monkeys S, E and R extracellular recordings in V1 were performed with multi-contact 'U' probes (Plexon) with 24 contact points spaced 100μm apart. A fluid line allowed the application of pharmacological substances by pressure injection with a Hamilton syringes (1μL). The depth of the probe was determined by measuring the CSD evoked by a full-screen 100% contrast checkerboard. We estimated the location of the border between layer 5 and layer 4C as the polarity reversal from current sinks in layer 4C to current sources in the deep layers (**Figure S1**).

In monkeys B, J and C we obtained extracellular recordings in V1 and V4 using grids of 4x5 microelectrodes (Cyberkinetics Neurotechnology Systems Inc.). For the power and coherence analysis we locally referenced the LFP to an electrode within the same array. For the electrical microstimulation experiments we delivered trains of 5 biphasic pulses of 500μs duration at a frequency of 200Hz with an amplitude in the range of 30-100μA. The anode and cathode electrode were on the same array, reducing the stimulation artifact in the other area where we recorded LFP's. Statistical significance was assessed using paired Student's *t*-tests. See **Supplementary Information** for further information about the paradigm, neuronal recordings and data analysis.

References

1. Zeki,S.M. Functional specialisation in the visual cortex of the rhesus monkey. *Nature* **274**, 423-428 (1978).

2. Felleman,D.J. & Van Essen,D.C. Distributed hierarchical processing in the primate cerebral cortex. *Cereb. Cortex* **1**, 1-47 (1991).

3. Lamme,V.A.F. & Roelfsema,P.R. The distinct modes of vision offered by feedforward and recurrent processing. *Trends Neurosci.* **23**, 571-579 (2000).

4. Engel,A.K., Fries,P., & Singer,W. Dynamic predictions: oscillations and synchrony in top-down processing. *Nat. Rev. Neurosci.* **2**, 704-716 (2001).

5. Wang,X.J. Neurophysiological and computational principles of cortical rhythms in cognition. *Physiol Rev.* **90**, 1195-1268 (2010).

6. von Stein,A., Chiang,C., & Konig,P. Top-down processing mediated by interareal synchronization. *Proc. Natl. Acad. Sci. U. S. A* **97**, 14748-14753 (2000).

7. Adrian,E. Brain Rhythms. *Nature* **153**, 360-362 (1944).

8. Yu,J. & Ferster,D. Membrane potential synchrony in primary visual cortex during sensory stimulation. *Neuron* **68**, 1187-1201 (2010).

9. Berger,H. Über das elektroenkephalogramm des menschen. *Arch. Psychiatr. Nervenkr* **87**, 527-570 (1929).

10. Klimesch,W., Sauseng,P., & Hanslmayr,S. EEG alpha oscillations: the inhibition-timing hypothesis. *Brain Res. Rev.* **53**, 63-88 (2007).

11. Jensen,O. & Mazaheri,A. Shaping functional architecture by oscillatory alpha activity: gating by inhibition. *Front Hum. Neurosci.* **4**, 186 (2010).

12. Fries,P., Reynolds,J.H., Rorie,A.E., & Desimone,R. Modulation of oscillatory neuronal synchronization by selective visual attention. *Science* **291**, 1560-1563 (2001).

13. Buffalo,E.A., Fries,P., Landman,R., Buschman,T.J., & Desimone,R. Laminar differences in gamma and alpha coherence in the ventral stream. *Proc. Natl. Acad. Sci. USA* **108**, 11262-11267 (2011).

14. Singer,W. & Gray,C.M. Visual feature integration and the temporal correlation hypothesis. *Annu. Rev. Neurosci.* **18**, 555-586 (1995).

15. Thiele,A. & Stoner,G.R. Neuronal synchrony does not correlate with motion coherence in cortical area MT. *Nature* **421**, 366-370 (2003).

16. Roelfsema,P.R., Lamme,V.A.F., & Spekreijse,H. Synchrony and covariation of firing rates in the primary visual cortex during contour grouping. *Nature Neurosci.* **7**, 982-991 (2004).

17. Fries,P. Neuronal gamma-band synchronization as a fundamental process in cortical computation. *Annu. Rev. Neurosci.* **32**, 209-224 (2009).

18. Roberts,M.J. *et al.* Robust gamma coherence between macaque V1 and V2 by dynamic frequency matching. *Neuron* **78**, 523-536 (2013).

19. Chalk,M. *et al.* Attention reduces stimulus-driven gamma frequency oscillations and spike field coherence in V1. *Neuron*114-125 (2010).

20. Lima,B., Singer,W., Chen,N.H., & Neuenschwander,S. Synchronization dynamics in response to plaid stimuli in monkey V1. *Cereb. Cortex* **20**, 1556-1573 (2010).

21. Ray,S. & Maunsell,J.H. Differences in gamma frequencies across visual cortex restrict their possible use in computation. *Neuron* **67**, 885-896 (2010).

22. Jia,X., Smith,M.A., & Kohn,A. Stimulus selectivity and spatial coherence of gamma components of the local field potential. *J. Neurosci.* **31**, 9390-9403 (2011).

23. Siegel,M., Donner,T.H., & Engel,A.K. Spectral fingerprints of large-scale neuronal interactions. *Nat. Rev. Neurosci.* **13**, 121-134 (2012).

24. Dehaene,S. & Changeux,J.P. Experimental and theoretical approaches to conscious processing. *Neuron* **70**, 200-227 (2011).

25. Self,M.W., Kooijmans,R.N., Super,H., Lamme,V.A., & Roelfsema,P.R. Different glutamate receptors convey feedforward and recurrent processing in macaque V1. *Proc. Natl. Acad. Sci. U. S. A* **109**, 11031-11036 (2012).

26. Lund,J.S. Anatomical organization of macaque monkey striate visual cortex. *Annu. Rev. Neurosci.* **11**, 253-288 (1988).

27. Rockland,K.S. & Virga,A. Terminal arbors of individual "feedback" axons projecting from area V2 to V1 in the macaque monkey: a study using immunohistochemistry of anterogradely transported Phaseolus vulgaris-leucoagglutinin. *J. Comp. Neurol.* **285**, 54-72 (1989).

28. Anderson,J.C. & Martin,K.A. The synaptic connections between cortical areas V1 and V2 in macaque monkey. *J. Neurosci.* **29**, 11283-11293 (2009).

29. Mitzdorf,U. Current source-density method and application in cat cerebral cortex: investigation of evoked potentials and EEG phenomena. *Physiol. Rev.* **65**, 37-100 (1985).

30. Buzsaki,G., Anastassiou,C.A., & Koch,C. The origin of extracellular fields and currents--EEG, ECoG, LFP and spikes. *Nat. Rev. Neurosci.* **13**, 407-420 (2012).

31. Schroeder,C.E., Tenke,C.E., Givre,S.J., Arezzo,J.C., & Vaughan,H.G., Jr. Striate cortical contribution to the surface-recorded pattern-reversal VEP in the alert monkey. *Vision Res.* **31**, 1143-1157 (1991).

32. Lamme,V.A.F. The neurophysiology of figure-ground segregation in primary visual cortex. *J. Neurosci.* **15**, 1605-1615 (1995).

33. Lamme,V.A.F., Supèr,H., & Spekreijse,H. Feedforward, horizontal, and feedback processing in the visual cortex. *Curr. Opin. Neurobiol.* **8**, 529-535 (1998).

34. Hupe,J.M. *et al.* Cortical feedback improves discrimination between figure and background by V1, V2 and V3 neurons. *Nature* **394**, 784-787 (1998).

35. Poort,J. *et al.* The role of attention in figure-ground segregation in areas V1 and V4 of the visual cortex. *Neuron* **75**, 143-156 (2012).

36. Haegens,S., Nacher,V., Luna,R., Romo,R., & Jensen,O. alpha-Oscillations in the monkey sensorimotor network influence discrimination performance by rhythmical inhibition of neuronal spiking. *Proc. Natl. Acad. Sci. U. S. A* **108**, 19377-19382 (2011).

37. Ray,S. & Maunsell,J.H. Different origins of gamma rhythm and high-gamma activity in macaque visual cortex. *PLoS. Biol.* **9**, e1000610 (2011).

38. Brovelli,A. *et al.* Beta oscillations in a large-scale sensorimotor cortical network: directional influences revealed by Granger causality. *Proc. Natl. Acad. Sci. U. S. A* **101**, 9849-9854 (2004).

39. Maier,A., Adams,G.K., Aura,C., & Leopold,D.A. Distinct superficial and deep laminar domains of activity in the visual cortex during rest and stimulation. *Front. Syst. Neurosci.* **4**, (2010).

40. Xing,D., Yeh,C.I., Burns,S., & Shapley,R.M. Laminar analysis of visually evoked activity in the primary visual cortex. *Proc. Natl. Acad. Sci. U. S. A* **109**, 13871-13876 (2012).

41. Livingstone,M.S. Oscillatory firing and interneuronal correlations in squirrel monkey striate cortex. *J. Neurophysiol.* **75**, 2467-2485 (1996).

42. Bollimunta,A., Mo,J., Schroeder,C.E., & Ding,M. Neuronal mechanisms and attentional modulation of corticothalamic alpha oscillations. *J. Neurosci.* **31**, 4935-4943 (2011).

43. Roelfsema,P.R., Tolboom,M., & Khayat,P.S. Different processing phases for features, figures, and selective attention in the primary visual cortex. *Neuron* **56**, 785-792 (2007).

44. Scholte,H.S., Spekreijse,H., & Roelfsema,P.R. The spatial profile of visual attention in mental curve tracing. *Vision Res.* **41**, 2569-2580 (2001).

45. Houtkamp,R., Spekreijse,H., & Roelfsema,P.R. A gradual spread of attention during mental curve tracing. *Percept. Psychophys.* **65**, 1136-1144 (2003).

46. Roelfsema,P.R., Lamme,V.A.F., & Spekreijse,H. Object-based attention in the primary visual cortex of the macaque monkey. *Nature* **395**, 376-381 (1998).

47. Castelo-Branco,M., Neuenschwander,S., & Singer,W. Synchronization of visual responses between the cortex, lateral geniculate nucleus, and retina in the anesthetized cat. *J. Neurosci.* **18**, 6395-6410 (1998).

48. Ito,J., Nikolaev,A.R., & van Leeuwen C. Spatial and temporal structure of phase synchronization of spontaneous alpha EEG activity. *Biol. Cybern.* **92**, 54-60 (2005).

49. Bosman,C.A. *et al.* Attentional stimulus selection through selective synchronization between monkey visual areas. *Neuron* **75**, 875-888 (2012).

50. Bullock,T.H. & McClune,M.C. Lateral coherence of the electrocorticogram: a new measure of brain synchrony. *Electroencephalogr. Clin. Neurophysiol.* **73**, 479-498 (1989).

51. Lindemann,M., Raethjen,J., Timmer,J., Deuschl,G., & Pfister,G. Delay estimation for cortico-peripheral relations. *J. Neurosci. Methods* **111**, 127-139 (2001).

52. Traynelis,S.F. *et al.* Glutamate receptor ion channels: structure, regulation, and function. *Pharmacol. Rev.* **62**, 405-496 (2010).

53. Silva,L.R., Amitai,Y., & Connors,B.W. Intrinsic oscillations of neocortex generated by layer 5 pyramidal neurons. *Science* **251**, 432-435 (1991).

54. Roopun,A.K. *et al.* Period concatenation underlies interactions between gamma and beta rhythms in neocortex. *Front. Cell. Neurosci.* **2**, 1 (2008).

55. Larkum,M.E., Zhu,J.J., & Sakmann,B. A new cellular mechanism for coupling inputs arriving at different cortical layers. *Nature* **398**, 338-341 (1999).

56. Larkum,M. A cellular mechanism for cortical associations: an organizing principle for the cerebral cortex. *Trends Neurosci.* **36**, 141-151 (2013).

57. Ulrich,D. Dendritic resonance in rat neocortical pyramidal cells. *J. Neurophysiol.* **87**, 2753-2759 (2002).

58. Gilbert,C.D. & Wiesel,T.N. Morphology and intracortical projections of functionally characterised neurones in the cat visual cortex. *Nature* **280**, 120-125 (1979).

59. Fitzpatrick,D., Lund,J.S., & Blasdel,G.G. Intrinsic connections of macaque striate cortex: afferent and efferent connections of lamina 4C. *J. Neurosci.* **5**, 3329-3349 (1985).

60. Binzegger,T., Douglas,R.J., & Martin,K.A. A quantitative map of the circuit of cat primary visual cortex. *J. Neurosci.* **24**, 8441-8453 (2004).

61. Thomson,A.M. Neocortical layer 6, a review. *Front Neuroanat.* **4**, 13 (2010).

62. Girard,P., Hupé,J.-M., & Bullier,J. Feedforward and feedback connections between area V1 and V2 of the monkey have similar rapid conduction velocities. *J. Neurophysiol.* **85**, 1328-1331 (2001).

63. Patten,T.M., Rennie,C.J., Robinson,P.A., & Gong,P. Human cortical traveling waves: dynamical properties and correlations with responses. *PLoS. ONE.* **7**, e38392 (2012).

64. Bahramisharif,A. *et al.* Propagating neocortical gamma bursts are coordinated by traveling alpha waves. *J. Neurosci.* **33**, 18849-18854 (2013).

65. Bastos,A.M. *et al.* Visual areas exert feedforward and feedback influences through distinct frequency channels. *Neuron* **85**, 390-401 (2015).

66. Vierling-Claassen,D., Cardin,J.A., Moore,C.I., & Jones,S.R. Computational modeling of distinct neocortical oscillations driven by cell-type selective optogenetic drive: separable resonant circuits controlled by low-threshold spiking and fast-spiking interneurons. *Front Hum. Neurosci.* **4**, 198 (2010).

67. Contreras,D., Durmuller,N., & Steriade,M. Absence of a prevalent laminar distribution of IPSPs in association cortical neurons of cat. *J. Neurophysiol.* **78**, 2742-2753 (1997).

68. Butovas,S. & Schwartz,C. Spatiotemporal effects of microstimulation in rate neocortex: a parametric study using mutielectrode recordings. *J. Neurophysiol.* **90**, 3024-3039 (2003).

69. Histed,M.H., Bonin,V., & Reid,R.C. Direct activation of sparse, distributed populations of cortical neurons by electrical microstimulation. *Neuron* **63**, 508-522 (2009).

70. Bullier,J., McCourt,M.E., & Henry,G.H. Physiological studies on the feedback connection to the striate cortex from cortical areas 18 and 19 of the cat. *Exp. Brain Res.* **70**, 90-98 (1988).

71. Movshon,J.A. & Newsome,W.T. Visual response properties of striate cortical neurons projecting to area MT in macaque monkeys. *J. Neurosci.* **16**, 7733-7741 (1996).

72. Markov,N.T. *et al.* Weight consistency specifies regularities of macaque cortical networks. *Cereb. Cortex* **21**, 1254-1272 (2011).

73. Dagnino,B., Gariel,M.A., & Roelfsema,P.R. Feedforward and feedback propagation of electrically induced activity in the visual cortex. SfN Abstracts, Society for Neuroscience, San Diego, CA. no 638.08. 2013.

74. Lopes da Silva,F.H., Vos,J.E., Mooibroek,J., & van Rotterdam,A. Relative contribution of intracortical and thalamo-cortical processes in the generation of alpha rhythms, revealed by partial coherence analysis. *Electroencephalogr. Clin. Neurophysiol.* **50**, 449-456 (1980).

75. Benevento,L.A. & Rezak,M. Extrageniculate projections to layers VI and I of striate cortex (area 17) in the rhesus monkey (Macaca mulatta). *Brain Res.* **96**, 51-55 (1975).

76. Ogren,M.P. & Hendrickson,A.E. The distribution of pulvinar terminals in visual areas 17 and 18 of the monkey. *Brain Res.* **137**, 343-350 (1977).

77. Saalmann,Y.B., Pinsk,M.A., Wang,L., Li,X., & Kastner,S. The pulvinar regulates information transmission between cortical areas based on attention demands. *Science* **337**, 753-756 (2012).

78. Hakami,T. *et al.* NMDA receptor hypofunction leads to generalized and persistent aberrant gamma oscillations independent of hyperlocomotion and the state of consciousness. *PLoS. ONE.* **4**, e6755 (2009).

79. Herrero,J.L., Gieselman,M.A., Sanayei,M., & Thiele,A. Attention-induced variance and noise correlation reduction in macaque V1 is mediated by NMDA receptors. *Neuron* **78**, 729-739 (2013).

80. Fries,P., Womelsdorf,T., Oostenveld,R., & Desimone,R. The effects of visual stimulation and selective visual attention on rhythmic neuronal synchronization in macaque area V4. *J. Neurosci.* **28**, 4823-4835 (2008).

81. Gray,C.M. & Singer,W. Stimulus-specific neuronal oscillations in orientation columns of cat visual cortex. *Proc. Natl. Acad. Sci. USA* **86**, 1698-1702 (1989).

82. Yu,J. & Ferster,D. Membrane potential synchrony in primary visual cortex during sensory stimulation. *Neuron* **68**, 1187-1201 (2010).

83. Hipp,J.F., Engel,A.K., & Siegel,M. Oscillatory synchronization in large-sclae cortical networks predicts perception. *Neuron* **69**, 387-396 (2011).

84. Sejnowski,T.J. & Paulsen,O. Network oscillations: emerging computational principles. *J. Neurosci.* **26**, 1673-1676 (2006).

85. Bonnefond,M. & Jensen,O. Alpha oscillations serve to protect working memory maintenance against anticipated distracters. *Curr. Biol.* **22**, 1969-1974 (2012).

86. Shushruth,S. *et al.* Strong recurrent networks compute the orientation tuning of surround modulation in the primate primary visual cortex. *J. Neurosci.* **32**, 308-321 (2012).

87. Gilad,A., Meirovithz,E., & Slovin,H. Population responses to contour integration: early encoding of discrete elements and late perceptual grouping. *Neuron* **78**, 389-402 (2013).

88. Nassi,J.J., Lomber,S.G., & Born,R.T. Corticocortical feedback contributes to surround suppression in V1 of the alert primate. *J. Neurosci.* **33**, 8504-8517 (2013).

89. Chen,Y. *et al.* Task difficulty modulates the activity of specific neuronal populations in primary visual cortex. *Nature Neurosci.* **11**, 974-982 (2008).

90. Niebergall,R., Khayat,P.S., Treue,S., & Martinez-Trujillo,J.C. Multifocal attention filters targets from distracters within and beyond primate MT neurons' receptive field boundaries. *Neuron* **72**, 1067-1079 (2011).

91. Roelfsema,P.R., Lamme,V.A.F., Spekreijse,H., & Bosch,H. Figure-ground segregation in a recurrent network architecture. *J. Cognit. Neurosci.* **14**, 525-537 (2002).

92. Shao,Z. & Burkhalter,A. Different balance of excitation and inhibition in forward and feedback circuits of rat visual cortex. *J. Neurosci.* **15**, 7353-7365 (1996).

93. Moore,T. & Armstrong,K.M. Selective gating of visual signals by microstimulation of frontal cortex. *Nature* **421**, 370-373 (2003).

SUPPLEMENTARY INFORMATION

Supplementary Results

Catch trials

Figure S5H compares the MUA response elicited by a homogeneous background (the catch condition, **Figure S5C**) to the response elicited in the background condition with a figure far from the RF (the ground condition, **Figure S5B**). The presence of a figure outside the neurons' RF caused a slight additional suppression of the MUA response (time window from 200-30ms after stimulus onset, t-test, $P<0.001$). Similarly, the gamma LFP-MUA coherence was slightly lower if the neurons' receptive field fell on the background than in the catch condition (**Figure S5E**). Both effects are presumably caused by the selection of a figure outside the RF in the ground condition, and are in accordance with the finding that attentional selection increases the MUA responses as well as gamma oscillations (**Figure 2A**,**D**). The LFP power in the alpha band was somewhat higher in the ground than in the catch condition, but effect did not occur for the LFP-MUA coherence.

Granger causality

Figure S15 illustrates the full multivariate Granger causality frequency spectrum between layers. Causality that is directed upwards (towards the pia) is plotted in red and downwards in blue. For the low frequencies, Granger causality was directed from the deep layers towards layer 4 (note that the largest low frequencies peaks are red) and also from the superficial layers towards layer 4 with a remarkably narrow peak, which was consistently located at 10Hz. This finding supports the hypothesis that the deep and very superficial layers influence activity in the middle layers, and is in accordance with the profile of phase differences between these layers for the alpha rhythm (**Figure 3**) and also with the coherence analysis (**Figure S13**). In contrast, the peak in the Granger causality analysis in the gamma range revealed directional influences from layer 4AB to layer 3 and, in addition, a directional influence from layer 4C and layer 6 towards layer 5. This profile therefore matches the laminar profile of phase differences evident in the trough triggering analysis (**Figure 3**) and in the coherence analysis across layers (**Figure S13**). A previous study also

investigated Granger causality across layers in monkey V1[1]. We notice that the electrodes used in the present study allowed a more fine-grained analysis of the CSD patterns due to the smaller spacing between electrodes (100um as opposed by 150um in ref. 25). We confirm some of the previous findings, but also obtained important additional insights. First, we found that the strongest generator in the alpha range was in the deep layers, in line with the results from Bollimunta et al.[1,2]. Second, we also observed a generator in the very superficial layers driving downwards. Third, we found that the generator of the alpha was in layer 5/6, not in layer 4 as reported by Bollimunta et al.[1]. This result is in line with our analysis of the CSD-MUA coherence, which demonstrated that MUA locking to the alpha rhythm coincided with a sink in layer 5 (**Figure 3B**,**C**). A possibility explanation for the discrepancies between the studies is provided by the improved spatial resolution provided by the narrower spacing between the contact points of our laminar probes, which also enabled a better localization of the boundary between layers 4c and 5 and thereby a more accurate alignment of different penetrations.

Supplementary Methods

Stimuli and Task

We trained 6 adult macaque monkeys (S, E, R, B, J and C) to perform the texture segregation task. A trial began with the fixation point (a red circle of 0.3° diameter) presented on a grey background and the monkey began the trial by directing gaze to a one degree fixation window centred on the fixation point. After 300ms of fixation the texture stimulus was presented. After a further 300ms, the fixation circle was extinguished and the monkey was required to make a saccadic eye-movement into a target-window (4 degrees diameter) centered on the figure position. Correct responses were rewarded with apple juice. Trials in which the animal broke fixation before the fixation point was extinguished were aborted. On 25% of trials we presented a homogeneous texture without a figure (catch condition) and the animals were rewarded for carrying on fixating within the fixation window for a further 400ms. All stimulus conditions were presented in a pseudorandom order.

All stimuli were generated using in-house software and were presented on a CRT monitor with a resolution of 1024x768 pixels and refresh rate of 85Hz, which was viewed from a distance of 75cm. The figure-ground stimuli were full-screen bitmaps of textures consisting of black oriented line elements (45 and 135 orientation) on a white background. Two bitmaps of each texture orientation (i.e. two leftwards oriented and two rightwards oriented textures) were made with randomly placed elements (5345 elements per bitmap with a thickness of 1 pixel and a length of 16 pixels). To make the figure stimuli, a square region of one bitmap of 4 x 4 degrees with the center located on the RF was copied onto the same position of a full-screen bitmap of the orthogonal orientation. Four different versions of each stimulus were made by combining each texture with a figure from one of the two orthogonal textures. These four texture-combinations were shown in a counter-balanced order, ensuring that on average precisely the same contour elements were present inside the RF across the different conditions. Two background conditions were created by rotating the location of the figure 120 or 240 degrees around the fixation point.

Surgical procedures

The animals underwent two surgeries under general anesthesia that was induced with ketamine (15mg/kg injected intramuscularly) and maintained after intubation by ventilation with a mixture of 70% N_2O and 30% O_2, supplemented with 0.8% isoflurane, fentanyl (0.005mg/kg intravenously) and midazolam (0.5mg/kg/h intravenously). In the first operation a head holder was implanted and in monkeys S, E, B, J and C a gold ring was inserted under the conjunctiva of one eye for the measurement of eye position (we measured the eye position of monkey R with a camera system). The monkeys were then trained until they could reliably perform the task. In monkeys S, E and R a recording chamber (Crist Instruments) was subsequently implanted over the operculum of V1 and a craniotomy was performed inside the chamber for the laminar recordings. In monkeys B, J and C multiple grids of 4x5 microelectrodes with 1-1.5 mm length needles (Cyberkinetics Neurotechnology Systems Inc.) were chronically implanted in areas V1 and V4. The 1 mm electrode tips are likely to end up in layer 4 and the 1.5mm tips in layer 4 or just below in layer 5. All procedures complied with the NIH Guide for Care and Use of Laboratory Animals (National Institutes of Health, Bethesda, Maryland), and were approved by the

institutional animal care and use committee of the Royal Netherlands Academy of Arts and Sciences.

Data acquisition and preprocessing

Neuronal data was collected with TDT (Tucker Davis Technology) recording equipment using a high-impedance headstage (RA16AC) and a preamplifier (either RA16SD or PZ2) with a high-pass filter of 2.2Hz, a low-pass filter of 7.5 kHz (-3dB point) and sampled with a rate of 24.4kHz. As in previous studies[3-5], the digitized signals were band-pass filtered (500Hz-5kHz), full-wave rectified and low-pass filtered (200Hz) to produce an envelope of the multi-unit activity (MUA). This MUA signal provides an average of spiking activity of a number of neurons in the vicinity of the tip of the electrode and the population response obtained with this method is therefore expected to be identical to the population response obtained by pooling across single units[6]. For the spectral properties of neuronal activity, MUA gives a higher signal-to-noise ratio than single unit data[3,7]. We applied a low-pass filter (<200Hz) to record the local field potential (LFP).

We used multi-contact 'U' probes (Plexon) for the laminar recordings with 24 contact points spaced 100μm apart (**Figure 1B**). Either the metal shaft of the probe or a silver/silver chloride wire in the recording chamber served as reference. We lowered the electrode across the dura with a micro-manipulator (Narishige, Japan) at a relatively fast rate (~100μm/s) to minimize dimpling of the cortex and ascertained when the first contact point passed the dura by careful visual inspection of the LFP and we then reduced the speed to ~10μm/s.

We calculated the one-dimensional current source density (CSD) from the LFP following Mitzdorf[8] as:

$$CSD(x) = -\sigma \cdot \frac{\phi(x-h) - 2\phi(x) + \phi(x+h)}{h^2}$$

Where ϕ is the voltage, x is the point at which the CSD is calculated, h is the spacing of electrodes for the computation (here we used a spacing of 200μm) and σ is the conductivity of cortical tissue (we used a value of $0.4 S.m^{-1}$)[9]. The CSD is a measure of the currents flowing towards or away from electrode contact points[10,11].

To determine the depth of the electrode we measured the CSD evoked by a full-screen 100% contrast checkerboard (presented for 250ms while the monkey fixated, check size 0.3°)[8,12]. We estimated the location of the border between layer 5 and layer 4C as the polarity reversal from current sinks in layer 4C to current sources in the deep layers around 40ms after stimulus onset[10,12] (**Figure S1**). We placed the electrode so that the CSD reversal was as close as possible to the 8th contact from the tip to ensure coverage of all cortical layers. We estimated the position of the other layers on the basis of histological data[13,14]. We mapped the receptive fields (RFs) of every recording site of the electrode (see below for the RF mapping methods). When the RFs of the recording sites in different layers did not overlap, indicating that the probe was not perpendicular to the cortical surface, the probe was retracted and inserted at a different location. In the final analysis we aligned the data from different penetrations using the CSD reversal of the visual response evoked by the figure-ground stimuli. We removed line noise by fitting a 50Hz sinusoid to the LFP signal of each trial and subtracting it. We calculated the signal-to-noise-ratios (SNR) of every MUA recording site as the height of the peak of the stimulus-evoked response divided by the standard deviation of activity in the prestimulus period. Only recording sites with an SNR>3 were included in the analysis.

In monkeys B and J recordings were made with microelectrode grids in V1 and V4 with overlapping receptive fields (**Figure S17**). To measure the local V1 and V4 LFP for the power and coherence analysis, we referenced the LFP to an electrode within the same array. Hardware filters in the preamplifier stage induce phase shifts in the signal[15]. We measured the shift for every frequency and corrected for them in the frequency domain.

Eye movements were recorded either with a scleral search coil using the double-induction techniqu[16] and sampled at 1017Hz, or using a video eye-tracker (Thomas recordings) with a sampling rate of 350Hz.

Electrical microstimulation

We carried out electrical microstimulation experiments in monkeys B and C using the microelectrode grids in V1 and V4. We delivered trains of 5 biphasic pulses of 500μs duration (250μs per phase) at a frequency of 200Hz with an amplitude in the range of 30-

100μA using a custom-made constant current stimulator. In the first phase of the pulse, one electrode of the V1 or V4 array served as cathode and another electrode in the same array as anode and the polarity was reversed in the second phase. An advantage of this stimulation configuration is that it reduced the stimulation artifact in the other area where we recorded the LFP.

Drug injections

Some of the laminar probes contained a fine glass capillary tube for the injection of fluids into the cortex. The exit point of the tube was commonly between contacts points 7 and 8. The tubes were filled using polyethylene tubing and Hamilton syringes (1μL). Drugs were dissolved either in filtered water or artificial cerebrospinal fluid. The drug was filtered using a sterile microfilter (Millipore, 0.23μm filter). All drugs were obtained from Sigma and were used in the following concentrations: 50 mM APV, 5–10 mM CNQX, and 50–100 μM ifenprodil. We used pressure injection to administer small volumes (25–80 nL) with a Hamilton syringe, either in 10nL steps or in a larger bolus.

Receptive field mapping

We measured the V1 receptive field dimensions by determining the onset and offset of the response to a slowly moving light bar for each of eight movement directions[17]. The MUA RF size in V1 was 1.2 deg on average (standard deviation = 0.28 deg) and the eccentricity was between 1.8 and 5.5 deg (median = 3.7 deg). We mapped the V4 RFs by presenting white dots (0.5-1 deg diameter, luminance 82cd/m^2) on a grey background (luminance 14cd/m^2) at different positions of a grid (0.5 deg spacing). We defined the RF borders as the locations where activity fell below 50% of the maximum[18]. With this definition, the median V4 RF area was 13.6 deg^2 (range 6.5 to 37.7 deg^2). RFs in V4 were considerably larger than those in V1 but there was substantial overlap (**Figure S17**). In the figure condition of the task the V1 RFs fell in the center of the figure.

Data analysis and statistics

Figure 2A shows the MUA population response evoked by the figure and the background. Before pooling responses across the individual MUA recording sites we normalized their activity by subtracting the average spontaneous activity in a window of 150ms before stimulus onset and then dividing by the peak response in the background condition.

We used wavelet analysis and correlation analysis to calculate spectral estimates[19]. The Fourier transform of the signal $x^r(t)$ of every recording site j and every trial r was calculated and convolved with a set of complex Morlet-filters to obtain the time- and frequency-dependent spectrum:

$$F_j^r(t,\omega) = \int dt' g(t,t',\lambda_c,\lambda_b) x_j^r(t')$$

With the complex Morlet filters given by:

$$g(t,t',\lambda_c,\lambda_b) = \frac{1}{\lambda_b\sqrt{\pi}} e^{-\frac{(t-t')^2}{\lambda_b^2}} e^{-i\frac{(t-t')}{\lambda_c}} \text{ with } \lambda_c = 2\pi/\omega \text{ and } \lambda_b = \alpha\lambda_c .$$

This can be understood as a complex exponential with wavelength λ_c, windowed by a Gaussian with a standard deviation equal to $\lambda_b/\sqrt{2}$. λ_b is set equal to λ_c times the scaling parameter α, making the length of the wavelet linearly dependent on the frequency. α was set to 1, making the standard deviation of the wavelet envelope equal to $\lambda_c/\sqrt{2}$. The effective temporal bandwidths of the wavelets therefore corresponded to $100/\sqrt{2}$ ms for alpha and about $17/\sqrt{2}$ ms for gamma. The time representation of the wavelet envelopes were truncated at $\pm 3\lambda_b$. The wavelet envelopes were allowed to extend beyond the chosen time window by maximally half a Gaussian.

The power spectrum of site j was defined as:

$$P_j(t,\omega) = \frac{1}{N}\sum_{r=1}^{N} \left| F_j^r(t,\omega) \right|$$

where N is the total number of trials[20]. The cross spectral density function for recording sites j and k was calculated for each trial r as:

$$S_{jk}^{r}(t,\omega) = \frac{1}{T} F_{j}^{r}(t,\omega)^{*} F_{k}^{r}(t,\omega)$$

where the * denotes the complex conjugate. This equation can also be expressed as:

$$S_{jk}^{r}(t,\omega) = C_{jk}^{r}(t,\omega) - iQ_{jk}^{r}(t,\omega)$$

where the real part, denoted by $C_{jk}^{r}(t,\omega)$, is the coincidence spectral density function and the imaginary part $Q_{jk}^{r}(t,\omega)$ is the quadrature spectral density function. The coherence function was calculated from the cross spectral density as:

$$Coh_{jk}(t,\omega) = \frac{\left|\sum_{r=1}^{N} S_{jk}^{r}(t,\omega)\right|}{\sqrt{\sum_{r=1}^{N} S_{jj}^{r}(t,\omega) \sum_{r=1}^{N} S_{kk}^{r}(t,\omega)}}$$

and the instantaneous phase function as:

$$Ph_{jk}(t,\omega) = -\tan^{-1} \frac{\sum_{r=1}^{N} Q_{jk}^{r}(t,\omega)}{\sum_{r=1}^{N} C_{jk}^{r}(t,\omega)}$$

To compute the LFP-MUA and CSD-CSD coherence, we selected sites on the laminar probe with a distance of 200μm.

The analysis window was from 150 to 350ms after the presentation of the visual stimulus (unless otherwise noted). For these analyses the average LFP signal over all trials was subtracted from the signal of every trial, separately for each condition and each channel to focus on internally generated rhythms. To estimate the contribution of stimulus locked activity to the coherence measurements we repeated the analysis for shuffled trials but observed no clear peaks (dashed lines in **Figure S3**), which confirmed that oscillatory activity was not time-locked to the stimulus onset (see also **Figure 2B**, **6D**, **S20A**,**B**). Furthermore, the effects of the task on the LFP power and LFP-MUA did not critically

depend on the subtraction of the stimulus-evoked LFP potential (**Figure S20C-F**) as they occurred in a time-window after the strongest components of the evoked potential.

We carried out permutation tests to determine the p-values for differences in LFP power between conditions, separately for low frequencies (below 25Hz) and high frequencies (above 30Hz) (**Figure S2A-C**). Specifically, we shuffled the class labels (figure or ground) 10.000 times, for each permutation we determined the mean power spectrum across recording, calculated the difference spectrum, selected the two frequency bins with the highest and lowest differences in power and stored those values. This resulted in a distribution of 20.000 values from which p-values could be determined by calculating the upper and lower percentiles corresponding to that p-value (for example the 0.05 and 99.95 percentiles for a p-value of 0.001)[21]. CircStat, a toolbox for circular statistics, was used for all statistical analyses involving phases[22].

Because oscillatory activity is not necessarily linked to external events that can serve as triggers to average individual waves of activity, we used the troughs of oscillatory activity in the LFP as reference points[23,24]. To select genuine oscillatory activity, we selected the 50% of trials with highest power in the relevant frequency band (we obtained equivalent results if we included all trials). We determined the troughs by filtering the LFP of one recording site in layer 4C (~250μm above the CSD reversal between layer 4C and layer 5) in the desired frequency band (8-12Hz for alpha and 55-65Hz for gamma) (**Figure S6**). Only troughs occurring in a period from 150-350ms after stimulus onset were stored, after which the filtered signal was not used further. Time windows around the troughs were then used to average the LFP, the CSD and the MUA of all channels, after subtraction of the mean response (equivalent to subtraction of the shift-predictor). The size of these time windows was 1.5 times the period of the mean filtered frequency, and we excluded windows that extended beyond 100-350ms after stimulus onset. All trough-triggered traces were added together, divided by the total number of troughs per monkey and subsequently averaged across monkeys. We expressed the amplitude of the fluctuations in the MUA revealed by this analysis (**Figure 3**) as fraction of the mean MUA response in the window from 150-350ms after stimulus onset, after smoothing with a sliding window of 5ms for gamma and 25ms for alpha.

To measure the phase shifts in MUA between layers, we averaged LFP-triggered MUA across laminar compartments (**Figure 3D**,**H**). We assigned recording sites between 550 and 50μm below the CSD reversal to the deep layers, between 50 and 550μm above the reversal to layer 4, and between 650 and 1050 μm above the reversal to the superficial layers. To estimate phase differences between the MUA in different compartments we fitted a sinusoid with the frequency of the band-pass filter used to determine the LFP troughs. Statistical significance of these time delays was calculated over penetrations (i.e. recording days). We extended this analysis by determining LFP-troughs for a wide range of frequencies (in steps of 2 Hz using a band-pass filter with a width of 4Hz, i.e. 2Hz overlap between adjacent frequency bins) to investigate how the MUA phase differences between laminar compartments depend on frequency (**Figure S7**).

We used the MVGC toolbox[25] to compute Granger causality with a model order of 50ms[1,2]. We used the CSD to compute the Granger causality between layers and the LFP (global reference) for Granger causality between V1 to V4. We used bootstrapping to estimate the standard error of the means (10.000 samples) and permutation tests to calculate the significance of the difference in Granger causality between layers and between V1 and V4 averaged in the alpha and gamma band (10.000 permutations). We controlled for multiple comparisons between layers by calculating for each permutation the full matrix of comparisons between laminar compartments averaged within the alpha and gamma band, for each permutation only the maximum and minimum value was taken within this matrix. This resulted in a distribution of 20.000 values from which we determined the p-values (the 0.05 and 99.95 percentiles for a p-value of 0.001).

Design of anatomical figures

For the lateral view of the macaque brain in Fig, 1A we adapted drawings of Nieuwenhuis et al.[26] and Krieg[27]. The Nissl section illustrating the different layers in **Figures 1B** and **S19A** was adapted from O'Kusky and Colonnier[14].

Supplementary Figures

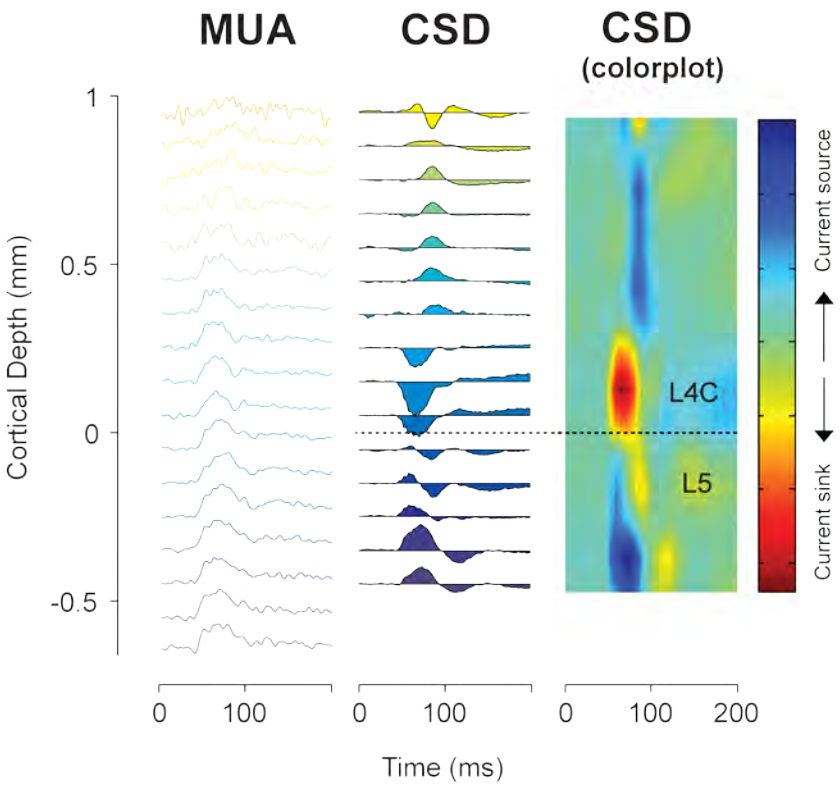

Figure S1 | Example of laminar recordings. An example penetration showing the MUA (left graph) and CSD (middle and right graph) triggered by a full-screen, full-contrast checkerboard stimulus. Simultaneous responses from 17 contacts are shown stacked. In the leftmost columns blue colours indicate deeper channels and green/yellow colours indicate shallow channels. MUA was normalized to the peak of the response for each recording site. In the right column the red colours show current sinks and the blue colours current sources. The dashed line shows the boundary between layers 4 and 5, estimated as the transition between the earliest sink and source evoked by the appearance of the visual stimulus.

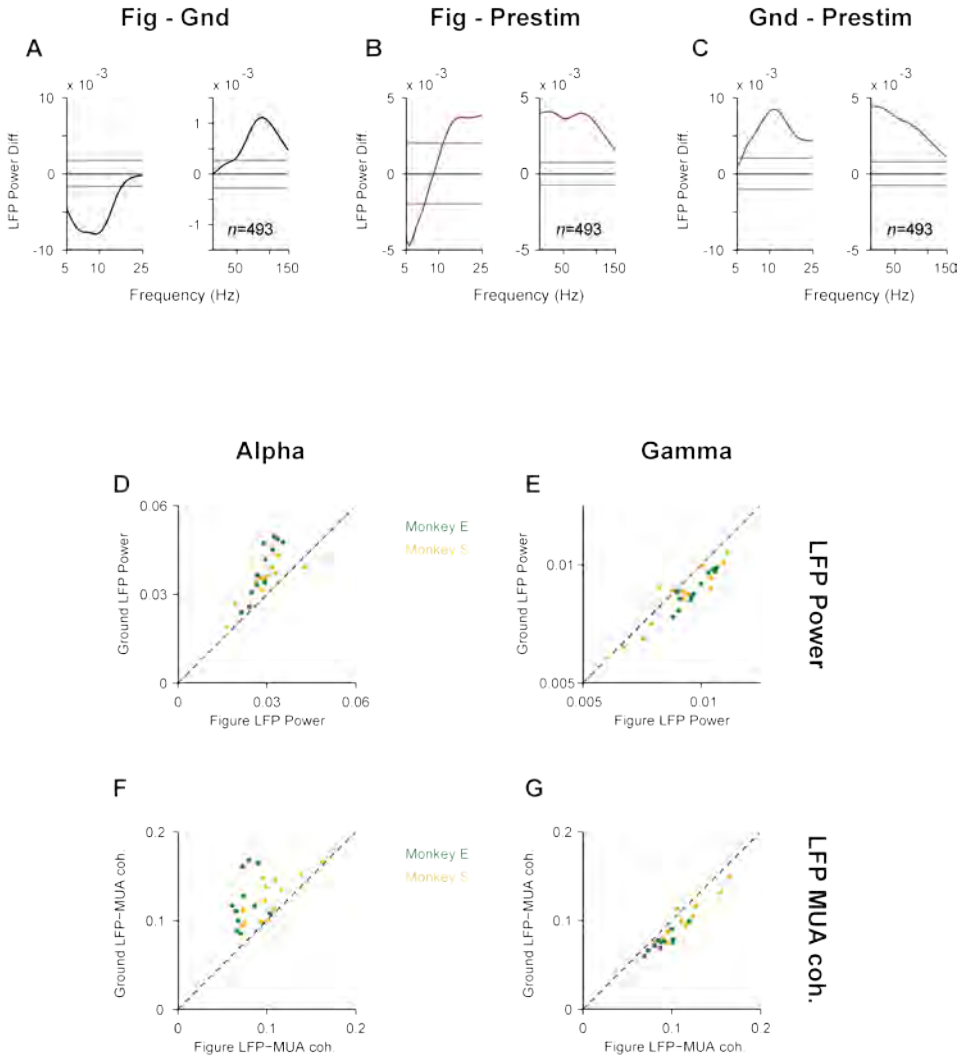

Figure S2 | Supplementary statistics for LFP power and LFP-MUA coherence. (**A**) Difference in LFP power between the response evoked by the figure and the background in a window from 150-350ms after stimulus onset. (**B**) Difference in LFP power between the response evoked by the figure and the pre-stimulus period (200-0ms before stimulus onset). (**C**) Difference in LFP power between the response evoked by the background and the pre-stimulus period. Grey lines indicate p<0.001 (signed permutation test; *n*=493 recording sites). (**D**-**G**) Scatter plots for LFP power (D,E) and LFP-MUA coherence (F,G) for the alpha (D,F) and gamma band (E,G) elicited by the figure (abscissa) and background (ordinate). Yellow circles indicate penetrations for monkey S (13 penetrations) and green circles for monkey E (11 penetrations) (*t*-test, *Ps*<0.001 for all comparisons).

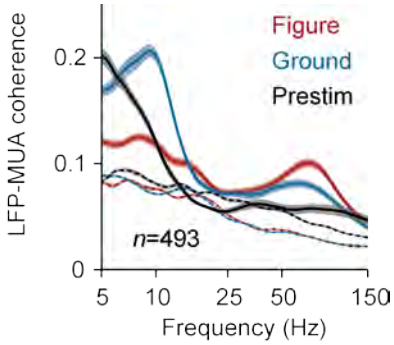

Figure S3 | Average LFP-MUA coherence in the figure (red trace) and background condition (blue trace) during the modulation period, and the pre-stimulus period (black trace). The dashed lines indicate the LFP-MUA coherence for shuffled trials. Notice that these spectra fell below the unshuffled trials and showed no clear peaks, indicating that oscillatory activity was significant and not time-locked to the stimulus onset. Shaded areas show s.e.m. in all plots (n=493 recording sites), when they are difficult to see the s.e.m. is small.

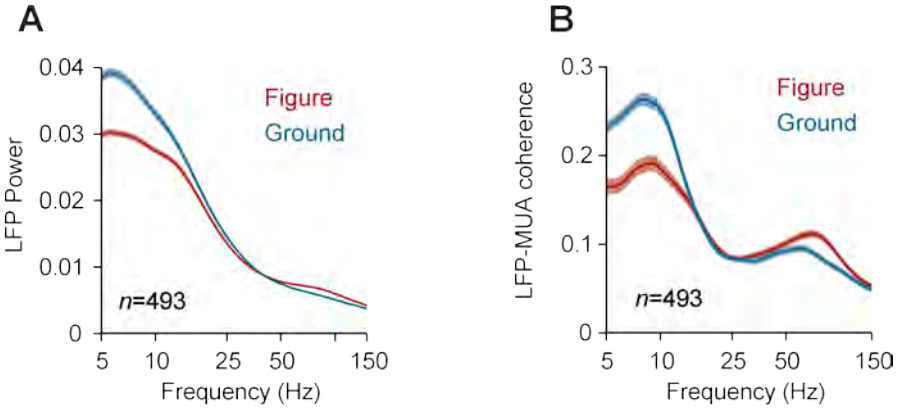

Figure S4 | Control analysis with extended time-window. LFP power spectrum (**A**) and LFP-MUA coherence (**B**) in a window from 150-450ms in trials with a reaction time longer than 420ms, for the figure (red trace) and ground condition (blue trace).

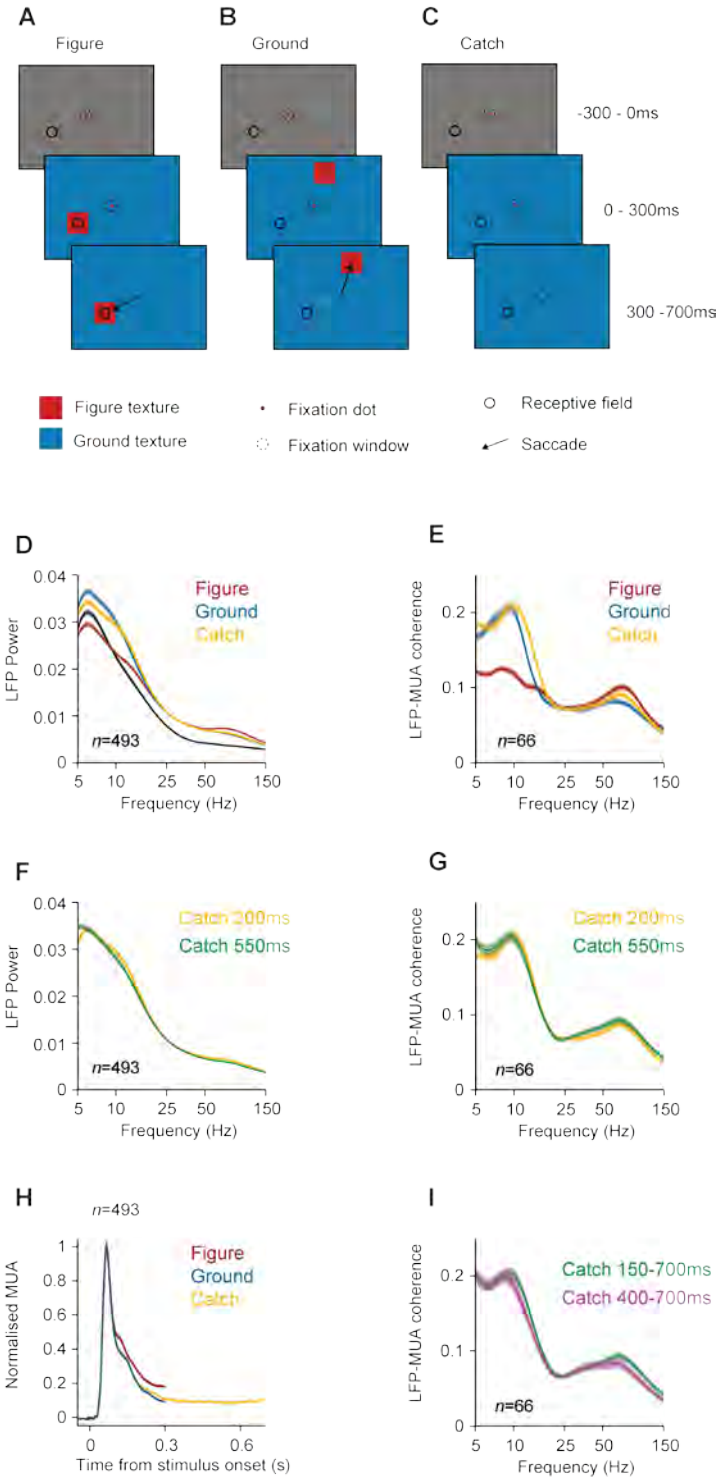
A
Figure
B
Ground
C
Catch
-300 - 0ms
0 - 300ms
300 -700ms
Figure texture
Ground texture
Fixation dot
Fixation window
Receptive field
Saccade
D
LFP Power
Figure
Ground
Catch
n=493
Frequency (Hz)
E
LFP-MUA coherence
Figure
Ground
Catch
n=66
Frequency (Hz)
F
LFP Power
Catch 200ms
Catch 550ms
n=493
Frequency (Hz)
G
LFP-MUA coherence
Catch 200ms
Catch 550ms
n=66
Frequency (Hz)
H
n=493
Normalised MUA
Figure
Ground
Catch
Time from stimulus onset (s)
I
LFP-MUA coherence
Catch 150-700ms
Catch 400-700ms
n=66
Frequency (Hz)

Figure S5 | Power spectra and LFP-MUA coherence in catch trials. Schematic representation of the time course of the task and the different trial types. The monkeys started a trial by fixating within a small window (indicated by the dashed circle) centered on a fixation point (indicated by the red dot). After 300ms, a figure-ground texture appeared (the blue region illustrates the background, the red square illustrates the location of the figure). (**A**-**C**) In the figure condition (A), a figure was centered on the neurons' receptive field (circle) and in the ground conditions (B) the figure appeared at one of two other locations so that the receptive field fell on the background. The monkeys were rewarded for an eye movement to the figure (arrow). There were also 25% catch trials with a homogenous texture of one orientation. The monkey was rewarded for maintaining fixation for another 400ms (C), so that we could analyze the power spectrum in a longer time window. (**D**, **E**) LFP power spectrum (D) and LFP-MUA coherence (E) for the figure condition (red trace), the ground condition (blue trace) and the catch condition (yellow trace), in a time window from 150-350ms after stimulus onset. (***F***, **G**) Comparison of the LFP power (F) and LFP-MUA coherence (G) in the catch condition in a 200ms (150-350ms after stimulus onset, yellow trace) and a 550ms time-window (150-700ms after stimulus onset, green trace). Shaded areas show s.e.m. in all plots (*n*=493 recording sites). (**H**) Average MUA response in V1 evoked by the figure (red trace), the background (blue trace) and the catch condition (n=493 recording sites). The traces for the figure and ground condition are truncated at the time when the monkey was allowed to make a saccade. Note that the MUA in catch trials reaches a relatively stable level in the later period of the trial. (**I**) Average LFP-MUA coherence in the catch condition in a window from 150-700ms after stimulus onset (green) and 400-700ms after stimulus onset (purple). Shaded areas show s.e.m. in all plots (n=493 recording sites).

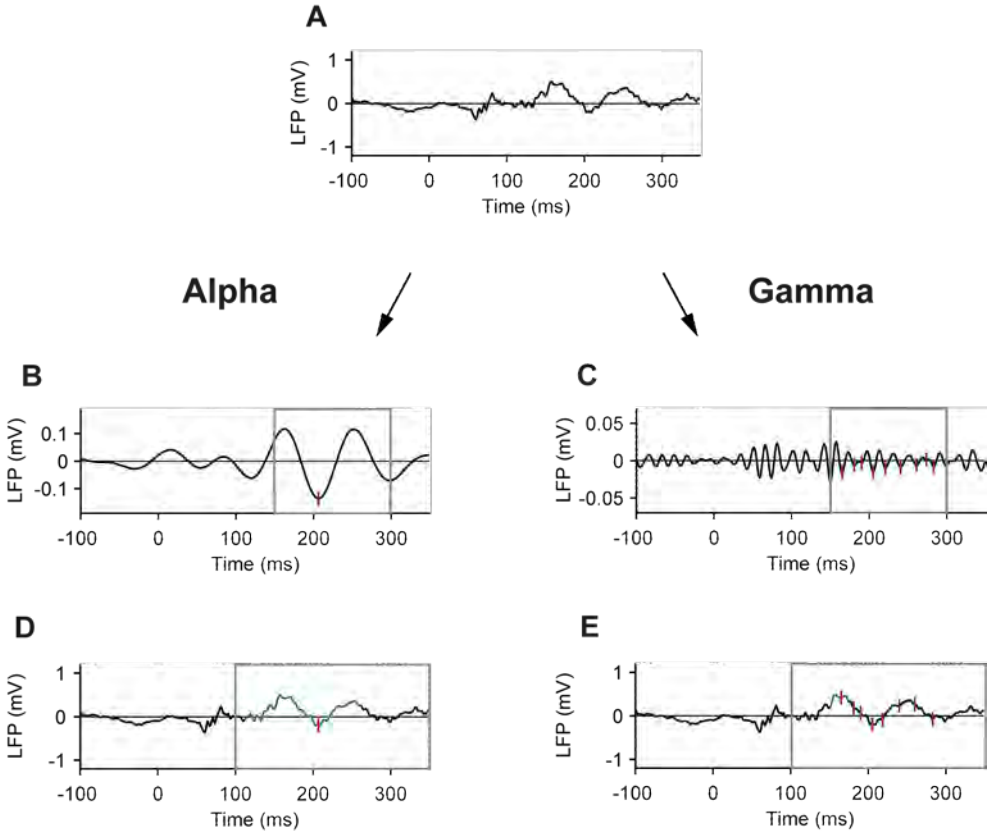

Figure S6 | Trough-triggering analysis. (**A**) LFP trace of a representative trial where the RF of a recording site fell on the background, after subtraction of the mean evoked potential. Note the presence of alpha and gamma oscillations. (**B**,**C**) To determine the timing of troughs of the oscillations, the LFP was filtered between 8-12Hz (B) and 55-65Hz (C). Red marks indicate troughs within the computational window (150-300ms, grey rectangle). (**D**,**E**) The troughs detected in the filtered signal were mapped back onto the broad-band LFP for averaging.

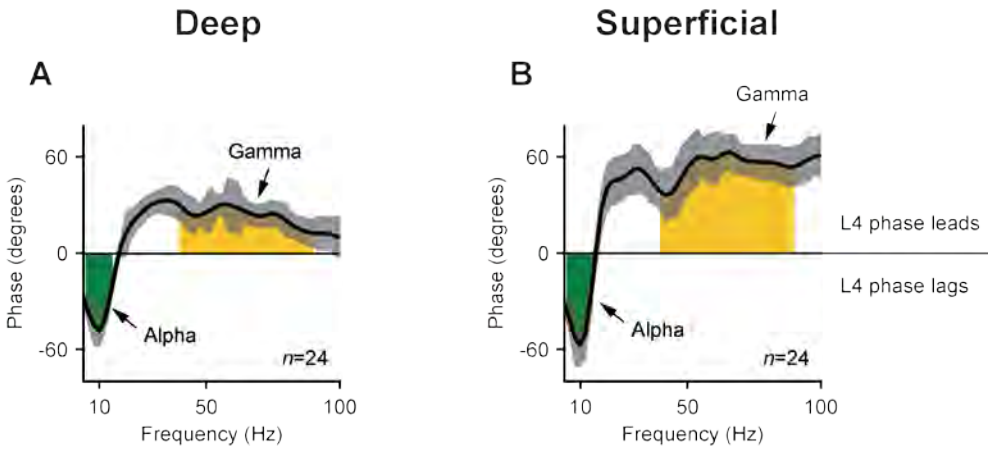

Figure S7 | MUA phase in deep and superficial layers relative to layer 4. MUA phase in the deep (**A**) and superficial layers (**B**) relative to the MUA in layer 4 for different frequencies. We aligned the MUA on the troughs of the LFP in layer 4 for different frequencies with a band-pass filter (width of 4Hz). Positive values denote a phase lead of layer 4. Green and yellow areas indicate the frequencies that we assigned to the alpha (5-15Hz) and gamma (40-90Hz) range. Shaded areas show s.e.m. (*n*=24 penetrations).

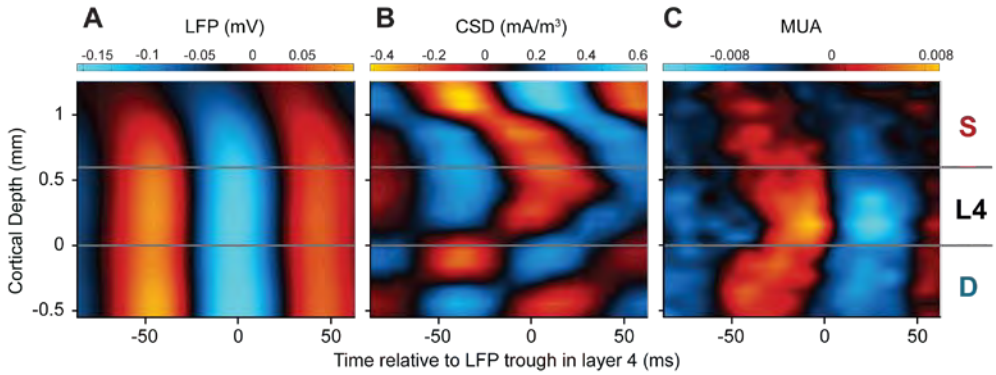

Figure S8 | Laminar profile of alpha oscillations in the prestimulus period. (**A**) Laminar profile of the LFP (mV) relative to the alpha troughs in a window from 150-0ms before stimulus onset, averaged across 24 penetrations. Negative potentials are shown in blue, positive potentials in red. (**B**) Average laminar profile of the CSD (mA/m3) relative to LFP troughs in layer 4 for the alpha rhythm. Current sinks are shown in red, sources in blue. (C) MUA aligned to the LFP troughs in layer 4. Red colors show MUA that is higher than the average and blue colors MUA lower than the average.

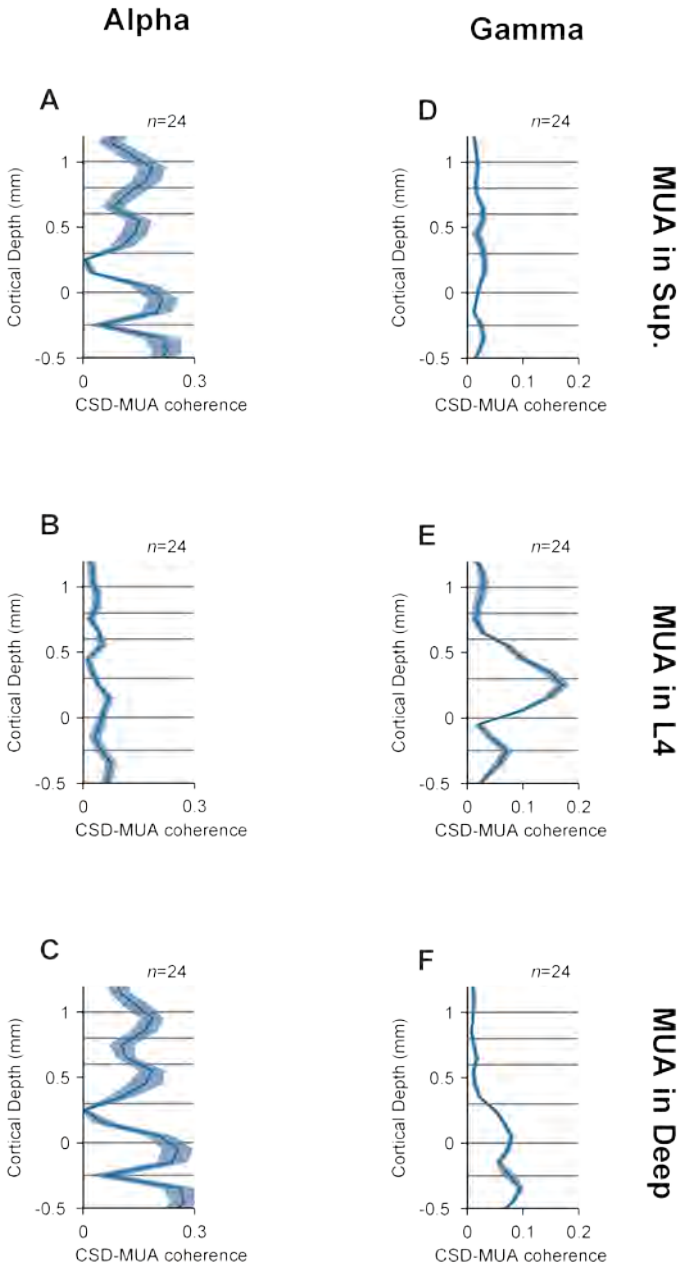

Figure S9 | Laminar profile of CSD-MUA coherence for the alpha band (**A**-**C**) and the gamma band (**D**-**F**) separately for the MUA averaged across superficial layers (A,D), layer 4 (B,E) and deep layers (C,F).

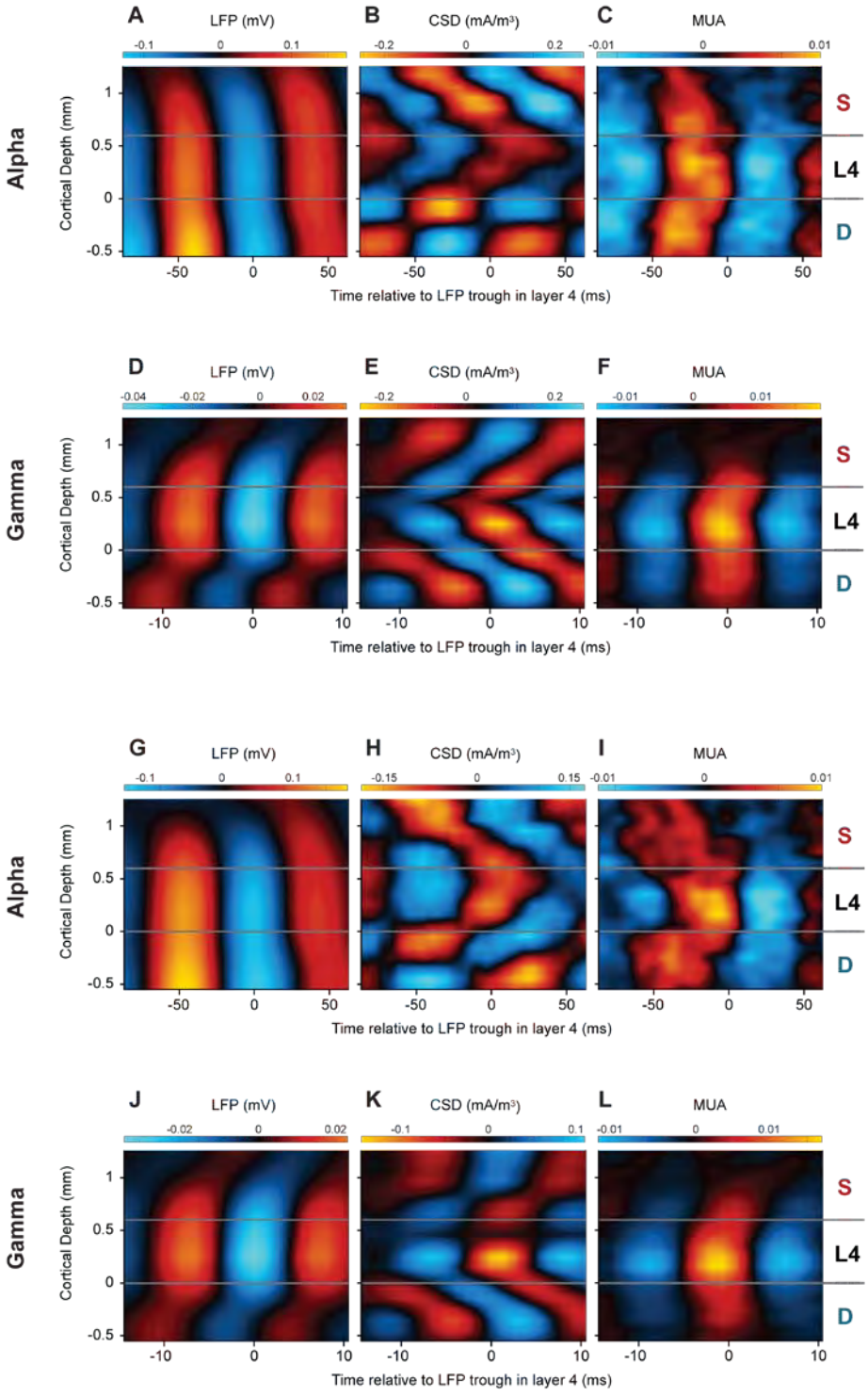
A
LFP (mV)
B
CSD (mA/m³)
C
MUA
Alpha
Cortical Depth (mm)
S
L4
D
Time relative to LFP trough in layer 4 (ms)
D
LFP (mV)
E
CSD (mA/m³)
F
MUA
Gamma
G
LFP (mV)
H
CSD (mA/m³)
I
MUA
Alpha
J
LFP (mV)
K
CSD (mA/m³)
L
MUA
Gamma

Figure S10 | Laminar profile of cortical oscillations separately for monkey E (**A**-**F**) and monkey S (**G**-**L**). (A) Laminar profile of the LFP (mV) relative to the alpha troughs in a window from 150-300ms after stimulus onset, averaged across 11 penetrations of monkey E. Negative potentials are shown in blue, positive potentials in red. (B) Average laminar profile of the CSD (mA/m3) relative to LFP troughs in layer 4 for the alpha rhythm. Current sinks are shown in red, sources in blue. (C) MUA aligned to the LFP troughs in layer 4. Red colors show MUA that is higher than the average and blue colors MUA lower than the average. (D-F) Same analysis as in A-C, but now the data was aligned to the troughs of the gamma rhythm (55-65Hz) in layer 4. (G-L) Same analysis as in A-F but averaged across 13 penetration for monkey S.

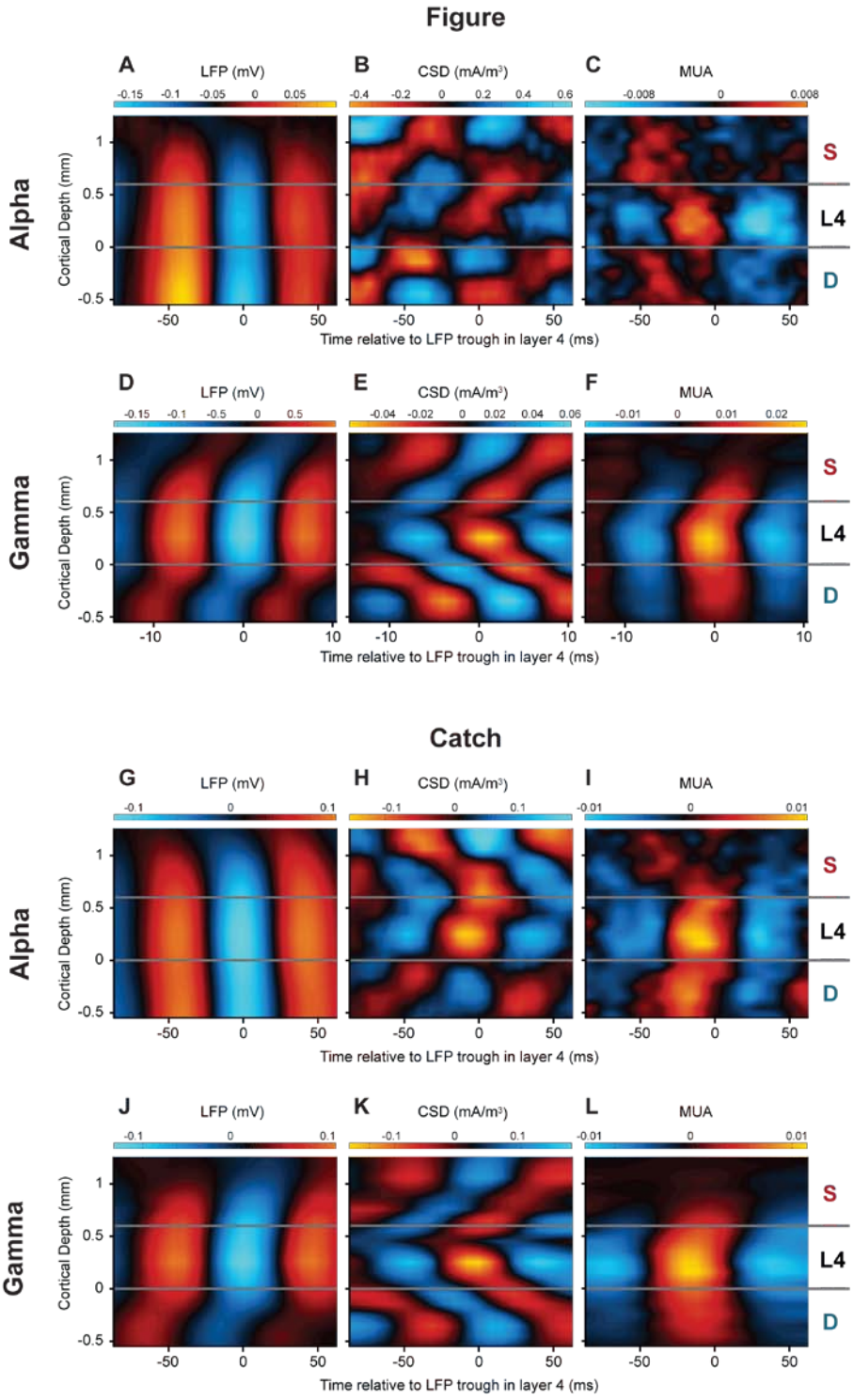
Figure
A
LFP (mV)
-0.15 -0.1 -0.05 0 0.05
B
CSD (mA/m³)
-0.4 -0.2 0 0.2 0.4 0.6
C
MUA
-0.008 0 0.008
Alpha
Cortical Depth (mm)
1
0.5
0
-0.5
-50 0 50
S
L4
D
Time relative to LFP trough in layer 4 (ms)
D
LFP (mV)
-0.15 -0.1 -0.5 0 0.5
E
CSD (mA/m³)
-0.04 -0.02 0 0.02 0.04 0.06
F
MUA
-0.01 0 0.01 0.02
Gamma
-10 0 10
Catch
G
LFP (mV)
-0.1 0 0.1
H
CSD (mA/m³)
I
MUA
-0.01 0 0.01
J
LFP (mV)
K
CSD (mA/m³)
L
MUA

Figure S11 | Laminar profile of cortical oscillations for different task conditions. (**A**-**C**) Laminar profile of cortical oscillations if the figure fell in the neurons' RF. (A) Laminar profile of the LFP (mV) relative to the alpha troughs in a window from 150-300ms after stimulus onset, averaged across 24 penetrations. Negative potentials are shown in blue, positive potentials in red. (B) Average laminar profile of the CSD (mA/m^3) relative to LFP troughs in layer 4 for the alpha rhythm. Current sinks are shown in red, sources in blue. (C) MUA aligned to the LFP troughs in layer 4. Red colors show MUA that is higher than the average and blue colors MUA lower than the average. (**D**-**F**) Same analysis as in A-C, but now the data was aligned to the troughs of the gamma rhythm (55-65Hz) in layer 4. (**G**-**L**) Same analysis as in A-F but for the catch trials in a late 300ms time window (400-700ms after stimulus onset).

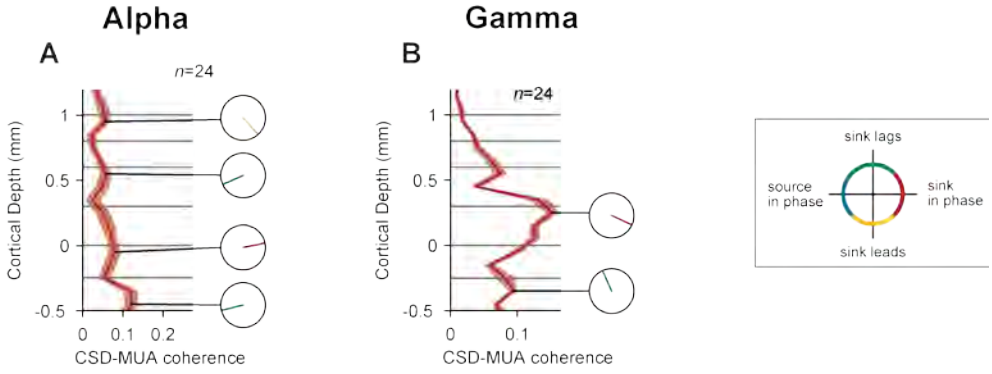

Figure S12 | Laminar profile of CSD-MUA coherence and phase for the figure condition. (**A**) Laminar profile of coherence between the layer-specific CSD and the MUA averaged across all layers, for the alpha band. There were four peaks in the coherence and the small circles show the phase of the CSD relative to the MUA. (**B**) Laminar profile of the CSD-MUA coherence in the gamma frequency range.

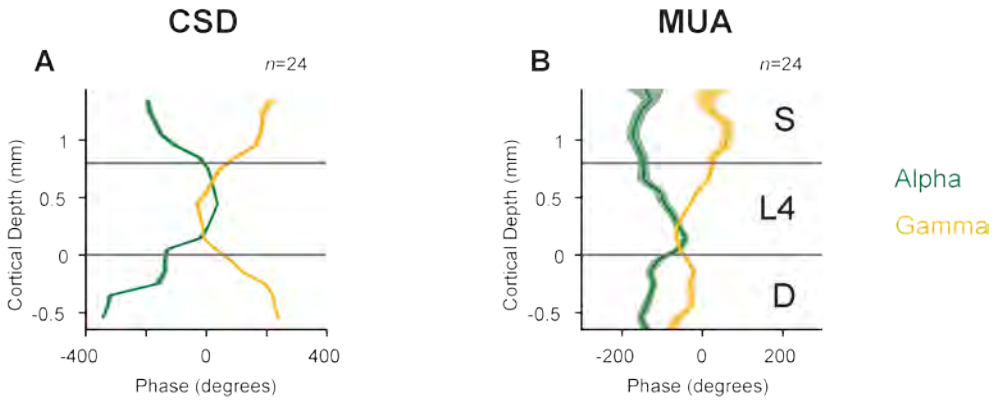

Figure S13 | Phase differences of the CSD and MUA in the different layers relative to the LFP in layer 4. (**A**) We used the LFP in layer 4 as reference signal and computed the phase of the CSD in the different layers for the alpha (green line) and gamma rhythm (yellow line). (**B**) Phase of the MUA in the different layers relative to the LFP in layer 4 for alpha and gamma activity. Shaded areas show s.e.m. (*n*=24 penetrations).

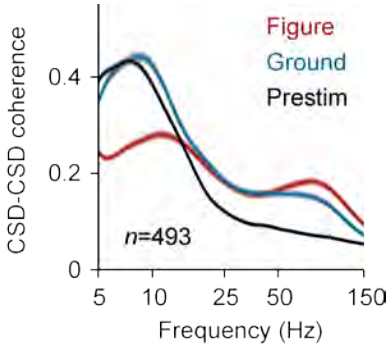

Figure S14 | Coherence of the CSD between sites on the laminar probe with a distance of 200µm in the figure (red trace) and background condition (blue trace) during the modulation period, and the pre-stimulus period (black trace). Shaded areas show s.e.m. in all plots (n=493 recording sites).

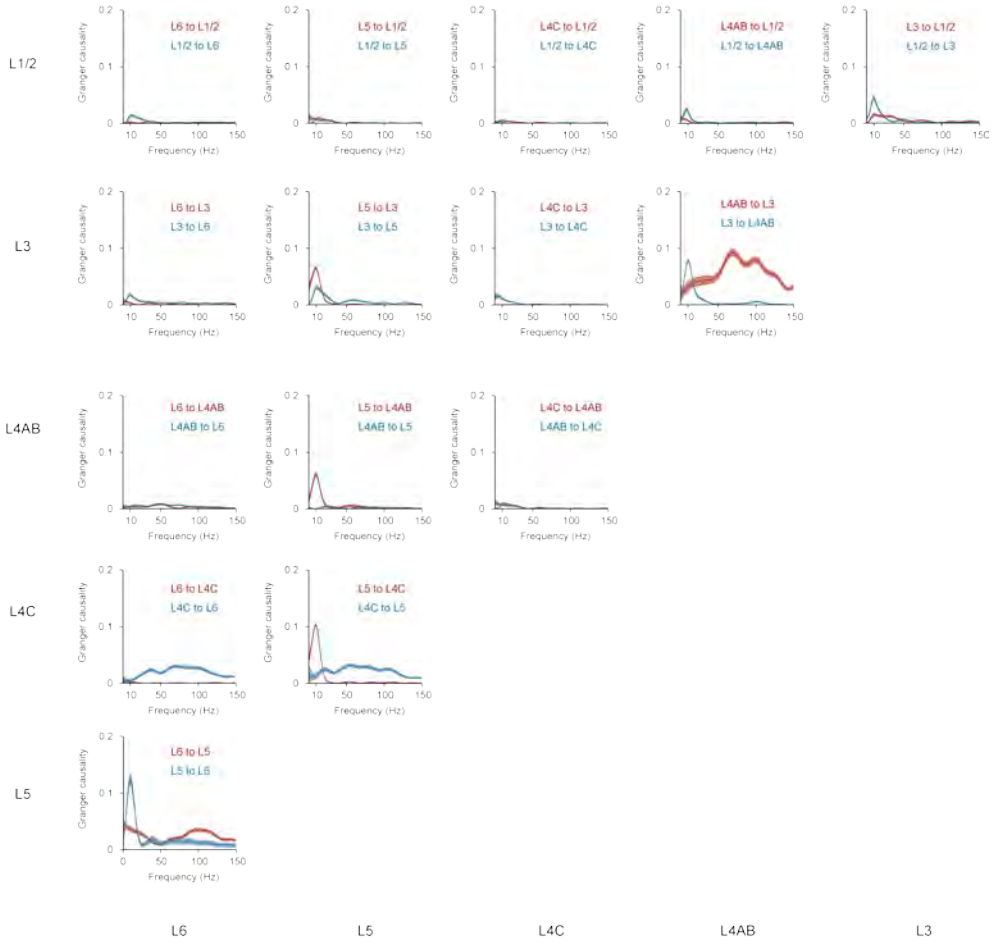

Figure S15 | Multivariate Granger causality of the CSD between the different layers in V1. Red lines indicate Granger causality in the upward direction (towards the pia), blue lines in the downward direction (towards the white matter). Shaded areas show s.e.m. (n=24 penetrations).

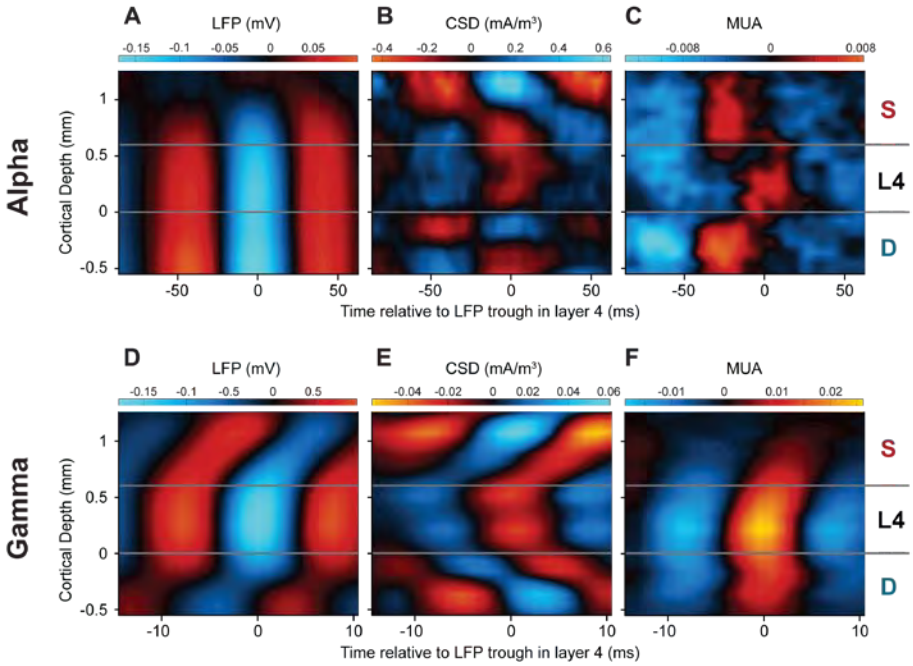

Figure S16 | Laminar profile of cortical oscillations in the curve tracing task. (**A**) Laminar profile of the LFP (mV) relative to the alpha troughs, in a window from 200-750ms after stimulus onset with the RF on the distractor curve, averaged across 16 penetrations. Negative potentials are shown in blue, positive potentials in red. (**B**) Average laminar profile of the CSD (mA/m^3) relative to LFP troughs in layer 4 for the alpha rhythm. Current sinks are shown in red, sources in blue. (**C**) MUA aligned to the LFP troughs in layer 4. Red colors show MUA that is higher than the average and blue colors MUA lower than the average. (**D**-**F**) Same analysis as in A-C, but now the data was aligned to the troughs of the gamma rhythm (55-65Hz) in layer 4.

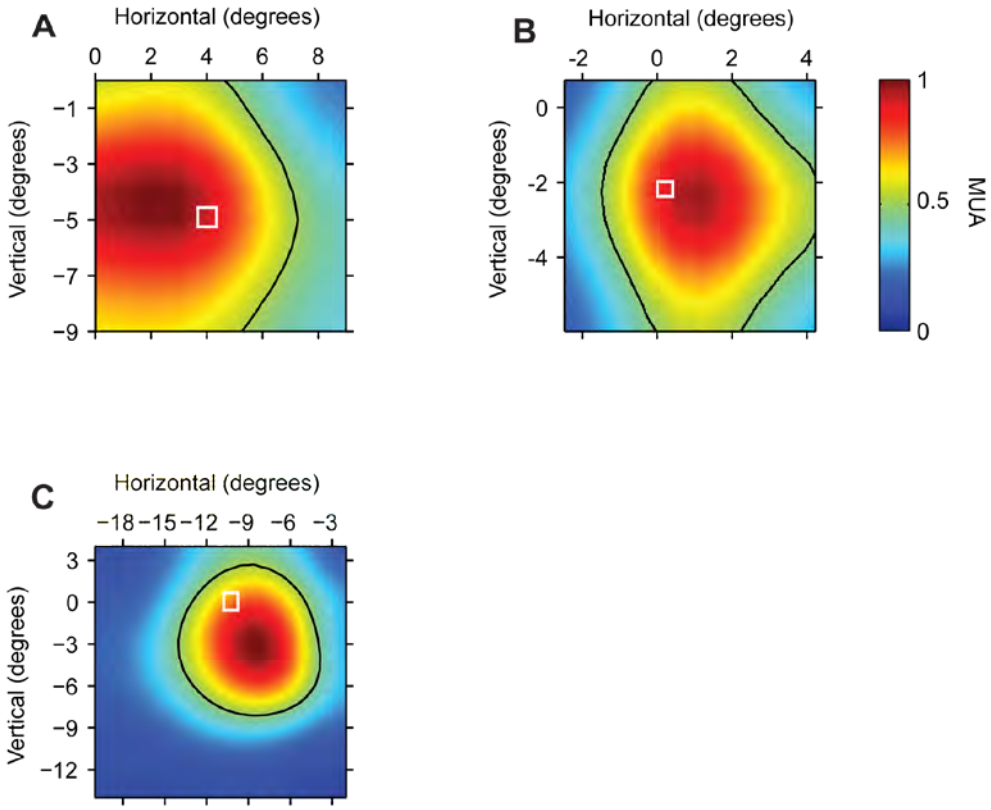

Figure S17 | RFs of recording sites in V1 (white squares) and V4 (color plots) in the three monkeys. Black line indicates region beyond which the V4 response falls below 50% of the maximum.

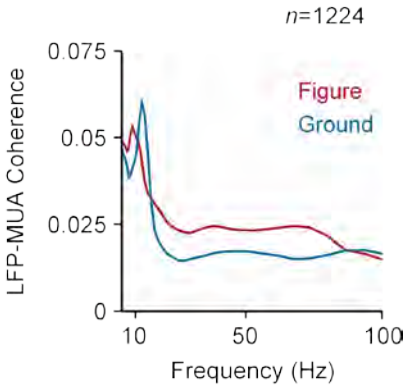

Figure S18 | Coherence between the (monopolar) LFP in V4 and the MUA in V1 in a window from 150-350 ms after stimulus onset when the neurons' receptive fields fell on the figure (red trace) or on the background (blue trace).

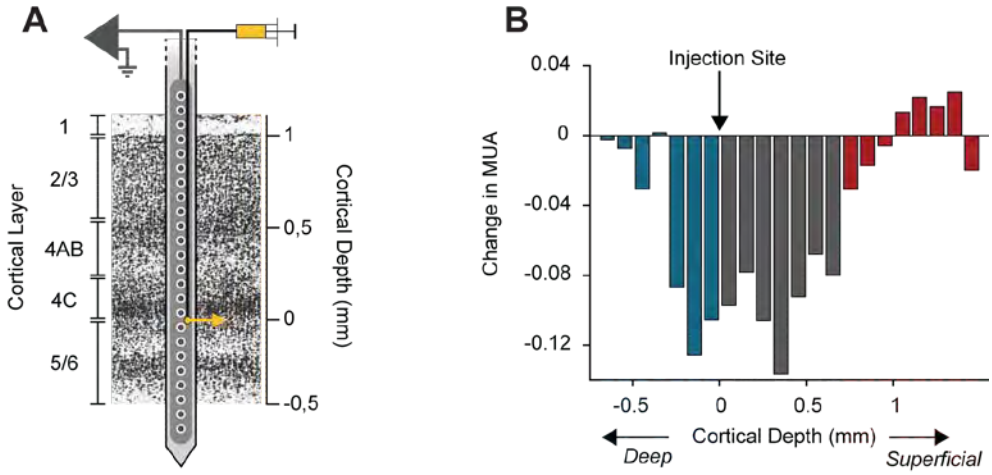

Figure S19 | Spread of pharmacological substances. (**A**) Drugs were injected through a fluid line. The yellow arrow indicates the approximate location of the fluid line exit. (**B**) An example recording where CNQX was injected at the boundary between layer 4c and layer 5 to measure the diffusion of the drug. The bars indicate the change in the average MUA response evoked by the appearance of the visual stimulus at each recording site (between 0-200ms after stimulus onset in normalized units) after injection of the drug. It can be seen that the drug diffuses from the injection site with a slight preference to spread towards the superficial sites, back along the shaft of the electrode. The maximum extent of the drug effect is ~1.5mm. The colors of the bars represent the different cortical layers, deep in blue, layer 4 in grey and superficial in red.

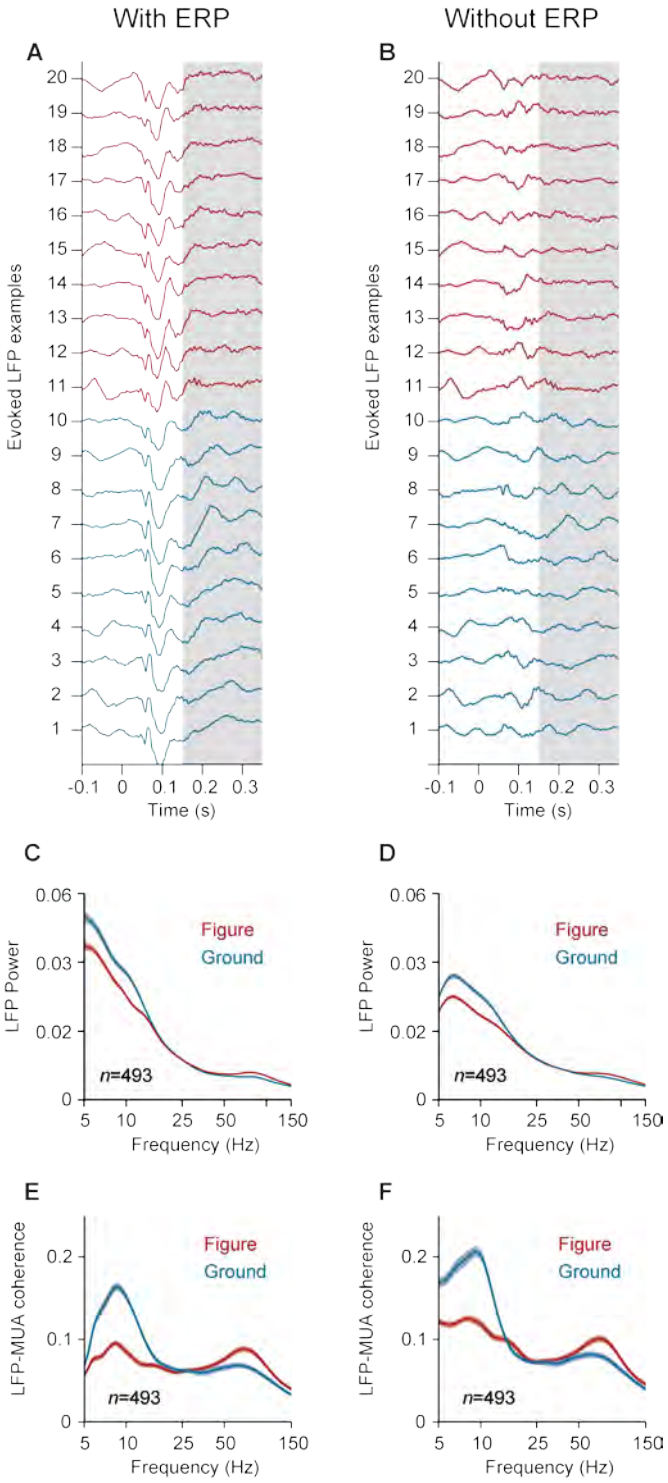
With ERP
Without ERP
A
B
Evoked LFP examples
Time (s)
C
D
LFP Power
Figure
Ground
n=493
Frequency (Hz)
E
F
LFP-MUA coherence

Figure S20 | Neuronal activity in single trials of the texture segregation task and the effect of subtracting the evoked potential. (**A**) LFP responses in successive trials of an example recording session without subtraction of the mean LFP response. Trials of the figure condition are shown in red and trials of the ground condition in blue. (**B**) LFP in the same trials after subtraction of the evoked potential. Grey area highlights the analysis window for frequency analysis (150-350ms after stimulus onset). (**C**,**D**) The average LFP power spectrum across all penetrations before (C) and after subtraction of the evoked potential (D). (**E**,**F**) The average LFP-MUA coherence spectrum across all penetrations before (E) and after subtraction of the LFP evoked potential (F). Red, figure condition; blue, ground condition. Shaded areas show s.e.m. (*n*=493 recording sites).

Supplementary References

1. Bollimunta,A., Mo,J., Schroeder,C.E., & Ding,M. Neuronal mechanisms and attentional modulation of corticothalamic alpha oscillations. *J. Neurosci.* **31**, 4935-4943 (2011).

2. Bollimunta,A., Chen,Y., Schroeder,C.E., & Ding,M. Neuronal mechanisms of cortical alpha oscillations in awake-behaving macaques. *J. Neurosci.* **28**, 9976-9988 (2008).

3. Supèr,H. & Roelfsema,P.R. Chronic multi-unit recordings in behaving animals: advantages and limitations. *Prog. Brain Res.* **147**, 263-282 (2005).

4. Logothetis,N.K., Pauls,J., Augath,M., & Oeltermann,A. Neurophysiological investigation of the basis of the fMRI signal. *Nature* **412**, 150-157 (2001).

5. Xing,D., Yeh,C.-I., & Shapley,R.M. Spatial spread of the local field potential and its laminar variation in visual cortex. *J. Neurosci.* **29**, 11540-11549 (2009).

6. Logothetis,N.K. The neural basis of the blood-oxygen-level-dependent functional magnetic resonance imaging signal. *Philos. Trans. R. Soc. Lond B Biol. Sci.* **357**, 1003-1037 (2002).

7. Zeitler,M., Fries,P., & Gielen,S. Assessing neuronal coherence with single-unit, multi-unit, and local field potentials. *Neural Comput.* **18**, 2256-2281 (2006).

8. Mitzdorf,U. Current source-density method and application in cat cerebral cortex: investigation of evoked potentials and EEG phenomena. *Physiol. Rev.* **65**, 37-100 (1985).

9. Logothetis,N.K., Kayser,C., & Oeltermann,A. In vivo measurement of cortical impedance spectrum in monkeys: implications for signal propagation. *Neuron* **55**, 809-823 (2007).

10. Mitzdorf,U. & Singer,W. Excitatory synaptic ensemble properties in the visual cortex of the macaque monkey: a current source density analysis of electrically evoked potentials. *J. Comp Neurol.* **187**, 71-83 (1979).

11. Buzsaki,G., Anastassiou,C.A., & Koch,C. The origin of extracellular fields and currents--EEG, ECoG, LFP and spikes. *Nat. Rev. Neurosci.* **13**, 407-420 (2012).

12. Schroeder,C.E., Tenke,C.E., Givre,S.J., Arezzo,J.C., & Vaughan,H.G., Jr. Striate cortical contribution to the surface-recorded pattern-reversal VEP in the alert monkey. *Vision Res.* **31**, 1143-1157 (1991).

13. Lund,J.S. Organization of neurons in the visual cortex, area 17, of the monkey (macaca mulatta). *J. Comp. Neurol.* **147**, 455-495 (1973).

14. O'Kusky,J. & Colonnier,M. A laminar analysis of the number of neurons, glia, and synapses in the adult cortex (area 17) of adult macaque monkeys. *J. Comp Neurol.* **210**, 278-290 (1982).

15. Nelson,M.J., Pouget,P., Nilsen,E.A., Patten,C.D., & Schall,J.D. Review of signal distortion through metal microelectrode recording circuits and filters. *J. Neurosci. Methods* **169**, 141-157 (2008).

16. Bour,L.J., Van Gisbergen,J.A.M., Bruijns,J., & Ottes,F.P. The double magnetic induction method for measuring eye movements: results in monkeys and man. *IEEE Trans. Biomed. Eng.* **31**, 419-427 (1984).

17. Kato,H., Bishop,P.O., & Orban,G.A. Hypercomplex and simple/complex cell classifications in cat striate cortex. *J. Neurophysiol.* **41**, 1072-1095 (1978).

18. Motter,B.C. Central V4 receptive fields are scaled by the V1 cortical magnification and correspond to a constant-sized sampling of the V1 surface. *J. Neurosci.* **29**, 5749-5757 (2009).

19. van der Togt,C., Kalitzin,S., Spekreijse,H., Lamme,V.A., & Super,H. Synchrony dynamics in monkey V1 predict success in visual detection. *Cereb. Cortex* **16**, 136-148 (2006).

20. Bendat,J.S. & Piersol,A.G. *Random data analysis and measurement procedures.* (John Wiley & Sons, Inc.,2000).

21. Fries,P., Womelsdorf,T., Oostenveld,R., & Desimone,R. The effects of visual stimulation and selective visual attention on rhythmic neuronal synchronization in macaque area V4. *J. Neurosci.* **28**, 4823-4835 (2008).

22. Berens,P. CircStat: A Matlab Toolbox for Circular Statistics. *Journal of Statistical Software* **31**, 1-21 (2009).

23. Steriade,M. & Amzica,F. Intracortical and corticothalamic coherence of fast spontaneous oscillations. *Proc. Natl. Acad. Sci. USA* **93**, 2533-2538 (1996).

24. Destexhe,A., Contreras,D., & Steriade,M. Spatiotemporal analysis of local field potentials and unit discharges in cat cerebral cortex during natural wake and sleep states. *J. Neurosci.* **19**, 4595-4608 (1999).

25. Barnett,L. & Seth,A.K. The MVGC multivariate Granger causality toolbox: a new approach to Granger-causal inference. *J. Neurosci. Methods* **223**, 50-68 (2014).

26. Nieuwenhuys,R., ten Donkelaar,H.J., & Nicholson,C. *The central nervous system of vertebrates* (Springer-Verlag,1998).

27. Krieg,W.J.S. *Interpretive atlas of the monkey's brain* (Brain Books, Evanston, Ill, 1975).

Chapter 5 | The contribution of AMPA and NMDA receptors to persistent firing in the dlPFC during working memory delays

Bram van Vugt[1], Timo van Kerkoerle[1], Devevrat Vartak[1] & Pieter R. Roelfsema

[1]These authors contributed equally to this work

ABSTRACT

Working memory refers to the ability to store and manipulate information over short periods of time. Persistent firing of neurons encoding the memorized information in the absence of sensory stimulation is generally regarded as the neural substrate of working memory. The underlying neural mechanisms of this internally sustained activity are not yet well established. One hypothesis holds that NMDA receptors (NMDA-Rs) are essential due to their slow decay times and unique voltage-dependent gating property. An alternative view holds that both NMDA and AMPA receptors (AMPA-R's) contribute to sustained activity, but whereas NMDA-Rs contribute in a multiplicative manner AMPA-R's contribute in an additive manner.

In this study we compared the contribution of AMPA-Rs and NMDA-Rs to persistent firing in the dorsolateral prefrontal cortex (dlPFC) of macaque monkeys performing a working memory task. We ejected small amounts of glutamatergic antagonists to prevent the complete abolishment of task-related activity, enabling us to differentiate contributions of the receptors during the different stages of the task. We found that both AMPA-Rs and NMDA-Rs contributed to internally sustained persistent activity. AMPA-R contributed equally to spontaneous and task-related activity, while NMDA-Rs showed a larger contribution to the visual response and sustained activity compared to spontaneous activity. Furthermore, the contribution of NMDA receptors to task-related activity of visual cells was comparable to its contribution to task-related activity of delay cells. Our results provide new insights into the contribution of AMPA-Rs and NMDA-Rs to spiking activity during working memory.

INTRODUCTION

Working memory refers to the ability to store and manipulate information over short periods of time on the order of seconds[1]. As this ability is one of the most crucial elements of cognition in daily life and is affected in disorders such as schizophrenia[2] and Alzheimer's disease[3], understanding the neural basis of working memory would be of great medical and social significance.

The content of working memory can either be retrieved from long-term storage or extracted from sensory information. Although working memory has been observed in the tactile[4] and the auditory[5] domain, most studies investigating working memory focused on the visual modality. These studies showed that, dependent on the brain region, the content of working memory can be based on individual stimulus features like motion[6] or color[7], integrated objects[8] or the location of the stimulus[9-12].

A common task to probe spatial working memory is the oculomotor delayed-response (ODR) task (**Figure 1A**), in which subjects are required to keep a cued location in working memory in order to make a correct saccade to that location at the end of the trial. Several studies[9,10,13-15] found that that the firing of a subset of neurons in the dorsolateral prefrontal cortex (dlPFC) of the macaque monkey represents a spatially specific memory trace for a to be remembered location; these so called 'delay cells' are activated by a visual cue that is presented in their receptive field (RF), but also remain active when the visual cue is extinguished and the location of the visual cue has to be maintained in memory. Other cells in the dlPFC are only active during the cue period and return to baseline during the delay period, these are called 'visual cells'.

Although the absence or presence of this memory trace predicts whether the monkey remembers the location of the visual cue at the end of the trial and therefore shows that internally sustained neural firing is the neuronal substrate for working memory, which neural mechanisms underlie this activity is still not known. Several mechanisms however have been proposed. It has been argued for instance that this sustained firing involves reverberatory excitation between neurons within a cortical area[16,17] or reciprocal excitatory loops between cortical areas[15,18-20]. Other proposals involve intrinsic dynamics of single neurons, in which specific membrane conductances underlie the sustained activity that is

observed during working memory related processes. Among others, acetylcholine receptors[21-23], dopamine receptors[24], noradrenaline receptors[25,26] and NMDA-Rs[27,28] have been proposed over the years as possible candidates. Modeling work has indicated that for a population of neurons to maintain persistently active over time, the synaptic connections between excitatory neurons need to have a slower decay time constant compared to the inhibitory connections[27,29]. As NMDA receptors (NMDA-Rs) have slow kinetics and contain a voltage-dependent magnesium block that is relieved by a fast AMPA receptor (AMPA-R) controlled depolarization of the cell[30], the idea that working memory relies crucially on NMDA-Rs has gained more popularity. The slow decay time of NMDA-Rs can produce a stable and robust working memory network, while the voltage dependent property of these receptors gate persistent activity by an initial transient input.

Recently, Wang et al.[31] tested whether NMDA-Rs are critically important for persistent firing by the activity from delay cells in the macaque dlPFC during the ODR task. They found that an NMDA-R antagonist almost completely abolishes task-related firing in delay cells. AMPA-R antagonists also decreased persistent activity, but weaker than NMDA-R antagonists and mainly so during the later phase of the delay period. However, it is conceivable that the high antagonist dosages that were used occluded any differential dependence of activity on glutamate receptors in the different task epochs. In accordance with this view, Wang et al. [31] also used AMPA-R blocker dosages with less impact on neuronal firing rate and these experiments revealed a more specific effect that was most pronounced during the late phase of the delay activity. Similarly, differential effects of the AMPA-R and the NMDA-R have been observed in a previous study, in which was shown that that AMPA-Rs contribute more strongly to feedforward processing while NMDA-Rs contribute more strongly to feedback processing in primary visual cortex (V1) of the macaque monkey[32].

In contrast to these proposals that AMPA-Rs and NMDA-Rs have specific effects on different types of activity like sustained firing in the dlPFC and feedforward and feedback processing in V1, other studies described general and non-specific effects of AMPA-Rs and NMDA-Rs on spiking activity. AMPA-Rs for instance have been shown to contribute additively to spiking activity[33], although other studies in primary sensory areas have found that the initial visual response was more sensitive to CNQX[34,35]. On the other hand, NMDA-

Rs have been shown to contribute multiplicatively to spiking activity[33]. Based on these studies, a general and additive contribution of AMPA-Rs to spiking activity is expected to be relatively independent on the intensity of the input drive, thereby showing a strong contribution of AMPA-Rs to baseline firing and task-related firing throughout the whole period of the task. A general and multiplicative contribution of NMDA-Rs to spiking activity would predict a relatively small contribution of NMDA-Rs during spontaneous baseline firing compared to the initial visual response and later sustained firing. In the present study we aimed to directly compare the contribution of AMPA-Rs and NMDA-Rs to spontaneous activity, visually driven activity and persistent activity. We used microiontophoresis to block NMDA-Rs and AMPA-Rs and used low ejection currents that decrease activity without completely abolishing task-related activity, enabling us to differentiate contributions of NMDA-Rs and AMPA-Rs during the different stages of the task. Furthermore, we also tested whether NMDA-R's were selectively involved in sustained activity by comparing the effect of NMDA antagonists on delay cells versus visual cells.

RESULTS

We trained two monkeys on the ODR task (**Figure 1A**), and we used a probe[36] (**Figure 1B**) which allowed us to combine reliable recording of single unit activity (**Figure 1C**) with iontophoresis in the dlPFC.

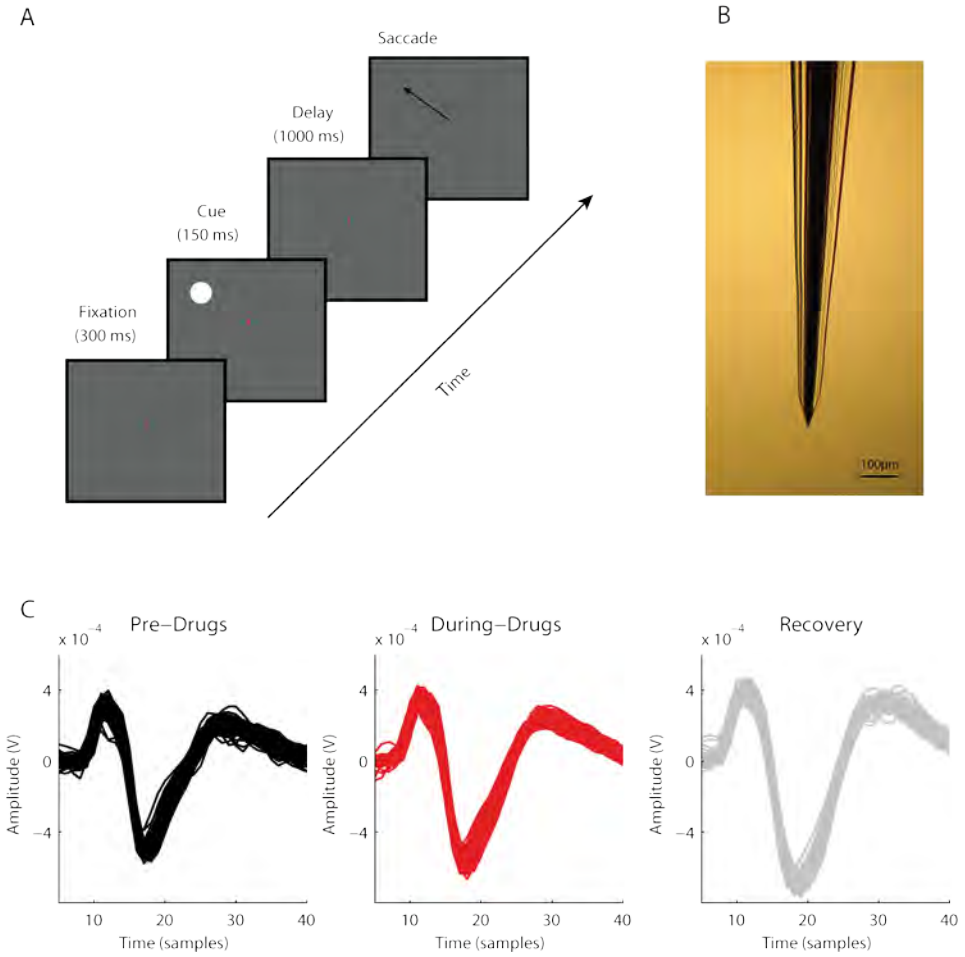

Figure 1 | Experimental paradigm. (**A**) ODR task, the monkey kept fixation for as long as the red fixation point was visible and made a saccade to the location where the cue had been presented. (**B**) Example of the three barrel glass electrode, (the scale bar indicates 100um). (**C**) Example single unit recorded in the block of trials before drug delivery (black), during drug delivery (red) and in the recovery period (gray).

Contribution of NMDA-Rs during the ODR task

At the time we started collecting the data, performance for both monkeys in the ODR task was high (99.9% for monkey B, 98% for monkey J) (**Figure 2**). To elucidate the contribution of NMDA-Rs, we iontophoretically administered the NMDA-R antagonist APV in two monkeys (B and J). Three blocks of ~80 trials were recorded; a recording block of ~80 trials without drug delivery by maintaining the holding current (from now on called pre-drug recordings), a recording block of ~80 trials where the drugs was administered by applying the ejection current (from now on called during-drug recordings) and finally a recording block of ~80 trials without drug delivery, again by maintaining the holding current (from now on called recovery recordings). The local application of APV did not have consistent effects on accuracy. Although APV decreased the accuracy of monkey B to 99.4% ($p < 0.005$; t test, n=33), accuracy increased only slightly to 99.5% during the recovery block (not significantly different from the APV block; $p > 0.4$, n=23) (**Figure 2A**). APV did not influence the accuracy of monkey J. It was 98% in the pre-drug epoch, 97,9% during APV administration and 97,6% in the recovery block (all $p > 0.4$; t test, n=23) (**Figure 2B**).

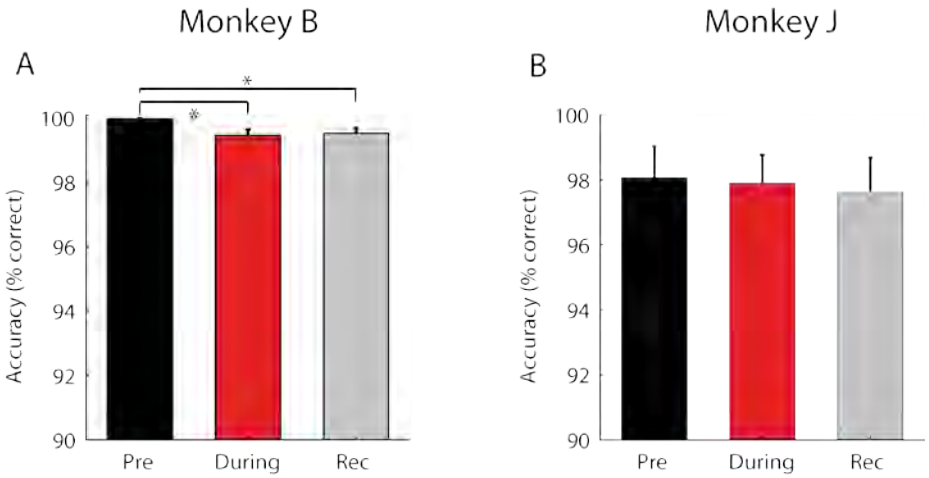

Figure 2 | Behavior ODR task during APV administration. Accuracy in the ODR task, in the block of trials before APV delivery (black bar), during APV delivery (red bar), and in the recovery period (grey bar), for (**A**) monkey B and (**B**) monkey J.

To investigate the role of NMDA-Rs in persistent firing, we recorded the activity of single neurons in the dlPFC during the ODR task. Only well isolated SU's that exhibited spatial selectivity were selected for further recording. We recorded activity from a total of 56 neurons (33 and 23 in monkeys B and J, respectively) that were held long enough to compare activity before drug application to that during APV administration. We lost the isolation of ten neurons (6 in monkey B and 4 in J) after drug application before the recovery block but we were able to record data for the other 47 neurons data during the recovery block. Most of the neurons (28 out of 33 for monkey B and 17 out of 23 for monkey J) exhibited persistent firing during the memory period.

Typical example recordings for both monkeys are illustrated in **Figure 3A**,**B**, and the population response is shown in **Figure 3C**,**D**. The neurons showed elevated firing during the full duration of the trial when the visual cue was presented at the preferred location of their RF, while showing a suppression of spiking activity in response to the presentation of the visual cue at the anti-preferred location of their RF (**Figure 3C**,**D**). In both monkeys, baseline activity before visual cue onset was suppressed during the recording block when APV was administered compared to pre-drug recordings ($p = < 10^{-6}$; t test, n = 66 for monkey B, $p < 0.01$; t test, n = 46 for monkey J) (Figure 3C,D). Administration of APV suppressed spiking activity during the full duration of the trial when the visual cue was presented at the preferred location in both monkeys ($p < 10^{-5}$; t test, n = 33 for monkey B, $p < 0.01$; t test, n = 23 for monkey J) (**Figure 3C**,**D**). In both monkeys the suppression was much larger at the preferred location than at the anti-preferred location, and in monkey J this suppression for cue presentation at the anti-preferred location was even absent. Blocking the NMDA-Rs therefore weakened the spatial tuning of the cells by reducing the difference in spiking activity between cue presentation at the preferred location versus the anti-preferred location. To measure the spatial tuning we computed d', which measures of the reliability of the response in single trials. Calculating the d' for each cell shows that the spatial tuning was weaker for most cells in both monkeys (**Figure 3E**,**F**) after blocking NMDA-Rs. In monkey B, APV caused a decrease in d' from an average of 1.66 to a value of 1.20 ($p < 10^{-4}$; t test, n = 33) and from 1.75 to 1.37 in monkey J ($p < 10^{-3}$; t test, n = 23).

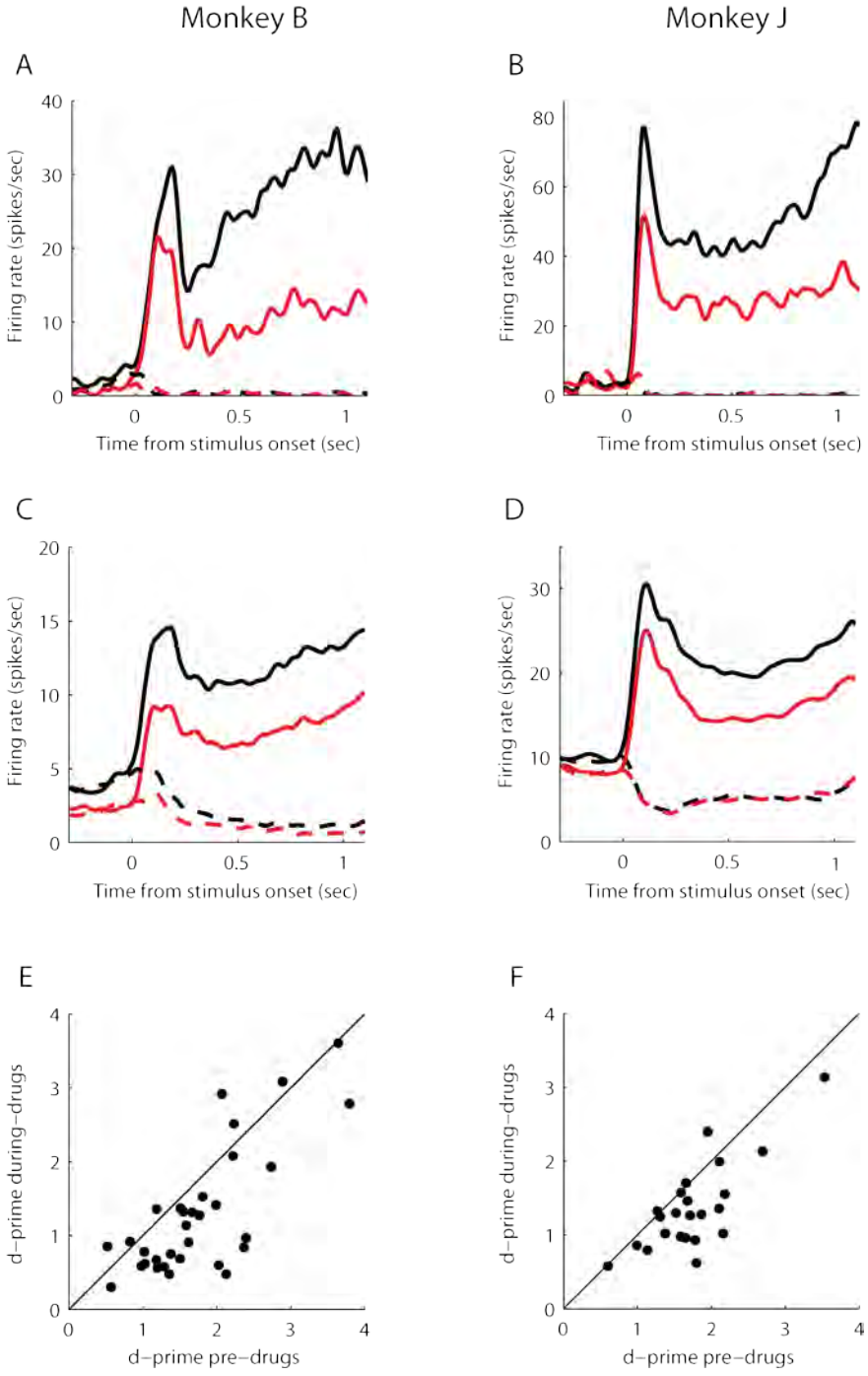
Monkey B
Monkey J
A
B
C
D
E
F
Firing rate (spikes/sec)
Time from stimulus onset (sec)
d–prime during–drugs
d–prime pre–drugs

Figure 3 | Effect of APV on spiking activity during ODR task. Example units (**A**,**B**) and population response (**C**,**D**), illustrating the effect of APV on the ODR task for (A,C) monkey B (N=34) and (B,D) monkey J (N=23). The preferred location (continuous lines) and anti-preferred location (dashed lines), before (black lines) and during APV delivery (red lines). (**E**,**F**) Abscissa, d' before APV delivery; ordinate, d' during APV delivery for (E) monkey B and (F) monkey J. Every data point represents a single unit.

Spiking activity slowly restored to normal levels when drug administration was stopped. Although not complete, all the cells showed a recovery response that returned in the direction of pre-drug recordings, both for baseline spiking activity before visual cue onset ($p < 10^{-5}$; t test, n = 54 for monkey B, $p < 10^{-3}$; t test, n = 38 for monkey J) as well as for spiking activity for the remainder of the trial when the visual cue was presented at the preferred ($p < 0.05$; t test, n = 27 for monkey B, $p < 0.05$; t test, n = 19 for monkey J) or at the anti-preferred location ($p < 0.05$; t test, n = 27 for monkey B, $p < 0.05$; t test, n = 19 for monkey J) (**Figure S2**).

To investigate whether NMDA-Rs contributed differentially to spiking activity during different periods of the ODR task, we plotted the absolute difference between spiking activity before and during the administration of APV (**Figures 4**). For both monkeys the influence on the firing rate was higher during the task-related activity than during the spontaneous activity ($p < 10^{-4}$; t test, n = 33 for monkey B, $p < 10^{-3}$; t test, n = 23 for monkey J). This drug effect was similar during the visually driven period and period of persistent activity. This suggests that NMDA-Rs are not selectively involved in maintaining sustained activity, but have a general multiplicative effect on spiking activity. This is interpretation is further supported by an analysis of cells that exhibited a visually response but no delay activity (**Figure 5**), which also showed a suppression of firing during the administration of APV in both monkeys ($p < 0.05$; t test, n = 6 for monkey B and $p < 0.05$; t test, n = 6 for monkey J).

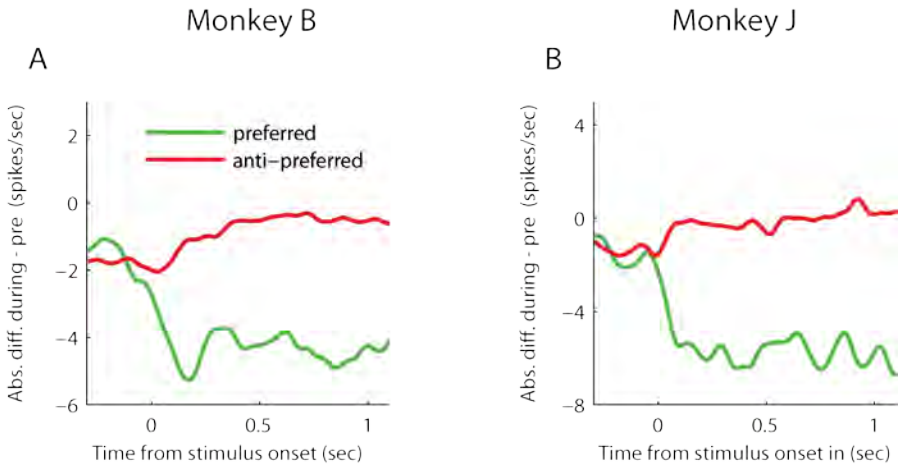

Figure 4 | Effect of APV on spiking activity during ODR task. Absolute difference of spiking activity during the ODR task during APV delivery minus before APV delivery for the preffered location (green line) and anti-preferred location (red line), for (**A**) monkey B and (**B**) monkey J.

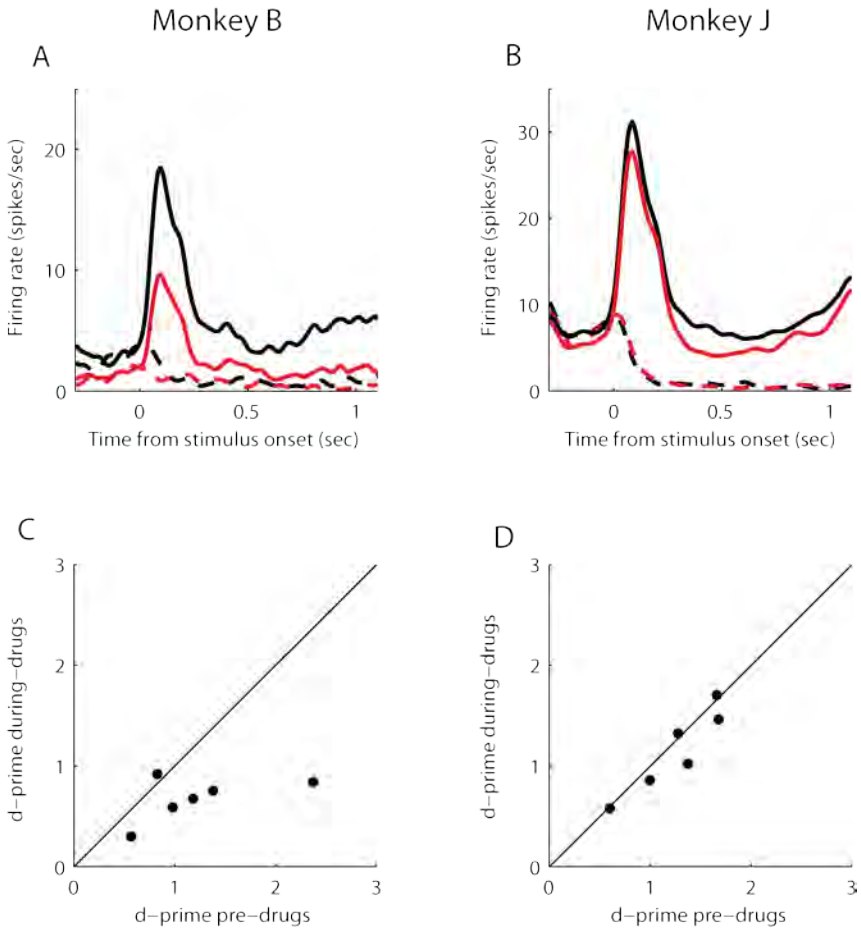

Figure 5 | Effect of APV on spiking activity of visual cells during ODR task. (**A**,**B**) Population response of the effect of APV on the ODR task for (A) monkey B (N=7) and (B) monkey J (N=7). The preferred location (continuous lines) and anti-preferred location (dashed lines), before (black lines) and during APV delivery (red lines). (**C**,**D**) Abscissa, d' before APV delivery; ordinate, d' during APV delivery for monkey B (C) and monkey J (D). Every data point represents an individual visual cell.

Contribution of AMPA-Rs during the ODR task

To investigate the role of AMPA-Rs in persistent firing we iontophoretically administered the AMPA-R antagonist CNQX in monkeys E and monkey J. As in the APV experiment, the monkey's accuracy before drug application was high (99.2% for monkey J, 96% for monkey E), and CNQX did not influence accuracy (both monkeys, $p > 0.7$) (**Figure 6**).

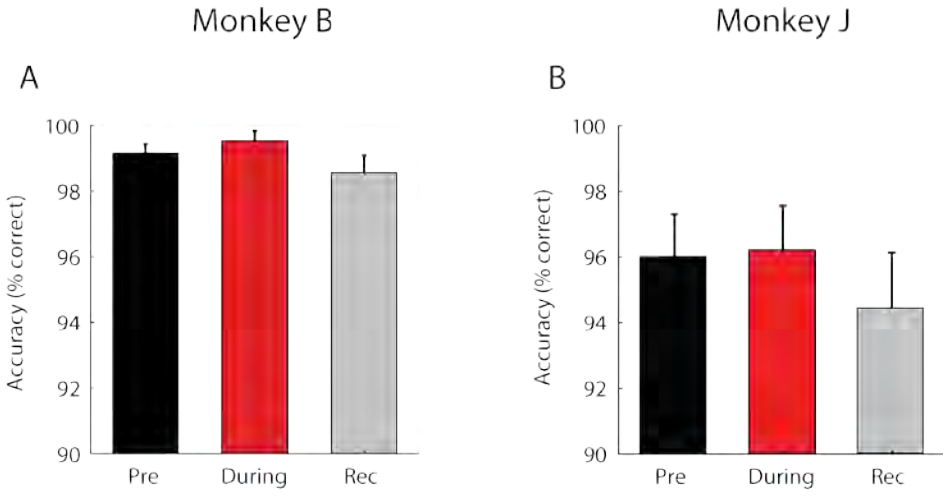

Figure 6 | Behavior in the ODR task during CNQX administration. Accuracy in the ODR task, in the block of trials before CNQX delivery (black bar), during APV delivery (red bar), and in the recovery period (grey bar), for (**A**) monkey J and (**B**) monkey E.

We recorded a total of 48 neurons with CNQX application (27 in monkey J and 21 in monkey E), and more than half of them exhibited sustained firing during the memory period (15 out of 27 for monkey J and 14 out of 21 for monkey E). Of these neurons 29 were kept long enough to examine activity in the recovery, after drug application. Typical example recordings are illustrated in **Figure 7A**,**B**, and the population response is shown in **Figure 7C**,**D**. In both monkeys, baseline spiking activity before visual cue onset was suppressed during the CNQX administration compared to pre-drug recordings ($p < 10^{-5}$; t test, n = 54 for monkey J; $p < 0.05$; t test, n = 28 for monkey E) (**Figure 7C**,**D**). For both monkeys, administration of CNQX suppressed spiking activity during the full duration of the trial when the visual cue was presented at the preferred location ($p < 10^{-3}$; t test, n = 27

for monkey J, $p < 10^{-3}$; t test, n = 14 for monkey E). When the visual cue was presented at the anti-preferred location there was a significant reduction of activity in Monkey J ($p < 10^{-3}$; t test, n = 27) but not for Monkey E ($p > 0.05$; t test, n = 14) (**Figure 7C**,**D**). To examine the influence of CNQX on the tuning, we calculated d's. In monkey J CNQX caused a decrease in d' from an average of 0.81 to a value of 0.7 ($p < 10^{-3}$; t test, n = 27) whereas for monkey E the decrease in d' was from 0.99 to 0.64 ($p < 0.05$; t test, n = 14) (**Figure 6E**,**F**).

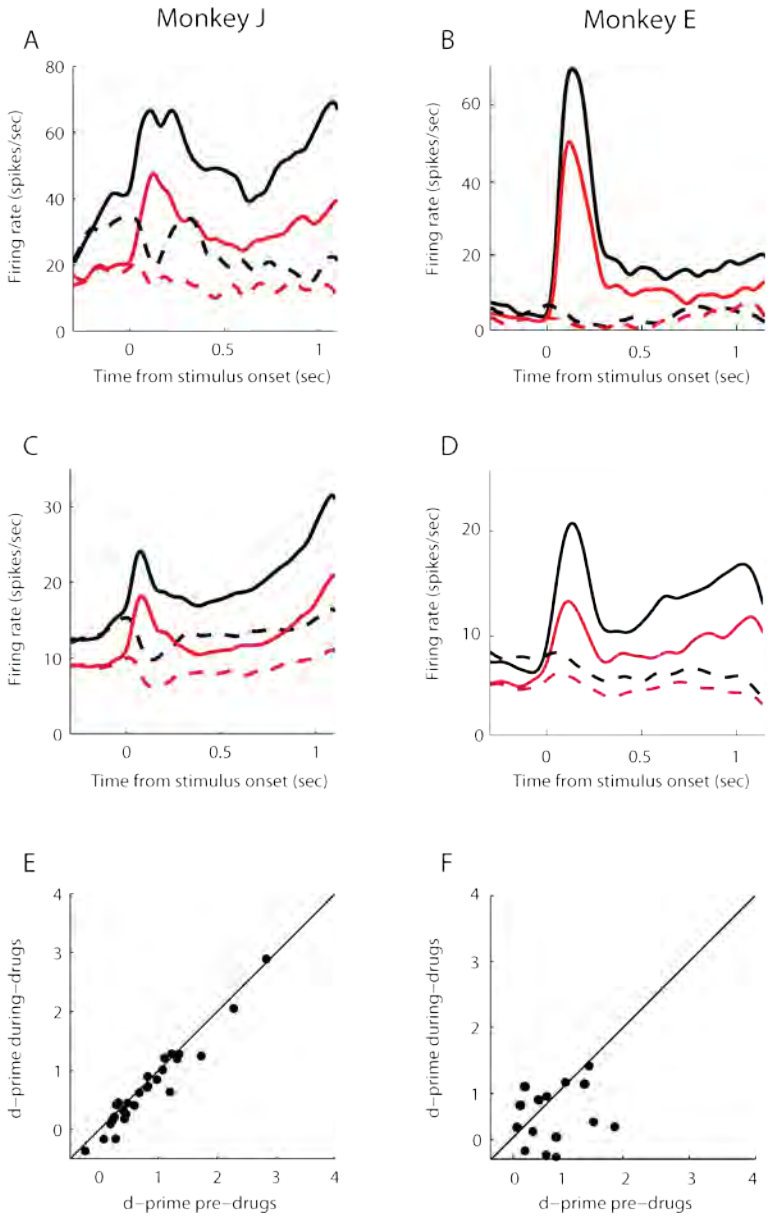

Figure 7 | Effect of CNQX on spiking activity during ODR task. Example units (**A**,**B**) and population response (**C**,**D**) illustrating the effect of CNQX on neuronal activity during the ODR task for (A,C) monkey J (N=27) and (B,D) monkey E (N=14). The preferred location (continuous lines) and anti-preferred location (dashed lines), before (black lines) and during APV delivery (red lines). (**E**,**F**) Abscissa, d' before CNQX delivery; ordinate, d' during CNQX delivery for monkey J (E) and monkey E (F). Every data point represents an individual unit.

Although spiking activity was still observed during recovery blocks, it did not restore to normal levels when administration of CNQX was stopped. For some SU's (9 out of 19 for monkey J, 4 out of 14 for monkey E) the spiking activity did not even return in the direction of the response before the administration of CNQX. As the waveforms of the residual spiking activity of the isolated SU's were very similar during the recovery recordings compared to the pre-drug and during-drug recordings, this absence of restoration to normal levels of spiking activity was not due to effects that can be ascribed to the stability of the SU recordings. Instead, as several studies have shown that activity does not go back to pre-drug levels after the administration of CNQX[32,37]. This lack of recovery of spiking activity was most likely the result of the long-lasting effects of blocking AMPA-Rs after CNQX administration.

To investigate the contribution of AMPA-Rs during different periods of the ODR task, we again plotted the absolute difference between spiking activity before and during the administration of CNQX (**Figures 8**). While for monkey J the contribution of AMPA-Rs to spiking activity increased progressively during the trial (**Figure 8A**), this was not that evident for monkey E (**Figure 8B**).

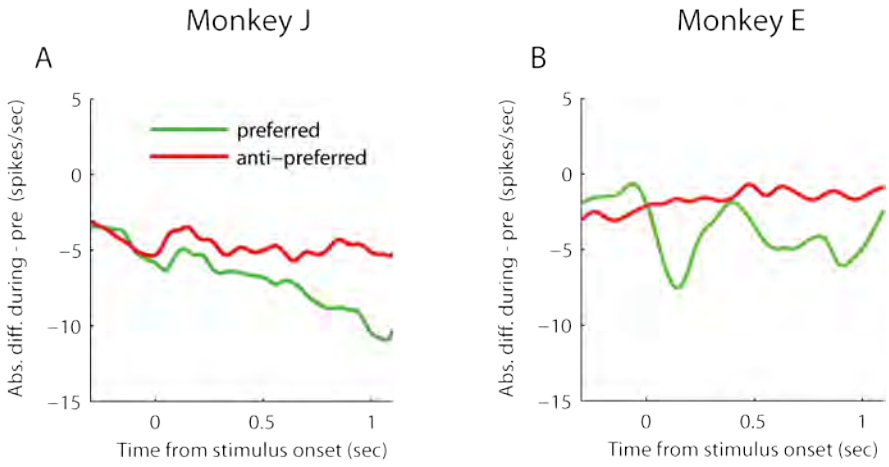

Figure 8 | Effect of CNQX on spiking activity during ODR task. Absolute difference in spiking activity during the ODR task of during CNQX versus before CNQX delivery for the preferred location (green line) and the anti-preferred location (red line), for (**A**) monkey J and (**B**) monkey E.

DISCUSSION

In this study we investigated the neural mechanisms underlying persistent firing by determining to which degree this sustained firing is dependent on different glutamate receptors. By iontophoretically blocking AMPA- and NMDA receptors we compared the specific contribution of these receptors to activity in the dlPFC during the ODR task. We used very small ejection currents and applied the drugs for only short periods of time to perturb activity without blocking it to obtain a sensitive measure of the role of the different receptors.

Although our results show that blocking glutamatergic receptors can have substantial effects on the spiking activity, our study did not find any consistent effects in the behavior of the monkeys (**Figures 2**, **6**), similar to previous studies using iontophoretic drug application[24,31]. This is expected as the spatial spread of iontophoretically applied drugs is very limited[38,39], thereby affecting only a small population of neurons.

We found that both the AMPA-R and the NMDA-R contribute to task-related firing during the ODR task. The effects of AMPA-Rs we observed were more of an additive nature, the contribution of the AMPA-R to spiking activity was relatively independent of the level of firing (**Figure 7C**,**D**) . Blocking AMPA-Rs showed a strong decrease in spontaneous baseline firing, which was comparable to the strong decrease in task-related firing throughout the whole period of the ODR task. In contrast to the additive effects of the AMPA-Rs, the effects of the NMDA-Rs were of a multiplicative nature, NMDA-Rs contributed more strongly to firing rates of activated neurons and less to the firing rate of neurons not already activated (**Figure 3C**,**D**).

Due to the different effects of the AMPA-R and the NMDA-R on the contribution of spiking activity these glutametergic receptors also have different effects on the spatial tuning of the cell. AMPA-Rs contributed to the strong response when the visual cue was presented at the preferred location and also to the weaker response when the visual cue was presented at the anti-preferred location. Blocking AMPA-Rs therefore reduced the difference in activity between preferred and anti-preferred location only slightly. In other words, the spatial tuning remained relatively similar (**Figure 7E**,**F**). Blocking NMDA-Rs

had a stronger impact on the spatial tuning given their multiplicative effect. Blockade of the NMDA-Rs reduced the activity elicited at the preferred location much more than the response elicited at the anti-preferred location. As a result, the spatial tuning for most of the recorded cells was strongly reduced (**Figure 3E**,**F**).

Although our results show that AMPA-Rs and NMDA-Rs contribute differentially to task-related spiking activity during the ODR task, they do not make a convincing case for a specific and critical role of NMDA-Rs in persistent firing. Previous studies proposed that persistent activity is realized by the voltage-dependent gating property of the NMDA-R, producing a positive feedback loop between membrane depolarization and excitatory inward currents which is able to outlast transient input[31]. While blocking NMDA-Rs during the ODR task does reduce task-related spiking activity, several observations in our study show that this reduction is not specific to persistent activity. First, both AMPA-Rs and NMDA-Rs contributed to task-related spiking activity, and the contribution of AMPA-Rs to persistent activity (**Figure 7C**,**D**) was at least as strong as that of NMDA-Rs (**Figure 3C**,**D**). Second, the contribution of NMDA-Rs to the initial visual response was comparable to the contribution to persistent activity during the delay period (**Figure 3C**,**D**). Third, the reduction in task-related spiking activity as well as the weakened spatial tuning after blocking NMDA-Rs also occurred for the visual cells without persistent activity (**Figure 5**).

Our results therefore revealed a general contribution of NMDA-Rs to spiking activity, which is similar for the visual response and persistent activity that increases with the neuronal firing rate. Such a multiplicative contribution of NMDA-Rs is comparable to results from previous studies on the contributions of NMDA-Rs on spiking activity in the cat visual cortex[33]. Similarly, the contribution to activity of AMPA-R that depended less on the tuning of neurons is in line with previous studies in the cat visual cortex[33,40].

At first sight, our conclusions may seem to be incompatible with the results of Wang et al.[41], who found that that persistent firing is critically dependent on NMDA-Rs whereas AMPA-Rs contribute to sustain network activity by permitting NMDA-R contributions to delay-cell firing. One difference between studies was the choice of antagonists. We used the competitive NMDA-R antagonist APV, whereas Wang et al. used MK801, which is non-competitive, and the selective NR2B NMDA subunit antagonist Ro25-6981. Furthermore, we used CNQX to block AMPRA-Rs, whereas Wang et al. used NBQX in addition to

CNQX. However, we believe that the most important difference between studies is in the dosage of the drugs. Specifically, Wang et al. almost completely abolished delay activity with NMDA antagonists. By using smaller dosages, we were able to reveal that the NMDA-R blockers have a multiplicative effect in all phases of the task. Wang et al. found that the effects of NMDA-R antagonists on delay activity were stronger than the effects of AMPA-R antagonists, but it is conceivable that this difference is also due to a dosage effect. Wang et al. might also have seen a more complete suppression with higher dosages of the AMPA-R blockers. Taken together, the results suggest that the multiplicative contribution of NMDA-Rs to spiking activity occurs irrespective of whether activity is spontaneous, stimulus driven, or related to working memory.

Our findings therefore support the view that AMPA and NMDA receptors contribute to persistent firing. But they are not the only ones. Blocking dopamine receptor D1 (DRD1) for instance revealed an 'inverted-U' dose-response relationship, too little or too much DRD1-R activity reduces persistent firing[24]. Furthermore, a2A-adrenoceptors[25,26] and cholinergic muscarinic receptors[21-23] also impact on persistent firing, in part by acting on non-selective cation permeable transient receptor potential channels (TRPC)[42] and hyperpolarization activated cyclic nucleotide-gated potassium channels[26,43]. Thus, many receptors contribute to persistent firing, which implies that one must be careful attributing persistent firing to one specific receptor.

Another important question is how persistent activity is maintained. Maintenance could involve reverberatory excitation between neurons within a cortical area[16,17] or reciprocal excitatory loops between cortical areas[15,18-20]. In the first scenario, internally sustained persistent firing is generated by reciprocal excitation between pyramidal neurons with similar spatial properties. In the second scenario, the internally sustained persistent firing is maintained by reciprocal excitatory loops between cortical areas or by loops through subcortical structures, including the basal ganglia. Internally sustained persistent firing is also observed in other brain areas, notably the posterior parietal cortex[44,45], medial superior temporal cortex[6] and the inferotemporal cortex[46-48]. Furthermore, a study by Chafee and Goldman-Rakic[19] combined local cooling of either parietal and prefrontal cortex and recording in the other area during a working memory task. They showed that inactivation

of one of these areas could both increase and decrease the activity of individual neurons in the other region, without a clear effect on behavior.

Our results therefore are in line with a general contribution of AMPA-Rs and a general and more specific multiplicative contribution of NMDA-Rs on spiking activity during the ODR task. This is a relevant finding, both for models on the neural mechanisms during working memory and for clinical application. As our results rule out that internally sustained persistent firing is specifically dependent on NMDA-Rs, future research is required to elucidate the mechanisms that underlie working memory. Importantly, these mechanisms are not mutually exclusive and scenarios in which both the intrinsic dynamics of single neurons, as well as reverberatory excitation between neurons within or between cortical areas are important, remain likely.

METHODS

Surgical procedures

All procedures complied with the NIH Guide for Care and Use of Laboratory Animals (National Institutes of Health, Bethesda, Maryland) and were approved by the institutional animal care and use committee of the Royal Netherlands Academy of Arts and Sciences.

We recorded neural activity from three adult macaque monkeys (Macaca Mulatta: monkeys B, J and E). During surgeries general anesthesia was induced with ketamine (15mg/kg injected intramuscularly) and maintained after intubation by ventilation with a mixture of 70% N_2O and 30% O_2, supplemented with 0.8% isoflurane, fentanyl (0.005mg/kg intravenously) and midazolam (0.5mg/kg/h intravenously). In a first surgery, the monkeys were implanted with a head post for head stabilization. The monkeys were then trained on the ODR task until they could reliably perform the task. In a second surgery we performed a craniotomy (centered on stereotaxic coordinates: 21mm anterior, and 17mm lateral) and implanted a titanium chamber (Crist Instruments) for electrophysiological recordings and iontophoretical administration of APV and CNQX. After implantation the location of the arcuate and principal sulci relative to the recording chamber were determined using ultrasound imaging, and FEF was located by using electrical microstimulation (**Figure 1C**).

Behavioral task

Monkeys B, J and E were first trained on the ODR task[10] (**Figure 1A**). A fixation point (a red circle of 0.3° diameter) was presented on a grey background and the monkey started the trial by directing gaze to a 1.5degree diameter fixation window centered on the fixation point (0.1 degree diameter red dot). After 300ms of fixation a visual cue (white circle of 2 degree diameter) was presented at either the preferred or the anti-preferred location. After 150ms the visual cue was extinguished but the monkey had to maintain fixation for another 1000ms before the fixation point was extinguished, which indicated to the monkey that he was required to make a memory guided eye-movement into a target-window (4 degrees diameter) that was centered on the location of the previous visual cue. Correct responses were rewarded with apple juice. Trials in which the animal broke fixation before the

fixation point was extinguished were aborted, and stimulus conditions were presented in a pseudorandom order.

All stimuli were generated using in-house software (Tracker) and were presented on a CRT monitor with a resolution of 1024x768 pixels and refresh rate of 85Hz, which was viewed from a distance of 40cm. Eye movements were recorded with a video eye-tracker (Thomas recordings) with a sampling rate of 350Hz.

Electrophysiology and iontophoresis

We recorded single units with tungsten-in-glass electrodes fused with two side barrels[36] (**Figure 1D**) that were used for iontophoretic drug administration by applying a small electric current to a tungsten wire that was inserted in these side barrels. The impedances of the measuring electrodes ranged from 400 kOhm to 2 MOhm (median ~1 MOhm) and the impedance of the ejection barrels from 15 to 150 MOhm (median ~20 MOhm).

The signal from the recording electrode was recorded with Tucker Davis Technology (TDT) equipment using a high-impedance headstage (RA16AC) and a preamplifier (RA16SD) with a hardware high-pass filter of 2.2Hz, a low-pass filter of 7.5 kHz (-3dB point) and sampled with a rate of 24.4kHz. Spikes were initially determined by setting a voltage threshold. If necessary, spike sorting was done offline using waveclus software[49].

For iontophoresis, we dissolved the NMDA-R antagonist 2-amino-5-phosphonovalerate (APV) (Sigma-Aldrich) and the AMPAR antagonist 6-cyano7-nitroquinoxaline-2,3-dione (CNQX) (Sigma-Aldrich) at 0.02 M in triple-distilled water (pH ~8.0). APV and CNQX are negatively charged, and we retained them in the glass-pipettes by delivering a positive potential (+15nA for APV and +20nA for CNQX) and ejected them by delivering a negative potential. The ejection currents were set to the amount needed for a noticeable difference in the spiking activity recorded while the monkey performed the ODR task. For APV, ejection currents ranged from -2nA to -7nA for monkey B and from -5nA to -15nA for monkey J. For CNQX, ejection currents ranged from -10nA to -20nA in both monkeys (J and E).

RF mapping

RF's were measured using the same ODR task that was used during the recordings. First the preferred and anti-preferred direction was determined using 8 locations at 8 degrees eccentricity. The eccentricity was subsequently mapped in 4 degree steps for the preferred and anti-preferred direction only. Most of the RF's of the recorded single unit's (SU's) were at 18 degrees eccentricity for monkey B, at 13 degrees eccentricity for monkey J and at 18 degrees eccentricity for monkey E.

Data acquisition

As determined by ultrasound imaging, SU activity was recorded anterior to the arcuate sulcus (**Figure S1**). A blunt guide tube, made to tightly fit around the probe, was rigidly attached to a microdrive for mechanical stability (Narishige group). We pre-dimpled the dura with the guide tube and electrode (~1mm), penetrated the dura with the electrode, and pulled back the guide tube and electrode to un-dimple the dura. The electrode was left to settle for about 20 minutes. The probe was then very carefully advanced until a SU was encountered. After stabilizing the recording of the spiking activity of the SU, the RF properties of the SU were determined using the ODR task. Only isolated SU's that showed spatial selectivity were selected for further recording, and most neurons that we recorded from (45 out of 57 for the APV dataset, 32 out of 51 for the CNQX dataset) showed sustained firing during the memory period. For most SU's (47 out of 57 for the two APV datasets, 29 out of 48 for the two CNQX datasets), three blocks of ~80 trials were recorded; a recording block of ~80 trials without drug delivery by maintaining the holding current (from now on called pre-drug recordings), a recording block of ~80 trials where the drugs was administered by applying the ejection current (from now on called during-drug recordings) and finally a recording block of ~80 trials without drug delivery, again by maintaining the holding current (from now on called recovery recordings). During-drug recordings were started once an effect was noticeable in the spiking activity, usually 3 to 4 minutes after the ejection current was applied and the drugs were applied continuously throughout the recording period. Recovery recordings were started once the effect of drug delivery faded, usually 5-10 minutes after the holding current was re-maintained after drug delivery. The waveforms of the recorded spiking activity during one example recording are

shown in Figure 1E. For a small fraction of the recordings (10 out of 57 for the two APV datasets, 13 out of 48 for the two CNQX datasets) the SU was lost during the waiting period after drug delivery and no recovery recording could be performed.

Data analyses

All spike data was binned in 10ms windows. The ODR task was divided into two epochs; spontaneous activity and task-related activity. The spontaneous epoch lasted from 300ms before stimulus onset up to stimulus onset and the task-related epoch lasted from stimulus onset up to saccade onset.

To quantify the spatial tuning for each cell individually, the d' for task-related activity was calculated by (mean preferred location - mean anti-preferred location) / sqrt(0.5*(std preferred location)^2+(std anti-preferred location)^2).

Statistical analyses

For statistical comparisons to test whether the drugs changed spiking activity during spontaneous and task-related activity, two-sided t-tests were used to compare spiking activity between pre-drug, during drug and recovery recordings. Results were only reported if significant p-values were less than 0.05 for both monkeys individually and when averaged across monkeys.

References

1. Baddeley,A. Working memory: theories, models, and controversies. *Annu. Rev. Psychol.* **63**, 1-29 (2012).
2. Driesen,N.R. *et al.* Impairment of working memory maintenance and response in schizophrenia: functional magnetic resonance imaging evidence. *Biol. Psychiatry* **64**, 1026-1034 (2008).
3. Schroeter,M.L. *et al.* Executive deficits are related to the inferior frontal junction in early dementia. *Brain* **135**, 201-215 (2012).

4. Romo,R., Brody,C.D., Hernandez,A., & Lemus,L. Neuronal correlates of parametric working memory in the prefrontal cortex. *Nature* **399**, 470-473 (1999).

5. Rama,P. *et al.* Dissociable functional cortical topographies for working memory maintenance of voice identity and location. *Cereb. Cortex* **14**, 768-780 (2004).

6. Mendoza-Halliday,D., Torres,S., & Martinez-Trujillo,J.C. Sharp emergence of feature-selective sustained activity along the dorsal visual pathway. *Nat. Neurosci.* **17**, 1255-1262 (2014).

7. Mohr,H.M., Goebel,R., & Linden,D.E. Content- and task-specific dissociations of frontal activity during maintenance and manipulation in visual working memory. *J. Neurosci.* **26**, 4465-4471 (2006).

8. Wilson,F.A.W., Ó Scalaidhe,S.P., & Goldman-Rakic,P.S. Dissociation of object and spatial processing domains in primate prefrontal cortex. *Science* **260**, 1955-1958 (1993).

9. Fuster,J.M. & Alexander,G.E. Neuron activity related to short-term memory. *Science* **173**, 652-654 (1971).

10. Funahashi,S., Bruce,C.J., & Goldman-Rakic,P.S. Mnemonic coding of visual space in the monkey's dorsolateral prefrontal cortex. *J. Neurophysiol.* **61**, 331-349 (1989).

11. Courtney,S.M., Ungerleider,L.G., Keil,K., & Haxby,J.V. Transient and sustained activity in a distributed neural system for human working memory. *Nature* **386**, 608-611 (1997).

12. Fletcher,P.C. & Henson,R.N. Frontal lobes and human memory: insights from functional neuroimaging. *Brain* **124**, 849-881 (2001).

13. Niki,H. Differential activity of prefrontal units during right and left delayed response trials. *Brain Res.* **70**, 346-349 (1974).

14. Watanabe,M. Prefrontal unit activity during delayed conditional discriminations in the monkey. *Brain Res.* **225**, 51-65 (1981).

15. Miller,E.K., Erickson,C.A., & Desimone,R. Neural mechanisms of visual working memory in prefrontal cortex of the macaque. *J. Neurosci.* **16**, 5154-5167 (1996).

16. Goldman-Rakic,P.S. Cellular basis of working memory. *Neuron* **14**, 477-485 (1995).

17. Barak,O. & Tsodyks,M. Persistent activity in neural networks with dynamic synapses. *PLoS. Comput. Biol.* **3**, e35 (2007).

18. Fuster,J.M., Bauer,R.H., & Jervey,J.P. Functional interactions between inferotemporal and prefrontal cortex in a cognitive task. *Brain Res.* **330**, 299-307 (1985).

19. Chafee,M.V. & Goldman-Rakic,P.S. Inactivation of parietal and prefrontal cortex reveals interdependence of neural activity during memory-guided saccades. *J. Neurophysiol.* **83**, 1550-1566 (2000).

20. Gazzaley,A. & Nobre,A.C. Top-down modulation: bridging selective attention and working memory. *Trends Cogn. Sci.* **16**, 129-135 (2012).

21. Krnjevic,K., Pumain,R., & Renaud,L. The mechanism of excitation by acetylcholine in the cerebral cortex. *J. Physiol* **215**, 247-268 (1971).

22. Andrade,R. Cell excitation enhances muscarinic cholinergic responses in rat association cortex. *Brain Res.* **548**, 81-93 (1991).

23. Egorov,A.V., Hamam,B.N., Fransèn,E., Hasselmo,M.E., & Alonso,A.A. Graded persistent activity in entorhinal cortex neurons. *Nature* **420**, 173-178 (2002).

24. Vijayraghavan,S., Wang,M., Birnbaum,S.G., Williams,G.V., & Arnsten,A.F. Inverted-U dopamine D1 receptor actions on prefrontal neurons engaged in working memory. *Nat. Neurosci.* **10**, 376-384 (2007).

25. Li,B.M., Mao,Z.M., Wang,M., & Mei,Z.T. Alpha-2 adrenergic modulation of prefrontal cortical neuronal activity related to spatial working memory in monkeys. *Neuropsychopharmacology* **21**, 601-610 (1999).

26. Wang,M. *et al.* Alpha2A-adrenoceptors strengthen working memory networks by inhibiting cAMP-HCN channel signaling in prefrontal cortex. *Cell* **129**, 397-410 (2007).

27. Lisman,J.E., Fellous,J.-M., & Wang,X.-J. A role for NMDA-receptor channels in working memory. *Nature Neurosci.* **1**, 273-275 (1998).

28. Wang,X.-J. Synaptic reverberation underlying mnemonic persistent activity. *Trends Neurosci.* **24**, 455-462 (2001).

29. Brunel,N. & Wang,X.J. Effects of neuromodulation in a cortical network model of object working memory dominated by recurrent inhibition. *J. Comput. Neurosci.* **11**, 63-85 (2001).

30. Hestrin,S., Nicoll,R.A., Perkel,D.J., & Sah,P. Analysis of excitatory synaptic action in pyramidal cells using whole-cell recording from rat hippocampal slices. *J. Physiol* **422**, 203-225 (1990).

31. Wang,M. *et al.* NMDA receptors subserve persistent neuronal firing during working memory in dorsolateral prefrontal cortex. *Neuron* **77**, 736-749 (2013).

32. Self,M., Kooijmans,R.N., Supèr,H., & Roelfsema,P.R. Different glutamate receptors convey feedforward and recurrent processing in macaque V1. Proc.Natl.Acad.Sci.U.S.A . 2012.

33. Fox,K., Sato,H., & Daw,N. The effect of varying stimulus intensity on NMDA-receptor activity in cat visual cortex. *J. Neurophysiol.* **64**, 1413-1428 (1990).

34. Armstrong-James,M., Walker,E., & Callahan,C.A. The contribution of NMDA and non-NMDA receptors to fast and slow transmission of sensory information in the rat SI barrel cortex. *J. Neurosci.* **13**, 2149-2160 (1993).

35. Self,M.W., Kooijmans,R.N., Super,H., Lamme,V.A., & Roelfsema,P.R. Different glutamate receptors convey feedforward and recurrent processing in macaque V1. *Proc. Natl. Acad. Sci. U. S. A* **109**, 11031-11036 (2012).

36. Thiele,A., Delicato,L.S., Roberts,M.J., & Gieselmann,M.A. A novel electrode-pipette design for simultaneous recording of extracellular spikes and iontophoretic drug application in awake behaving monkeys. *J. Neurosci. Methods* **158**, 207-211 (2006).

37. Leininger,E. & Belousov,A.B. Recovery of network-driven glutamatergic activity in rat hippocampal neurons during chronic glutamate receptor blockade. *Brain Res.* **1251**, 87-102 (2009).

38. Kelly,J.S. & Renaud,L.P. Physiological identification of inhibitory interneurones in the feline pericruciate cortex. *Neuropharmacology* **13**, 463-474 (1974).

39. Rao,S.G., Williams,G.V., & Goldman-Rakic,P.S. Destruction and creation of spatial tuning by disinhibition: GABA(A) blockade of prefrontal cortical neurons engaged by working memory. *J. Neurosci.* **20**, 485-494 (2000).

40. Sato,H., Hata,Y., & Tsumoto,T. Effects of blocking non-N-methyl-D-aspartate receptors on visual responses of neurons in the cat visual cortex. *Neuroscience* **94**, 697-703 (1999).

41. Wang,M. *et al.* NMDA receptors subserve persistent neuronal firing during working memory in dorsolateral prefrontal cortex. *Neuron* **77**, 736-749 (2013).

42. Yan,H.D., Villalobos,C., & Andrade,R. TRPC Channels Mediate a Muscarinic Receptor-Induced Afterdepolarization in Cerebral Cortex. *J. Neurosci.* **29**, 10038-10046 (2009).

43. Thuault,S.J. *et al.* Prefrontal cortex HCN1 channels enable intrinsic persistent neural firing and executive memory function. *J. Neurosci.* **33**, 13583-13599 (2013).

44. Chafee,M.V. & Goldman-Rakic,P.S. Matching patterns of activity in primate prefrontal area 8a and parietal 7ip neurons during spatial working memory task. *J. Neurophysiol.* **79**, 2919-2940 (1998).

45. Colby,C.L., Duhamel,J.R., & Goldberg,M.E. Visual, presaccadic, and cognitive activation of single neurons in monkey lateral intraparietal area. *J. Neurophysiol.* **76**, 2841-2852 (1996).

46. Fuster,J.M. & Jervey,J.P. Inferotemporal neurons distinguish and retain behaviorally relevant features of visual stimuli. *Science* **212**, 952-955 (1981).

47. Fuster,J.M. & Jervey,J.P. Neuronal firing in the inferotemporal cortex of the monkey in a visual memory task. *J. Neurosci.* **2**, 361-375 (1982).

48. Miyashita,Y. Neuronal correlate of visual associative long-term memory in the primate cortex. *Nature* **335**, 817-820 (1988).

49. Quiroga,R.Q., Nadasdy,Z., & Ben-Shaul,Y. Unsupervised spike detection and sorting with wavelets and superparamagnetic clustering. *Neural Comput.* **16**, 1661-1687 (2004).

SUPPLEMENTARY INFORMATION

Supplementary Figures

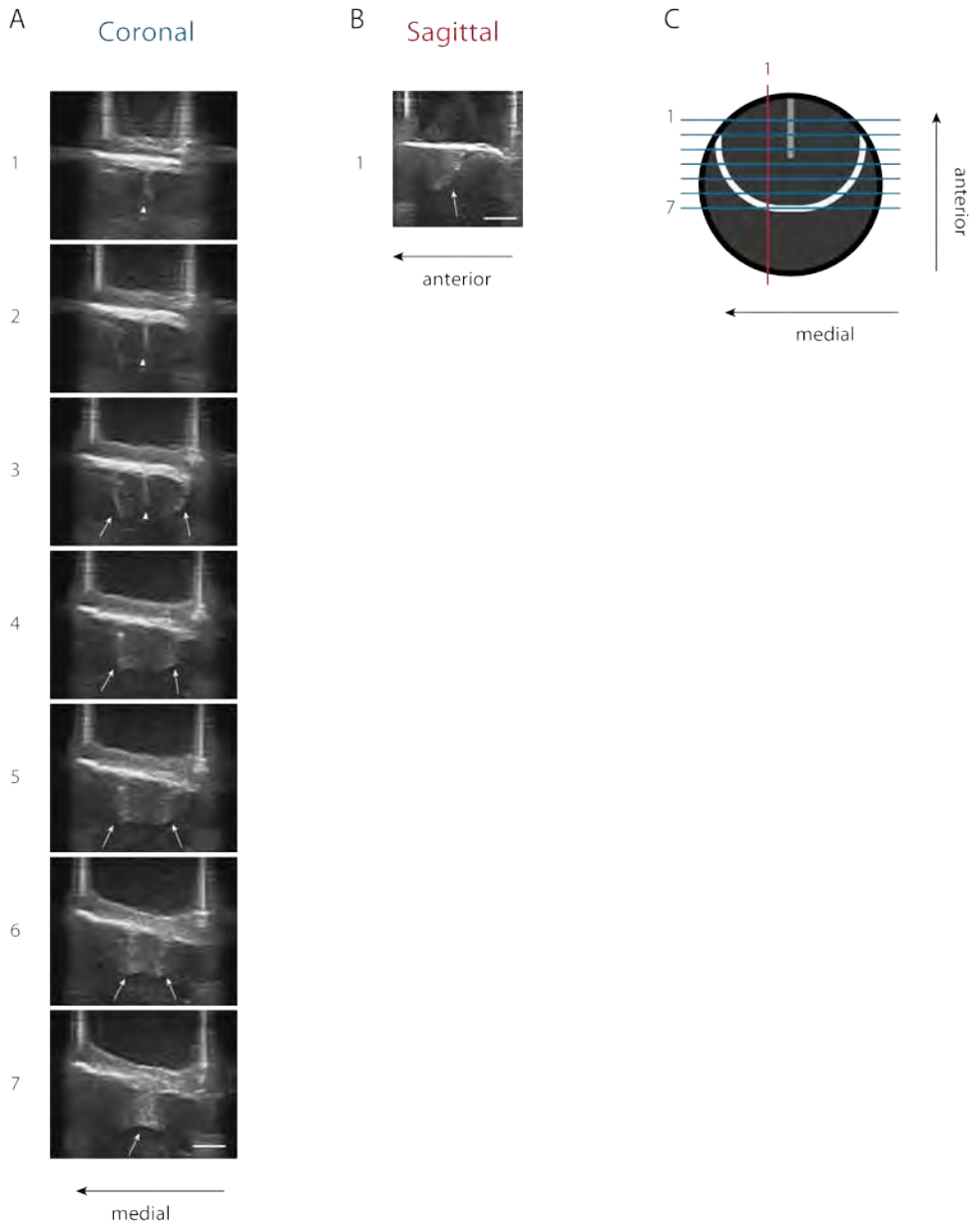

Supplementary Figure 1 | Location of recording chamber. Coronal (**A**) and sagittal (**B**) ultrasound images of the recording chamber of monkey B. White arrows point to the arcuate sulcus, white arrowheads point to the principal sulcus. (**C**) Schematic drawing indicating the location of the different slices relative to the arcuate sulcus (white line) and principal sulcus (grey line). White scale bars, 10mm.

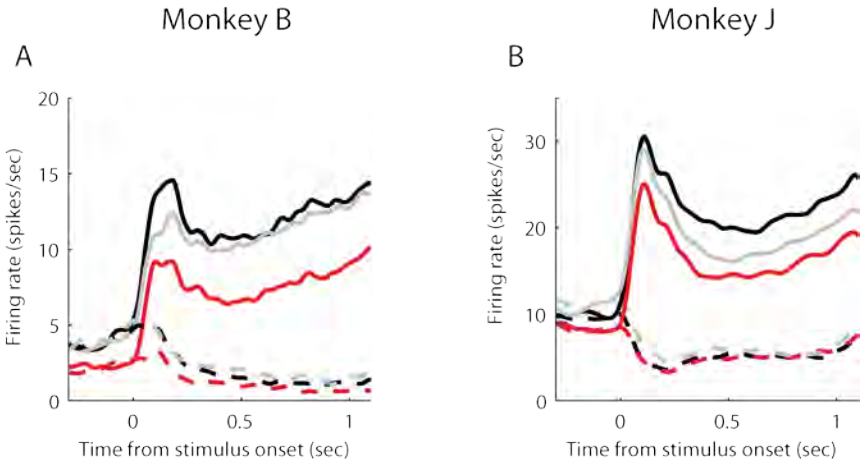

Supplementary Figure 2 | Population ODR Task APV with recovery. The effect of APV on population response of the ODR and recovery for (**A**) monkey B (N=34) and (**B**) monkey J (N=23). The preferred location (continuous lines) and anti-preferred location (dashed lines), before (black lines) and during APV delivery (red lines). Grey lines illustrate activity in the recovery episode.

Chapter 6 | Discussion and conclusions

In the introduction of this thesis we described the neural mechanisms underlying our remarkable visual perception. How feedforward processing creates new response properties at every cortical level, culminating in the highly selective neurons in IT, for example to faces. At the same time, feedback connections are crucial in selective attention and working memory, enabling us to dynamically select and maintain information that is behaviorally relevant for us. While the neural mechanisms of feedforward processing are relatively well understood[1-5], the mechanisms of feedback remain largely unclear. In this thesis we therefore sought to investigate the function and mechanisms of feedback processing in monkey visual cortex.

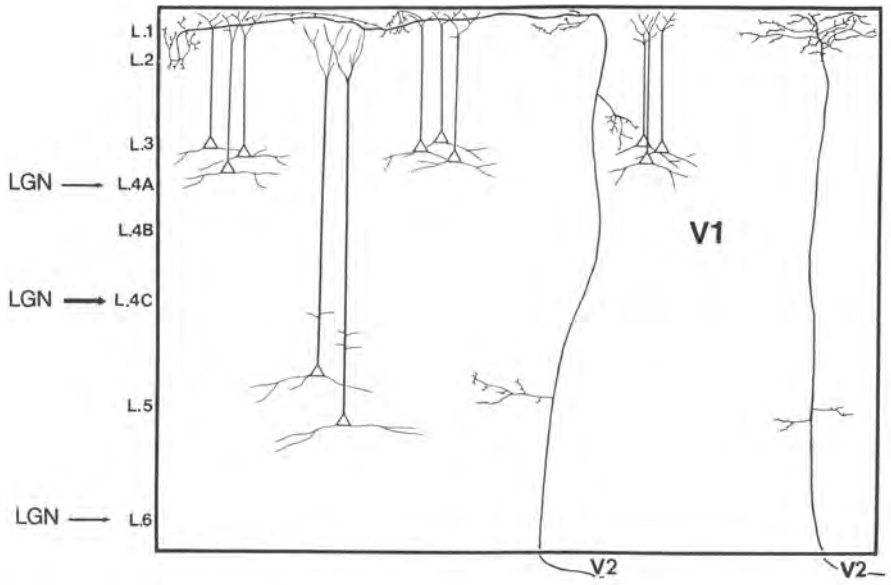

Figure 1 | Illustration showing the different layers in V1 that are targeted by feedforward and feedback connections. Feedforward input from the LGN arrives in layer 4C and to a lesser degree in layer 6 and 4A, while feedback from V2 arrives in layer 1-3 and 5. Some pyramidal cells within V1 are also indicated, note that layer 5 cells are able to receive feedback on both their basal and apical dendritic trees. (Adapted from ref. 7.)

Feedforward and feedback processing have notoriously been hard to disentangle because both streams are generally activated together. However, the two processing streams are still

segregated at the level of cortical layers, this particularly well established for V1. Feedforward input from the thalamus to V1 arrives very specifically in layer 4C and to a lesser extent in layer 6 and layer 4A[6], while feedback from higher visual areas arrives in the very superficial layers and layer 5 (**Figure 1**)[7,8]. This laminar profile provides a way to distinguish feedforward from feedback influences by recording neural activity simultaneously in the different layers of the cortex.

Chapter 2

First of all, we used laminar recordings to measure activity separately for all the layers in the primary visual cortex (V1) of monkeys performing the figure-ground task. This task has been suggested to rely on feedback from higher visual areas to V1, enhancing the firing rate at the figure location relative to background locations[9-12]. As expected, the figure and ground stimuli evoked a characteristic feedforward profile, with an early current sink in layer 4C at the same time as the peak in spiking activity.

In contrast, the figure-ground modulation showed sustained current sinks in layers 1-3 and 5 (Figure **2A**), closely matching the layers that are targeted by feedback in V1. Furthermore, the change in spiking activity caused by figure-ground modulation was strongest in the superficial and deep layers, and weaker in layer 4C (**Figure 2B**). This indicates that the figure-ground task generates sustained feedback input from higher visual areas to area V1, potentially enhancing the activity of neurons at the figure location.

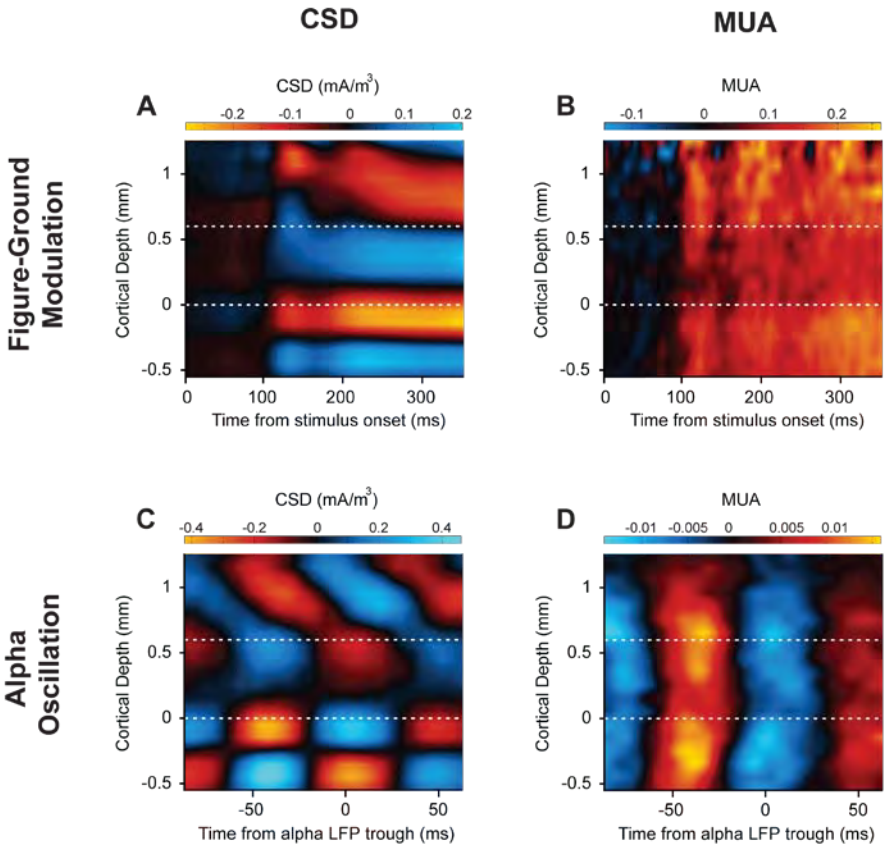

Figure 2 | Laminar profile of feedback in figure-ground modulation and alpha oscillations. (**A**,**B**) Stimulus-evoked responses of the (A) CSD and (B) MUA for the figure relative to the background condition. Current sinks (putatively reflecting excitatory synaptic input) are shown in red, current sources are shown in blue. (**C**,**D**) Average laminar profile of the (C) CSD and (D) MUA relative to LFP troughs in layer 5 for the alpha rhythm (8-12Hz).

Chapter 3

Next, we used laminar recordings while monkeys performed the curve-tracing task, allowing us to study the role of feedback in selective attention and working memory. We found a consistent working memory trace in both synaptic and spiking activity in V1. This trace could be disrupted by a mask but returned afterwards. Furthermore, we again found characteristic signatures of feedback for both selective attention and working memory, with current sinks in the superficial layers and layer 5, at the same time as in increase in spiking

activity which was strongest in the superficial and deep layers. This provides evidence that feedback to V1 is involved in the selection of objects that are behaviorally relevant and the maintenance of that information when the stimulus is no longer present.

Chapter 4

We went on to analyze the rhythmic activity that is induced by the figure-ground and the curve-tracing tasks, finding very similar effects for both tasks. The gamma rhythm was enhanced at the task-relevant location and positively correlated with spiking activity at a trial-by-trial basis. In contrast, the alpha rhythm was suppressed at the task-relevant location, enhanced at task-irrelevant locations and negatively correlated with spiking activity. This indicates that the gamma rhythm corresponds to increased activity while the alpha rhythm could represent active inhibition at task-irrelevant locations, confirming previous studies[13-15].

We next investigated the laminar profile of the alpha and gamma rhythm in V1. The gamma waves showed a characteristic feedforward profile, with an initial sink in layer 4C at the same time with an increase in spiking activity which spread across the cortical column. In contrast, the alpha waves showed a feedback profile with initial current sinks in the very superficial layers and layer 5 (**Figure 2C**). These sinks were aligned to an increase in spiking activity as well, which was strongest in the deep and superficial layers (**Figure 2D**). The sinks and the increase in spiking activity were not sustained as in the figure-ground modulation (**Figure 2A**,**B**), but were followed by a phase of suppression with sources in the superficial layers and layer 5 and a decrease in spiking activity. This indicates that the gamma rhythm propagated in the feedforward direction while the alpha rhythm propagated in the feedback direction through V1.

Further experiments using pharmacological intervention, electrical microstimulation and directionality measures between V1 and V4 confirmed that the gamma rhythm propagated in the feedforward direction while the alpha rhythm propagated in the feedback direction through monkey visual cortex.

Chapter 5

Finally, we investigated the neural mechanisms of the source of feedback by recording in the prefrontal cortex of monkeys performing selective attention and working memory tasks. We showed a center-surround organization of sustained activity for both of these tasks, with an enhancement of activity at task-relevant and a suppression of activity at task-irrelevant locations. By combining iontophoresis with single-unit recordings, we found that NMDA and AMPA receptors both contribute to the maintenance of task-relevant information in the prefrontal cortex during selective attention and working memory.

Two modes of feedback

Taken together, we found two signatures of feedback, one which was sustained and enhanced on task relevant locations (**Chapter 2** & **3**; **Figure 2A**,**B**), the other which was synchronized in the alpha range and enhanced on task irrelevant locations (**Chapter 4**; **Figure 2C**,**D**). Feedback is supported by excitatory neurons and the main effect is therefore generally thought to be excitatory[16,17], corresponding well with the sustained feedback profile that we found on task relevant locations. However, the alpha rhythm is enhanced at task irrelevant locations and was found to be negatively correlated with firing rates (**Chapter 4**).

A way to unify these seemingly contradicting results is by proposing a model in which feedback itself has a center-surround organization, with a sustained enhancing influence at the center and rhythmic inhibitory influence in the surround (**Figure 3**). In this model, the gamma rhythm is generated in V1 by feedforward input from the LGN[18, although see 19]. (For simplicity the feedforward input to V1 is shown as unaffected by feedback, although attentional effects in the lateral geniculate nucleus (LGN) have been found as well[20,21].) The sustained feedback in the center enhances the gamma activity in V1, while the feedback in the surround entrains the activity in the alpha rhythm, corresponding to a phasic suppression of activity at the troughs of the alpha rhythm. It is still an open question whether the level of activity at the peaks of the alpha rhythm in the surround is higher or the same as the activity in the center.

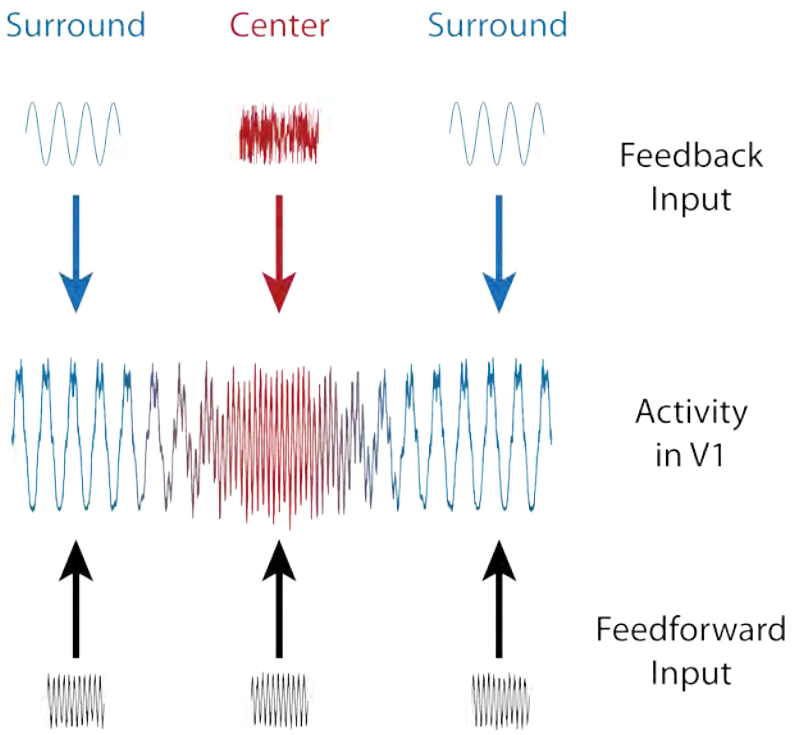

Figure 3 | Model of feedforward and feedback processing. The gamma rhythm arrives in V1 by feedforward input. Feedback input has a center-surround organization with sustained feedback at the center and an alpha synchronized feedback in the surround. The sustained feedback enhances the feedforward input to V1 while the alpha synchronized feedback potentially suppresses activity. The suppression in the surround is more pronounced at the troughs than at the peaks of the alpha cycle.

Center-surround organization of feedback

Studies in monkeys have previously found a center-surround organization in the effects of cortical feedback on early visual areas. A seminal study used electrical microstimulation in frontal eye field (FEF)[22], a higher cortical area which has been shown to provide direct feedback connections to early visual areas[23]. They found modulation of activity in visual area V4 with a center-surround organization: receptive fields that were at the focus of the stimulation showed enhancement of their activity while neighboring receptive fields showed suppression of activity.

A recent study in mouse visual cortex by the lab of Yang Dan investigated the effect of cortical feedback with the use of new optical and genetic tools[24]. They found an area in mouse prefrontal cortex which provided strong feedback to V1. Stimulating this area or the axons coming from this area, generated an activation pattern with a center-surround organization in V1. They went on to expose the cortical circuit in V1 that was underlying this organization, and found that the surround suppression was caused indirectly by the activation of a specific type of inhibitory neurons in V1, called somatostatin cells.

Indirect evidence for the organization of feedback can be found by investigating the spatial profile of selective attention. Schall et al. specifically studied the spatial profile of attention in monkey FEF[25], they found an enhancement at the focus of attention and a suppression that was strongest close to this focus, leveling off towards the far surround. Studies using fMRI and MEG have found similar so-called 'Mexican-hat' profiles of attention in visual areas, with a circle of enhancement at the center and a ring of inhibition around it that often remains suppressive into the far surround[26-29].

Both direct and indirect evidence therefore indicate that the effects of feedback on early visual areas has a center-surround organization. This could be related to the proposed model that feedback itself has a center-surround organization as well. The surround inhibition that is found within higher cortical areas like FEF could spread via feedback connections to lower visual areas, synchronizing the surround in the alpha range. The center-surround effect could then be locally enhanced at every level of the visual hierarchy, by the center-surround mechanism as described by Yang Dan.

Cortical mechanisms of the alpha rhythm

The cortical mechanisms of the gamma rhythm have been quite well established[30-32], indicating a crucial role of local loops between pyramidal cells and parvalbumin interneurons. In contrast, it is much less clear how the alpha rhythm is generated, nor how alpha could be related to surround suppression.

Based on the work of Yang Dan, it is conceivable that somatostatin cells are crucial for the generation of the alpha rhythm. For example, alpha could be generated by an interaction of cortical feedback and somatostatin cells, in a similar way as loops between pyramidal cells

and parvalbumin interneurons have been shown to underlie the gamma rhythm[30-32]. Some modeling work has implicated a neuron with the slow-inhibitory characteristics of somatostatin cells in the generation of low frequency oscillations[33,34], but no direct evidence has yet been found to support this. Arguing against this, a recent study in anesthetized mouse visual cortex showed that direct stimulation of somatostatin cells actually suppress low frequency oscillations and enhance high frequency activity[35]. To directly test whether somatostatin cells are involved in the alpha rhythm, it would be necessary to investigate it's temporal dynamics as has been extensively done for parvalbumin cells[30,31].

There are also other possible mechanisms that could be involved in the alpha rhythm. Work from the lab of Scanziani has shown that activating pyramidal cells in layer 6 of mouse visual cortex suppresses neuronal activity in the rest of the column[36], via fast spiking inhibitory neurons in the deep layers that project to all other layers in the column[37]. This is in line with earlier work in monkey visual cortex, implicating layer 6 in receptive field surround inhibition[38]. It could be that a subpopulation of layer 6 cells is driving the suppression of activity that we see during the alpha cycle, however, we saw a suppression of activity across layers, including layer 6 (**Figure 2D**). Moreover, a study in monkey V4 by Vinck et al. showed that fast-spiking cells (putative interneurons) fired at the same phase of the alpha cycle as regular cells, although they probably mostly recorded in the superficial layers[39].

A recent study by the group of Fellin has selectively activated pyramidal cells in layer 5 of mouse visual cortex[40]. Similar to the work of the lab of Scanziani, they found that this strongly modulated neurons across the cortical column, but instead by enhancing their activity. This is in line with work by the group of Larkum in mice which showed that coincident input to the apical and basal dendrites of layer 5 neurons is a powerful mechanism that can modulate the activity of neurons across layers[41,42]. This would match well with the feedback profile that we found with current sinks in layer 1-2 and 5 at the same time as the increase of spiking activity (**Figure 2C**,**D**).

The work by Larkum indicated that coincident input to the layer 5 cells can cause the cells to be in two different states, either a sustained or a bursting mode[42]. The finding that layer 5 cells can be in a bursting mode is related to a rich literature on low frequency oscillations in cortical slices, indicating intrinsic properties of layer 5 pyramidal cells in the generation of

these oscillations[43-46]. Moreover, the study by the group of Fellin also found that ongoing low frequency activity can be modulated by activating and inactivating layer 5 cells *in vivo*[40]. As the deep layers provide the dominant source of feedback in the cortex[47], layer 5 cells could determine the two modes of feedback by being in a state of either sustained or low frequency activity. This would imply that the alpha rhythm involves a phase of after-hyperpolarization, the troughs during the alpha cycle would simply represent the lack of excitatory feedback instead of a phase of active inhibition.

Bursting activity and the pulvinar

It could be said that bursting activity is unrelated to the alpha rhythm because it is not a stable oscillation and the main frequency component of bursts is generally lower than 10Hz. However, a recent paper by Harris et al. showed that bursting activity at a single cell level corresponds to oscillations around 10Hz at the population level[48].

Bursting activity and the alpha rhythm measured in cats and dogs was originally thought to be dependent on the LGN[49,50], which would contradict our finding that the alpha rhythm propagates in the feedback direction. However, work by Sherman has shown that bursting activity in monkeys is dramatically stronger in the pulvinar than in the LGN[51], and V1 only receives input from the pulvinar in the layers which are targeted by cortical feedback, the very superficial layers and deep layers[52,53]. Moreover, the pulvinar in turn receives strong input from cortical layer 5 cells[53].

This link to the pulvinar is particularly interesting because it has been implicated both in the generation of the alpha rhythm[54,55] and in selective attention[55,56]. Whereas our results highlight the involvement of cortical feedback in the generation of the alpha rhythm, these previous studies suggest an additional role for the pulvinar, or a loop between the cortex and the pulvinar.

The well studied phenomenon of bursting activity could thereby be related to the alpha oscillatory activity that we observed, which would also be in line with recent work in monkey V4 showing that bursting activity is lower at attended location[57]. Our work would suggest that this effect could partly be due to an enhancement of bursting activity at distractor locations.

Functional role of cortical rhythms

The reviewed literature suggests that the cortical mechanisms of the alpha rhythm are still debated. A loop between interneurons and excitatory cells could be involved, but the intrinsic properties of deep layer pyramidal cells might be sufficient as well. Moreover, our work indicated cortical feedback connections, while previous literature also suggests a role for the pulvinar. Although this is an important issue to solve, an independent question is whether the alpha rhythm is actively involved in the suppression of task irrelevant information or whether it is an epiphenomenon of the underlying cortical mechanisms. Deep layer cells could just happen to get synchronized around 10Hz for example, without any functional relation to information processing. Although the gamma rhythm has received much more attention, it's functional significance is also still lively debated[58-64]. The question whether cortical rhythms have a functional role in visual cognition will most likely be very hard to settle.

Conclusions

Taken together, in this thesis we revealed an important neural component of the source of feedback in prefrontal cortex. Furthermore, we found two signatures of feedback in V1: one in the stimulus-evoked responses of task-relevant versus task-irrelevant locations, and the other in the alpha rhythm which was found to be enhanced at task-irrelevant locations. This suggests that selective attention not only corresponds to a center-surround organization in prefrontal cortex but also in feedback itself, with a sustained or tonic mode of processing at the focus of attention and an alpha synchronized mode in the attentional surround.

Until recently, it has been hard to study the role of projections in the cortex because most neuroscientific techniques only record activity within individual areas. The CSD is powerful in separating feedforward from feedback input, but it remains an indirect measure. Recent technical developments like multi-photon imaging and optogenetics[65,66] have the potential to directly investigate the role of feedforward and recurrent connections, and it's relationship to cortical rhythms. It will therefore be highly exciting to discover how the functional connectivity within and between brain areas gives rise to our exquisite visual perception, and what the role of cortical rhythms in this will turn out to be.

References

1. Hubel,D.H. & Wiesel,T.N. Ferrier lecture. Functional architecture of macaque monkey visual cortex. *Proc. R. Soc. Lond B Biol. Sci.* **198**, 1-59 (1977).

2. Van Essen,D.C., Anderson,C.H., & Felleman,D.J. Information processing in the primate visual system: an integrated systems perspective. *Science* **255**, 419-423 (1992).

3. Kobatake,E. & Tanaka,K. Neuronal selectivities to complex object features in the ventral visual pathway of the macaque cerebral cortex. *J. Neurophysiol.* **71**, 856-867 (1994).

4. Riesenhuber,M. & Poggio,T. Hierarchical models of object recognition in cortex. *Nature Neurosci.* **2**, 1019-1025 (1999).

5. Roelfsema,P.R. Cortical algorithms for perceptual grouping. *Annu. Rev. Neurosci.* **29**, 203-227 (2006).

6. Lund,J.S. Anatomical organization of macaque monkey striate visual cortex. *Annu. Rev. Neurosci.* **11**, 253-288 (1988).

7. Rockland,K.S. & Virga,A. Terminal arbors of individual "feedback" axons projecting from area V2 to V1 in the macaque monkey: a study using immunohistochemistry of anterogradely transported Phaseolus vulgaris-leucoagglutinin. *J. Comp. Neurol.* **285**, 54-72 (1989).

8. Anderson,J.C. & Martin,K.A. The synaptic connections between cortical areas V1 and V2 in macaque monkey. *J. Neurosci.* **29**, 11283-11293 (2009).

9. Lamme,V.A., Zipser,K., & Spekreijse,H. Figure-ground activity in primary visual cortex is suppressed by anesthesia. *Proc. Natl. Acad. Sci. U. S. A* **95**, 3263-3268 (1998).

10. Lamme,V.A.F., Supèr,H., & Spekreijse,H. Feedforward, horizontal, and feedback processing in the visual cortex. *Curr. Opin. Neurobiol.* **8**, 529-535 (1998).

11. Hupe,J.M. *et al.* Cortical feedback improves discrimination between figure and background by V1, V2 and V3 neurons. *Nature* **394**, 784-787 (1998).

12. Poort,J. *et al.* The role of attention in figure-ground segregation in areas V1 and V4 of the visual cortex. *Neuron* **75**, 143-156 (2012).

13. Klimesch,W., Sauseng,P., & Hanslmayr,S. EEG alpha oscillations: the inhibition-timing hypothesis. *Brain Res. Rev.* **53**, 63-88 (2007).

14. Jensen,O. & Mazaheri,A. Shaping functional architecture by oscillatory alpha activity: gating by inhibition. *Front Hum. Neurosci.* **4**, 186 (2010).

15. Bonnefond,M. & Jensen,O. Alpha oscillations serve to protect working memory maintenance against anticipated distracters. *Curr. Biol.* **22**, 1969-1974 (2012).

16. Johnson,R.R. & Burkhalter,A. Microcircuitry of forward and feedback connections within rat visual cortex. *J. Comp Neurol.* **368**, 383-398 (1996).

17. Shao,Z. & Burkhalter,A. Different balance of excitation and inhibition in forward and feedback circuits of rat visual cortex. *J. Neurosci.* **15**, 7353-7365 (1996).

18. Castelo-Branco,M., Neuenschwander,S., & Singer,W. Synchronization of visual responses between the cortex, lateral geniculate nucleus, and retina in the anesthetized cat. *J. Neurosci.* **18**, 6395-6410 (1998).

19. Bastos,A.M., Briggs,F., Alitto,H.J., Mangun,G.R., & Usrey,W.M. Simultaneous recordings from the primary visual cortex and lateral geniculate nucleus reveal rhythmic interactions and a cortical source for gamma-band oscillations. *J. Neurosci.* **34**, 7639-7644 (2014).

20. O'Connor,D.H., Fukui,M.M., Pinsk,M.A., & Kastner,S. Attention modulates responses in the human lateral geniculate nucleus. *Nat. Neurosci.* **5**, 1203-1209 (2002).

21. McAlonan,K., Cavanaugh,J., & Wurtz,R.H. Guarding the gateway to cortex with attention in visual thalamus. *Nature* **456**, 391-394 (2008).

22. Moore,T. & Armstrong,K.M. Selective gating of visual signals by microstimulation of frontal cortex. *Nature* **421**, 370-373 (2003).

23. Markov,N.T. *et al.* Weight consistency specifies regularities of macaque cortical networks. *Cereb. Cortex* **21**, 1254-1272 (2011).

24. Zhang,S. *et al.* Selective attention. Long-range and local circuits for top-down modulation of visual cortex processing. *Science* **345**, 660-665 (2014).

25. Schall,J.D., Sato,T.R., Thompson,K.G., Vaughn,A.A., & Juan,C.H. Effects of search efficiency on surround suppression during visual selection in frontal eye field. *J. Neurophysiol.* **91**, 2765-2769 (2004).

26. Kastner,S. & Pinsk,M.A. Visual attention as a multilevel selection process. *Cogn Affect. Behav. Neurosci.* **4**, 483-500 (2004).

27. Muller,N.G. & Kleinschmidt,A. The attentional 'spotlight's' penumbra: center-surround modulation in striate cortex. *Neuroreport* **15**, 977-980 (2004).

28. Slotnick,S.D., Schwarzbach,J., & Yantis,S. Attentional inhibition of visual processing in human striate and extrastriate cortex. *Neuroimage.* **19**, 1602-1611 (2003).

29. Hopf,J.M. *et al.* Direct neurophysiological evidence for spatial suppression surrounding the focus of attention in vision. *Proc. Natl. Acad. Sci. U. S. A* **103**, 1053-1058 (2006).

30. Cardin,J.A. *et al.* Driving fast-spiking cells induces gamma rhythm and controls sensory responses. *Nature* **459**, 663-667 (2009).

31. Sohal,V.S., Zhang,F., Yizhar,O., & Deisseroth,K. Parvalbumin neurons and gamma rhythms enhance cortical circuit performance. *Nature* **459**, 698-702 (2009).

32. Tiesinga,P. & Sejnowski,T.J. Cortical enlightenment: are attentional gamma oscillations driven by ING or PING? *Neuron* **63**, 727-732 (2009).

33. Vierling-Claassen,D., Cardin,J.A., Moore,C.I., & Jones,S.R. Computational modeling of distinct neocortical oscillations driven by cell-type selective optogenetic drive: separable resonant circuits controlled by low-threshold spiking and fast-spiking interneurons. *Front Hum. Neurosci.* **4**, 198 (2010).

34. Lee,J.H., Whittington,M.A., & Kopell,N.J. Top-down beta rhythms support selective attention via interlaminar interaction: a model. *PLoS. Comput. Biol.* **9**, e1003164 (2013).

35. Chen,N., Sugihara,H., & Sur,M. An acetylcholine-activated microcircuit drives temporal dynamics of cortical activity. *Nat. Neurosci.* **18**, 892-902 (2015).

36. Olsen,S.R., Bortone,D.S., Adesnik,H., & Scanziani,M. Gain control by layer six in cortical circuits of vision. *Nature* **483**, 47-52 (2012).

37. Bortone,D.S., Olsen,S.R., & Scanziani,M. Translaminar inhibitory cells recruited by layer 6 corticothalamic neurons suppress visual cortex. *Neuron* **82**, 474-485 (2014).

38. Bolz,J. & Gilbert,C.D. Generation of end-inhibition in the visual cortex via interlaminar connections. *Nature* **320**, 362-365 (1986).

39. Vinck,M., Womelsdorf,T., Buffalo,E.A., Desimone,R., & Fries,P. Attentional modulation of cell-class-specific gamma-band synchronization in awake monkey area v4. *Neuron* **80**, 1077-1089 (2013).

40. Beltramo,R. *et al.* Layer-specific excitatory circuits differentially control recurrent network dynamics in the neocortex. *Nat. Neurosci.* **16**, 227-234 (2013).

41. Larkum,M.E., Senn,W., & Luscher,H.R. Top-down dendritic input increases the gain of layer 5 pyramidal neurons. *Cereb. Cortex* **14**, 1059-1070 (2004).

42. Larkum,M. A cellular mechanism for cortical associations: an organizing principle for the cerebral cortex. *Trends Neurosci.* **36**, 141-151 (2013).

43. Silva,L.R., Amitai,Y., & Connors,B.W. Intrinsic oscillations of neocortex generated by layer 5 pyramidal neurons. *Science* **251**, 432-435 (1991).

44. Sanchez-Vives,M.V. & McCormick,D.A. Cellular and network mechanisms of rhythmic recurrent activity in neocortex. *Nat. Neurosci.* **3**, 1027-1034 (2000).

45. Ulrich,D. Dendritic resonance in rat neocortical pyramidal cells. *J. Neurophysiol.* **87**, 2753-2759 (2002).

46. Le Bon-Jego,M. & Yuste,R. Persistently active, pacemaker-like neurons in neocortex. *Front Neurosci.* **1**, 123-129 (2007).

47. Rockland,K.S. & Pandya,D.N. Laminar origins and terminations of cortical connections of the occipital lobe in the rhesus monkey. *Brain Res.* **179**, 3-20 (1979).

48. Luczak,A., Bartho,P., & Harris,K.D. Gating of sensory input by spontaneous cortical activity. *J. Neurosci.* **33**, 1684-1695 (2013).

49. Lopes da Silva,F.H., van Lierop,T.H.M.T., Schrijer,C.F., & Storm,v.L. Organization of thalamic and cortical alpha rhythms: spectra and coherences. *Electroencephalogr. Clin. Neurophysiol.* **35**, 627-639 (1973).

50. Lorincz,M.L., Kekesi,K.A., Juhasz,G., Crunelli,V., & Hughes,S.W. Temporal framing of thalamic relay-mode firing by phasic inhibition during the alpha rhythm. *Neuron* **63**, 683-696 (2009).

51. Ramcharan,E.J., Gnadt,J.W., & Sherman,S.M. Higher-order thalamic relays burst more than first-order relays. *Proc. Natl. Acad. Sci. U. S. A* **102**, 12236-12241 (2005).

52. Benevento,L.A. & Rezak,M. Extrageniculate projections to layers VI and I of striate cortex (area 17) in the rhesus monkey (Macaca mulatta). *Brain Res.* **96**, 51-55 (1975).

53. Ogren,M.P. & Hendrickson,A.E. The distribution of pulvinar terminals in visual areas 17 and 18 of the monkey. *Brain Res.* **137**, 343-350 (1977).

54. Lopes da Silva,F.H., Vos,J.E., Mooibroek,J., & van Rotterdam,A. Relative contribution of intracortical and thalamo-cortical processes in the generation of alpha rhythms, revealed by partial coherence analysis. *Electroencephalogr. Clin. Neurophysiol.* **50**, 449-456 (1980).

55. Saalmann,Y.B., Pinsk,M.A., Wang,L., Li,X., & Kastner,S. The pulvinar regulates information transmission between cortical areas based on attention demands. *Science* **337**, 753-756 (2012).

56. Robinson,D.L. & Petersen,S.E. The pulvinar and visual salience. *Trends Neurosci.* **15**, 127-132 (1992).

57. Anderson,E.B., Mitchell,J.F., & Reynolds,J.H. Attention-dependent reductions in burstiness and action-potential height in macaque area V4. *Nat. Neurosci.* **16**, 1125-1131 (2013).

58. Ray,S. & Maunsell,J.H. Differences in gamma frequencies across visual cortex restrict their possible use in computation. *Neuron* **67**, 885-896 (2010).

59. Brunet,N., Vinck,M., Bosman,C.A., Singer,W., & Fries,P. Gamma or no gamma, that is the question. *Trends Cogn Sci.* **18**, 507-509 (2014).

60. Siegle,J.H., Pritchett,D.L., & Moore,C.I. Gamma-range synchronization of fast-spiking interneurons can enhance detection of tactile stimuli. *Nat. Neurosci.* **17**, 1371-1379 (2014).

61. Hermes,D., Miller,K.J., Wandell,B.A., & Winawer,J. Stimulus Dependence of Gamma Oscillations in Human Visual Cortex. *Cereb. Cortex* **25**, 2951-2959 (2015).

62. Hermes,D., Miller,K.J., Wandell,B.A., & Winawer,J. Gamma oscillations in visual cortex: the stimulus matters. *Trends Cogn Sci.* **19**, 57-58 (2015).

63. Ray,S. & Maunsell,J.H. Do gamma oscillations play a role in cerebral cortex? *Trends Cogn Sci.* **19**, 78-85 (2015).

64. Bastos,A.M., Vezoli,J., & Fries,P. Communication through coherence with inter-areal delays. *Curr. Opin. Neurobiol.* **31**, 173-180 (2015).

65. Denk,W., Strickler,J.H., & Webb,W.W. Two-photon laser scanning fluorescence microscopy. *Science* **248**, 73-76 (1990).

66. Boyden,E.S., Zhang,F., Bamberg,E., Nagel,G., & Deisseroth,K. Millisecond-timescale, genetically targeted optical control of neural activity. *Nat. Neurosci.* **8**, 1263-1268 (2005).

Appendix | Summary

Acknowledgement

Summary

One of the great questions in science is how our visual perception of the world is generated by our brain. It is known that visual information from our eyes travel in a feedforward direction through a hierarchy of areas in the cortex, transforming the visual information from simple line-like features in the first visual area (V1) to more complex features like faces in higher visual areas. However, there is an equally strong stream in the opposite direction, and the function and mechanisms of this feedback stream is less well understood. In this thesis we sought to investigate feedforward versus feedback processing in the visual cortex of monkeys performing cognitive tasks.

By recording simultaneously in the different layers of V1 we found a characteristic signature of both the feedforward and the feedback flow of activity. We showed that the feedback input to V1 was enhanced at locations corresponding to task relevant elements of a stimulus, enhancing the activity of neurons at those locations. Moreover, the feedback input and the activity in V1 remained enhanced when the stimulus disappeared. This suggests that even the earliest visual area is involved in the selection of task relevant information, as well as in the maintenance of that information when the stimulus is absent.

The visual cortex also generates rhythmic activity at both a low and a high frequency. We found that the low frequency or 'alpha' rhythm travelled selectively in the feedback direction, while the high frequency or gamma rhythm travelled in the feedforward direction through the visual cortex. This finding can now also be used to distinguish these two processing streams in the visual cortex, for example with EEG and MEG in humans.

Finally, we recorded activity of individual neurons in an area in the brain that is thought to provide the source of feedback in the cortex, the dorsolateral prefrontal cortex (dlPFC). By using local application of drugs, we showed that both slow (NMDA) and fast (AMPA) receptors contribute to the encoding of task relevant information in the dlPFC.

Persbericht

Van kijken naar zien: hoe de hersenen onze waarneming filteren

Elke ochtend als je wakker wordt, open je je ogen en zie je de wereld, in al zijn vormen en kleuren. Eén van de belangrijke vragen in de wetenschap is hoe deze ervaring wordt gecreëerd door ons brein.

Visuele informatie komt binnen in je ogen en wordt verzonden naar het eerste visuele gebied (V1) achter in je hoofd. Vervolgens stroomt het naar visuele hersengebieden meer vooraan in je hoofd. De hersencellen in opeenvolgende gebieden verwerken steeds complexere elementen van de visuele wereld, van kleine lijntjes in V1, naar gezichten of auto's in hogere visuele gebieden.

Naast deze zogenoemde 'feedforward' stroom van informatieverwerking is er ook een 'feedback' stroom die in omgekeerde richting loopt. Hoewel die feedback stroom van activiteit ongeveer even sterk is als de feedforward stroom, is het nog onduidelijk wat de rol van deze omgekeerde stroom in de hersenen is. Het wordt gedacht dat feedback belangrijk is voor visuele aandacht, bijvoorbeeld het lezen van een woord in deze zin.

Onderzoek toont aan dat visuele aandacht beschadigd is in ziektes als schizofrenie, autisme en ADHD, maar ook in ouderdom. Dit impliceert dat bij deze mensen feedback verbindingen specifiek zijn aangetast.

Om de neuronale mechanismen van feedforward en feedback verbindingen beter te begrijpen hebben we apen getrained in het uitvoeren van visuele aandacht taakjes, soortgelijk aan de taakjes waarvan bekend is dat ze minder goed kunnen worden uitgevoerd door mensen met neurologische aandoeningen als schizofrenie en ADHD. De apen keken daarbij naar een computerscherm waarop een plaatje werd getoond met relevante en irrelevante informatie. Ze werden beloond als ze een oogbeweging maakten naar het relevante gedeelte van het plaatje. Door tegelijkertijd de activiteit te meten met electrodes die in de hersenen waren geplaatst, konden we zowel de feedforward als de feedback stroom meten tijdens het uitvoeren van cognitieve taakjes.

We vonden dat de achterwaartse stroom inderdaad continu versterkt was in gebieden in de hersenen waar relevante elementen van een plaatje worden verwerkt. Achterwaartse stromen zorgen er dus voor dat je bijvoorbeeld een woord dat je wilt lezen beter kan zien.

De stromen in ons hoofd kunnen ook in golven bewegen in plaats van continu verhoogd of verlaagd zijn. We vonden dat snelle golven van activiteit in de voorwaartse richting stromen, terwijl langzame golven in de achterwaartse richting stromen. Ook vonden we dat de langzame golven sterker waren in hersengebieden waar irrelevante elementen van een plaatje worden verwerkt. Achterwaartse stromen, die in langzame golven bewegen, zorgen er daarom misschien voor dat de irrelevante woorden rondom het woord dat je wilt lezen worden onderdrukt. Onze hersenen filteren dus wat we zien door belangrijke gedeeltes te verterken en onbelangrijke gedeeltes te onderdrukken.

Dit onderzoek geeft een unieke manier om te begrijpen hoe de tegenovergestelde stromen in de hersenen ervoor zorgen dat we ons kunnen focussen op informatie die belangrijk voor ons is, en wat er in onze hersenen mogelijk mis gaat als dat niet meer goed lukt.

Acknowledgement

Finally, I would like to thank a couple of people who have been crucial for my PhD.

Pieter, ik kan me nog goed herinneren dat we voor de eerste keer afspraken om te praten over een mogelijke stage. Je gebruikte het woord cortico-corticale verbindingen, en ik vroeg je wat dat betekende. Sinds die dag is er veel veranderd, je hebt me het vertrouwen gegeven om te mogen werken in een veld wat we beiden fantastisch vinden, om me te kunnen ontwikkelen van een natuurkunde student naar een 'system neuroscientist'. Wat ik enorm in je waardeer is je enthousiasme voor de wetenschap, gecombineerd met een altijd klaar heldere geest, en een weigering om op te houden met werken totdat iets echt goed is, in technisch en theoretisch opzicht maar ook in de manier waarop je het communiceert naar anderen. Ik heb ook enorm veel waardering voor je manier van leiding geven, allereerst vriendelijk, nooit neerbuigend. Alles kan besproken, op niets ligt een taboe, je focust je op de wetenschappelijke inhoud, niet om de vorm. Dat creert een unieke sfeer van vrijheid en creativiteit, gecombineerd met een rigoreus scherpe blik en een oog voor detail. Daarbij ben ik je enorm dankbaar dat altijd tijd voor me hebt vrij gemaakt, op die momenten was je ook altijd volledig bij het gesprek, hoe druk je het ook had. Ik heb enorm veel van je geleerd, en hoop dat te mogen blijven doen.

Robert Desimone, Pascal Fries, Ole Jensen, Huib Mansvelder and Eus van Someren, your work has been crucial in shaping me as a scientist. It is a great privilege and pleasure to defend my thesis before you.

I also would like to express my sincere gratitude to Charles Gilbert, for giving me the possibility to work on and finish my PhD in your lab, when time allowed it.

Wim Vanduffel, dank voor je steun en vertrouwen in de eerste jaren van mijn carriere. Je bent voor mij een exceptionele wetenschapper die een grote geest combineert met een groot hart.

Matt, you know it was partly you that kept me in Amsterdam, instead of pursuing a PhD in the US. Your friendly and joyful personality and your keen sense of social relations within the lab made my PhD so much more fun and easy going. Moreover, I am highly grateful to have learned all the skills of monkey electrophysiology from you. And I know you remember the many times I entered your office, bugging you about neuroscience, cognitive psychology, psychophysics and statistics. As you kept on having answers, I kept on coming back to pick your extensive mind. I also should thank you for having Louise as a student, allowing me to meet the love of my life.

Chris, een van de eerste herinneringen die ik aan je heb is dat je me op een vroege maandag ochtend vertelde dat ik waarschijnlijk een longontsteking had, en dat ik toch echt naar de huisarts moest. M'n huisarts wist het niet, longontsteking, ingeklapte long of een longembolie, maar na onderzoek in het ziekenhuis bleek dat je gelijk had. Je bent een stille kracht in het lab, die altijd klaar staat om te helpen, niet alleen met medisch advies, maar ook voor allerhande technische en software-matige problemen. Ik ben je ook enorm dankbaar voor je introductie tot frequentie analyse, je vriendschap met Stiliyan Kalitzin, je ideeën over synchroniciteit en de vele pareltjes van artikelen die je me hebt aangeraden. Maar de beste herinnering aan jou zijn de talloze avonden dat we samen hebben gegeten in de kantine van het AMC. De gesprekken over neurowetenschappen, filosofie, film, politiek enzovoorts. Het is altijd een plezier om naar je te luisteren, je eloquent taalgebruik, je geest die vol zit met vragen, inzichten en verhalen. Met name hebt me uitgedaagd om mijn vooronderstellingen te blijven onderzoeken, om te begrijpen dat er verschillende niveau's van verklaringen en modellen bestaan (cellulair, netwerk, cognitief) en om altijd de vraag in het oog te houden: "Wat leert ons dat over hoe het brein werkt?".

Stiliyan Kalitzin, thank you very much for sharing the wavelet analysis scripts, and for your help to understand and expand them.

Kor, jouw rust tijdens operaties, en je kennis van anesthesie is cruciaal geweest voor mijn werk. Je jaren lange ervaring, maar ook je vriendschap en het vertrouwen dat je me gaf, in het trainen van apen en aan de operatie tafel, hebben het mogelijk gemaakt dat ik enorm veel heb kunnen leren. Ook Dave en Anneke ben ik enorm dankbaar voor de geweldige zorg voor onze jongens.

Bram en Bruno, dank voor de geweldige tijd samen. Ons kantoor samen zal altijd bij me blijven als de ideale werkplek. Lange discussies als we er zin in hadden, hard werken als dat nodig was. Ik voelde me volledig op m'n gemak bij jullie, als collega's en als vrienden. Ik ga er vanuit dat we elkaar blijven zien.

Gio, thank you convincing me to be PhD representatives at the NIN, it was a fun and interesting time together that made me appreciate even more how great of a person you are. I'm confident that you will have beautiful and successful life with Yael and David!

Danique, je enthousiasme voor de wetenschap en je ambitie blijven een inspiratie voor me. Dank dat je me hebt overtuigd om stellingen toe te voegen aan dit boekje, en dank dat ik soms een dropje mocht stelen uit je la.

Arezoo and Aurel, it was great to be able to spend time together with you in the lab. I have gained a lot from your knowledge about neuroscience and electrophysiology, and I've truly enjoyed your company. Ilia, it was so much fun to work with you on the alpha game. I really hope your company will be a success.

Roxana, Jeanette, Chris, Dev, Marie-Alice, Liviu and the other members of the lab, thank you for all the help and for making the time in the lab so much more fun!

Ruud, Rinus en Joost, dank voor alle hulp, van het aanpassen van de microdrives tot aan het bouwen van de kooien van Faraday. Jullie kennis van technieken materialen hebben me veel geleerd. Ook heeft jullie enthousiasme voor jullie vak me laten zien dat jullie de leukste banen hebben van het NIN.

Rein, dank voor al je hulp en je inzichten in de werking van versterkers, het voorkomen van ruis, en netjes solderen. Ronald en Pieter, hartelijk dank voor al jullie hulp, van draadjes en krimpkousjes tot de hulp bij de opstelling om zelf electrodes te kunnen maken.

Tini, Wilma, Heidi en Ernita, hartelijk dank voor al jullie vriendelijke en efficiente hulp bij de organisatie van zoveel praktische zaken. Tini, met name ook hartelijk dank bij alle hulp om te kunnen promoveren. Het was erg fijn om te weten dat het zo goed geregeld werd, vanuit New York was dat erg lastig geweest. Marcia, Wil en Hanneke, hartelijk dank voor alle dagelijkse hulp in mijn dagen op het NIN.

All the other colleagues at the NIN, it was great to spend time with you, and for making the NIN such a great place!

Anouk, Ilja, Annelinde, Iris, Martijn, Yair, Tomas, Roy, Steven en alle anderen, dank voor alle inspirerende gesprekken en de leuke avonden. Ik heb me altijd verbazingwekkend op m'n gemak gevoeld bij jullie, wat vooral komt door het overduidelijke plezier dat jullie gezamelijk hebben.

Meneer Extra, dank voor je geweldige wiskunde lessen en je vertrouwen al toen ik zo jong was. Ik was toen misschien nog niet zo geinteresseerd om er iets mee te doen, maar je vertrouwen in mijn capaciteiten heeft me geholpen om voor het eerst echt aan de slag te gaan, tijdens mijn studie natuurkunde en later tijdens mijn PhD.

Marcel van den Hout, dank voor je voorbeeld functie als hoogleraar psychologie.

Ludwig Wittgenstein, thank you for helping me to avoid pursuing a career in philosophy.

John Arsenault, thanks for your help with this thesis, and for being an inspiring friend. I hope one day we'll be able to work together again.

Martijn Cloos, dank voor je immer hoopvolle blik, tijdens onze studie natuurkunde in Amsterdam, en nu weer in New York.

Michiel Schuurman, dank voor al je hulp bij het vormgeven van dit boekje en de cover van PNAS. De Pantone kleurencirkel die ik van je heb gekregen blijft bij m'n bureau hangen om me te helpen in het kiezen van kleuren voor de figuren die ik maak.

Guido Cilissen, dank voor je help bij het maken van het mooie inkijkje in het apenbrein. Het was erg leuk om het samen met je te ontwerpen.

Emiel, ik zal nooit vergeten dat we samen in de Melkweg zaten en dat je me vroeg, het beeld van deze mandarijnenschil, waar zit dat in je hoofd? Dit is het vlammetje dat me nog altijd leidt in mijn onderzoek.

Wouter, Giso, Japie, Mathijs, Alexandra, Bram, Isabella, Elise, Wyne, Kat, Erika, Alex, Fieke en alle anderen, dank voor de momenten dat jullie er waren om m'n hart en ziel te verlichten in de soms donkere dagen.

Rafael, je vriendschap heeft veel voor me betekend, met name ook in de moeilijke eerste tijd in New York, toen ik zoveel behoefte had om bij mensen te zijn die Floor kenden, bij de mensen waar enkele woorden genoeg. Maar je bent denk ik ook al heel jong cruciaal voor me geweest om ambitieus te durven zijn, om verder te durven kijken, en mezelf te ontwikkelen. Het is wat dat betreft misschien ook niet zo toevallig dat we samen in New York terecht zijn gekomen, om de Amerikaanse droom te gaan leven.

Dominique, dank voor je liefde en steun. Je bent zoveel jaren zo belangrijk geweest. Alle keren dat ik laat thuis kwam van werk en zei, "Ik heb het, het werkt!", om de avond erop weer te moeten zeggen, "Misschien toch niet..". Michel en Emmeliek, ik ben jullie erg dankbaar voor jullie gastvrijheid en steun, en Michel voor je overtuigend advies om natuurkunde af te maken.

Pa, je niet aflatende steun heeft het mogelijk gemaakt dat ik zowel de studie natuurkunde als filosofie af heb kunnen maken, wat cruciaal is geweest om zowel de natuurwetenschappelijke achtergrond als de visie te kunnen ontwikkelen om in de neurowetenschap te gaan promoveren. Je blijvend vertrouwen in mij is cruciaal voor mijn leven en mijn carriere. Mutti, dank voor alle liefde en wijsheid. Je bent enorm belangrijk geweest in mijn keuze voor de neurowetenschappen door je oprechte interesse in de mens in al zijn facetten, en door je ambitie en het plezier in alles wat je doet.

Floor, je was de beste moeder, en de meest inspirerende persoon. De keren dat ik bij je op bezoek kwam in de Govert Flinck straat in Amsterdam, je sprankelende interesse in de psychologie, de originaliteit en kwaliteit van je ideeen, de manier waarop je je kleedde en je huis inrichtte. Ik was altijd onder de indruk, en trots dat ik je kende. Je gezin en het huis met mijn broer Paul in Amersfoort was voor mij een baken van rust en plezier. Altijd was er wel iets te doen, iets nieuws te beleven, nieuwe ideeën om over te praten. Het was voor mij de perfecte plek in deze wereld. Het is ruw en onbegrijpelijk dat je er niet meer bent. Het maakt dat deze wereld minder mooi is geworden. Er is iets weggerukt, alsof er ineens geen bomen meer zijn. Tegelijkertijd blijf je altijd bij ons, zul je een voorbeeld blijven voor hoe een moeder en een vrouw kunnen zijn, een heldin. Ik zal je altijd missen.

Paul, Nino, Sara, Meike, Tijmen, Jasmijn, Felix en Roos, het is fantastisch om jullie broertje en oom te mogen zijn. Jullie gezinnen blijven een baken van rust en plezier voor mij.

Louise, mijn super liefste. Het avontuur om naar New York te gaan heeft ons geleerd hoe sterk we samen zijn, onze liefde blijft maar groeien. Met jou samen zijn is mijn favoriete bezigheid, die zekerheid en jouw vertrouwen geven me de rust en de vrijheid om ook het werk te kunnen doen wat ik zo leuk vind. Ik heb zoveel zin in onze toekomst samen, ik kijk er naar uit, met een glimlach en een gerust hart.